THE UNIVERSITY OF QUEENSLAND

AUSTRALIA

Fundamentals of thin intumescent coatings for the design of fire-safe structures

Andrea Lucherini

Master of Science (Civil Engineering – Structural Engineering)
Bachelor of Science (Civil and Environmental Engineering)

A thesis submitted for the degree of Doctor of Philosophy at
The University of Queensland in 2020
School of Civil Engineering

Fundamentals of thin intumescent coatings for the design of fire-safe structures

by

Andrea Lucherini

This thesis has been supervised by

Dr Cristian Maluk

Prof José L. Torero

Dr Juan P. Hidalgo

The examining committee consisted of

Prof Serge Bourbigot

Dr Antonio Bilotta

Abstract

At present, intumescent coatings represent a mainstream solution for protecting load-bearing structural steel systems during a fire. Upon heating, intumescent coatings swell to form a thick low-density and low-thermal-conductivity porous char that prevents the substrate material from reaching high temperatures that may compromise structural integrity and stability.

Within the structural fire safety engineering practice, the performance of intumescent coatings is commonly assessed adopting simplified engineering methods solely based on the standard temperature-time fire curve in fire resistance furnace tests. However, numerous researchers have emphasised the limitations of this methodology due to the influence of several factors, such as the fire heating conditions, on the intumescent process and the overall insulation effectiveness. Consequently, the current design framework does not represent an adequate design practice to ensure the fire safety of structures. In a world moving towards performance-based engineering solutions, there is a need for explicitly understanding how different factors (e.g. heating conditions) may influence the effectiveness of intumescent coatings.

This research study aimed at building the fundamentals for developing robust engineering methods for the performance-based design of structural elements protected with intumescent coatings, considering their effectiveness for a wide range of potential conditions. Various studies were carried out in order to understand how different factors affect the performance of intumescent coatings. An experimental methodology was proposed to analyse their performance through a detailed characterisation of the thermo-physical response during thermal exposure. Steel plates coated with a commercial solvent-based thin intumescent coating were exposed to various well-defined and highly-repeatable heating conditions in accordance with the Heat-Transfer Rate Inducing System (H-TRIS) test method. The influence of the applied initial Dry Film Thickness (DFT) and the substrate thermal conditions were also investigated. Moreover, complementary studies using standard experimental methodologies were conducted in order to characterise the intumescent coating by defining its physical, thermal and optical properties and studying the chemical reactions and the thermal decomposition processes at different temperatures and under different heating regimes.

Experimental results showed that the tested intumescent coating required incident heat fluxes higher than 20-23 kW/m^2 in order to initiate the swelling process. Thresholds for the onset of swelling in terms of steel (100-250℃) and coating (350-500℃) temperatures were defined and it was found that the onset of swelling is directly influenced by the heating conditions and the initial coating thickness. The H-TRIS experiments also evidenced how the swelling process and the resulting swelled coating thickness govern the thermal and physical response of intumescent coatings, therefore their effectiveness. In particular, the heating conditions govern the swelling rate of the intumescent coating, while the initial coating thickness governs the maximum swelled coating thickness.

During swelling, the coated steel plates tended to 300-350℃, while their temperature increased above 350℃ when the swelling process was completed. As confirmed by the thermo-gravimetric analysis, this temperature range corresponds to the coating swelling reaction, which typically occurs around 350-400℃ and it can be considered completed above 400℃. These outcomes suggest that the swelling reaction occurs in the proximity to the substrate-coating interface: the virgin coating swells and protects the substrate by displacing the already-swelled coating towards the direction of the heat source. This was confirmed by the experiments involving different substrate thermal conditions. The physical and thermal properties of the substrate control the capacity of the system to concentrate/dissipate heat at the substrate-coating interface, consequently the temperature evolution of the reacting coating and the swelling process. Accordingly, high swelling rates were recorded for insulating substrate conditions (timber), while low swelling rates for conditions characterised by significant heat losses (water-cooled heat sink).

Based on the experimental results, a finite-difference heat transfer model was formulated in order to simulate the thermal and physical response of swelling intumescent coatings. The coating swelling was implemented by adding finite elements at the substrate-coating interface and the intumescent coating was modelled as swelled porous char with constant material properties. Following this approach, the modelling of intumescent coatings mainly became a quasi steady-state physical problem, largely driven by a correct prediction of the coating swelling rate and the evolution of the swelled coating thickness: empirical correlations were derived based on the experimental outcomes. Consequently, the coating material

properties have limited influence and the model loses accuracy for transient states. Nevertheless, for the tested experimental conditions, the model is capable of generally describing the heat transfer through swelling intumescent coatings by predicting the evolution of the coating surface and steel temperatures.

The experimental and modelling research presented herein shows how the thermal and physical response of intumescent coatings can be predicted by gauging their swelling process and implementing a simplified finite-difference heat transfer model. The swelling process and the resulting swelled coating thickness govern the effectiveness of thin intumescent coatings. Different factors (e.g. heating conditions) affect the swelling process in different ways (e.g. swelling rate), therefore the insulating effectiveness.

Declaration

This thesis is composed of my original work, and contains no material previously published or written by another person except where due reference has been made in the text. I have clearly stated the contribution by others to jointly-authored works that I have included in my thesis.

I have clearly stated the contribution of others to my thesis as a whole, including statistical assistance, survey design, data analysis, significant technical procedures, professional editorial advice, financial support and any other original research work used or reported in my thesis. The content of my thesis is the result of work I have carried out since the commencement of my higher degree by research candidature and does not include a substantial part of work that has been submitted to qualify for the award of any other degree or diploma in any university or other tertiary institution. I have clearly stated which parts of my thesis, if any, have been submitted to qualify for another award.

I acknowledge that an electronic copy of my thesis must be lodged with the University Library and, subject to the policy and procedures of The University of Queensland, the thesis be made available for research and study in accordance with the Copyright Act 1968 unless a period of embargo has been approved by the Dean of the Graduate School.

I acknowledge that copyright of all material contained in my thesis resides with the copyright holder(s) of that material. Where appropriate I have obtained copyright permission from the copyright holder to reproduce material in this thesis and have sought permission from co-authors for any jointly authored works included in the thesis.

Publications included in this thesis

Lucherini A., Torero J.L. and Maluk C. *Effects of substrate thermal conditions on the swelling of thin intumescent coatings*. Interflam 2019: Fire Resistance, Fire and Materials, pp. 1-14, 2020 (https://doi.org/10.1002/fam.2840).
– incorporated as Chapters 7.

Contributor	Statement of contribution
Author Andrea Lucherini (candidate)	Conception and design (90%) Analysis and interpretation (90%) Drafting and production (90%)
Author José L. Torero	Conception and design (5%) Analysis and interpretation (5%) Drafting and production (5%)
Author Cristian Maluk	Conception and design (5%) Analysis and interpretation (5%) Drafting and production (5%)

Lucherini A. and Maluk C. *Intumescent coatings used for the fire-safe design of steel structures: A review*. Journal of Constructional Steel Research, vol. 162, no. 105712, 2019 (https://doi.org/10.1016/j.jcsr.2019.105712).
– incorporated as Chapters 2.

Contributor	Statement of contribution
Author Andrea Lucherini (candidate)	Conception and design (90%) Analysis and interpretation (90%) Drafting and production (90%)
Author Cristian Maluk	Conception and design (10%) Analysis and interpretation (10%) Drafting and production (10%)

Lucherini A. and Maluk C. *Assessing the onset of swelling for thin intumescent coatings under a range of heating conditions*. Fire Safety Journal, vol. 106, pp. 1-12, 2019 (https://doi.org/10.1016/j.firesaf.2019.03.014).

– incorporated as Chapters 5 and part of Chapter 4.

Contributor	Statement of contribution
Author Andrea Lucherini (candidate)	Conception and design (90%) Analysis and interpretation (90%) Drafting and production (90%)
Author Cristian Maluk	Conception and design (10%) Analysis and interpretation (10%) Drafting and production (10%)

Submitted manuscripts included in this thesis

Lucherini A., Hidalgo J.P., Torero J.L. and Maluk C. *Influence of heating conditions and initial thickness on the effectiveness of thin intumescent coatings*. "13th International Symposium on Fire Safety Science (IAFSS)" Special Issue, Fire Safety Journal, Under Review.
– incorporated as Chapters 6.

Contributor	Statement of contribution
Author Andrea Lucherini (candidate)	Conception and design (85%) Analysis and interpretation (85%) Drafting and production (85%)
Author Juan P. Hidalgo	Conception and design (5%) Analysis and interpretation (5%) Drafting and production (5%)
Author José L. Torero	Conception and design (5%) Analysis and interpretation (5%) Drafting and production (5%)
Author Cristian Maluk	Conception and design (5%) Analysis and interpretation (5%) Drafting and production (5%)

Other publications during candidature

Journal publications

Lucherini A., Razzaque Q.S. and Maluk C. *Exploring the fire behaviour of thin intumescent coatings used on timber*. Fire Safety Journal, vol. 109, no. 102887, 2019.

Yerman L., Wall H., Carrascal J., Browning A., Chandraratne D., Nguyen C., Wong A., Goode T., Kyriacou D., Campbell M., Cao J., Do T., Casimiro-Soriguer D., **Lucherini A.**, Zárate S., Wyn H.K., Bolaños A., Solarte A., Górska C., Le B.-D., Tran S., Le Q. and Torero J.L. *Experimental study on the fuel requirements for the thermal degradation of bodies by means of open pyre cremation*. Fire Safety Journal, vol. 98, pp. 63-73, 2018.

Lucherini A., Giuliani L. and Jomaas G. *Experimental study of the performance of intumescent coatings exposed to standard and non-standard fire conditions*. Fire Safety Journal, vol. 95, pp. 42-50, 2018.

Emberley R., Gorska Putynska C., Bolanos A., **Lucherini A.**, Solarte A., Soriguer D., Gutierrez Gonzalez M., Humphreys K., Hidalgo J.P., Maluk C., Law A. and Torero J.L. *Description of Small and Large-Scale CLT Fire Tests*. Fire Safety Journal, vol. 91, pp. 327-335, 2017.

Conference publications

Lucherini A., Torero J.L. and Maluk C. *Effects of thermal conditions of steel on the fire performance of thin intumescent coatings*. Proceedings of the 15th International Conference and Exhibition on Fire Science and Engineering (Interflam), Royal Holloway College, London, UK, 2019.

Razzaque Q.S., **Lucherini A.** and Maluk C. *Intumescent coatings on timber – Exploring what it is actually doing*. Proceedings of the 5th Pacific Timber Engineering Conference (PTEC 2019), The University of Queensland, 2019.

Lucherini A. *Experimental fire studies on intumescent coatings used for steel structures*. Proceedings of 2nd Australian Young Researchers' Conference (YRC) of the Institution of Structural Engineers (IStructE), Queensland University of Technology, Brisbane, Australia,

2018.

Lucherini A., Abusamha N., Segall-Brown J. and Maluk C. *Experimental study on the onset of swelling for thin intumescent coatings*. Journal of Physics: Conference Series, Volume 1107, 3rd European Symposium on Fire Safety Science (ESFSS), n. 032017, 2018.

Lucherini A. *Effectiveness of thin intumescent coatings used for fire-safe steel structures*. Proceedings of the Inaugural Australian Young Researchers' Conference (YRC) of the Institution of Structural Engineers (IStructE), The University of Queensland, Brisbane, Australia, 2017.

Lucherini A. and Maluk C. *Novel test methods for studying the fire performance of thin intumescent coatings*. Proceedings of the 2nd International Fire Safety Symposium (IFireSS), University of Naples, Italy, pp. 565-572, 2017.

Conference posters

Lucherini A., Torero J.L. and Maluk C. *Effects of thermal conditions of steel on the fire performance of thin intumescent coatings*. 15th International Conference and Exhibition on Fire Science and Engineering (Interflam), Royal Holloway College, London, UK, 2019.

Lucherini A., Hidalgo J.P. and Maluk C. *Experimental study on the heat transfer within the swelling phase of thin intumescent coatings*. 11th Asia-Oceania Symposium on Fire Science and Technology (AOSFST), Taipei, Taiwan, 2018.

Lucherini A. and Gutierrez Gonzalez M. *Engineering the revolution of tall timber construction*. 2nd Biennial State Conference Doing Timber Business in Queensland: Room to Grow, Brisbane, Australia, 2018.

Lucherini A., Abosamha N. and Maluk C. *Investigating the activation of thin intumescent coatings*. 12th International Symposium on Fire Safety Science (IAFSS), Lund, Sweden, 2017.

Lucherini A., Abosamha N. and Maluk C. *Investigating the activation of thin intumescent coatings*. EAIT Postgraduate Conference (EPC), The University of Queensland, Australia, 2017.

Contributions by others to the thesis

No contributions by others.

Statement of parts of the thesis submitted to qualify for the award of another degree

No works submitted towards another degree have been included in this thesis.

Research involving human or animal subjects

No animal or human subjects were involved in this research.

Acknowledgements

This thesis represents the result of almost the last four years of my life with all its joy and suffering, with all its success and defeats. Nevertheless, what is important is that this journey has made me grow, experience the unknown, visit unparalleled places, accentuate my strengths and weaknesses, and futher define my values and life goals. In general, growing up and getting to know myself even better and deeper.

This journey did not happen without unexpected events and heartache, alongside satisfaction and moments in which you are truly breathing life and flying above the clouds. However, despite everything, this experience has been wonderful and unforgettable, simply because it happened and I had the freedom to make my choices and take responsibility, chase my dreams and aspire to become the person I desire, being truly myself.

I do not know how to start because I would like to thank innumerable people for their unique mental, physical and spiritual support, without whose help I would never have fully enjoyed this experience and achieved this enormous goal.

First of all, I would like to thank Anna Paola, who I would like to dedicate this composition to, because each part of my PhD journey, as any moment of my life in the last few years, has been encompassed by her. Despite the extreme distance and difficulties, this journey has been overflowing with unforgettable emotions, from immense joy to the deepest sadness. During this intricate journey, she dug into my rigid personality, opened up my shell with her smile, firmly held my hand and demonstrated that happiness is achievable, even though it is not a painless process. The uncountable experiences with her helped me understanding who I truly am and what really matters in life. I am and I will always be infinitely grateful to her for all this and what I am not able to describe in simple words. Wherever in the world, Australia, Fiji, France, Italy, UK or the Caribbean, she has always been there for me, as well as her fantastic family: Maria Eleonora, Ersilia, Corrado, Lucio and Bond.

I would like to warmly thank my extraordinary family for the continuous support during almost ten long and tough years of university. I am extremely grateful to babbo Fabio and mamma Bruna, who always supported my choices and have continuously encouraged me in the realisation of my aspirations, even though my dreams tore us apart with many kilometres of

distance. I loved how they have carefully been looking after me, deeply enjoying a meal, a weekend or any moment in my presence, always enthusiastic and making me feel special. I would like to thank my brother Francesco for having taken down the barriers between us, opening our hearts as two real brothers who help each other in any circumstance and discuss any possible aspect of life. I would like to thank my not-so-little sister Laura for always taking care of me, being keen to join me in doing anything and always listening to her big-brother's words as something to learn from and appreciate.
I would like to thank all my extended family, especially grandparents and close relatives who supported me even from afar, making themselves feel close with their warmth: nonna Emilia for always looking forward to my return in Italy to hug me and serve me the best meals of my life; nonno Benito and nonno Ettore, I carry you in my heart and I will be always grateful to you for being present in any moment and embodying the best model inspiration for my life.

I would like to thank my academic supervisor and advisors for offering me this unique opportunity and supporting me during the whole research project. I am particularly grateful to Dr Cristian Maluk, the person who believed in me and guided me throughout the demanding journey of pursuing a Doctor of Philosophy. I am very grateful for his constant inspiration, guidance, encouragement and valuable advice. I have learnt immensely from him and he constantly demonstrated his trust and esteem by helping and motivating me, even in the most challenging situations and darkest moments.
I would like to thank Dr Juan Hidalgo, associate advisor and also a great friend. We arrived in Australia at the same time and we started discovering this new world together. I am grateful to him because he continuously supported me throughout my research project by coming up with brilliant ideas and helping me to solve intricate problems.
I would like to thank the one-of-a-kind Prof. José Torero, a person of a boundless knowledge and experience who constantly guided me in my research journey and growth. Meeting him, even though only a few times per year, enlightened my research: I enjoyed and appreciated every single moment conversing with him and I can not put into words the amount of things learnt from him.
I would like to gratefully acknowledge Qazi Samia Razzaque, Edward Kwok, Long Le and Andrew Abrahams for providing expert technical support and begin enthusiast in starting a collaboration project on intumescent coatings between the University of Queensland and

Remedial Building Services Australia Pty Ltd.
I would like to thank my research family, the Fire Group "Fuego" at the University of Queensland for their company, technical and psychological assistance, laughter, fire engineering discussions and all the moments spent together in the lab or in conferences around the world. In particular, I am grateful to my forever-markets friend Martyn, the illustrious Cotorras (Mateo "Mala", Jaime "Americana", Luis "Anciana", Sergio "Pato" and Julian "Pollo"), the Ticos Aaron and Angela, the pâtissière Tam and the team "Los Toreros". I would like to also acknowledge the priceless help of Jero, Stewart, David and Andres. I am also thankful to some visiting research students that made a big difference during their short stay in Australia (Martín, Pascal, Martina, Laura and Silvia), the students who collaborated on the research project on intumescent coatings (Nemer, Adam, Bastien and Diana), the beloved people from the Advanced Engineering Building, my tutoring colleagues and academics, in particular Dr David Lange and Dr Ron Blackwell.
I would like to thank the fire group family at the University of Edinburgh, who welcomed me warmly and helped me make the most out of my short research visiting experience. I am particularly grateful to Prof. Grunde Jomaas for always being a great mentor and supporting my personal life and career, and Prof. Luke Bisby for offering me this great opportunity and fostering very interesting and challenging research discussions. I would like to acknowledge Valentina and Martina, Vasilis and George for being - apart from colleagues - great friends and sharing memorable adventures in Edinburgh.
I would like to thank the London Fire Safety Engineering team of Over Arup & Partners, in particular Dr Panos Kotsovinos and Dr Egle Rackauskaite, for offering me a unique educational and stimulating experience and showing me how the real world works from the perspective of an outstanding engineering firm.

Furthermore, I would also like to thank all my close friends, the family that I chose during this long journey. Met in Italy, Denmark, Australia or somewhere around the world, I shared these university years with them intensely, full of wonderful experiences and saturated with unforgettable memories.
I would like to thank Kurtis, Marj, Nelly, Jana, Claudia and Finn for being the ideal housemates and best friends that anyone would love to share dinners, drinks, parties and adventures. I will never forget you and you will always have a place in my heart, and a friend (and

a place to visit and stay) in Italy! With all our friends that have been part of "Unfairfield" or "Audenshaw Shennanigans", I would like to mention our other housemates that made our days even more fun: Amber, Blaze, Maggie, Chai, Lola, Cleo, Fernando and Guilherme.
I am very grateful to all the extended Brisbane and West End community, which made me feel surprisingly at home on a remote island on the opposite side of the globe. In particular, I would like to thank Andreaccio, Dima, Zev, Larissa, Maria, Mikael, Izzy, Megan and the Cam Family, especially Debbie and Sian.
I am grateful to Kaz, my Australian godmother, who welcomed and introduced me to this astonishing country, completely different to what I was used to. In these years, I loved this country with its incredible animals and breathtaking natural sceneries: I would have never imagined that such country and experience would have totally changed my life perspective.

Finally, I would like to acknowledge my Italian friends, the ones I met a long time ago and I shared many years of my life. I rarely see them, but I maintain special relationships with them: they are the ones who make me miss home and they transform each of my visits into a big party or a cosy dinner.
I would like to thank Michele for being the best friend anyone would love to have, the Famiglia Buttieri (Quero, Luca, Pino, Salvo, Cumenda, Renatone, Franceschiello, Enrico e Pasqua) for making our university friendships endless starting or continuing in Bologna, all the A.D.A. members for keeping together an association based on true values, my memorable friends from university (Pippo, Mancio, Cocchina and Carmela) and Arezzo (Bido, Gianlu, Valda, Zizzi and Sile), the Sociocche Laura and Stefania, Giorgio, Bisa, Gaetone and FranciNucci, my team-mates from the Atletico Piazzetta, and my high-school professors Nicola Salvadori and Maria Grotti.
Lastly, friends that I met along my intricate journey around the world, I am still close to them and I am looking forward to hugging them again: Lucie and Francesca, Carlos, Riccardo, Pablo and David, Julian, Manuel Elena and Andrea, Eleonora Elena and Lorenzo.

Financial support

I would like to gratefully acknowledge the following financial supports received during the completion of the degree of Doctor of Philosophy (PhD):

Candidate Development Award (CDA), awarded by Graduate School of The University of Queensland, Australia, for 2-weeks secondment at Arup, London, UK and for the participation in the 15th International Conference and Exhibition on Fire Science and Engineering (Interflam), Royal Holloway College, London, UK, June-July 2019.

UQ Civil RHD Travel Assistant Grant, awarded by the School of Civil Engineering of The University of Queensland, Australia, for the participation in the 10th International Conference on Structures in Fire (SiF), Belfast, UK, February 2018.

International Postgraduate Research Scholarship, awarded by The University of Queensland, for living allowance stipend and full cost of tuition fees during the Doctoral of Philosophy (PhD) at The University of Queensland, Australia, July 2016.

Philanthropic Grants for Early Career Engineering Researchers (Dr Cristian Maluk), awarded by the Faculty of Engineering, Architecture and Information Technology (EAIT) at The University of Queensland, Australia, 2016.

Keywords

Intumescent coatings, fire safety, heat transfer, structures, H-TRIS, fire-safe design, fire testing, heating conditions, swelling.

Australian and New Zealand Standard Research Classifications (ANZSRC)

ANZSRC code: 090503, Construction Materials, 50%
ANZSRC code: 091299, Materials Engineering not elsewhere classified, 30%
ANZSRC code: 090506, Structural Engineering, 20%

Fields of Research (FoR) Classification

FoR code: 0905, Civil Engineering, 50%
FoR code: 1204, Engineering Design, 30%
FoR code: 0912, Material Engineering, 20%

to Anna Paola

for always being there
and always will be

Contents

List of Figures

List of Tables

Nomenclature, acronyms and terminology

Symbols

Symbol	Unit	Definition
L	[m]	Characteristic length
d	[m]	Thickness
$\dot{d}$	[m/min]	Swelling rate
A	[m^2]	Surface area
V	[m^3]	Volume
A/V	[m^{-1}]	Section factor
t	[sec]	Time
T	[K]	Temperature
c_p	[J/kgK]	Specific heat capacity
R	[m^2K/W]	Thermal resistance
Δt	[sec]	Time increment
Δx	[m]	Space discretisation
ΔT	[K]	Temperature difference
ΔH_r	[J/kg]	Heat of reaction
E''_{th}	[J/m^2]	Accumulative thermal energy flux
F_{12}	[-]	View factor
g	[m/s^2]	Gravitational acceleration (9.81)
h	[W/m^2K]	Heat transfer coefficient
$\dot{q}''$	[W/m^2]	Heat flux
$\dot{g}'''$	[W/m^3]	Volumetric generated/absorbed heat flux
$\dot{m}''$	[kg/sm^2]	Mass reaction rate

Symbol	Unit	Definition
Bi	[-]	Biot number
$\overline{Nu}_L$	[-]	Nusselt number
Pr	[-]	Prandlt number
Ra_L	[-]	Rayleigh number

Greek Letters

Symbol	Unit	Definition
α	[- / m^2/s]	Absorptivity / Thermal diffusivity
β	[K^{-1}]	Volumetric thermal expansion coefficient
∂	[-]	Differential
Δ	[-]	Incremental
ε	[-]	Emissivity
λ	[μm / W/mK]	Wavelength / Thermal conductivity
ρ	[- / kg/m^3]	Reflectivity / Density
σ	[W/m^{2}K^4]	Stefan-Boltzmann constant ($5.67 \cdot 10^{-8}$)
ν	[m^2/s]	Kinematic viscosity
τ	[-]	Transmissivity

Superscripts

Superscript	Definition
$i = 1, 2, 3...$	Time step

Subscripts

Subscript	Definition
s	Steel
c	Coating / Intumescent coating
p	Protection material

Subscript	Definition
g	Fire gas phase
$swell$	Swelling
$surf$	Surface
th	Thermal
0	Initial
fin	Final
in	In/into the system
out	Out/outside the system
$back$	Back side, substrate
$panel$	Radiant panel
$cond$	Conduction / Conductive
$conv$	Convection / Convective
rad	Radiation / Radiative
net	Net
inc	Incident
$loss$	Losses
eff	Effective
app	Apparent
$j = 1, 2, 3...N$	Node number
$k = 1, 2, 3...$	Material type
tot	Total
$const$	Constant
$mean$	Mean value
max	Maximum value
min	Minimum value
exp	Experiment/Experimental
mod	Model/Modelled
∞	Ambient
air	Air
$film$	Film

Acronyms

Acronym	Definition
ASTM	American Society for Testing and Materials
APP	Ammonium Polyphosphate
BS	British Standard
CEN	Comité Europeén de Normalization
CLT	Cross-Laminated Timber
CTBUH	Council on Tall Buildings and Urban Habitat
DFT	Dry Film Thickness
DSC	Differential Scanning Calorimetry
DTG	Differential Thermo-Gravimetric analysis
EN	European standard
FEM	Finite Element Method
FTIR	Fourier-Transform Infrared Spectroscopy
H-TRIS	Heat-Transfer Rate Inducing System
IAFSS	International Association for Fire Safety Science
IC	Intumescent Coating
IR	Infra-Red
ISO	International Organization for Standardization
ISS	Integrating Sphere System
LFA	Laser Flash Analysis
MCT	Method of Critical Temperatures
MEL	Melamine
MLC	Mass-Loss Calorimeter
PER	Pentaerythritol
RMSE	Root-Mean-Square Error
STA	Simultaneous Thermal Analysis
TPS	Transient Plane Source
TGA	Thermo-Gravimetric Analysis
WFT	Wet Film Thickness

1

Introduction

1.1 Background

The continuously growing urbanisation and world population are pushing for the development of vertical cities and the construction of high-rise buildings. In these cases fire safety may be a concern because, along with assuring an appropriate fire safety strategy for the safe evacuation of the building occupants, the structural integrity and stability must be ensured in the event of a fire [1]. For this purpose, steel represents an optimal construction material due to its ductility, weight-strength ratio, durability and potential for modular constructibility [2]. However, as all other construction materials, the stability and integrity of steel structures may be compromised during and after a fire due to loss of strength and stiffness, as well as thermally induced forces and displacements [3].

The application of thermal barriers characterised by low thermal conductivity is the traditional solution to reduce the temperature increase of the load-bearing structure during a fire [4]. Conventional solutions, such as gypsum plasterboards or cementitious spray-on systems, are usually deemed to be relatively inexpensive and easy to apply, but aesthetically unpleasant and an undesirable choice for the modern slender structures with visible steelwork. The unique advantages of *intumescent coatings* (also known as reactive coatings), such as the low impact on the attractive architectural appearance of bare steel structures and their flexibility for both on- and off-site applications, have fostered their success and extensive use all over the world [5-7].

Consequently, intumescent coatings nowadays represent a dominant fire safety solution for protecting load-bearing structural steel systems during fire. Furthermore, their unique advantages pushed the construction industry into looking at the possibility of applying intumescent coatings to protect different substrate materials. For example, the application of intumescent coatings can mitigate the destructive effects of fire-induced concrete spalling, prevent surface ignition and reduce the charring rate within wooden elements [8-9].

Intumescent coatings are thermally reactive materials, usually composed of a combination of organic and inorganic components bound together in a polymer matrix [10-11]. At ambient temperature, intumescent coatings appear as a pigmented thin coating, applied to a Dry Film Thickness (DFT) in the order of few millimetres (thin intumescent coatings, usually solvent-based or waterborne) or few centimetres (thick intumescent coatings, usually epoxy-

based) [5]. When exposed to sufficient heat, they swell to form a thick low-density and low-thermal-conductivity porous char that prevents the substrate material from reaching high temperatures [12]. Thin intumescent coatings can swell up to 100 times their initial thickness following typical reaction stages in the so-called intumescent process [13].

1.2 Research gaps and motivation

Within the structural fire safety engineering practice, the performance of intumescent coatings is commonly assessed based on the standard fire resistance test in furnaces. In these tests, the temperature experienced by coated samples exposed to the standard temperature-time fire curve are recorded up to failure (however it is defined) [14-17]. Based on these temperatures, simplified implicit engineering methods (tabulated fire ratings or effective thermal conductivity method) are typically adopted for the structural fire safety design [13]. However, intumescent coatings are chemically reactive materials and numerous researchers have emphasised the influence of the several factors, such as heating conditions, on the intumescent process and the overall insulation effectiveness [10-13, 18-21]. In particular, slow-growing fires or low heating regimes may have a negative impact on the insulating performance of intumescent coatings by causing an incomplete swelling, or even melting and delamination [12, 19].

As a consequence, the current procedures do not represent a comprehensive design practice for fire-safe structures. They do not fully assess the effectiveness of intumescent coatings through a thorough understanding of the physical and thermal behaviour of swelling intumescent coatings. Prior studies have highlighted how the current design procedures may be excessively conservative or severely on the unsafe side and there is no clear understanding on whether the results obtained during a standard fire resistance furnace test can or cannot be extended to other conditions [22]. Most importantly, these simplified engineering methods simulate the temperature evolution of coated samples in furnaces exposed to a single heating scenario, not addressing the whole range of potential heating regimes occurring in a fire. In a world moving towards performance-based engineering solutions, there is an extreme need for fundamentally understanding how different factors may influence the effectiveness of intumescent coatings, for instance heating conditions and applied initial

coating thickness. By obtaining this scientific and practical knowledge, it will be possible to formulate and validate models able to produce realistic and reliable predictions. This will enable performance-based engineering solutions for a robust design of fire-safe structures that explicitly considers the effectiveness of intumescent coatings under a range of potential conditions [13].

The available literature presents limited research studies that have looked at assessing the effectiveness of intumescent coatings through their thermal and physical behaviour [13]. This progress is commonly inhibited by inadequate testing methodologies and experimental setups. In particular, the current expensive and time consuming large-scale procedures based on standard fire resistance tests in furnaces have been questioned due to the poor repeatability and the uncertain thermal boundary conditions imposed on test samples [23-24]. Furthermore, the closed environment of standard furnaces does not allow for accurate visual inspection of test samples during the heating exposure, a key aspect to comprehend the thermo-physical response of intumescent coatings [19]. Finally, the concept of standard fire as unique testing fire condition clearly defines the expected performance of intumescent coatings and therefore it inhibits advances in developing new effective products for a wide range of conditions [12].

1.3 Research objectives

Intending to contribute towards engineering solutions for the robust performance-based design of fire-safe structures protected with intumescent coatings, the research project aimed at investigating fundamental aspects related to the behaviour of intumescent coatings for a wide range of potential conditions. Within the scope of this research project, various studies using standard and novel experimental methodologies were carried out in order to understand how the effectiveness of thin intumescent coatings may be affected by different factors. Figure 1.1 presents a schematic overview of the research project. In particular, the research project aims at:

- Developing an experimental methodology to systematically study the effectiveness of thin intumescent coatings for a wide range of potential physical and thermal conditions.
- Experimentally gauging the effectiveness of thin intumescent coatings through a detailed characterisation of their thermal and physical response during the heating exposure.
- Characterising thin intumescent coatings by defining their thermo-physical properties, the chemical reactions and thermal decomposition processes at different temperatures and under different heating conditions.
- Understanding the conditions and temperature ranges that promote the onset of swelling for thin intumescent coatings.
- Studying the influence of different factors on the effectiveness of thin intumescent coatings: heating conditions, applied initial coating thickness and substrate thermal conditions.
- Formulating a finite-difference model able to simulate the thermal and physical response of thin intumescent coatings for a wide range of potential physical and thermal conditions.
- Producing fundamental outcomes for proposing a rigorous performance-based design framework which explicitly considers the effectiveness of intumescent coatings for a wide range of potential conditions.

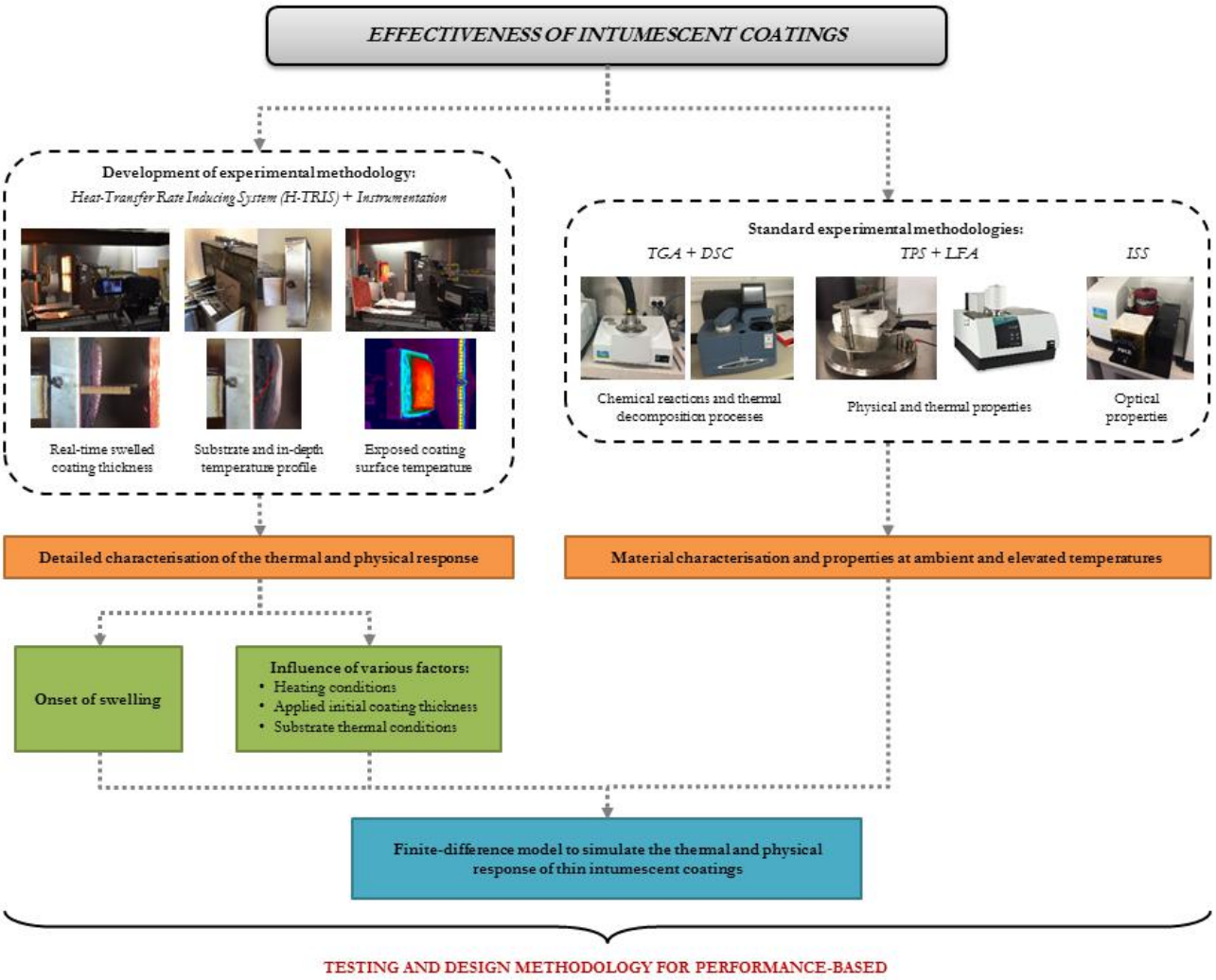

Figure 1.1: Schematic illustration of the research project.

1.4 Thesis outline

This thesis is composed of nine chapters and four appendices. Each chapter was conceived as a standalone chapter and thus some notes are repeated in a number of chapters, wherever they are relevant. In this section each chapter, aside from the current introductory chapter, is briefly described.

Chapter 2 - *Literature review*

A literature review highlights how the mainstream use of intumescent coatings for the design of fire-safe structures has fostered the recent extensive research into the development of effective intumescent coatings and the assessment of their performance as thermal barrier to structural elements and materials. Numerous researchers have proposed comprehensive approached and methodologies to overcome the challenges related to the current design framework based on standard fire resistance furnace testing. The literature review describes the most recent developments in the field of testing and assessment of the effectiveness of intumescent coatings. Apart from the chemical formulation, the substrate boundary conditions, the applied initial coating thickness, the heating conditions and the testing methodology appear to be the key governing factors and all of them should be considered for performance-based design methods in structural fire safety engineering.

Chapter 3 - *Material and methods*

An experimental methodology aimed at analysing the effectiveness of intumescent coatings is presented. The methodology is based on the Heat-Transfer Rate Inducing System (H-TRIS) test method and it uses arrays of high-performance radiant panels coupled with a computer-controlled linear motion system to impose well-defined and highly-repeatable thermal boundary conditions at the exposed surface of test samples. The experimental methodology is proposed to study various fundamental aspects related to intumescent coatings for a wide range of conditions in terms of heating exposures, applied initial coating thickness and substrate characteristics. The experimental setup is purposely instrumented in order to systematically gauge all the possible information to describe the thermal and physical response of intumescent coatings during the heating exposure.

Chapter 4 - *Material characterisation*

A set of complementary studies using standard experimental methodologies is presented in order to characterise different aspects of a solvent-based thin intumescent coating, chosen as product exemplar. The Thermo-Gravimetric Analysis (TGA) and Differental Scanning Calorimetry (DSC) experiments uniquely identify the product by investigating the chemical reactions and thermal decomposition processes occurring in the intumescent coating at different temperatures and under different heating regimes. Experiments involving the Transient Plane Source (TPS), the Laser Flash Analysis (LFA) and the Integrating Sphere System (ISS) enable the quantification of the physical, thermal and optical properties of the intumescent coating at ambient and elevated temperatures. These experiments are proposed in order to integrate the experiments conducted using the H-TRIS test method and achieve a preliminary understanding on how heat transfer and thermal processes develop in the tested intumescent coating.

Chapter 5 - *Onset of swelling*

This chapter investigates the onset of swelling for thin intumescent coatings, a key feature for providing effective thermal insulation to the protected substrate. Steel plates coated with the thin intumescent coating are exposed to a wide range of heating conditions using the H-TRIS test method. The onset of swelling is examined by analysing the evolution of the swelled coating thickness and substrate temperatures. The experimental study focuses on defining the conditions that promote or prevent the onset of swelling for thin intumescent coatings, for example by specifying a critical constant incident heat flux and defining thresholds in terms of steel and coating temperatures. The influence of the heating conditions and the applied initial coating thickness on the problem is also investigated. Finally, a first simplified finite-difference heat transfer model is formulated in order to simulate the temperature increase of uncoated and coated steel samples prior to onset of swelling.

Chapter 6 - *Influence of heating conditions and initial coating thickness*

Adopting the experimental methodology using the H-TRIS test method, this chapter analyses the effectiveness of the thin intumescent coatings through a detailed characterisation of their thermal and physical response. Steel plates coated with the thin intumescent coating are

exposed to a wide range of heating conditions. In addition, the influence of the applied initial coating thickness is studied. These aspects are investigated by comparing the evolution of the steel temperature, the swelled coating thickness, the coating surface temperature and the in-depth temperature profiles within the swelling intumescent coating during the thermal exposure. The experimental study aims at understanding how different factors may influence the swelling reaction and the effectiveness of thin intumescent coatings.

Chapter 7 - *Influence of substrate thermal conditions*

Adopting the experimental methodology using the H-TRIS test method, this chapter focuses on the influence of the substrate thermal conditions on the behaviour of thin intumescent coatings. Steel plates coated with the thin intumescent coating are exposed to a constant incident heat flux of 50 kW/m^2 and different substrate thermal conditions are simulated using different samples holders: insulating conditions and three conditions involving a water-cooled heat sink with different cooling rates. The same experiments are also performed on timber samples coated with the same thin intumescent coating. The effects of the substrate thermal conditions are investigated by comparing the evolution of the substrate temperature, the coating surface temperature and the swelled coating thickness. The experimental study aims at understanding the effects of the substrate thermal conditions on the effectiveness of thin intumescent coatings, in particular examining in depth their swelling mechanism.

Chapter 8 - *Heat transfer modelling*

Based on the experimental outcomes, a finite-difference heat transfer model is formulated in order to simulate the thermal and physical response of swelling intumescent coatings applied on steel plates for the tested ranges of heating conditions and applied initial coating thickness. In general, the numerical model aims at offering a engineering tool for the performance-based design of fire-safe structures protected with thin intumescent coatings. The chapter describes the process for the formulation of the heat transfer model with all its simplifications and assumptions. In particular, the swelling of thin intumescent coating is implemented by adding finite elements and the intumescent coating is modelled as swelled porous char with constant material properties. Accordingly, the effectiveness of thin intumescent coatings is primarily dependent on their ability to develop swelled porous char and

the proposed model mainly relies on a correct prediction of the coating swelling rate and the evolution of the swelled coating thickness. The model accuracy is assessed by comparing the evolution of the steel substrate temperature, the coating surface temperature, the swelled coating thickness and the in-depth temperature profiles within the sweling intumescent coating during the thermal exposure. An extended sensitivity analysis and external validation are also performed in order to assess the model accuracy with respect some key governing parameters and understand its limitations.

Chapter 9 - *Conclusions and recommendations for future research*
The main conclusions drawn on the basis of the research studies presented and discussed within this thesis are highlighted and commented. Recommendations for future research on the behaviour of thin intumescent coatings for the design of fire-safe structures are also presented.

Bibliography

[1] Drysdale D. "An introduction to fire dynamics". John Wiley & Sons, Ltd, 3rd Edition, 2011.

[2] Wang Y.C. "Steel and composite structures: behaviour and design for fire safety". Taylor & Francis Group, 2002.

[3] Usmani A.S., Rotter J.M., Lamont S., Sanad A.M. and Gillie M. "Fundamental principles of structural behaviour under thermal effects". Fire Safety Journal, vol. 36, pp. 721–744, 2001.

[4] Buchanan A.H. and Abu A.K. "Structural design for fire safety". John Wiley & Sons, 2nd Edition, 2017.

[5] Mariappan T. "Recent developments of intumescent fire protection coatings for structural steel: A review". Journal of Fire Sciences, vol. 34, no. 2, pp. 1-44, 2016.

[6] Weil E.D. "Fire-protective and flame-retardant coatings – A state-of-the-arte review". Journal of Fire Science, vol. 29, pp. 259-296, 2011.

[7] Puri E.G., Khanna A.S. "Intumescent coatings: a review on recent progress". Journal of Coatings Technology and Research, vol. 14, pp.1-20, 2017.

[8] Lu F. and Fontana M. "Intumescent coating against explosive spalling of HPC in fire". Proceedings of 5th International Workshop on Concrete Spalling due to Fire Exposure, Borås, Sweden, pp. 365-374, 2017.

[9] Lucherini A., Razzaque Q.S. and Maluk C. "Exploring the fire behaviour of thin intumescent coatings used on timber". Fire Safety Journal, vol. 109, pp. 102887, 2019.

[10] Li G.Q., Lou G.B., Zhang C., Wang L. and Wang Y. "Assess the fire resistance of intumescent coatings by equivalent constant thermal resistance". Fire Technology, vol. 48, pp. 529-546, 2012.

[11] Wang L., Dong Y., Zhang D., Zhang D. and Zhang C. "Experimental study of heat transfer in intumescent coatings exposed to non-standard furnace curves". Fire Technology, vol. 51, no. 1, pp. 627-643, 2015.

[12] Elliott A., Temple A., Maluk C. and Bisby L. "Novel testing to study the performance of intumescent coatings under non-standard heating regimes". Fire Safety Science – Proceedings of the 11th International Symposium, University of Canterbury, New Zealand, pp. 652-665, 2014.

[13] Lucherini A. and Maluk C. "Intumescent coatings used for the fire-safe design of steel structures: A review". Journal of Constructional Steel Research, vol. 162, no. 105712, 2019.

[14] International Organization for Standardization (ISO). "ISO834-1:1999 Fire resistance tests - Elements of building construction - Part 1: General requirements for fire resistance testing".

Geneva, Switzerland, 1999.

[15] Comité Europeén de Normalization (CEN). "EN 1363-1:2012 Fire resistance tests - Part 1: General Requirements". Brussels, Belgium, 2012.

[16] Comité Europeén de Normalization (CEN). "EN 1363-2:2012 Fire resistance tests - Part 2: Alternative and additional procedures". Brussels, Belgium, 1999.

[17] Comité Europeén de Normalization (CEN). "EN 13381-8:2013 Test methods for determining the contribution to the fire resistance of structural members - Part 8: Applied reactive protection to steel members". Brussels, Belgium, 2013.

[18] Zhang Y., Wang Y., Bailey C.G. and Taylor A.P. "Global modelling of fire protection performances of an intumescent coating under different furnace conditions". Journal of Fire Science, vol. 31, no.1, pp. 51-72, 2012.

[19] Lucherini A., Giuliani L. and Jomaas G. "Experimental study of the performance of intumescent coatings exposed to standard and non-standard fire conditions". Fire Safety Journal, vol. 95, pp. 42-50, 2018.

[20] de Silva D., Bilotta A and Nigro E. "Experimental investigation on steel elements protected with intumescent coating". Construction and Building Materials, vol. 205, pp. 232-244, 2019.

[21] Cirpici B.K., Wang Y.C. and Rogers B. "Assessment of the thermal conductivity of intumescent coatings in fire". Fire Safety Journal, vol. 81, pp. 74-84, 2016.

[22] Kolsek J. and Cesarek P. "Performance-based fire modelling of intumescent painted steel structures and comparison to EC3". Journal of Constructional Steel Research, vol. 104, pp. 91-103, 2015.

[23] Maluk C., Bisby L., Terrasi G., Krajcovic M., Torero J.L. "Novel fire testing methodology: why, how and what now?". Proceedings of the Mini Symposium on Performance-based Fire Safety Engineering of Structures as part of the 1st International Conference on Performance Based land Life Cycle Structural Engineering, pp. 448-458, 2012.

[24] Maluk C., Bisby L., Krajcovic M. and Torero J.L. "A Heat-Transfer Inducing System (H-TRIS) Test Method". Fire Safety Journal, vol. 105, pp. 307-319, 2019.

2

Literature review

2.1 Fire safety of structures

Every year, building fires are the worldwide cause of numerous deaths, along with tremendous economic and social impact [1]. Despite the perceived low occurrence of fires in buildings, a fire event can have disastrous consequences; hence, an appropriate *fire safety strategy* must be considered in situations where fire may be a problem (e.g. high-rise structures). At the backbone of the fire safety in buildings, structural integrity during and after a fire has to be ensured [2]. Therefore, *structural integrity and stability* represent a core aspect of the fire safety strategy and it must be considered among all the other aspects of the design process of a fire-safe structure [3].

For example, *steel structures* are a mainstream building structural system and the Council on Tall Buildings and Urban Habitat (CTBUH) recently reported that the worldwide 54% of composite multi-level projects over 200 metres comprises a steel frame with metal decking [4]. The benefits of high strength-weight ratio and ductility enable engineers with the possibility for designing fascinating slim and light structures. Moreover, the modular nature of steel structures allows for reduced construction costs, both temporal and economic [5].

However, as all other building construction materials, the structural integrity of steel structures can be compromised during and after fire. In particular, steel experiences significant strength and stiffness reduction at elevated temperatures. According to Eurocode design guidelines [6], at temperatures of 550-600℃ structural steel retains about 50% of its ambient temperature strength. Also, steel has a high thermal conductivity; hence, steel structures are perceived as solids elements that may heat up rapidly during fire.

Traditionally, the behaviour of steel structures in fire has been understood to be dominated by the effects of *strength loss* induced by heat. However, structural systems can possess enormous reserves of strength by adopting large-displacements configurations [7]. This was evidenced by the relatively appropriate residual capacity after the Cardington full-scale fire tests on a composite steel framed structure [8]. However, the same series of fire tests highlighted that thermal expansions and large deflections of steel members induce particular negative and potentially dangerous actions on heated structures [7]. In particular, *thermally induced forces and displacements* during fire can become critical to the point of governing the structural performance and they can induce deformations and thermal stresses that

could cause structural instability and/or progressive failure [2, 7, 9].

Structural fire safety engineering can be used to manage the risks associated with partial or complete structural collapse during or after a fire in a building. As regards to steel structures, the application of *thermal barriers* is a widely used method to avoid steel from reaching critical temperatures during fire. This is usually done by covering or wrapping the structural members with low density and low thermal conductivity materials that can reduce the rate of temperature increase of the load-bearing steel structure [2]. Traditionally, there had been a range of commercially available thermal barrier solutions that encapsulate steel structures using concrete encasement, calcium silicate or gypsum plaster boards, cementitious spray-on systems or flexible fire blankets.

These *conventional fire safety solutions* are relatively inexpensive and they can be easily adopted for a wide range of applications. Nevertheless, they are usually deemed to be aesthetically unpleasant and therefore they do not represent the most desirable choice for slender and light buildings with visible steelwork [10]. For this reason, the steel industry experienced a rapid growth in the use of intumescent coatings.

2.2 Intumescent coatings

Intumescent coatings (also known as reactive coatings) are nowadays a mainstream solution used to protect load-bearing structural steel systems during fire [11]. In 2016, the Dow Jones predicted that "the intumescent coatings market size is forecast to be worth $1.16 billion by 2022 [...] and to reach 145.6 kilo tons by 2022" [12]. The rapid growth in the use of intumescent coatings in the built environment is associated with the low impact in the attractive architectural appearance of bare steel structures, along with their light-weight and their flexibility for both on- and off-site applications [13-15].

Upon heating, intumescent coatings swell to form a low density and low thermal conductivity foamed char (Figure 2.1); hence, preventing temperature increase of steel that could cause structural instability and/or progressive failure [16, 17].

Intumescent coatings are thermally reactive materials, usually composed of a combination of organic and inorganic components bound together in a polymer matrix [19-21]. Intumescent coatings formulations are usually composed of an acid source (*"catalyst"*), a carbonaceous

Figure 2.1: Steel profile section protected with a thin intumescent coating, before (left) and after (right) fire testing [18].

compound (*"carbonific"*), a blowing agent (*"spumific"*), binders and additives: their functions have been widely described in the literature and during the last decades the formulations have been optimized so as to form an effective protective char. Innovative improvements are continuously proposed within the intumescent coating industry: the inclusion of pigments to provide better weather proofing ability and decorative surface finish [22]; the use of fibres of different natures as hybrid reinforcement to increase the coating mechanical strength [23]; the introduction of nano-silica to promote the formation of a more compact char layer [24]; the substitution of the carbon source with vegetable compounds, as ginger powder and coffee husk [25]; the addition of fillers, nanoparticles, silicones, resins and flame retardants. These are just a few examples of the enormous effort that the research community focused on intumescent coatings is taking for the development of better, more efficient and reliable coating formulations [11, 16, 26-29].

The composition of *thin intumescent coatings* is typically solvent-based or water-based and they are usually applied to a Dry Film Thickness (DFT), no thicker than a few millimetres. They are mainly applied in the built environment and used for cellulosic fire conditions. On the other hand, *thick intumescent coatings* are usually epoxy-based (two-component systems) and applied to thicknesses in the order of few centimetres. Unlike the thin ones, thick intumescent coatings have mainly industrial application and they are used for hydrocarbon fire conditions [11, 15].

Intumescent coatings are usually applied in three different components: primer, base coat and top-coat. The *primer* ensures good adhesion between the metal substrate and the

coating and provides increased corrosion resistance [30]. The *top-coat* can be required for decorative or durability reasons when exposed to weathering and aggressive environment [11]. The *application procedure* represents a key aspect for the effectiveness of intumescent coatings. Before application, the substrate has to be appropriately prepared and cleaned from any contaminants in order to create a rough surface and facilitate the application and adhesion of the coating [31]. Nowadays, steel members are usually coated by airless spray application, fast method that can be applied also to irregular shapes [32]. They can be also applied using conventional methods, such as brush and rollers. The application of the coating in an accurate thickness on steel sections is always a complicated procedure due to its dependency on several conditions (e.g. temperature, humidity). The quality of the final product must be always verified and the minimum required thickness ensured [18].

2.2.1 The intumescent process

The *intumescent process* by which intumescent coatings react, swell and char can be described by the different stages shown in Figure 2.2. According to several studies, the following stages of intumescence may be defined [20, 21, 29, 33-35]:

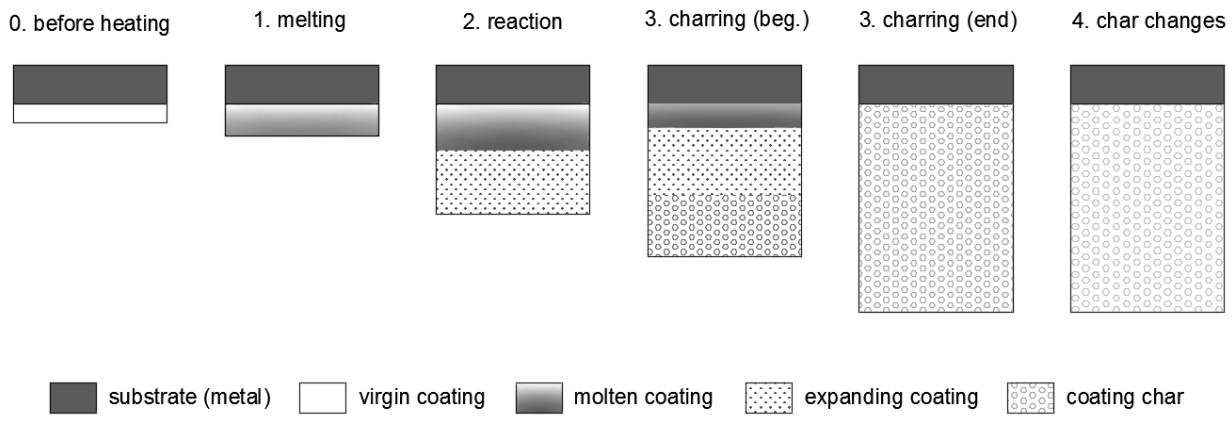

Figure 2.2: Schematic of the various stages of the intumescent process.

1. *Thermal decomposition (melting zone)* - when the coating is exposed to a heat source and reaches a critical temperature, the inorganic acid source undergoes a thermal decomposition: the surface melts and converts into a viscous fluid [36].

2. *Swelling (reaction zone)* - the blowing agent is then activated, causing an endothermic reaction that absorbs heat from the substrate and decomposes to release a large amount of gaseous products. The gas bubbles are trapped in the coating, causing the molten matrix to swell up to 100 times its original thickness and forming a low density and low thermal conductivity porous media that acts as thermal barrier for the metal substrate [37]. The swelling process continues until the blowing agent is exhausted or the carbon matrix is not viscous enough to continue to confine the gas bubbles.

3. *Char formation (charring zone)* - as the temperature increases, the porous media hardens and releases the residual volatiles to form char. At this stage, the char structure is highly carbonaceous and is usually characterised by a black/grey colour at the exposed surface.

4. *Char structural changes (char degradation zone)* - the carbonaceous char is oxidised and CO_2 is released: the black and compact char structure slowing changes into a white brittle dusty foam at the exposed surface.

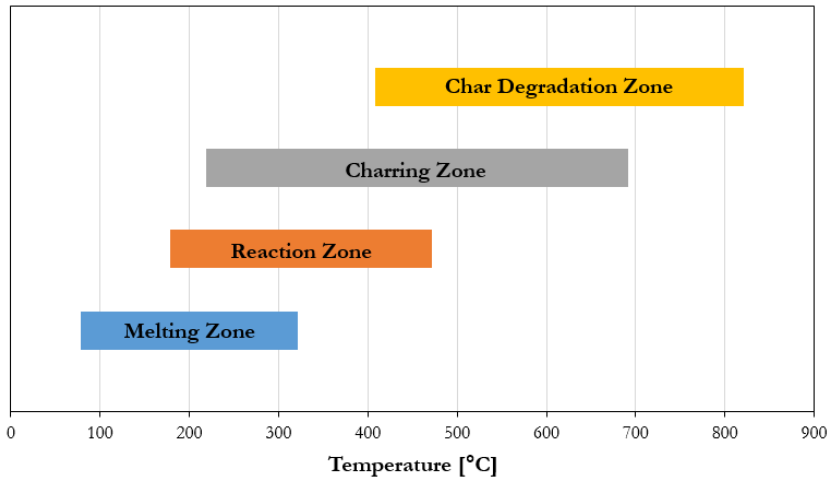

Figure 2.3: Threshold temperature for the different stages of the intumescent process.

The classification of stages and zones and their respective threshold temperature have been reported to occur within a range of temperatures (Figure 2.3), influenced by variation in coatings formulations and fire testing procedures adopted by different researchers [19, 33, 35, 36, 38-48]. The evolution of the four stages is strongly dependent on the composition of the chemicals and their mixture. However, the order and the matching of the chemical

and physical processes are essential, as they must happen in an appropriate sequence, as the temperature is raised [36]. In particular, the *onset of swelling* as the initiation of the swelling phase has a key role in the development of the intumescent char structure. It usually defines the end of the melting zone and the beginning of the reaction zone [49]. According to the above-mentioned prior studies, the onset of swelling can occur in a wide range of temperatures, typically when the coating is between 200 and 300 °C.

2.3 Literature review objectives

During the past decades, the fire research community has extensively investigated the performance of intumescent coatings used in steel structures. The majority of prior research studies can be defined by two categories: (1) studies focused on the chemistry of intumescent coatings and (2) studies focused on assessing the fire performance of intumescent coatings as thermal barrier to structural elements. The first category, led by *chemists*, widely developed and invented new ingredients and formulations to improve the physical and thermal behaviour of intumescent coatings exposed to heat. The second category, led by *fire safety engineers and scientists*, investigated the heat transfer and the overall effectiveness of intumescent coatings as fire safety solution for different structural elements and materials. The state-of-the-art of chemical mixtures and formulations of intumescent coatings have been reviewed by several researchers [11, 28, 29, 35]. However, in the literature no comprehensive review is available on the enormous amount of research studies focused on the fire performance of steel elements protected with intumescent coatings. This review covers the more recent developments in the field of fire testing and analysis of the fire performance of steel elements protected with intumescent coatings.

2.4 Current design framework

The current design framework for demonstrating integrity of structural systems during and after fire is based on compliance with the *standard fire resistance furnace test* (Figure 2.4). Single full-scale structural members, loaded or unloaded, are tested to failure (however this is defined) under a standard heating condition (Figure 2.5), defined by a temporal evolution

of temperature inside the furnace [50-52]. As many other structural components and materials, the performance of a load-bearing steel elements protected with intumescent coatings is typically assessed based on compliance with the standard fire resistance furnace test, where single coated elements are usually exposed to the *cellulosic fire curve* from one or all sides. In other applications, different standard curves may be the required: for example, the *hydrocarbon fire curve* for applications in the oil and gas industry (Figure 2.5) [53-55].

Figure 2.4: Example of unloaded standard fire resistance furnace test [18].

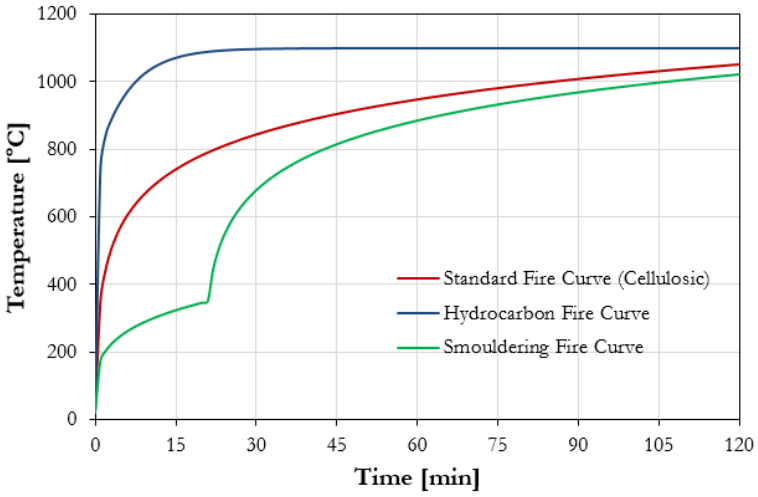

Figure 2.5: Prescribed temperature-time fire curves.

The failure criteria for steel structures is usually based on the *Method of Critical Temperatures* (MCT) [6]. The fire resistance level of the protected steel element is defined based on the time when a critical temperature is reached, usually defined as the temperature at which the single structural member no longer withstand its given loading. The failure criteria for structural steel is at the discretion of the designer charged with designing for the fire-safe structure. A fire-safe design is executed considering the structural capacity at ambient temperature and, in particular, the utilization factor of each structural member during fire. Nevertheless, the steel critical temperature is often prescribed around 550-600 ℃, based on the assumption that, due to safety factors, most of the structural elements are loaded at 50% of their ambient temperature capacity and a failure will occur when the materials had a 50% reduction in strength [6, 56].

2.4.1 Tabulated fire ratings

The outcomes from a series of standard fire resistance furnace tests can be used to build *tabulated fire ratings* (refer to Table 2.1), where manufacturers present the minimum required DFT of the intumescent product for achieving a time to reach a critical temperature in the standard fire resistance furnace test [2, 53]. In order to design a fire-safe structure, engineers choose the optimal solution from tabulated ratings based on the following input parameters:

- target fire resistance rating;
- critical design temperature, either prescribed or based on utilization factors;
- steel section factor, which is in essence the ratio between exposed surface and volume of the protected steel element (A_p/V);
- type of cross-section (open or closed sections); and
- element type (mainly beams or columns).

Table 2.1: Example of tabulated fire ratings for the design of steel structural element protected with intumescent coatings.

Fire Resistance Class R60 – Beams and Columns, Open Sections (H and I)									
Design Temperature [°C]	350	400	450	500	**550**	600	650	700	750
Section Factor A_p/V [m^{-1}]	Required Dry Film Thickness (DFT) of …… [mm]								
…	…	…	…	…	…	…	…	…	…
100	1.556	1.122	0.924	0.634	0.484	0.384	0.305	0.236	0.190
105	1.842	1.149	0.983	0.678	0.508	0.403	0.320	0.247	0.191
110	2.099	1.176	1.042	0.723	0.532	0.422	0.335	0.258	0.191
115	2.256	1.203	1.091	0.776	0.591	0.442	0.350	0.269	0.194
120	2.414	1.230	1.112	0.843	**0.650**	0.461	0.365	0.279	0.202
125	-	1.257	1.134	0.909	0.708	0.480	0.380	0.290	0.210
130	-	1.284	1.155	0.976	0.763	0.499	0.395	0.301	0.218
135	-	1.311	1.176	1.043	0.812	0.518	0.410	0.312	0.226
140	-	1.338	1.197	1.094	0.861	0.545	0.425	0.322	0.234
145	-	1.365	1.219	1.117	0.910	0.589	0.440	0.333	0.243
150	-	1.392	1.240	1.141	0.959	0.633	0.454	0.344	0.251
…	…	…	…	…	…	…	…	…	…

Table 2.1 offers an example of the process to design a steel structural element protected with intumescent coatings using tabulated fire ratings: in order to ensure a fire resistance rating of R60 to a steel I-beam with a section factor equal to 120 m^{-1}, the structural element

requires an applied DFT of intumescent coating equal to 0.65 mm, assuming a steel critical temperature of 550℃ (corresponding to a utilization factor of 0.6, according to Eurocode [6]).

2.4.2 Effective thermal conductivity method

Another tool for designing fire-safe steel structures using intumescent coatings is the European assessment method based on the concept of *effective thermal conductivity* (Annex E of EN 13381-8 [53]). This design method is based on a lumped capacitance 1D heat transfer approximation of the transient heat conduction equation, where a low-density insulation material, such as swelled intumescent coatings, is approximated as a thermal mass included between the fire gas temperature T_g and the protected steel temperature T_s The complex thermal-physical behaviour of intumescent coatings is simplified in an effective parameter, neglecting the change in thickness and assuming the thermal capacitance of the coating negligible compared to the protected steel (Figure 2.6). According to this method, the effective thermal conductivity of an intumescent coating λ_p at time t can be determined with the following formulation:

$$\lambda_p = d_p c_{p,s} \rho_s \frac{V}{A_p} \frac{T_s^{t+\Delta t} - T_s^t}{\left[T_g^{t+\Delta t} - T_s^t\right] \Delta t} \tag{2.1}$$

where d_p is the applied initial dry film thickness of intumescent coating [m], $c_{p,s}$ is the specific heat capacity of steel [J/kgK], ρ_s is the density of steel [kg/m^3], A_p/V is the section factor of the protected steel member [m^{-1}], $T_s^{t+\Delta t}$ is the steel temperature at time $t + \Delta t$ [K], T_s^t is the steel temperature at time t [K], $T_g^{t+\Delta t}$ is the fire gas temperature at time $t + \Delta t$ [K] and Δt is the time increment [sec]. The resulting temperature-dependent effective thermal conductivity defines an equivalent thermal barrier provided by the intumescent coating to the steel substrate during a standard fire resistance furnace test.

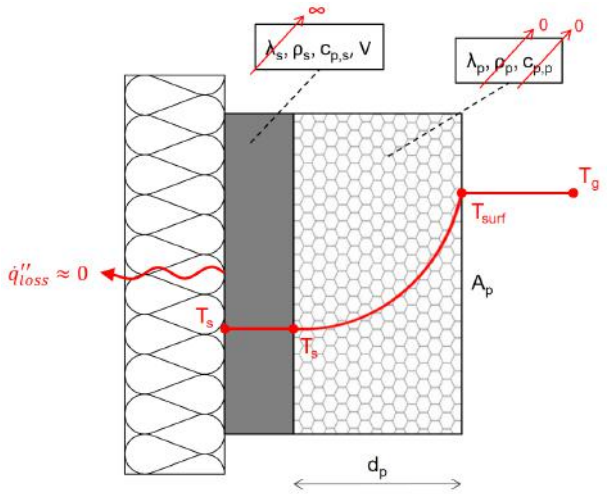

Figure 2.6: Schematic of the simplified heat transfer problem for the effective thermal conductivity method.

2.5 Key challenges for the design of structures protected with intumescent coatings

The concept of *fire resistance* was first introduced at the beginning of the 20th century and the testing framework has only slightly changed over the years [57]. This concept is based on the time-to-failure of single elements tested in the standard fire resistance furnace test. During the last decades, the relevance of using the standard temperature-time fire curve and standard fire resistance furnace tests have been questioned due to high operating costs, poor repeatability, inappropriate thermal boundary conditions and poor statistical confidence [58, 59]. Also in the case of intumescent coatings, standard fire resistance tests always require extensive time and economical effort because of the large number of full-scale tests required to cover the vast range of steel configurations and coating thicknesses necessary for approval and material classification [60, 61].

In addition, unlike other non-reactive fire protection systems, numerous research studies have emphasised the influence of heating conditions on the performance of intumescent coatings (Figure 2.7). Intumescent coatings are chemically reactive materials and their thermo-physical behaviour have shown to be influenced by the testing fire exposure [17, 20, 21, 33, 58, 62-67]. Particularly, some researchers have shown that slow-growing fires or low heating regimes may cause an incomplete swelling of the reactive coating, or even facilitate melting and/or delamination. These phenomena can have a negative impact on the

overall effectiveness of the intumescent coating and lead to unsatisfactory insulation to the steel structure [17, 58, 67].

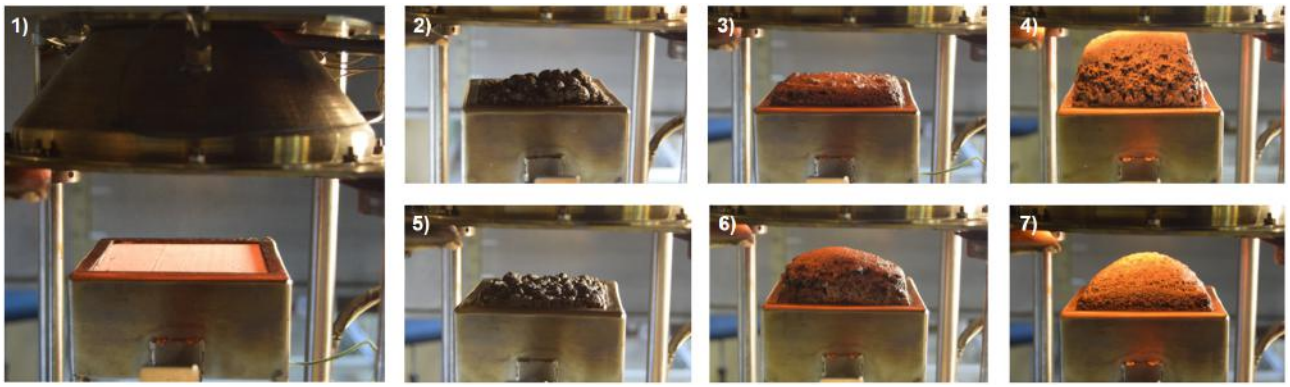

Figure 2.7: The influence of the heating conditions on the fire performance of thin intumescent coatings: char structures obtained from different cone calorimeter tests: 1) prior to heating; 2-4) PaintA and 5-7) PaintB under 20, 40 and 60 kW/m^2 [18].

However, the current design framework wrongly assumes that the thermo-physical properties of intumescent coatings are independent of the fire conditions. Normally, the standard furnace fire resistance test is the only considered fire scenario and its results are extended to all the other conditions. Nevertheless, owing the reactive nature of intumescent coatings, the results obtained from standard fire resistance tests may not be consistent and reliable under different sets of heating conditions [21, 33, 68]. The current design procedures do not represent a rigorous design practice for fire-safe steel structure: they are overly simplified, sometimes excessively conservative, sometimes severely on the unsafe side [64, 69]. The assessment of the performance of intumescent coatings under several potential fire conditions should be the common practice for determining whether the insulating properties obtained from the standard tests could be used in other fire scenarios. Each product and formulation would behave differently, even in an opposite manner [67].

The concept of standard fire as only testing fire scenario also inhibits advances in understanding how reactive coatings behave in non-standard fire conditions [17]. The worldwide success of intumescent coatings as a fire safety solution boosted manufacturers to develop innovative intumescent coatings products and compositions [22-25]. However, there is a severe shortcoming in these research studies related to the expected performance and the testing procedures. Novel products are usually tested according to the standard fire expos-

ure and, consequently, the industry aims at developing new intumescent coating products to pass these kinds of tests, in which the fire exposure is fixed and it is not a governing variable [19].

The engineering community have also strongly criticised the assumptions and limitations of the currently available engineering tools for the design of intumescent coatings. For instance, numerous uncertainties are related to the tabulated fire ratings. The embedded implicit safety factors do not ensure a clear level of safety and the linear interpolations between different tests have been questioned due to the clear non-linear relationship between the intumescent performance and several factors, such as section factor and applied DFT. The importance of applying the right amount of coating has been recently underlined, emphasising the possible dangerous effects: the steel section may not have sufficient fire protection in case of a lower DFT, while a too thick DFT may promote coating delamination and falling off [70]. Moreover, the European effective thermal conductivity method treats intumescent coatings as chemically non-reactive materials because it implicitly assumes that their thermo-physical properties are temperature-dependent only and the rate of heating (e.g. due to different fire conditions, different coating thickness, different section factors) has little effect [63]. The method simplifies the response of intumescent coatings by considering the applied initial thickness and inaccurate physical and thermal properties, e.g. thermal capacity and density. Therefore, the effective thermal conductivity does not clearly represent the effectiveness of intumescent coatings because it incorporates several phenomena that occur in the intumescent process, such as endo- and exothermic reactions [62]. Its strong simplifications are reflected by the high variance of the values reported in literature: in few studies, values lower than thermal conductivity of air were reported [71]. Lastly, the assumption of adiabatic conditions on the steel member (1D heat transfer or perfect 4-sided exposure) and the evaluation of the coating temperature as average value between the gas phase temperature of the fire and the steel substrate temperature have been arguments of debate.

Furthermore, the tabulated ratings based on the fire resistance concept only clearly show the final time of reaching the steel critical temperature. This completely ignores the time evolution of the temperature in the structural member during the fire exposure, from ambient up to the critical limit. As a consequence, the only possible methods which can be adopted for the

structural fire design are simplified procedures, such as the method of critical temperatures [6]. In this method, the structural fire design is performed on individual structural members rather than considering the entire structural system. Besides, the method does not consider the mechanical boundary conditions of the structural elements, such as members free or restrained to thermal expansion. Therefore, the design of structural fire protection does not investigate the overall stability and the interaction between structural members during the fire event. These simplifications on the unsafe side omit dangerous destructive effects like thermally-induced forces and displacements in a fire event [7, 64].

In addition, the current design framework does not consider the influence of certain secondary factors that affect the performance of intumescent coatings. An example is the effect of the atmospheric oxygen content during fire testing. According to the standard procedure, the atmosphere surrounding the test sample in a standard furnace shall have an oxygen concentration above 4% when testing non-combustible materials [54]. Griffin et al. have demonstrated how the oxygen content of the exposing atmosphere can significantly affect the mode and rate of char formation and degradation, thus affect the thermal shielding property of the intumescent coating [39]. Considering different test environments would be optimal to investigate how standard fire ratings may be applied to situations with different oxygen content. The location of the gas burners inside the furnace and the consequent convective flows are another important aspect, since they govern the coating char detachment.

Finally, since most of the chemical components in the intumescent formulations are organic, they react with the exposed environment and their effectiveness deteriorates with time. Particularly, intumescent coatings suffer from solar radiation, moisture cycles and thermal fatigue, along with any atmospheric contaminants. As the fire protection performance must be ensured throughout the entire life of the building structure, there is a necessity to investigate the long-term durability of intumescent coatings exposed to different environmental conditions. Many studies have reported the vulnerability of intumescent coatings to ageing and weathering [72]. For example, the swelling ratio of a degraded coating can be reduced by over 70% and the steel temperature can increase by about 200℃, compared to the fresh coating [73]. In the case of seawater exposure, the fire-resistant properties can be drastically lost only after one month of immersion [74]. Also, ageing in indoor environments can severely reduce the insulting and reactive properties of intumescent coatings and there is

a necessity to renovate intumescent coatings in existing old buildings [75, 76]. However, the current design framework does not take into account the degradation of intumescent coatings in time: the design assessment and testing are performed only on virgin coatings and there are no existing regulations on how to verify the intumescent reactivity of degraded coatings [68].

2.6 Relevant research studies

During the last decades, many researchers have been involved in the study of the performance of intumescent coatings in terms of thermal shielding to the substrate material. In order to overcome the challenges of the current design framework, numerous research studies have proposed comprehensive approaches and methodologies to investigate the effectiveness of intumescent coatings exposed to different heating conditions and tested using different experimental set-ups.

2.6.1 Standard fire resistance furnaces

Testing single protected steel and composite elements using furnaces of different sizes is still the prevalent methodology to assess the effectiveness of intumescent coatings. Past researchers have exposed a large variety of test samples to the standard temperature-time curve in furnaces, from bench scale to large scale. Concrete-steel composite joints, steel plates, welded and bolted steel connections, steel columns, concrete-filled steel hollow structural sections and steel cellular beams are examples of structural systems tested in furnaces in order to understand the performance of virgin or degraded intumescent coatings exposed to fire [68, 69, 73, 77-83]. In the majority of the research studies, the standard fire curve is the main heating condition imposed on unloaded protected samples and the evolution of protected steel temperatures is the only control parameter of performance.
However, some other researchers started implementing different non-standard temperature-time fire curves in furnace testing. The European *smouldering fire or slow heating curve* represents a first regulated attempt to assess the fire performance of intumescent coatings under slow-growing fires (Figure 2.5) [53]: it is characterised by a low heating regime for the first 20 minutes and then it continues following the standard fire curve [17, 63, 75, 76, 80,

81]. Other researchers tested coated steel plates under different temperature-time curves, such as the European *parametric fire curves* (more or less severe than the standard fire) or large-power fires in large spaces according to the Chinese code [21, 33, 84, 85].

2.6.2 Cone calorimeter

Due to the high costs and time-consuming nature of standard furnace testing, several researchers started developing bench-scale and laboratory-scale experiments to investigate the intumescent coating behaviour under different fire conditions. A conventional technique is to expose coated steel samples to constant radiant heat fluxes using a cone calorimeter [62, 86]. In a more controlled testing environment, the thermal shielding capacity of intumescent coatings has been carefully studied with respect to several factors, such as the imposed external heat flux, the coating thickness, the sample size and the role of the back thermal boundary conditions [60, 87, 88]. Few researchers also combined the cone calorimeter with novel techniques: for example, Wang et al. used thermographic phosphors in order to measure the intumescent coating surface temperature and consequently calculate the transient thermal conductivity [89, 90].

However, more recently few researchers started underling the limitations of cone calorimetry testing. Firstly, results from cone calorimeter investigations can be hardly compared due to differences in the test configurations. For instance, Fateh et al. showed how the distance between the sample and the bottom of the cone heater can affect the results, especially the back surface temperature of substrate materials [91]. Moreover, recent evidence suggests that the incident heat fluxes are distributed non-uniformly over the exposed top surface of test samples due to the unique geometry configuration between the truncated cone-shaped emitter and the squared recipient [92, 93]. Finally, this methodology suffers uncertainties in terms of net heat flux absorbed by the test sample during the swelling process: the external heat flux changes as the exposed coating surface moves closer to the cone heater and the swelling causes exposure of the perimeter phases [94].

2.6.3 Other experimental methods

Other researchers proposed innovative test methods and/or experimental set-ups in order to investigate different aspects of the performance of intumescent coatings under various heating conditions:

- The mechanical resistance of intumescent chars was studied by Jimenez et al. using a Bunsen burner and several novel methodologies to measure the compressive strength were compared by Reshetnikov et al. [95, 96].
- Fry studied different intumescent coatings applied on circular thin steel plates using an improved cone heater setup: using a laser beam, he was able to instantly evaluate the coating swelling and raise/lower the sample holder in order to maintain a constant incident heat flux at the sample surface [97].
- Calabrese et al. suggested the use of temperature sensors placed directly inside the swelling intumescent char exposed to a constant radiant heat flux: in this way, the thermal conductivity of the intumescent layer was calculated using the in-depth measurements following an inverse heat conduction problem approach [71, 98, 99].
- McNamee et al. experimentally investigated the coating effectiveness using two innovative experimental setups, which exposed the intumescent coatings to a horizontal flow as in a ceiling jet and to a vertical flow as in a fire plume [58].
- Morys et al. presented a complementary testing approach based a modified muffle furnace known as STT Mufu+ (Standard Temperature Time Muffle Furnace): small vertical plates can be efficiently tested under the standard temperature-time curve and the apparatus can be combined with other equipment, such as mechanical testing or high-temperature endoscope [100-102].
- Elliott et al. proposed to apply the H-TRIS (Heat-Transfer Rate Inducing System) method for studying the performance of reactive coatings subjected to different time-histories of incident radiant heat flux [17, 103]. The fire test method directly controls the thermal boundary conditions imposed on a test sample by moving an array of high-performance radiant panels: the approach offers considerable advantages over traditional testing in terms of reliability, repeatability, versatility, speed and costs and

it enables the visual inspection of test samples during fire testing (e.g. swelling rate). This approach was also adopted by Lucherini et al. that investigated the onset of swelling of thin intumescent coatings under a wide range of potential heating conditions [49, 104].

As a conclusion, the limitations of the current experimental framework inspired the research community to develop such a large variety of innovative experimental setups. Each test method tackles specific research gap and it optimises the investigation of particular aspects related to intumescent coatings. However, they are not widely adopted and the steel industry and the research community looking at the use of intumescence have not agreed on a universal testing methodology yet.

2.6.4 Numerical and computational modelling

The swelling of intumescent coatings under heat is a complicated multicomponent phenomenon, involving a complex combination of different material phases, mixtures and reactions. Many variables are extremely difficult to measure and the intumescent process is hard to describe. However, many researchers attempted to develop several numerical and mathematical models of various complexities in order to simulate the intumescent process and the heat transfer through swelling intumescent systems.

Starting from the innovative model developed by Cagliostro et al. based on mass and heat transfer and fundamental chemical reaction kinetics within a non-reacted coating, many one-dimensional mathematical models have been implemented during the last decades [105]. Starting from different assumptions, each of them is able to simulate different aspects of the complex behaviour of intumescent coatings. For instance, using small-scale or large-scale experimental data, they can evaluate the thermal conductivity or the thermal resistance of intumescent chars or they can describe the heat transfer within intumescent coatings based on chemical kinetics, mass and energy conservation [19, 39, 61, 106, 107]. Researchers simplified the problem in different ways, like identifying independent global chemical reactions (e.g. melting, swelling and charring) or subdividing the coating into independent components (e.g. solid char, pores and gas phase) [19, 108, 109]. Other simple models are able to evaluate the fire resistance of various structural systems by predicting the temperature evolution

with good approximation based on the concept of equivalent constant thermal resistance or effective constant thermal conductivity [20, 65]. Also, few researchers implemented models able to accurately describe the heat transfer and swelling process of intumescent coatings using standard and non-standard furnace tests data [33, 87, 110]. These models require few input parameters derived from experimental data. However, these parameters are usually based on standard furnace testing only and they are difficult to directly quantify, such as the coating melting temperature or the intumescent char porosity. More recently, researchers focused on developing semi-empirical procedures for performance-based design calculations [64]. For example, Cirpici et al. created a revolutionary multi-layer model able to predict the intumescent coating behaviour and effective thermal conductivity under different conditions (steel section factor and applied initial DFT), also considering the different fire conditions [63]. Finally, few researchers focused on approximating the temperature profile within swelling intumescent coatings and the model implemented by Hsu represents the first example of comparison between predicted and measured in-depth temperature profiles within swelling coatings [111, 112].

Finally, some researchers also attempted to model the behaviour of steel structures protected with intumescent coatings using different finite-element software. TNO-Diana, SAFIR16 and ABAQUS are the most common FEM software adopted in different studies aimed at simulating the failure modes and/or temperature evolutions of various protected samples exposed to fire [75, 83, 114, 115]. However, due to the complexity of the intumescent reaction, this software relies on several assumptions. For instance, common simplifications are modelling a constant geometry mesh and a temperature-dependent effective thermal conductivity function that considers the phase change from the original solid coating into the swelled coating. In most of the cases, the coating insulating properties are estimated only considering the standard fire exposure. As a conclusion, these models still have many uncertainties related to input parameters and material properties and they must be used with great care and critical eye.

As in the case of testing methods, a countless amount of numerical and computational models of various complexities can be found in literature. However, a universal simple, rather than complex model that can simulate the performance of intumescent coating has not yet been developed or, at least, it has not been generalised for the vast variety of available

commercial products and potential fire conditions.

2.7 Analysis and discussion

2.7.1 Key governing factors

Huge efforts taken by past researchers have yielded a deep understanding of intumescent coatings used in the construction industry. From the extensive review shown herein, it is possible to point out the main factors that govern the performance and effectiveness of intumescent coatings used for the design of fire-safe load-bearing steel structures. Nevertheless, it is usually difficult to establish a clear general trend among past research studies and some outcomes of past research studies even contradict each other. As already mentioned in the motivation, the influence of different chemical formulations of intumescent coatings is not in the scope of this review. According to the extensive review shown herein, the key governing factors are:

- *Substrate boundary conditions*. They are a key parameter that governs how rapid the temperature of a steel section may increase during a fire or cool after burnout. The common way to quantify them is through the section factor A_p/V, calculated as the ratio between the section perimeter exposed to fire and the area or mass of the heated steel [2]. A larger section factor usually results in a rapid increase in the steel temperature [79]. As regards intumescent coatings, researchers have found out that a high section factor leads to a faster swelling and greater swelling ratios [33, 97]. On the other hand, the influence of the section factor on the coating thermal conductivity is not clear: sometimes, coatings had higher thermal conductivity for higher section factors; sometimes, lower [65, 66].
- *Applied coating thickness*. The applied thickness of the intumescent coating on a steel element is normally the control parameter for ensuring the required level of fire protection. It is usually quantified as wet film thickness (WFT) during the application process, but engineers usually design for a certain Dry Film Thickness (DFT). Many assume that a higher DFT always guarantees a higher level of thermal protection, given by a lower limiting steel temperature. However, increasing the DFT does not

always yield to an insulation property benefit [21]. Also, outcomes of past research have shown that the increase in performance is marginal for a higher DFT [17, 71, 98, 99]. Contrarily, outcomes of other experimental investigations showed that a higher DFT might produce higher thermal conductivity [63, 65, 66]. This can be confirmed by research studies where lower DFTs have shown a more rapid swelling and higher swelling ratios due to the complete development of the intumescent char [33, 60, 97]. Without any doubt, higher DFTs have a higher potential of adhesion failure or facilitate the pull-back phenomenon at web openings in cellular beams [75, 82].

- *Heating conditions*. Numerous experimental investigations have highlighted many influencing aspects related to the heating conditions, however these are controlled or measured. Outcomes of research studies have evidenced how varied heating conditions can lead to different char structures, swelling ratios and overall swelling processes [21, 33, 88, 110]. For instance, Cirpici et al. registered lower swelling ratios and higher effective thermal conductivities for higher heating rates, while Fry evaluated higher thermal conductivities for higher heat fluxes [63, 97]. In general, when exposed to fast-growing fires, intumescent coatings undergo a more complete reaction to produce desired swelled char structures [33]. In particular, the complete development of the intumescent coating tested by Han et al. was achieved for incident radiant heat fluxes above 35 kW/m^2, while Lucherini et al. showed that the minimum incident heat flux to reach onset of swelling was above 23 kW/m^2 [49, 60]. In addition, for temperatures above 600-700°C, the carbonaceous char loses its strength and compactness due to thermal oxygenation [102]. On the contrary, when exposed to slow-growing fires, intumescent coatings are not able to fully react to form the desired swelled char and they have inadequate performances [21, 33]. In a few cases, during experimental testing, low heating regimes even caused melting and delamination of the coating or char cracking with incomplete swelling [17, 67].
- *Fire test method*. Numerous researchers have underlined how the fire testing method can influence the experimental outcomes of a research study on intumescent coatings [62, 67, 100]. Discrepancies can mainly come from different testing apparatus used (e.g. standard furnaces, cone calorimeter) and the corresponding testing conditions. For instance, the influence of the oxygen concentration on the intumescent chemical

kinetics justifies the different results from tests conducted in a well-ventilated air atmosphere (e.g. cone calorimeter) and the ones conducted in the low oxygen environment of standard furnaces [61, 91, 110]. In a similar manner, testing environments with different turbulence and convective flows can affect the coating adhesion, falling off and pull-back phenomena [58, 82].

Moreover, other characteristics of the protected steel member can also affect the insulating performance of intumescent coatings. The shape of the steel profile cross-section is an example: prior studies showed how the degradation and the crack formation on the intumescent char after long-term heating can be influenced by the steel profile shape, convex or concave [116]. Also, as already mentioned, cellular beams suffer pull-back phenomena at web openings [82, 83]. Finally, past experimental studies have shown that orientation of the coated steel sample can influence the intumescent process due to the variation of the main direction of migration of the gases released by the blowing agent (difference between a beam and a column orientation).

All the mentioned governing factors are based on the assumption that the type and thickness of the intumescent coating and its components (primer, coating and topcoat) are correctly specified, applied and well-maintained. The application process represents a delicate stage and it requires accurate keeping and diligent checks. Practitioners reported increasing cases of unsuccessful application, such as incompatible products or insufficient applied DFTs [58]. For instance, experience showed applications of intumescent coatings in confined spaces where physical obstacles prevented the swelling: for this reason, current engineering guidelines suggest to allow a swelling zone equal to 50 times the dry film thickness for thin intumescent coatings and 10-15 times the dry film thickness for thick intumescent coatings.

Finally, is worth highlighting the relevance of ensuring the durability of intumescent coatings during the entire design life of the structure. This is relevant to other fire protection solutions used in the built environment, likewise susceptible to long-term damages and deterioration, such as fire-rated boards and other spray-on systems. The current design framework does not take into account the long-term durability and performance of intumescent coatings. Periodical and diligent vigilance should somehow become a common practice in a similar manner as a revision of corrosion protection is periodically carried out, enforced by the

owners or possibly by the regulatory authorities having jurisdiction.

2.7.2 Design methods proposed in recent research studies

Apart from the regulated design framework, the research community is proposing new design methodologies for the assessment of the performance of intumescent coatings exposed to different fire conditions. Most of them focus on quantifying the insulating capacity by evaluating different forms of the coating thermal conductivity. In the literature, three main definitions of thermal conductivity can be identified:

- *Effective thermal conductivity*. The European method presented in Section 2.4.2 evaluates the coating thermal conductivity considering the initial dry film thickness of the coating [53]. The methodology incorporates several phenomena and strongly simplifies the intumescent coating response, but it is able to accurately reproduce the temperature evolution of the protected steel substrate. Cirpici et al. demonstrated how the values extracted from standard fire tests may be used to predict the steel temperatures for heating conditions less severe than the standard fire because the prediction results are on the safe side; however, the same results should not be used for more severe conditions because they will be unsafe [63]. Based on the envelope of experimental data, Elliott et al. proposed a methodology based on a steel-temperature-dependent "design" effective thermal conductivity curve [18]. This concept can be applied to any commercially available product and it can be used in the engineering practice. Figure 2.8 shows an example of the envelope obtained using the effective thermal conductivity curves found in the available literature.
- *Effective constant thermal conductivity*. Li et al. presented how protected steel temperatures can be calculated using the concept of effective constant thermal conductivity, defined as the temperature-averaged value of the temperature-dependent effective thermal conductivity within the temperature range of interest for fire resistance design of steel structures, usually 400-600℃ [65]. The value obtained from the standard test can be obtained for each type of intumescent coating and it may be used for various fire conditions as long as the steel temperature is higher than 400℃ [66]. In addition, the effects of different factors, such as steel section factor and DFT, can be incorpor-

ated through regression analysis. As in the previous case, using the effective constant thermal conductivity simplifies the design process, but it does not represent any fundamental physical property of the coating [66]. The recent publication from Li et al. was used to build Figure 2.9, where the most frequent values of constant effective thermal conductivity are calculated from a large number of fire tests on different steel sections protected with different intumescent coatings [66].

- *Apparent thermal conductivity*. Contrarily to effective values, the apparent thermal conductivity is evaluated considering the actual swelled coating thickness and relying on measurements of the in-depth temperatures within the swelled coating. Starting from experimental measurements, inverse heat transfer models are usually implemented in order to calculate the apparent thermal conductivity of intumescent coatings [71]. This methodology has been adopted in only a few research studies because of the experimental difficulties related to gauging accurate measurements of the in-depth temperature distributions without disturbing the swelling process. However, the apparent thermal conductivity enables the explicit calculation of the transient temperature gradients within swelled intumescent coatings using simple heat transfer finite-element models.

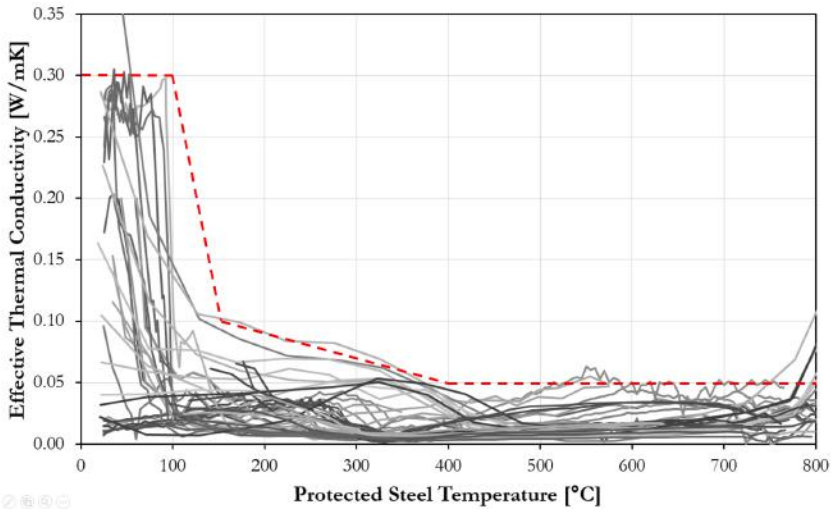

Figure 2.8: Effective thermal conductivity curves found in literature [17, 33, 65-67, 69, 75-77] and possible design methodology based on the envelope of experimental data.

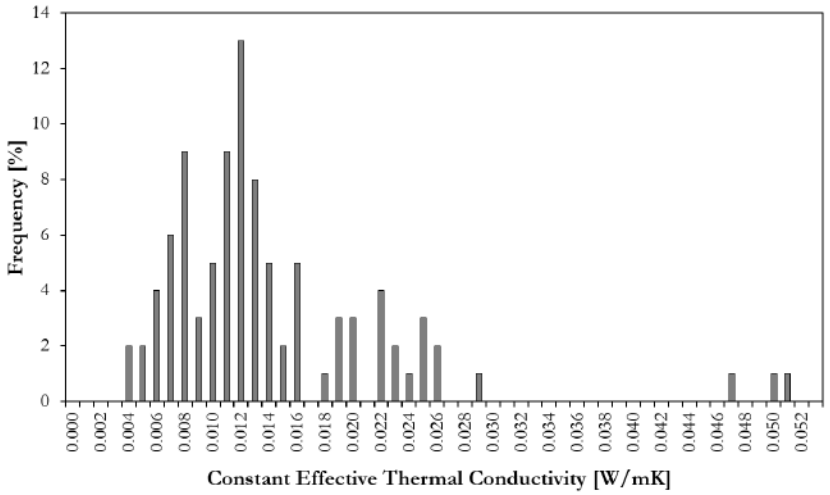

Figure 2.9: Constant effective thermal conductivity values calculated from a large number of fire tests on different steel sections protected with intumescent coatings (after Li et al. [66]).

2.8 Concluding remarks

The mainstream use of intumescent coatings used for the fire-safe design of steel structures has fostered extensive research into the development of effective intumescent coatings and the assessment of their performance during fire. Within the intumescent coating industry, researchers are continuously proposing new intumescent formulations that aim at delivering more efficient and reliable protective coatings. On the other hand, the fire-safe design of structural elements protected with intumescent coatings is still based on compliance with the standard fire resistance test in furnaces. Simplified implicit engineering methods (tabulated fire ratings or effective thermal conductivity method) based on a single fire scenario represented by the standard temperature-time fire curve are commonly adopted. However, numerous researchers have emphasised the potential influence of the heating conditions on the insulation effectiveness of intumescent coatings and some studies have actually shown how fire exposures different to the standard one may result in incomplete (or ineffective) swelling, melting or delamination of the intumescent coating. Due to its over-simplifications, limitations and uncertainties, the research community has extensively questioned the current design framework on multiple grounds. In order to overcome the abovementioned challenges, numerous researchers have completed comprehensive studies to investigate the effectiveness of intumescent coatings during fire, proposing different methodologies and us-

ing different experimental setups (e.g. cone calorimeters, widely used in fire safety science). Each approach has tackled specific research gaps and it has optimised the investigation of particular aspects related to intumescence.

The literature review presented herein showed the numerous variables that influence the complex response of intumescent coatings during fire: the thermal conditions of the substrate (e.g. steel structure), the applied coating thickness (wet or dry), the heating conditions and the fire test methodology. This work demonstrates that current engineering tools for designing fire-safe steel structures protected with intumescent coatings do not take into account most of the relevant variables relevant to the performance of intumescent coatings during fire.

The world is moving towards performance-based engineering solutions and this approach is currently becoming a common method in the space of structural fire safety engineering design. The rapid growth in the use of intumescent coatings is demanding performance-based engineering tools able to produce realistic and reliable predictions. However, the effectiveness of intumescent coatings has traditionally been assessed, in practice and research, without a fundamental understanding of the complex thermo-physical response.

It is needed that the research and practising communities move away from the rigid concept of standard fire resistance tests in furnaces for product development. Testing in a furnace has historically demonstrated to be time-consuming and resource-demanding and the over-reliance on standard fire testing and ratings hinder the growth of our understanding into the real fire performance of intumescent coatings, like any other fire protection solutions. The work shown herein demonstrated the need for scientific and practical knowledge on the thermal and physical behaviour of intumescent coatings under a range of heating scenarios (or fire scenarios) and not under a single heating scenario.

Different testing methods and different experimental setups can be adopted in order to tackle specific research gaps. Each methodology or setup has specific advantages and it can be more suitable for investigating certain aspects related to intumescence. However, researchers and practitioners must be aware of the shortcomings of each methodology and the limitations of the conclusions that can be drawn following a certain approach. For example, the testing environment around test methods similar to H-TRIS allows for continuous visual

inspection of fire-tested samples and careful control of the imposed thermal boundary conditions.

The research community should aim at defining a common methodology for a rigorous and systematic testing and design environment that allows the explicit quantification of the effectiveness of intumescent coatings exposed to various potential fire conditions. This will enable the growth of empirical knowledge on the fire behaviour of intumescent coatings in non-standard fire conditions. Simple rather than complex models should be formulated to quantify the dependency on thermal and physical properties of intumescent coatings exposed to different heating conditions and to produce realistic and reliable predictions of the fire performance of steel structures protected with intumescent coatings. All these tools would help to improve the design of fire-safe steel structures and simplify the current expensive and time-consuming large-scale test procedure.

Bibliography

[1] Lataille J.I. “Fire protection engineering in building design". Elsevier Science, 2003.

[2] Buchanan A.H. and Abu A.K. "Structural design for fire safety". John Wiley & Sons, 2nd Edition, 2017.

[3] Maluk C., Woodrow M. and Torero J.L. "The potential of integrating fire safety in modern building design". Fire Safety Journal, vol. 88, pp. 104-112, 2017.

[4] The Council on Tall Buildings and Urban Habitat. "An all-time record: 97 buildings of 200 meters or higher completed in 2014". CTBUH Year in Review: Tall Trends of 2014 and Forecasts for 2015, http://www.ctbuh.org/, 2014.

[5] Corus Construction and Industrial. "Fire resistance of steel-framed buildings". North Lincolnshire, 2006.

[6] Comité Europeén de Normalization (CEN). "EN 1993-1-2:2005 Eurocode 3: Design of steel structures - Part 1-2: General rules - Structural fire design". Brussels, Belgium, 2005.

[7] Usmani A.S., Rotter J.M., Lamont S., Sanad A.M. and Gillie M. "Fundamental principles of structural behaviour under thermal effects". Fire Safety Journal, vol. 36, pp. 721–744, 2001.

[8] Bravery PNR. "Cardington large building test facility, construction details for the first building - Technical report". British Steel plc (now CORUS), 1993. [Internal report]

[9] Cooke G.M.E. "A review of compartment fire tests to explore the behaviour of structural steel. Fire, static and dynamic tests of building structures". Proceedings of the Second Cardington Conference, E & F.N. Spon, London, pp. 17-32, 1996.

[10] Challener C. "Fire safety with specialty coatings". JCT Coatings Technology, vol. 4, no. 9, pp. 78-84, 2007.

[11] Mariappan T. "Recent developments of intumescent fire protection coatings for structural steel: A review". Journal of Fire Sciences, vol. 34, no. 2, pp. 1-44, 2016.

[12] Dow Jones. "Global market insights: intumescent coatings market worth $1.16 billion by 2022". Market Reports, Coatings World, vol. 21, no. 6, 2016.

[13] Allen C. "Choosing the right fireproofing for structures and equipment support". Chemical Engineering Progress, vol. 95, pp. 75-80, 1999.

[14] Dowling J. "Fire protection costs for structural steelwork". New Steel Construction, UK, 2003.

[15] Goode M. "Fire protection of structural steel in high-rise buildings". GCR 04-872, National Institute of Standards and Technology (NIST), 2004.

[16] Camino G., Costa L. and Martinasso G. "Intumescent fire-retardant systems". Polymer De-

gradation and Stability, vol. 23, pp. 359-376, 1989.

[17] Elliott A., Temple A., Maluk C. and Bisby L. "Novel testing to study the performance of intumescent coatings under non-standard heating regimes". Fire Safety Science – Proceedings of the 11th International Symposium, University of Canterbury, New Zealand, pp. 652-665, 2014.

[18] Lucherini A. "Experimental study of the behaviour of steel structures protected by different intumescent coatings and exposed to various fire scenarios". MSc thesis, Department of Civil Engineering, Technical University of Denmark (DTU), 2016.

[19] Yuan J. "Intumescent coating performance on steel structures under realistic fire conditions". PhD thesis, School of Mechanical, Aerospace and Civil Engineering, University of Manchester, 2009.

[20] Li G.Q., Lou G.B., Zhang C., Wang L. and Wang Y. "Assess the fire resistance of intumescent coatings by equivalent constant thermal resistance". Fire Technology, vol. 48, pp. 529-546, 2012.

[21] Wang L., Dong Y., Zhang D., Zhang D. and Zhang C. "Experimental study of heat transfer in intumescent coatings exposed to non-standard furnace curves". Fire Technology, vol. 51, no. 1, pp. 627-643, 2015.

[22] Kandola B.S., Akonda M.H. and Horrocks A.R. "Use of high-performance fibres and intumescents as char promoters in glass-reinforced polyester composites". Polymer Degradation and Stability, vol. 88, pp. 123-129, 2005.

[23] Amir N., Jalil N.A. and Ahmad F. "Characterization and study of char performance of glass wool and rockwool hybrid fibre reinforced intumescent coatings". ARPN Journal of Engineering and Applied Sciences, vol. 11, no. 20, 2016.

[24] Yan L., Xu Z. and Wang X. "Influence of nano-silica on the flame retardancy and smoke suppression properties of transparent intumescent flame-retardant coatings". Process in Organic Coatings, vol. 112, pp. 319-329, 2017.

[25] de Sa S.C., de Souza M.M., Peres R.S., Zmozinski A.V., Braga R.M., de Araujo Melo D.M. and Ferreira C.A. "Environmentally friendly intumescent coatings formulated with vegetable compounds". Process in Organic Coatings, vol. 113, pp. 47-59, 2017.

[26] Vandersall H.L. "Intumescent coating systems, their development and chemistry". Journal of Fire and Fiammability, vol. 2, pp. 97-140, 1971.

[27] Troitzsch J.H. "Methods for the fire protection of plastics and coatings by flame retardant and intumescent systems". Progress in Organic Coatings, vol. 11, pp. 41-69, 1983.

[28] Weil E.D. "Fire-protective and flame-retardant coatings – A state-of-the-arte review". Journal

of Fire Science, vol. 29, pp. 259-296, 2011.

[29] Puri E.G., Khanna A.S. "Intumescent coatings: a review on recent progress". Journal of Coatings Technology and Research, vol. 14, pp.1-20, 2017.

[30] Norgaard K.P. "Investigation of an Intumescent Coating System in Pilot and Laboratory-scale Furnaces". PhD thesis, CHEC Research Centre, Department of Chemical and Biochemical Engineering, Technical University of Denmark (DTU), Denmark, 2014.

[31] International Organization for Standardization (ISO). "ISO 8501-1:2007 Preparation of steel substrates before application of paints and related products. Visual assessment of surface cleanliness. Rust grades and preparation grades of uncoated steel substrates and of steel substrates after overall removal of previous coatings". Geneva, Switzerland, 2007.

[32] Wicks Z.W., Jones F.N., Pappas P.S. and Wicks D.A. "Organic coatings: science and technology". Wiley-Interscience, 3rd Edition, 2007.

[33] Zhang Y., Wang Y., Bailey C.G. and Taylor A.P. "Global modelling of fire protection performances of an intumescent coating under different furnace fire conditions". Journal of Fire Science, vol. 31, no.1, pp. 51-72, 2012.

[34] Horaceck H. and Pieh S. "The importance of intumescent systems for fire protection of plastic materials". Polymer International, vol. 49, pp. 1106-1114, 2000.

[35] Bourbigot S. and Duquesne S. "Fire retardant polymers: recent developments and opportunities". Journal of Material Chemistry, vol. 17, pp.2283-2300, 2007.

[36] Jimenez M., Duquesne S. and Bourbigot S. "Intumescent fire protective coating: toward a better understanding of their mechanism of action". Thermochimica Acta, vol. 449, no. 1-2, pp. 16-26, 2006.

[37] Taylor A.P. and Sall F.R. "Thermal analysis of intumescent coatings". European Polymer Paint Colour Journal, vol. 182, no. 4301, pp. 122-130, 1992.

[38] Oliveira R.B.R.S., Moreno Junior A.L. and Vieira L.C.M. "Intumescent paint as fire protection coating". IBRACON Structures and Materials Journal, vol. 10, no. 1, pp. 220-243, 2017.

[39] Griffin G.J., Bicknell A.D. and Brown T.J. "Studies on the effect of atmospheric oxygen content on the thermal resistance of intumescent fire-retardant coatings". Journal of Fire Science, vol. 23, no. 4, 2005.

[40] Bourbigot S., Le Bras M., Duquesne S. and Rochery M. "Recent advances for intumescent polymers". Macromolecular Materials and Engineering, vol. 289, no. 6, pp. 499-511, 2004.

[41] Anna P., Marosi Gy., Bourbigot S., Le Bras M. and Delobel R. "Intumescent flame retardant systems of modified rheology". Polymer Degradation and Stability, vol. 77, pp. 243-247, 2002.

[42] Neiningera S.M., Staggs J.E.J., Horrocks A.R. and Hill N.J. "A study of the global kinetics of thermal degradation of a fibre-intumescent mixture". Polymer Degradation and Stability, vol. 77, no. 2, pp. 187-194, 2002.

[43] Bourbigot S., Duquesne S. and Leroy J.-M. "Modeling of heat transfer of a polypropylene-based intumescent system during combustion". Journal of Fire Sciences, vol. 17, pp. 42-56, 1999.

[44] Bourbigot S., Le Bras M., Delobel R. and Tremillon J.M. "Synergistic effect of zeolite in an intumescence process". Journal of Chemistry Society, vol. 92, no. 18, pp.3435-3444, 1996.

[45] Le Bras M., Bourbigot S., Delporte C., Siat C. and Le Tallec Y. "New intumescent formulations of fire-retardant polypropylene - Discussion of the free radical mechanism of the formation of carbonaceous protective material during the thermo-oxidative treatment of the additives". Fire and Materials, vol. 20, pp. 191-203, 1996.

[46] Delobel R., Le Bras M. and Ouassou N. "Fire retardance of polypropylene by diammonium pyrophosphate-pentaerythritol: spectroscopic characterization of the protective coatings". Polymer Degradation and Stability, vol. 30, pp. 41-56, 1990.

[47] Delobel R., Ouassou N., Le Bras M. and Leroy J.M. "Fire retardance of polypropylene: action of diammonium pyrophosphate-pentaerythritol intumescent mixture". Polymer Degradation and Stability, vol. 23, pp. 349-357, 1989.

[48] Camino G., Costa L. and Trossarelli L. "Study of the mechanism of intumescence in fire retardant polymers: Part I - V". Polymer Degradation and Stability, vol. 8, pp. 13-22, 1984.

[49] Lucherini A. and Maluk C. "Assessing the onset of swelling for thin intumescent coatings under a range of heating conditions". Fire Safety Journal, vol. 106, pp. 1-12, 2019.

[50] International Organization for Standardization (ISO). "ISO834-1:1999 Fire resistance tests - Elements of building construction - Part 1: General requirements for fire resistance testing". Geneva, Switzerland, 1999.

[51] American Society for Testing and Materials (ASTM). "ASTM E119:2012 Standard Test Methods for Fire Tests of Building Construction and Materials". West Conshohocken, Pennsylvania, 2012.

[52] Standards Australia (AS). "AS 1530-4:2014 Methods for fire tests on building materials, components and structures - Part 4: Fire-resistance test of elements of construction". Sydney, Australia, 2014.

[53] Comité Europeén de Normalization (CEN). "EN 13381-8:2013 Test methods for determining the contribution to the fire resistance of structural members - Part 8: Applied reactive protection to steel members". Brussels, Belgium, 2013.

[54] Comité Europeén de Normalization (CEN). "EN 1363-1:2012 Fire resistance tests - Part 1: General Requirements". Brussels, Belgium, 2012.

[55] Comité Europeén de Normalization (CEN). "EN 1363-2:2012 Fire resistance tests - Part 2: Alternative and additional procedures". Brussels, Belgium, 1999.

[56] Standards Australia (AS). "AS 4100:1998 Steel structures". Sydney, Australia, 1998.

[57] Drysdale D. "An introduction to fire dynamics". John Wiley & Sons, Ltd, 3rd Edition, 2011.

[58] McNamee R.J., Storesund K. and Stolen R. "The function of intumescent paint for steel during different fire exposures". SP Sveriges Tekniska Foreskningsinstitut, SP Rapport 2016, vol.43, 2016.

[59] Maluk C., Bisby L., Terrasi G., Krajcovic M., Torero J.L. "Novel fire testing methodology: why, how and what now?". Proceedings of the Mini Symposium on Performance-based Fire Safety Engineering of Structures as part of the 1st International Conference on Performance Based land Life Cycle Structural Engineering, pp. 448-458, 2012.

[60] Han Z., Fina A., Malucelli G. and Camino G. "Testing fire protective properties of intumescent coatings by in-line temperature measurements on a cone calorimeter". Progress in Organic Coatings, vol. 69, pp. 475-480, 2010.

[61] Griffin G.J. "The modelling of heat transfer across intumescent polymer coatings". Journal of Fire Science, vol. 28, pp. 249-277, 2010.

[62] Bartholmai M., Schriever R. and Schartel B. "Influence of external heat flux and coating thickness on the thermal insulation properties of two different intumescent coatings using cone calorimeter and numerical analysis". Journal of Fire Materials, vol. 27, pp. 151-162, 2003.

[63] Cirpici B.K., Wang Y.C. and Rogers B. "Assessment of the thermal conductivity of intumescent coatings in fire". Fire Safety Journal, vol. 81, pp. 74-84, 2016.

[64] Kolsek J. and Cesarek P. "Performance-based fire modelling of intumescent painted steel structures and comparison to EC3". Journal of Constructional Steel Research, vol. 104, pp. 91-103, 2015.

[65] Li G.Q., Han J., Lou G.B. and Wang Y.C. "Predicting intumescent coating protected steel temperature in fire using constant thermal conductivity". Thin-Walled Structures, vol. 98, pp. 177-184, 2016.

[66] Li G.Q., Han J. and Wang Y.C. "Constant effective thermal conductivity of intumescent coatings: Analysis of experimental results". Journal of Fire Sceinces, vol 35, no. 2, pp. 132.155, 2017.

[67] Lucherini A., Giuliani L. and Jomaas G. "Experimental study of the performance of intumescent coatings exposed to standard and non-standard fire conditions". Fire Safety Journal, vol. 95,

pp. 42-50, 2018.

[68] Wang L.L., Wang Y.C., Yuan J.F. and Li G.Q. "Thermal conductivity of intumescent coating char after accelerated aging". Fire and Materials, vol. 37, pp. 440-456, 2012.

[69] Rush D., Bisby L., Gillie M., Jowsey A. and Lane B. "Design of intumescent fire protection for concrete filled structural hollow sections". Fire Safety Journal, vol. 67, pp. 13-23, 2014.

[70] Glendenning B. "Thick or thin: passive fire protection coatings". Fire Protection Engineering, no. 77, 2018.

[71] Bozzoli F., Mocerino A., Ranieri S. and Vocale P. "Inverse heat transfer modeling applied to the estimation of the apparent thermal conductivity of an intumescent fire retardant paint". Experimental Thermal and Fluid Science, vol. 90, pp. 143-152, 2018.

[72] Anees S.M. and Dasari A. "A review on the environmental durability of intumescent coatings for steels". Journal of Materials Science, vol. 53, pp. 124-145, 2018.

[73] Wang L.L., Wang Y.C. and Li G.Q. "Experimental study of hydrothermal aging effects on insulative properties of intumescent coating for steel elements". Fire Safety Journal, vol. 55, pp. 168-181, 2013.

[74] Jimenez M., Bellayer S., Revel B., Duquesne S. and Bourbigot S. "Comprehensive study of the influence of different aging scenarios on the fire protective behaviour of an epoxy based intumescent coating". Industrial & Engineering Chemical Research, vol. 52, no. 2, pp. 729-743, 2013.

[75] Bilotta A., De Silva D. and Nigro E. "Tests on intumescent paints for fire protection of existing steel structures". Construction and Building Materials, vol. 121, pp. 410-422, 2016.

[76] Bilotta A., De Silva D. and Nigro E. "General approach for the assessment of the fire vulnerability of existing steel and composite steel-concrete structures". Journal of Building Engineering, vol. 8, pp. 198-207, 2016.

[77] Dai X.H., Wang Y.C. and Bailey C. "A simple method to predict temperatures in steel joints with partial intumescent coating fire protection". Fire Technology, vol. 46, pp. 19-35, 2010.

[78] Dai X.H. Wang Y.C. and Bailey G.C. "Effects of partial fire protection on temperature developments in steel joints protected by intumescent coatings". Fire Safety Journal, vol. 44, pp. 376-386, 2009.

[79] De Silva D., Bilotta A. and Nigro E. "Experimental tests on intumescent coatings for protecting steel structures". Proceedings of the 9th International Conference on Structures in Fire (SiF), Princeton University, United States, pp. 1081-1089, 2016.

[80] Rush D., Bisby L.A., Jowsey A. and Lane B. "Residual capacity of fire-exposed concrete-filled

steel hollow section columns". Engineering Structures, vol. 100, pp. 550-563, 2015.

[81] Rush D., Bisby L., Gillie M., Jowsey A. and Lane B. "Furnace tests on unprotected and protected concrete filled structural hollow sections". Fire Safety Journal, vol. 78, pp. 71-84, 2015.

[82] Bailey C. "Indicative fire tests to investigate the behaviour of cellular beams protected with intumescent coatings". Fire Safety Journal, vol. 39, pp. 689-709, 2004.

[83] Nadjai A., Petrou K., Han S. and Ali F. "Performance of unprotected and protected cellular beams in fire conditions". Construction and Building Materials, vol. 105, pp. 579-588, 2016.

[84] Comité Europeén de Normalization (CEN). "EN 1991-1-2:2002 Eurocode 1: Action on structures – Part 1-2: General actions – Actions on structures exposed to fire". Brussels, Belgium, 2002.

[85] China Association for Engineering Construction Standardization (CSCS200). "Technical code for fire safety of steel structure in buildings". China Planning Press, Beijing, 2006.

[86] Bartholomai M. and Schartel B. "Assessing the performance of intumescent coatings using bench-scaled cone calorimeter and finite difference simulations". Journal of Fire Materials, vol. 31, pp. 187-205, 2007.

[87] Zhang Y., Wang Y., Bailey C.G. and Taylor A.P. "Global modelling of fire protection performance of an intumescent coating under different cone calorimeter heating conditions". Fire Safety Journal, vol. 50, pp. 51-62, 2012.

[88] Johansson N., Van Hees P., Jansson R. and Sjostrom J. "Behaviour of intumescent system subjected to different heating conditions". In S. Grayson Edition, Fire and Materials – 13th International Conference and Exhibition, pp. 187-196, 2013.

[89] Wang Y., Goransson U., Holmstedt G. and Omrane A. "A Model for prediction of temperature in steel structure protected by intumescent coating, based on tests in the cone calorimeter". Fire Safety Science – Proceedings of the 8th International Symposium, Tsinghua University, Beijing, China, pp. 235-246, September 2005.

[90] Omrane A., Wang Y.C., Goransson U., Holmstedt G. and Alden M. "Intumescent coating surface temperature measurement in a cone calorimeter using laser-induced phosphorescence". Fire Safety Journal, vol. 42, pp. 68-74, 2006.

[91] Fateh T., Guillaume E. and Joseph P. "An experimental study of the thermal performance of a novel intumescent fire protection coating". Fire Safety Journal, vol. 92, pp. 132-141, 2017.

[92] Wilson M.T., Dlugogorski B.Z. and Kennedy E.M. "Uniformity of radiation heat fluxes in cone calorimeter". Fire Safety Science – Proceedings of the 7th International Symposium, Gaithersburg, Maryland, USA, pp. 815-827, 2002.

[93] Schartel B., Bartholmai M. and Knoll U. "Some comments on the use of cone calorimeter data". Polymer Degradation and Stability, vol. 88, pp. 540-547, 2005.

[94] Kang S., Choi S. and Choi J. "Thermal boundaries of intumescent-type insulations in cone calorimeter testing". Fire Science and Technology 2015, Proceeding of 10th Asia-Oceania Symposium on Fire Science and Technology, pp. 705-714, 2015.

[95] Jimenez M., Duquesne S. and Bourbigot S. "Characterization of the performance of an intumescent fire protective coating". Surface & Coatings Technology, vol. 201, pp. 979-987, 2006.

[96] Reshetnikov I.S., Garashchenko A.N. and Strakhov V.L. "Experimental investigation into mechanical destruction of intumescent chars". Polymers for Advanced Technologies, vol. 11, pp. 392-397, 2000.

[97] Fry Z.S. "A laboratory scale study of intumescent coatings for protection of building structure member from fires". M.Sc. thesis, Department of Mechanical and Aerospace Engineering, Case Western Reserve University, 2014.

[98] Calabrese L., Bozzoli F., Bochicchio G., Tessadri B., Rainieri S. and Pagliarini G. "Thermal characterization of intumescent fire retardant paints". Journal of Physics: Conference Series, vol. 547, 2014.

[99] Calabrese L., Bozzoli F., Bochicchio G., Tessadri B., Vocale P. and Rainieri S. "Parameter estimation approach to the thermal characterization of intumescent fire retardant paints". Journal of Physics: Conference Series, vol. 655, 2015.

[100] Morys M., Illerhaus B., Sturm H. and Schartel B. "Revealing the inner secrets of intumescence: Advanced standard time temperature oven (STT Mufu+) - μ-computed tomography approach". Fire and Materials, vol. 41, pp. 927-939, 2017.

[101] Morys M., Illerhaus B., Sturm H. and Schartel B. "Size is not all that matters: Residue thickness and protection performance of intumescent coatings made from different binders". Journal of Fire Sciences, vol. 35, no. 4, pp. 1-19, 2017.

[102] Morys M., Illerhaus B., Sturm H. and Schartel B. "Variation of intumescent coatings revealing different modes of action for good protection performance". Fire Technology, vol. 53, pp. 1569-1587, 2017.

[103] Maluk C., Bisby L., Krajcovic M. and Torero J.L. "A Heat-Transfer Inducing System (H-TRIS) Test Method". Fire Safety Journal, vol. 105, pp. 307-319, 2019.

[104] Lucherini A. and Maluk C. "Novel test methods for studying the fire performance of thin intumescent coatings". Proceedings of 2nd International Fire Safety Symposium (IFireSS), Napoli, Italy, pp. 565-572, 2017.

[105] Cagliostro D.E., Riccitello S.R., Clark K.L. and Shimizu A.B. "Intumescent coating modelling". Journal of Fire and Flammability, vol. 6, pp. 205, 1975.

[106] Anderson C.E., Dziuk J. and Mallow W.A. "Intumescent reaction mechanisms". Journal of Fire Sciences, vol.3, pp. 161-194, 1985.

[107] Anderson C.E., Ketchum D.E. and Schartel B. "Thermal conductivity of intumescent chars". Journal of Fire Science, vol. 16, pp. 390-410, 1988.

[108] Di Blasi C. "Modeling the effects of high radiative heat fluxes on intumescent material decomposition". Journal of Analytical and Applied Pyrolysis, vol. 71, pp. 721-737, 2004.

[109] Di Blasi C., Branca C. and Horacek H. "Mathematical model for the nonsteady decomposition of intumescent coatings". AIChE Journal, vol. 47, pp. 2359-2370, 2001.

[110] Staggs J.E.J., Crewe R.J. and Butler R. "A theoretical and experimental investigation of intumescent behaviour in protective coatings for structural steel". Chemical Engineering Science, vol. 71, pp. 239-251, 2012.

[111] Zhang F., Sun Y. and Cheng Y. "Study on heat transfer in intumescent fire retardant epoxy coatings during combustion". Journal of Macromolecular Science, Part B: Physics, vol. 56, pp. 608-622, 2017.

[112] Hsu S.Y. "Modeling of heat transfer in intumescent fire-retardant coating under high radiant heat source and parametric study on coating thermal response". Journal of Heat Transfer, vol. 140, 2018.

[113] Krishnamoorthy R.R. and Bailey C.G. "Temperature distribution of intumescent coated steel framed connection at elevated temperature". Proceedings of Nordic Steel Construction Conference 2009, Malmo, Sweden, pp. 572-579, 2009.

[114] Atefi H., Nadjai A. and Ali F. "Numerical and experimental investigation of the thermal behaviour of coated cellular beams with intumescent coatings at elevated temperatures". Proceedings of the 2nd International Fire Safety Symposium (IFireSS), Napoli, Italy, pp. 257-264, 2017.

[115] Weisheim W., Schaumann P., Sander L. and Zehfub J. "Numerical model for the fire protection performance of intumescent coatings exposed to natural fires". Proceedings of the 10th International Conference on Structures in Fire (SiF), Belfast, UK, pp. 225-232, 2018.

[116] Andersen J.H. "Experimental study of the thermal resistance of intumescent coatings exposed to different heating rates". M.Sc. thesis, Department of Civil Engineering, Technical University of Denmark (DTU), 2015.

3

Material and methods

3.1 Introduction and background

The structural and fire safety engineering practice is moving towards performance-based designs and rigorous processes for the explicit fire-safe design of structures protected with intumescent coatings are extremely needed [1-3]. Numerous researchers have questioned the relevance of standard fire resistance furnace testing due to high operating costs, poor repeatability and inappropriate thermal boundary conditions [4]. As a consequence, several studies have proposed comprehensive approaches and experimental methodologies to investigate the behaviour of intumescent coatings exposed to various heating conditions and using different experimental set-ups. Due to specific advantages, different approaches and methodologies were proposed to tackle certain research gaps related to intumescence. However, researchers and practitioners must be aware of the shortcomings of each methodology and the limitations of the conclusions that can be drawn following a certain approach. For example, the cone calorimeter has been extensively adopted to study the performance of intumescent coatings under a well-defined incident heat flux in a open environment [5-7]. However, in the case of intumescent coatings, cone calorimetry testing suffers uncertainties in terms of net heat flux absorbed by the test sample during the swelling process: the external heat flux changes as the exposed coating surface moves closer to the cone heater and the swelling causes exposure of the perimeter phases [8]. On the other hand, small-scale experiments (e.g. TGA and DSC) are useful and reliable methodologies for studying the thermal decomposition of intumescent coatings and optimising their formulations, but they are not able to capture their swelling process [9-10]. As a conclusion, in the available literature many fundamental aspects related to intumescent coatings and their effectivness are still not fully understood and the research community has not agreed on specific testing methodologies yet.

The current chapter presents an experimental methodology designed for investigating the behaviour of intumescent coatings exposed to well-defined and highly-repeatable thermal boundary conditions. The methodology is based on the Heat-Transfer Rate Inducing System (H-TRIS) test method and uses arrays of high performance radiant panels coupled with computer-controlled linear motion systems to directly control the time-history of incident radiant heat flux at the exposed surface of real-scale coated samples. The methodology is

proposed to study fundamental aspects related to intumescence, such as the swelling and the thermo-physical response of intumescent coatings under a wide range of conditions in terms of heating or sample characteristics.

3.2 Experimental methodology

3.2.1 Heat-Transfer Rate Inducing System (H-TRIS) test method

In order to investigate and quantify the effectiveness of intumescent coatings exposed to a wide range of heating conditions, the *Heat-Transfer Rate Inducing System (H-TRIS)* test method was chosen as the appropriate experimental methodology [11]. The approach offers considerable advantages over conventional furnace testing in terms of reliability, repeatability, versatility, speed and costs [11]. In addition, H-TRIS allows for the direct and independent control of the thermal boundary conditions imposed on test samples by controlling a specified time-history of incident radiant heat flux at its exposed surface. This is possible by controlling the relative position between the exposed surface of the test sample and an array of high performance radiant panels coupled with a computer-controlled mechanical linear motion system [11]. In this way, H-TRIS can potentially impose any well-defined time-history of incident radiant heat flux, limited by the maximum and minimum proximities to the exposed surface of the test sample (minimum and maximum heat flux). Also, thanks to its open environment, the methodology enables the visual inspection of test samples during the heating exposure, technically challenging during a standard furnace test. More specifically, the H-TRIS test method allows for the measurement of the swelled coating thickness, a key aspect to comprehend the behaviour of intumescent coatings [1].

3.2.2 Assembly of H-TRIS test methods

Throughout the research project, three experimental setups based on the H-TRIS test method have been designed and assembled at the University of Queensland. The various versions of the H-TRIS test method represent different stages of the research project and they differ in size and ranges of thermal exposure, consequently each of them can have specific research applications:

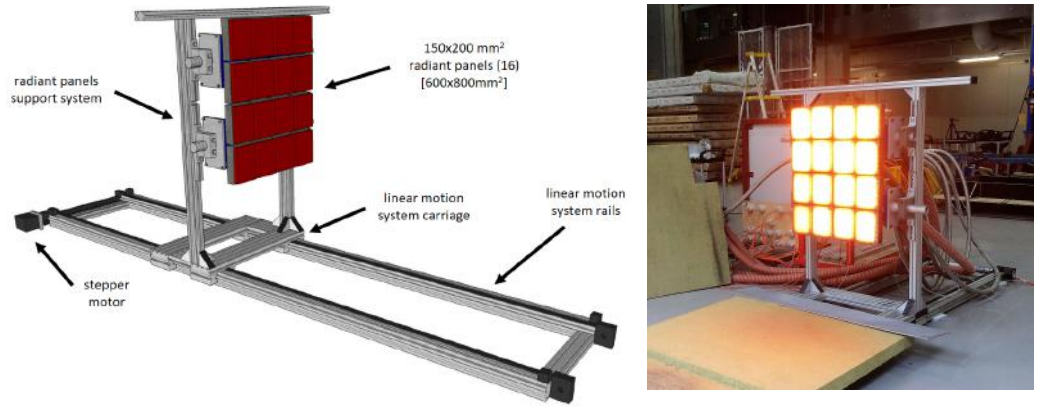

Figure 3.1: *Large-scale H-TRIS* at the Structures Laboratory of The University of Queensland.

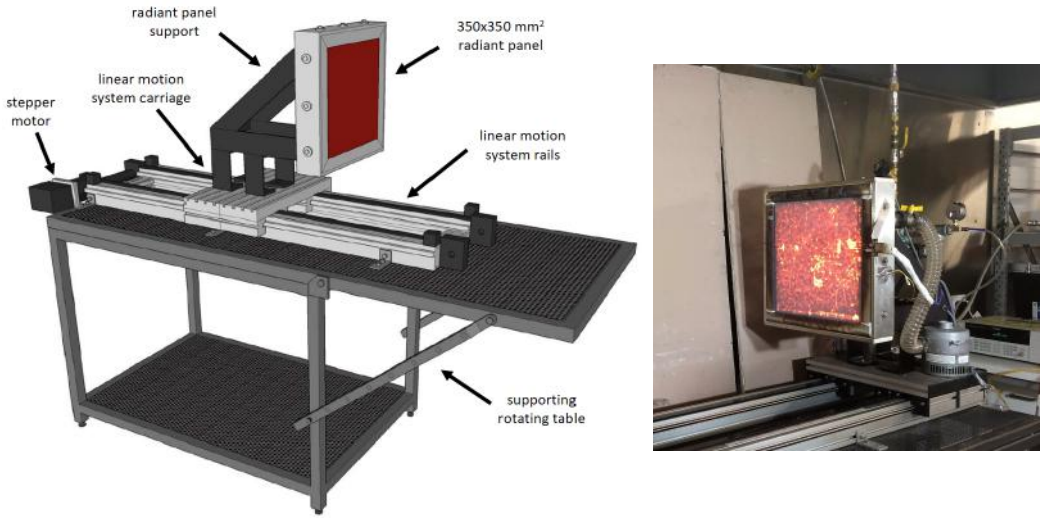

Figure 3.2: *Bench-scale H-TRIS 1.0* at the Fire Laboratory of The University of Queensland.

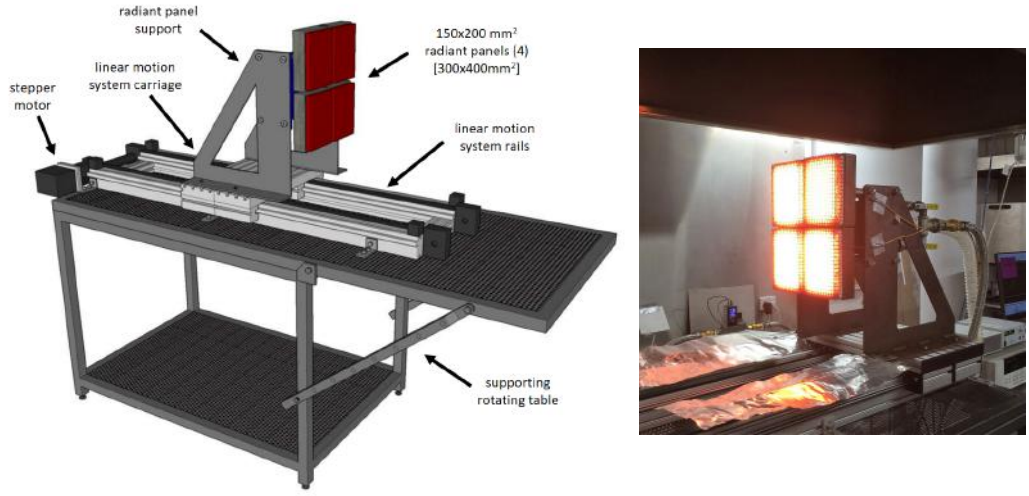

Figure 3.3: *Bench-scale H-TRIS 2.0* at the Fire Laboratory of The University of Queensland.

- *Large-scale H-TRIS*: composed of sixteen 150 x 200 mm^2 high-performance radiant panels (3.5 mm thick sintered metal fibre medium) creating a 600 x 800 mm^2 radiant heat source and able to impose heat fluxes up to 180 kW/m^2 (Figure 3.1).
- *Bench-scale H-TRIS 1.0*: composed of a single 355 x 355 mm^2 (14" x 14") high-performance radiant panel (thin ceramic fibre medium) and able to impose heat fluxes up to 60 kW/m^2 (Figure 3.2).
- *Bench-scale H-TRIS 2.0* (updated version): composed of four 150 x 200 mm^2 high-performance radiant panels (3.5 mm thick sintered metal fibre medium) creating a 300 x 400 mm^2 radiant heat source and able to impose heat fluxes up to 120 kW/m^2 (Figure 3.3).

All the radiant panels are fired by a air-natural gas mixture and they were mounted on linear motion systems that control the relative position between the radiant panels and the target exposed surface of the test sample. The systems are moved using a computer-controlled rotary stepper motor and they are programmed to automatically control the position of the radiant panels with high speed and accuracy. The mechanical linear motion systems have different dimensions based on the size of the H-TRIS apparatus. The *Large-scale H-TRIS* is composed of two linear rails 3500 mm long with a total travelling stroke of 3000 mm, while the two linear rails of the *Bench-scale H-TRIS* are 1500 mm long and they have a total travelling stroke of 1180 mm.

In addition, the *Bench-scale H-TRIS* is mounted on a special supporting table that was designed to allow for the rotation of the experimental plane. The inclination of the linear motion system, the sample holder and the radiant panel can be adjusted, from a horizontal to a vertical configuration, at steps of 15°, from 0° to 90° (Figure 3.4). In vertical configuration, the orientation of the linear motion system can also be rotated, allowing for experiments with the radiant panels array moving upwards or downwards (Figure 3.5). The system was designed to be fully modular and facilitate research studies aimed at understanding the influence of orientation, gravity and convective flows on test samples exposed to different heating regimes.

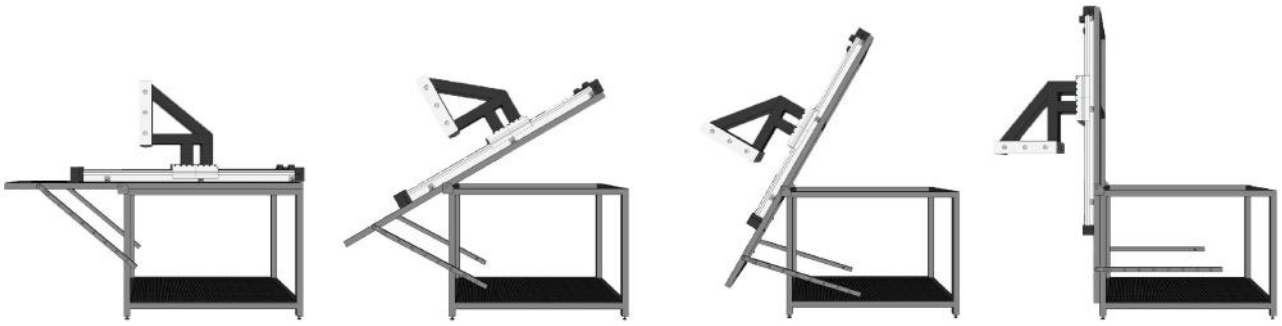

Figure 3.4: Possible experimental configurations of the *Bench-scale H-TRIS*: from horizontal (left) to vertical configuration (right) (*Bench-scale H-TRIS 1.0*).

Figure 3.5: Possible experimental configurations of the *Bench-scale H-TRIS*: vertical configuration with radiant panels array moving downwards (left), horizontal configuration (centre) and vertical configuration with radiant panels array moving upwards (right) (*Bench-scale H-TRIS 2.0*).

3.2.3 Thermal boundary conditions

Within the scope of this work, the heat transfer is considered unidimensional, following the main direction of the heat flow coming from the radiant panels into the target sample surface. In general, the thermal boundary conditions imposed on the exposed surface of test samples in accordance with the H-TRIS test method can be described as [11]:

$$\dot{q}''_{net} = \alpha \cdot \dot{q}''_{inc} - \dot{q}''_{loss} = \alpha \cdot \dot{q}''_{inc} - h_{conv}(T_{surf} - T_{\infty}) + F_{12}\varepsilon\sigma(T^4_{surf} - T^4_{\infty}) \tag{3.1}$$

where $\dot{q}''_{net}$ is the net heat flux absorbed by the exposed test sample [W/m^2], α is the absorptivity of the exposed test sample [-], $\dot{q}''_{inc}$ is the incident radiant heat flux at the exposed surface of the test sample [W/m^2], $\dot{q}''_{loss}$ is the heat losses at the exposed surface of the test sample due to convection and radiation [W/m^2], h_{conv} is the convective heat transfer coefficient [W/m^{2}K], T_{surf} is the surface temperature [K], T_{∞} is the ambient temperature [K], F_{12}: view factor [-], ε is the emissivity of the exposed test sample [-] and σ is the Stefan-Boltzmann

constant ($5.67 \cdot 10^{-8}$ W/m^{2}K^4).

The H-TRIS test method is able to accurately control the thermal boundary conditions at the exposed surface by simply moving the radiant panels array towards or away from the sample as necessary. In other terms, the H-TRIS can directly control the time-history of incident heat flux $\dot{q}''_{inc}$ at the exposed surface of the test sample during the thermal exposure [11]. Alternately, if an accurate heat transfer model (analytical or numerical) of the tested sample can be implemented, H-TRIS is able to impose specific time-histories of net heat flux $\dot{q}''_{net}$ by estimating the heat flux losses $\dot{q}''_{loss}$ as:

$$\dot{q}''_{loss} = h_{conv}(T_{surf} - T_{\infty}) + F_{12}\varepsilon\sigma(T^4_{surf} - T^4_{\infty}) \tag{3.2}$$

Figure 3.6 offers a simplified schematic of the thermal boundary conditions imposed by the H-TRIS test method on the exposed surface of a test sample.

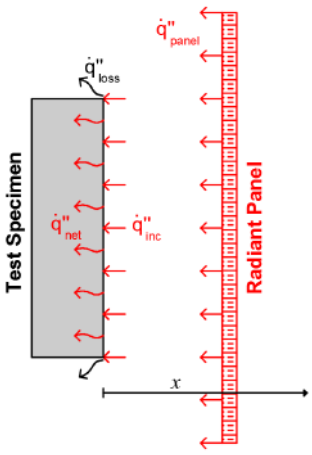

Figure 3.6: Simplified schematic illustration of the thermal boundary conditions imposed by the H-TRIS test method at the exposed surface of the test sample (drawn not in scale).

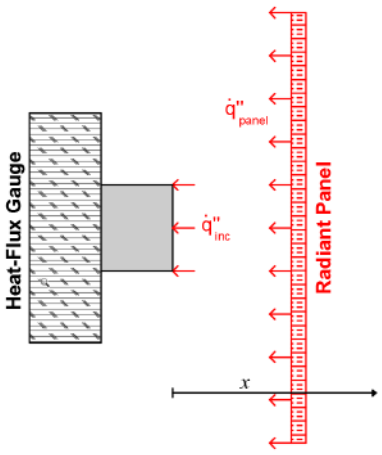

Figure 3.7: Simplified schematic illustration of thermal boundary conditions measured during the calibration procedure using a heat flux gauge (drawn not in scale).

3.2.4 Calibration procedure

In a pre-testing calibration procedure, the incident radiant heat flux defined by the relative position of the radiant panels array and the exposed surface of the test sample is measured using a *water-cooled Schimidt-Boelter heat flux gauge* (Figure 3.7) [11]. The heat flux gauge is placed at the centre of the target surface and it is mounted on a self-cooling cylindrical

probe in order to minimise the influence of convective flows near the gauge and avoid any damage to the instrumentation due to high temperatures [12-13]. Measurements at various positions are collected to generate a curve of incident radiant heat flux versus stand-off distance x from the radiant panels array (Figure 3.8).

Figure 3.8: H-TRIS calibration procedure (*Bench-scale H-TRIS 2.0*).

Figure 3.9 shows typical calibration curves of the three assembled H-TRIS apparatus. The error bars represent the range of deviation of the heat flux measurements due to the spatial distribution and the heat flux gauge accuracy. Based on their configurations, the three H-TRIS apparatus can reach different maximum heat flux values due to their size and the minimum proximity to the exposed surface of the test sample. The maximum incident heat fluxes are around 180 kW/m^2 for the *Large-scale H-TRIS*, 60 kW/m^2 for the *Bench-scale H-TRIS 1.0* and 110 kW/m^2 for the *Bench-scale H-TRIS 2.0*. Consequently, they can be used to impose different ranges of time-histories of incident radiant heat flux with different spacial distributions on the sample target surface.

All the radiant panels are set to operate at a certain constant panel temperature by controlling the natural gas flow to combustion mixture using a mass flow controller. Accordingly, each H-TRIS apparatus can be associated to a characteristic calibration curve. However, the calibration procedure may be influenced by various environmental factors, such as ambient temperature and humidity [11]. Consequently, the pre-test calibration procedure should be conducted before each set of experiments in order to ensure the consistency of the thermal boundary conditions imposed on test samples between various repetitions.

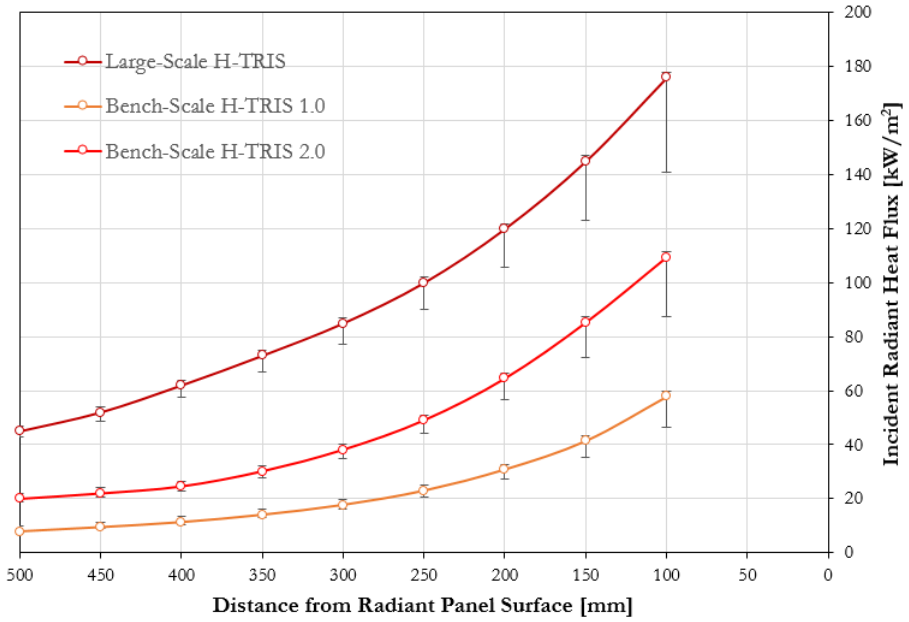

Figure 3.9: *Large-scale*, *Bench-scale 1.0* and *Bench-scale 2.0 H-TRIS* calibration curves: incident radiant heat flux at the target surface of the test sample versus stand-off distance from the radiant panels array.

In addition, the same procedure is periodically repeated at different locations on the target exposed surface in order to assess the spatial distribution of the thermal boundary conditions. The spacial distribution is directly dependent on the geometry of the system and the view factor, particularly on the ratio between the area of the target surface and the one of the radiant panels array [14]. Based on the assembled H-TRIS apparatus, a good practice is to choose the dimensions of the test sample (exposed surface) and the stand-off distance between the sample and the radiant panels in a way to ensure the spacial distribution of incident radiant heat flux better than 90% uniform.

The definition of the thermal boundary conditions imposed by the H-TRIS test method assumes a heat flux exclusively based on radiative heat transfer. Accordingly, H-TRIS should operate in order to avoid other modes of heat transfer to the test sample, such as convection or conduction. In particular, in order to avoid convective heat transfer between the test samples and the convective hot gases released by the radiant panels, a sufficient spacial separation between the radiant panels array and the exposure surface of the test sample must be ensured [15]. Depending on the different H-TRIS apparatus and test sample dimensions, a minimum distance to ensure radiative heat transfer and free convection at the sample surface can be calculated following conventional calculations or can be estimated

using thermal camera imaging as shown in Figure 3.10 [14, 16].

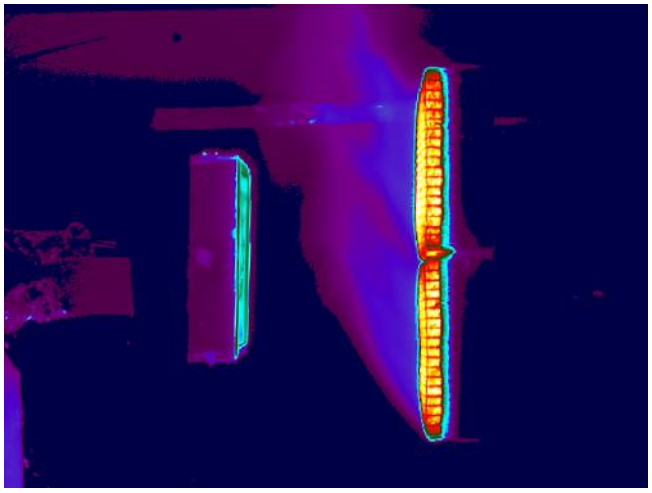

Figure 3.10: Thermal image obtained using an Infra-Red camera (*Bench-scale H-TRIS 2.0*, radiant panels - test sample distance = 200 mm).

3.3 Application to thin intumescent coatings

The H-TRIS test method was originally developed to study the propensity of high-strength concrete for explosive heat-induced spalling [11]. In the last decade, numerous research-driven and product development projects across multiple institutions (The University of Edinburgh, The University of Queensland, Technical University of Denmark...) have been undertaken using the H-TRIS test method for studying the fire-related aspects of various construction materials and system assemblies [1, 17-20]. Within the research study herein, the H-TRIS test method is adopted for studying the behaviour and effectiveness of thin intumescent coatings under a wide range of conditions in terms of heating, applied initial thickness and substrate characteristics. By accurately quantifying and controlling the thermal boundary conditions, thin intumescent coatings and key aspects related to intumescence are comprehensively investigated.

For example, as mentioned in the introduction section, some research studies have shown that a slow heating regime may have a negative impact on the insulating performance of intumescent coatings, or even show propensity for melting and/or delamination of the protection material. In particular, slow fires and low heating rates may also cause an incomplete swelling of the reactive material, leading to an unsatisfactory insulation to the protected structure

[1, 21-22]. Within this research project, the H-TRIS test method is adopted in order to investigate the onset of swelling of thin intumescent coatings exposed to slow fires, thus low time-histories of incident radiant heat flux. The careful control on the thermal boundary conditions will allow for a holistic understanding of the conditions that led to the initiation of the swelling process of thin intumescent coatings. Furthermore, thanks to the H-TRIS open environment, melting and delamination phenomena can be monitored and recorded.

In addition, there are limited research studies that have performed a comprehensive experimental gauging of the complex response of thin intumescent coating during thermal exposure (refer to Chapter 2). Within this research project, the H-TRIS test method is also embraced in order to characterise the thermal and physical response of thin intumescent coatings exposed to various heating conditions. In particular, thanks to its open environment, H-TRIS allows for the measurement of the real-time thickness of the swelled coating, the temperature evolution of the protected substrate material and the transient thermal gradient within the swelling intumescent coating. Using high-density and precision thermal sensors and various instrumentations, several aspects related to the effectiveness of thin intumescent coatings can be investigated and comprehended thanks to the advantages introduced by the H-TRIS test method compared to traditional furnace testing.

3.3.1 Test samples

The main test samples used in this research study were 200 x 200 mm^2 mild carbon steel plates, 10 mm thick, resulting in a section factor A_p/V (i.e. ratio between exposed surface and volume of steel) equal to 100 m^{-1} (Figure 3.11). Based on the assembled H-TRIS, the sample dimensions were chosen in order to achieve a surface distribution of incident radiant heat flux on the sample surface with a deviation lower than 10%.

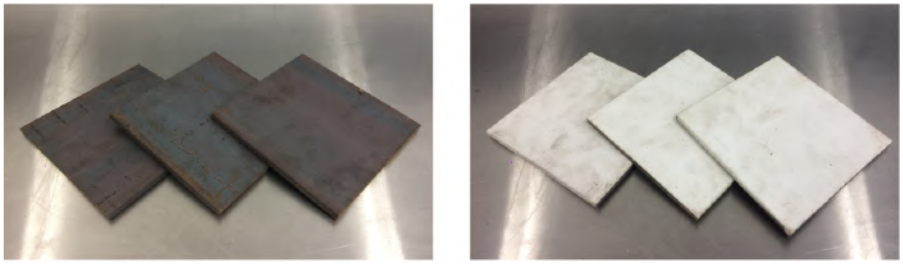

Figure 3.11: Test samples: unprotected steel plates (left) and coated steel plates (right).

The steel plates were first prepared for the application of the thin intumescent coating. The steel plates were cleaned and de-greased in order to remove salts, loose friable materials and any other contaminants. When the sample was dry, the top surface was sand-blasted in order to create a rough surface and facilitate the application and adhesion of the coating. A *"Sa2.5 - Near white metal"* surface preparation grade was ensured, complying with the Swedish Standard SIS 05 59 00 and the International Standard ISO 8501-1 [23-24].
The steel plates were professionally coated with a thin layer of intumescent coating by a registered contractor (Figure 3.12). The fire protection product is a commercially available solvent-based intumescent coating. The product is usually designed for structural steel members in the build environment for an internal, semi-exposed or external use and it is suitable for off-sire and on-site application. It is a fast-track coating and it does not require a primer in low-aggressive environments. According to the design specifications, the intumescent coating can provide up to 120 minutes fire protection to universal steel sections and cellular beams. The coating can be applied to a maximum Dry Film Thickness (DFT) of 6.5 mm. Unfortunately, the commercial name and formulation of the thin intumescent coating can not be shared due to confidentiality agreements.

Figure 3.12: Application of the intumescent coating on steel plates using airless spray equipment.

The thin intumescent coating was applied in one hand using airless spray equipment, without the use of any primer or topcoat (Figure 3.12). The test samples were dried at ambient temperature for about 1 week and then stored in a cold and dry environment. The preparation of test samples happened in two sessions throughout the research project: January 2017 and April 2018. In total, about 230 test samples were prepared and coated.
The initial target Dry Film Thicknesses (DFT) were 1000, 2000 and 3000 μm with an accur-

acy of $\pm$ 10%. In order to understand the quality of the executed work and the uniformity of the coating on the test samples, after one month of curing, the dry film thicknesses were measured by using a non-destructive coating thickness gauge (*Elcometer 456*) at five different locations (Figure 3.13): at the four plate corners and the plate centre. The measured values underlined the high difficulty of applying intumescent coatings in an accurate Dry Film Thickness (DFT): the procedure is thorny, dependent on several conditions (atmospheric pressure, temperature, humidity, applying device...) and difficult to control with good accuracy and repeatability. In general, the measured DFTs varied in a range between 800 and 3400 μm. In order to ensure the repeatability and compatibility between the different experiments, the test samples were selected based on the on the mean DFT measured over the steel plate surface and categorised into different groups (typically *"Low DFT"*, *"Medium DFT* and *"High DFT"*). In this document, the mean DFT values and their accuracy calculated for each coated steel plate are reported in each chapter, in the material and methods section.

Figure 3.13: Dry film thickness (DFT) measuring procedure using the non-destructive coating thickness gauge Elecometer 456 (device accuracy: $\pm$ 10 μm).

3.3.2 Description of the experiments

Depending on the different experimental investigations, uncoated and coated steel plates were individually tested using the H-TRIS test method (Figure 3.14). The test samples were exposed to a range of heating conditions, defined by time-histories of incident radiant heat flux: (1) constant incident radiant heat flux varying between 10 and 90 kW/m^2 and (2) linearly-increasing incident radiant heat flux between 0.5 and 3 kW/m^{2}min. All the experiments lasted for 30 or 60 minutes. The heating conditions were explicitly chosen in order

to subject the intumescent coating to various ranges of temperatures and heating rates, studying different aspects related to intumescence.

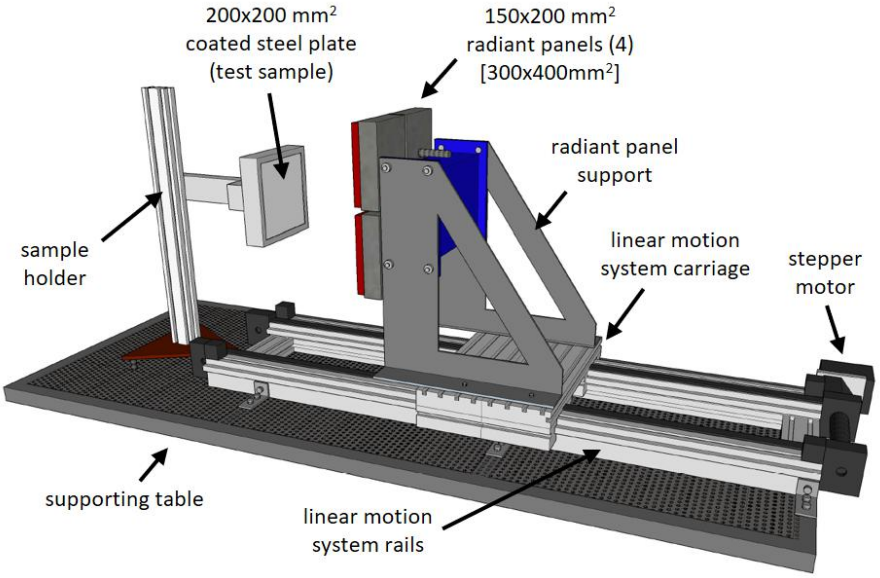

Figure 3.14: Detailed schematisation of the experimental setup based on the H-TRIS test method (*Bench-scale H-TRIS 2.0*).

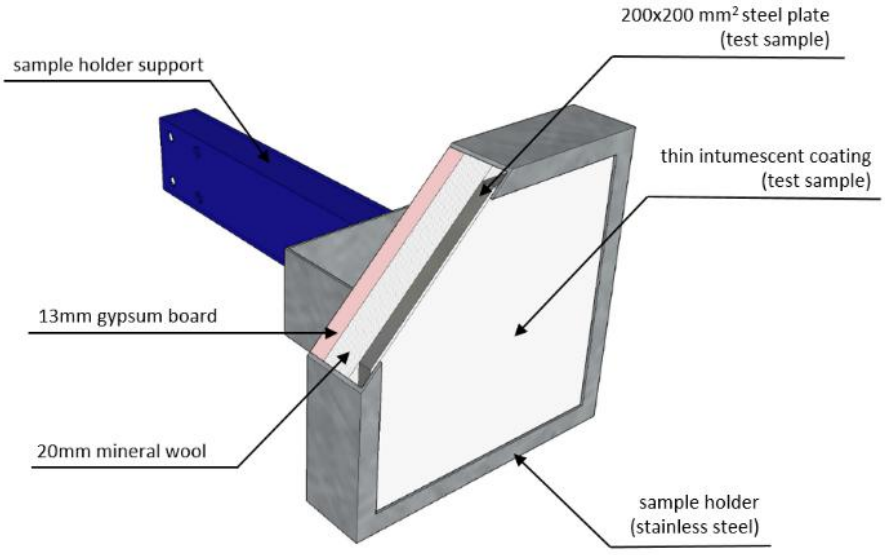

Figure 3.15: Detailed schematisation of the custom-built sample holder reproducing adiabatic thermal boundary conditions at the unexposed surface of the test sample.

During the thermal exposure, custom-built sample holders were used in order to hold the test sample aligned with the centre-point of the radiant panels array, in vertical orientation.

In most of the experiments, in order to replicate adiabatic thermal boundary conditions, heat losses at the back of the test sample were minimised by insulating the unexposed surface of test samples using a layer of 20 mm thick ceramic wool (ISOLITE ISOWOOL 1000 BLANKET 100) and 13 mm thick plasterboard (Knauf FireShield). The sample holder shown in Figure 3.15 was generally used, but in some experimental investigations (e.g. study on the effects of substrate thermal conditions), other custom-built sample holders were involved.

3.3.3 Instrumentation

Within this research study, the experimental setup based on coated steel plates and the H-TRIS test method was systematically instrumented in different ways based on the study objectives. In general, the experimental setup was instrumented in order to carefully gauge different aspects of the thermal and physical response of the intumescent coating during the heating exposure. For instance, several K-type thermocouples were installed in the test samples in order to measure the temperature evolution of the coated steel plate and the transient temperature profile within the intumescent coating. Moreover, the thickness of the swelled intumescent coating was measured by image processing of video footages taken using a high-resolution camera placed at the side of the test sample, aligned with the surface of the test sample. Finally, in some research studies, an Infra-Red camera was used in order to estimate the temperature evolution of the exposed coating surface.
A detailed description of the experimental setup and the implemented instrumentation is reported in each chapter, in the material and methods section.

3.4 Conclusions

In order to overcome the challenges and shortcomings of conventional fire testing, an experimental methodology aimed at analysing the effectiveness of intumescent coatings is presented. The methodology is based on the Heat-Transfer Rate Inducing System (H-TRIS), a well-established test method that enables the careful quantification and control of the thermal boundary conditions imposed on the exposed surface of test samples with high repeatability and low costs. Using a computer-controlled linear motion system, the apparatus controls the relative position between an array of high performance radiant panels and the test sample

in order to replicate well-defined time-histories of heat flux (incident or net).

The described experimental methodology is proposed to study the behaviour and effectiveness of thin intumescent coatings under a wide range of conditions in terms of heating, applied initial thickness and substrate characteristics. Experimental campaigns using steel plates coated with a commercially available solvent-based thin intumescent coating aim at comprehensively understanding various aspects related to intumescence in order to contribute towards performance-based design of fire-safe structures. For instance, the H-TRIS test method is adopted to investigate the onset of swelling and assess the effectiveness of intumescent coatings. The experimental setup was extensively instrumented in order to characterise the thermal and physical response of intumescent coatings during heating exposure by measuring the real-time swelled coating thickness, the exposed surface temperature, the substrate temperature and the in-depth transient temperature profile within its thickness.

Bibliography

[1] Elliott A., Temple A., Maluk C. and Bisby L. "Novel testing to study the performance of intumescent coatings under non-standard heating regimes". Fire Safety Science – Proceedings of the 11th International Symposium, University of Canterbury, New Zealand, pp. 652-665, 2014.

[2] Cirpici B.K., Wang Y.C. and Rogers B. "Assessment of the thermal conductivity of intumescent coatings in fire". Fire Safety Journal, vol. 81, pp. 74-84, 2016.

[3] Kolsek J. and Cesarek P. "Performance-based fire modelling of intumescent painted steel structures and comparison to EC3". Journal of Constructional Steel Research, vol. 104, pp. 91-103, 2015.

[4] Maluk C., Bisby L., Terrasi G., Krajcovic M. and Torero J.L. "Novel fire testing methodology: why, how and what now?". Proceedings of the Mini Symposium on Performance-based Fire Safety Engineering of Structures as part of the 1st International Conference on Performance Based land Life Cycle Structural Engineering, pp. 448-458, 2012.

[5] International Organization for Standardization (ISO). "ISO 5660–5661: International Standard, Fire Tests - Reaction to Fire - Part 1: Rate of Heat Release from Building Products (Cone Calorimeter Method)". Geneva, Switzerland, 1993.

[6] Bartholomai M., Schriever R. and Schartel B. "Influence of external heat flux and coating thickness on the thermal insulation properties of two different intumescent coatings using cone calorimeter and numerical analysis". Journal of Fire Materials, vol. 27, pp. 151-162, 2003.

[7] Zhang Y., Wang Y., Bailey C.G. and Taylor A.P. "Global modelling of fire protection performance of an intumescent coating under different cone calorimeter heating conditions". Fire Safety Journal, vol. 50, pp. 51-62, 2012.

[8] Kang S., Choi S. and Choi J. "Thermal boundaries of intumescent-type insulations in cone calorimeter testing". Fire Science and Technology 2015, Proceeding of 10th Asia-Oceania Symposium on Fire Science and Technology, pp. 705-714, 2015.

[9] Jimenez M., Duquesne S. and Bourbigot S. "Intumescent fire protective coating: toward a better understanding of their mechanism of action". Thermochimica Acta, vol. 449, no. 1-2, pp. 16-26, 2006.

[10] Bourbigot S. and Duquesne S. "Fire retardant polymers: recent developments and opportunities". Journal of Material Chemistry, vol. 17, pp.2283-2300, 2007.

[11] Maluk C., Bisby L., Krajcovic M. and Torero J.L. "A Heat-Transfer Inducing System (H-TRIS) Test Method". Fire Safety Journal, vol. 105, pp. 307-319, 2019.

[12] Filtz J.R., Lièvre M., Valin T., Hameury J., Wetterlund I., Persson B., Andersson P., Jansson R., Lemaire T., Öhlin M. and Myllymäki J. "Improving Heat Flux Meter Calibration for Fire Testing Laboratories (HFCAL)". Technical report elaborated for the Direction Générale des Affaires Economiques et Financières, Brussels, France, pp. 121, 2002.

[13] International Organization fro Standardization (ISO). "ISO 14934-4:2007 Fire tests – Calibration and Use of Heat Flux Meters – Part 4: Guidance on the Use of Heat Flux Meters in Fire Tests". Geneva, Switzerland, 2007.

[14] Incropera F.P., DeWitt D.P., Bergman T.L. and Lavine A.S. "Fundamental of heat and mass transfer". John Wiley & Sons, 6th Edition, 2006.

[15] Robertson A.F. "Development of an improved radiant heat source for fire testing". Fire and Materials, vol. 6, no. 2, 1982.

[16] Laschutza T. "Numerical and experimental investigation of a Thin Skin Calorimeter (TSC)". MSc thesis, School of Engineering, The University of Edinburgh, 2017.

[17] Maluk C., Bisby L. and Terrasi G.P. "Effects of polypropylene fibre type and dose on the propensity for heat-induced concrete spalling". Engineering Structures, vol. 141, pp. 584-595, 2017.

[18] Lucherini A., Razzaque Q.S. and Maluk C. "Exploring the fire behaviour of thin intumescent coatings used on timber". Fire Safety Journal, vol. 109, no. 102887, 2019.

[19] Bartlett A., Hadden R., Bisby L. and Law A. "Analysis of cross-laminated timber charring rates upon exposure to non-standard heating conditions". Fire and Materials, 2015.

[20] Hidalgo J.P. "Performance-based methodology for the fire safe design of insulation materials in energy efficient buildings". PhD thesis, School of Engineering, The University of Edinburgh, 2015.

[21] McNameer R.J., Storesund K. and Stolen R. "The function of intumescent paint for steel during different fire exposures". SP Sveriges Tekniska Foreskningsinstitut, SP Rapport 2016, vol. 43, 2016.

[22] Lucherini A., Giuliani L. and Jomaas G. "Experimental study of the performance of intumescent coatings exposed to standard and non-standard fire conditions". Fire Safety Journal, vol. 95, pp. 42-50, 2018.

[23] Svensk Standard. "SIS 05 59 00:1967 Preparation Of Steel Substrates Before Application Of Paints & Related Products - Visual Assessment Of Surface Cleanliness". Stockholm, Sweden, 1967.

[24] International Organization fro Standardization (ISO). "ISO 8501-1:2007 Preparation of steel

substrates before application of paints and related products - Visual assessment of surface cleanliness - Part 1: Rust grades and preparation grades of uncoated steel substrates and of steel substrates after overall removal of previous coatings". Geneva, Switzerland, 2007.

4

Material characterisation

4.1 Introduction and background

The literature review has highlighted how practitioners and researchers have developed several simplified formulas or mathematical/numerical models in order to predict and replicate the thermal barrier provided by swelling intumescent coatings to structural elements during fire. These models have a key role for the development of performance-based design solutions, which are becoming more popular and a common trend in the space of structural fire safety engineering design.

The current design framework offers only one regulated engineering method for the performance-based design of fire-safe steel structures protected with intumescent coatings: the European assessment method based on the concept of *effective thermal conductivity* (Annex E of EN 13381-8) [1]. This method simplifies the heat transfer through a reactive coating into an effective parameter (λ_{eff}) that replicates an equivalent thermal barrier provided by the intumescent coating to the steel substrate. The method is fully empirical as it relies on experimental measurements obtained in standard fire resistance furnace tests. In addition, this method is usually applied for standard fire conditions, whose results can not typically be extended to other heating conditions due to reactive nature of intumescent coatings.

In the last decades, many other models and design tools have been developed by the research community in order to overcome the limitations of the current design framework. However, none of these models has never been universally agreed or internationally regulated. Consequently, they are not widely adopted, also because of their limited application or high complexity. Moreover, all these models and formulations require a number of parameters and material properties to simulate the behaviour of intumescent coatings exposed to fire conditions. Due to the different approaches and methodologies, each model is based on different parameters and material properties, which sometimes are even defined differently (e.g. thermal conductivity). This yield to specific models that can be hardy generalised and differ case by case and for each intumescent product.

This lack of harmonisation and generalisation created confusion in the definition and evaluation of the physical and thermal properties of intumescent coatings, fundamental parameters for the development of any heat transfer model. Table 4.1 reports an extended literature review of the main material properties of intumescent coatings available in the literature.

Table 4.1: Review of the material properties of intumescent coatings available in literature.

Source	Data type	Swelling Ratio	Thermal conductivity	Heat capacity	Density	Emissivity
		d_c/DFT [-]	λ [W/mK]	c_p [J/kgK]	ρ [kg/m^3]	ε [-]
Weisheim 2019 [2]	Exp.+Mod.	34-44	0.10-1.40	-	50-1300	0.80
de Silva 2019 [3]	Exp.	18-32	0.01-0.05(λ_{eff})	1200	200	0.95
Wang 2019 [4]	Exp.	9-32	0.01-0.10(λ_{eff})	-	-	-
Luangtriratana 2018 [5]	Exp.	2-26	0.09-0.53	-	-	-
Kang 2018 [6]	Exp.+Mod.	-	0.05-0.40(λ_{app})	-	-	-
Bozzoli 2018 [7]	Exp.+Mod.	-	0.25-0.45(λ_{app})	-	-	-
Lucherini 2018 [8-9]	Exp.	10-83	0.03-0.50(R_{eff})	-	1300	0.92
Xu 2018 [10]	Exp.	5-43	0.01-0.03($\lambda_{eff,const}$)	-	-	-
Kang 2017 [11]	Exp.+Mod.	9-11	0.10-1.60(λ_{eff})	-	$f(T)$	0.77
Li 2017 [12]	Exp.	-	0.01-0.05($\lambda_{eff,const}$)	-	-	-
Cirpici 2016 [13]	Exp.	5-37	0.10-1.20(λ_{app}) 0.01-0.50(λ_{eff})	-	-	-
Li 2016 [14]	Exp.	-	0.01-0.04($\lambda_{eff,const}$)	-	-	0.92
Nadjai 2016 [15]	Exp.+Mod.	-	λ_{eff}	1000	1300	-
Bilotta 2016 [16-17]	Exp.+Mod.	-	53.3(virgin) 0.01-0.04(λ_{eff})	1200	200	0.95
Kolsek 2015 [19]	Exp.+Mod.	-	$f(DFT, A/V)$	1000	100	-
Wang 2015 [19]	Exp.	10-24	0.01-0.12(λ_{eff})	-	-	-
Elliott 2014 [20]	Exp.	19-48	0.05-0.35(λ_{eff})	-	-	-
Rush 2014 [21]	Exp.	-	0.35-0.50(λ_{eff})	-	-	-
EN13381-8 2013 [1]	-	-	λ_{eff}	1000	100	-
Gardelle 2013 [222]	Exp.	10-34	0.22-0.50	-	-	-
Muller 2013 [23]	Exp.	-	0.05-0.45	-	-	-
Wang 2013 [24]	Exp.	10-46	0.01-0.20(λ_{eff})	-	-	-
Gardelle 2012 [25]	Exp.	-	0.13-0.35	-	-	0.92
Zhang 2012 [26-27]	Mod.	15-50	-	1884	1400	-
Li 2012 [28]	Exp.+Mod.	-	0.03-0.06($R_{eff,const}$)	-	-	0.92
Wang 2012 [29]	Exp.+Mod.	10-46	0.01-0.15(λ_{eff})	-	-	-
Staggs 2012 [30]	Exp.+Mod.	10-12	0.36(char) 0.026(gas) 0.009(rad)	1498(virgin) 2170(gas) 663(char)	1200(virgin) 1(gas) 1186(char)	-
Staggs 2010 [31]	Mod.	-	0.10-0.50(λ_{eff})	-	-	-
Griffin 2010 [32]	Exp.+Mod.	10-60	0.20-0.24(virgin) $f(T)$(gas)	1500(virgin) $f(T)$(gas)	1100-1270(virgin) $f(T)$(gas)	0.92
Dai 2010 [33]	Exp.	-	0.01-0.50(λ_{eff})	1000	1300	-
Opstad 2010 [34]	Exp.+Mod.	-	0.02-0.08	840	1600	-
Yuan 2009 [35]	Exp.+Mod.	10-60	0.05-0.50(λ_{eff})	1884	1340-1400	1.00
Bartholmai 2007 [36]	Exp.+Mod.	-	0.06-0.20(R_{eff})	1	1	0.95
Omrane 2007 [37]	Exp.+Mod.	30-70	-	1000	1000	0.92
Griffin 2005 [38]	Exp.+Mod.	5-25	0.005-0.20(R/d)	-	-	-
Wang 2005 [39]	Mod.	-	<0.10(λ_{eff})	1000	1000	0.92
Bartholmai 2003 [40]	Exp.+Mod.	-	0.01-0.30(R_{eff})	1	1	0.95
Bourbigot 1999 [41]	Exp.+Mod.	-	0.60-1.00	2800-5300	-	-
Henderson 1985 [42]	Exp.+Mod.	-	0.70-1.00(virgin) 0.70-2.00(char)	$f(T)$(virgin) $f(T)$(char)	1810(virgin) 880-1440(char)	0.90
Anderson 1985 [43]	Exp.+Mod.	2-10	2.31(virgin) 0.83(char)	840	1490	-

The *thermal conductivity* usually represents the main performance criteria for an intumescent coating as it estimates its insulating capacity. However, due to the complex thermo-physical response, the evaluation of the thermal conductivity, as well as any other material property, is very challenging for swelling intumescent coatings. As a consequence, many researchers made an effort to evaluate this specific parameter in many different ways and making numerous assumptions [2-43]. The effective thermal conductivity λ_{eff} in accordance with the European assessment method is the most common way to evaluate the thermal conductivity of intumescent coatings [1, 3-4, 11, 13, 15, 16-17, 19-21, 24, 29, 31, 33, 35, 39]. The insulating capacity is simplified in an effective parameter, which incorporates the swelling of the intumescent coating, as well as several phenomena that occur in the intumescent process, such as endo- and exothermic reactions. In a few cases, the effective thermal resistance R_{eff} was preferred [8-9, 36, 40]. Other researchers proposed the concept of effective constant thermal conductivity $\lambda_{eff,const}$ calculated within the temperature range of interest for fire-safe design of steel structures (400-600°C) [10, 12, 14, 28]. Contrarily to effective values, other research studies evaluated the apparent thermal conductivity λ_{app} considering the actual swelled coating thickness and sometimes using in-depth temperature measurements within the swelled coating [6-7, 13]. Finally, only in a few research studies, the steady-state thermal conductivity was measured, for example using a TPS equipment [5, 22-23].

In many of the mentioned heat transfer models and formulations, the thermal capacitance of the intumescent coating is neglected in comparison with the thermal capacitance of the protected steel element. For example, this is the case of the European effective thermal conductivity method [1]. In these methods, the evaluation of the specific heat capacity c_p and the density ρ of the intumescent coating has a marginal importance. Rarely, the specific heat capacity is calculated through Differential Scanning Calorimetry (DSC) experiments and analysis [2]. The same concepts apply to the density of the intumescent coating which is rarely evaluated starting from mass/volume measurements and Thermo-Gravimetric Analysis (TGA) experiments [2].

Finally, the optical properties of materials, particularly emissivity and absorptivity, have a key role in thermal radiation and heat transfer: they govern the radiative heat transfer and heat losses between emitting surfaces. In the case of intumescent coatings, the optical properties are usually disregarded because the swelling coating is assumed as thermally thick material,

therefore its surface temperature can be approximated with the fire gas phase temperature (e.g. European effective thermal conductivity method [1]). In other cases, the absorptivity and emissivity of intumescent coatings are assumed a priori or implicitly obtained through the calibration of numerical models [37].

Generally, the research community has produced a vast amount of heat transfer models and formulations aimed at reproducing the response of intumescent coatings during fire. However, the material properties have never been universally defined and each specific model relies on its assumptions and characteristic parameters, which are often hard to evaluate (e.g. coating porosity and melting temperature) and they may differ product by product.

Within the scope of this research, a set of complementary studies using standard experimental methodologies were conducted in order to integrate the experiments conducted using the H-TRIS test method and achieve a preliminary understanding of the physical, thermal and optical properties of the tested intumescent coating at ambient and elevated temperatures. The experiments also investigated the chemical reactions and the thermal decomposition processes occurring in the intumescent coating at different temperatures and under different heating regimes. These studies represented a starting point for the material characterisation and modelling of any heat transfer process involving the tested intumescent coating.

4.2 Experimental methodologies

4.2.1 Thermo-Gravimetric Analysis (TGA)

Thermo-Gravimetric Analysis (TGA) is a common technique used to quantify the decomposition processes that a certain material experiences at different temperatures. These processes are determined in terms of mass loss with respect to temperature increases. This understanding is fundamental to characterise the performance of various materials under severe heating conditions. A thermogravimetric analyser commonly consists of a furnace where small samples contained in crucibles (order of a few milligrams) are placed on a calibrated load cell which records the evolution of the sample mass as a function of the sample temperature (temperature-varying experiments) or as a function of time (isothermal experi-

ments). Due to the small size of the tested sample and the relatively low heating rates, the influence of heat transfer is marginalised, hence the samples are not expected to experience a significant thermal gradient. In addition, the environment inside the furnace can be controlled in a way to create an oxidising atmosphere (air flow) or a reducing atmosphere (nitrogen flow) [44-45].

Thermo-Gravimetric Analysis (TGA) was performed on small powder samples of dry intumescent coating (8-10 mg). The test samples were prepared by finely cutting a small piece of dry intumescent coating and creating a fine homogeneous powder. The main aim of these experiments was to study the thermal decomposition of the intumescent coating and understand at which temperature ranges the different reactions occur, particularly the intumescent swelling reaction. The TGA experiments were carried out using a PerkinElmer STA 6000 (Figure 4.1). The intumescent coating was tested in the temperature range 30-900°C under four different constant heating rates: 5, 10, 20 and 30°C/min. Experiments were repeated twice in order to check the repeatability of the results. In addition, the influence of the surrounding atmosphere (air or nitrogen) was investigated. In all experiments, the flow rate of the atmospheric gas was kept equal to 20 ml/min.

4.2.2 Differential Scanning Calorimetry (DSC)

Differential Scanning Calorimetry (DSC) is usually performed in parallel to the Thermo-Gravimetric Analysis (TGA) in order to achieve a better understanding of the decomposition processes and phase changes of a certain material from the calorimetric point of view. DSC is a common technique to quantify the heat flows related to the thermal degradation processes that a certain material experiences at different temperatures. Similarly to a thermogravimetric analyser, the apparatus consists of a furnace where small samples contained in crucibles (order of a few milligrams) are located. In this case, a heat flux gauge is provided in order to measure the heat flows experienced by the sample crucible. The outcome is the evolution of the heat flow as a function of the sample temperature (temperature-varying experiments) or as a function of time (isothermal experiments). Similarly to TGA, in these experiments the influence of heat transfer is marginalised and the effects of different atmospheres (oxidising or reducing) can be investigated. Due to the close similarity of the two experiments, TGA and DSC are sometimes coupled in the same equipment: in this case, it

is known as *Simultaneous Thermal Analysis (STA)* [44, 46].

Differential Scanning Calorimetry (DSC) was performed on small powder samples of dry intumescent coating (8-10 mg). The test samples were prepared in the same way as for TGA experiments. The main aim of these experiments was to study the reactivity of the intumescent coating in terms of calorimetry. In particular, the experiments focused on quantifying the heat flow experienced by the sample in order to increase its own temperature, while it was experiencing different phases changes and reactions, such as melting and swelling. The DSC experiments were carried out using a Thermal Analysis (TA) Instrument Q2000 (Figure 4.2). The intumescent coating was tested under a constant heating rate of 10℃/min in reducing atmosphere (nitrogen) and in the temperature range 30-500℃. The experiment was repeated four times in order to check the repeatability of the results. In all experiments, the flow rate of the nitrogen was kept equal to 50 ml/min.

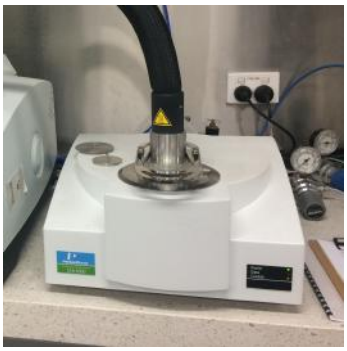

Figure 4.1: PerkinElmer STA 6000 for Thermo-Gravimetric Analysis (TGA).

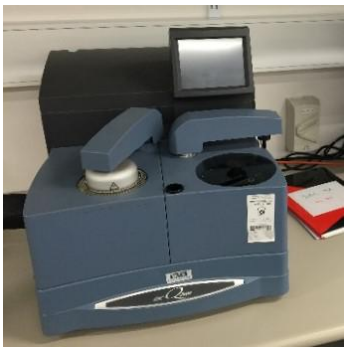

Figure 4.2: Thermal Analysis (TA) Instrument Q2000 for Differential Scanning Calorimetry (DSC).

4.2.3 Transient Plane Source (TPS)

A series of experiments using the *Transient Plane Source (TPS)* equipment was conducted in order to estimate the physical and thermal properties of the intumescent coating. The Transient Plane Source (TPS) method is a transient technique used for thermal characterisation of solid materials. This method is based on a transiently heated plane sensor that conducts electrical impulses and measures the thermal transport properties of materials, such as thermal conductivity, thermal diffusivity and volumetric specific heat capacity. Difference sensors (size or type) can be used based on the testing temperature range, the dimensions of the test sample and the thermal properties of the tested material. Particu-

larly, the sensor radius is usually selected depending on the sample thickness and material properties. The technique assumes semi-infinite solids and consequently the thermal wave produced by the sensor has to be contained within the sample thickness. Therefore, certain sensors are suitable for certain materials with specific sample dimensions. The testing time and power are usually set accordingly. The experiments are usually performed at ambient temperature using a dedicated sample holder, but the same process can be conducted at elevated temperature using a dedicated furnace and heat-resistant sensors [47-48].
The experiments using the Transient Plane Source (TPS) equipment were performed on several bench-scale prisms of intumescent coatings, cut in size depending on the type of measurement. The TPS experiments were carried out using a Hot Disk Thermal Constants Analyser TPS 1500 S (Figure 4.3a). Experiments were repeated at least twice for each different configuration and sample in order to check the repeatability of the results. The following groups of TPS experiments were conducted:

- *Experiments at ambient temperature on solid prisms of dry intumescent coating*. The samples dimensions were 100 x 60 x 18 mm^3 and the experiments were conducted in open environment (air) using the dedicated sample holder (Figure 4.3b).
- *Experiments at ambient temperature on swelled porous chars of the intumescent coating* obtained from the H-TRIS experiments. The measurement was carried out by placing the sensor between two outer surfaces of the swelled porous char (Figure 4.3c) or in-between the swelled porous char (Figure 4.3d). The test samples had sightly different dimensions, but the thickness was always higher than 20 mm. As in the previous case, the experiments were conducted in open environment (air) using the dedicated sample holder.
- *Experiments at elevated temperatures on solid prisms of dry intumescent coating*. The initial sample dimensions were 100 x 60 x 13 mm^3. The experiments were conducted under nitrogen-rich environment using the dedicated small cylindrical furnace (Figure 4.3e). Since the confined space of the cylindrical furnace did not allow the complete swelling of the intumescent coating, the experiments were performed for temperatures presumed to be below swelling conditions; hence, below 250℃. The measurements were conducted at 50℃ intervals, after a stabilisation time of at least 30 min.

Depending on the dimensions and the thermo-physical properties of the test sample, the testing power and time was set accordingly with a trial and error process. In general, the experiments were conducted using the Kapton5465 (3.189 mm radius) or the Kapton5501 sensor (6.403 mm radius) and applying a testing power 20-160 mW for a duration of 20-160 sec.

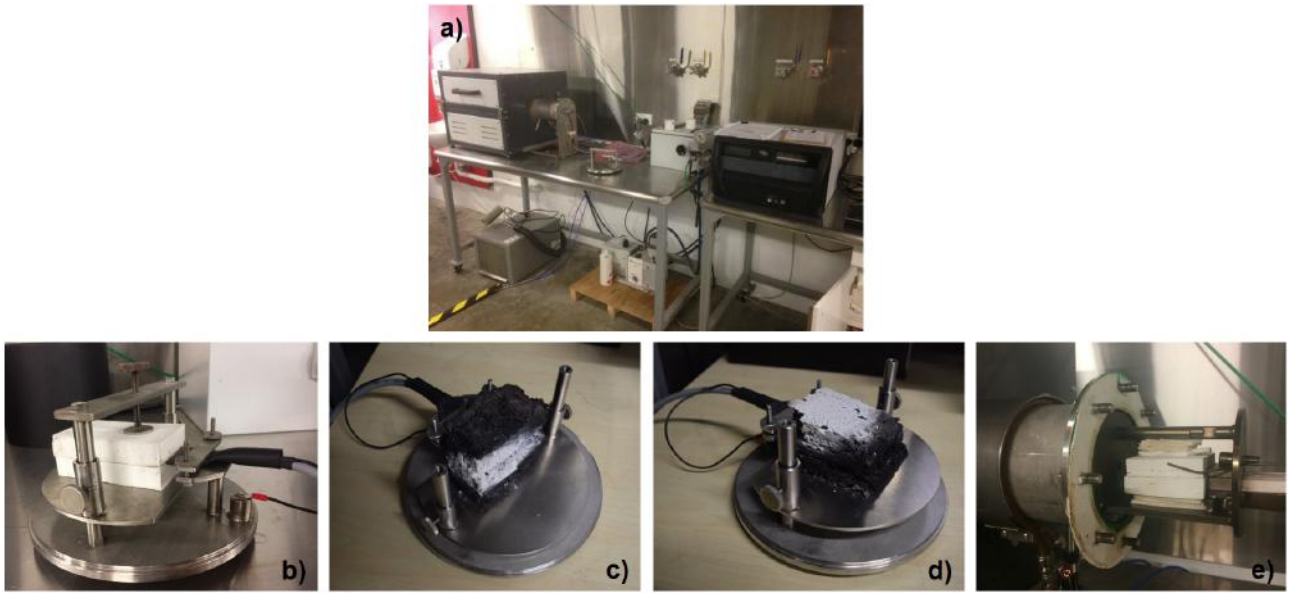

Figure 4.3: a) Hot Disk Thermal Constants Analyser TPS 1500 S equipment; b) Experiments at ambient temperature on solid prisms; c) d) Experiments at ambient temperature on swelled porous chars (surface-surface and inter-char); e) Experiments at elevated temperatures on solid prisms.

4.2.4 Laser Flash Analysis (LFA)

Another standard methodology to evaluate the thermal properties of materials is the *Laser Flash Analysis (LFA)*. The technique adopts equivalent principles to the TPS method, but the LFA methodology uses laser technology to measure the thermal transport properties of solid or liquid materials. During the experiments, test samples are heated by an electrical furnace with a constant heating rate and thermal properties of materials are measured using a pulsed laser and an Infra-Red detector. In this way, the LFA method allows for fast and reliable measurement of thermal diffusivity and thermal conductivity of materials over a broad temperature range (-120℃ to 2800℃) [49-50].

In collaboration with Netzsch, a series of LFA experiments were conducted to measure the thermal and physical properties of the intumescent coating and compare them to the one

obtained following the TPS method. Bench-scale circular disks of solid dry intumescent coating (12.7 mm diameter, 3 mm thick) were tested in a nitrogen-rich environment. The experiment was carried out once using the NETZSCH Laser Flash Apparatus LFA 467 HyperFlash (Figure 4.4). Prior to the measurement, the front and the back of the sample were coated with graphite to enhance the emission/absorption properties of the sample. Since the LFA methodology assumes constant physical properties of the test sample (i.e. constant thickness), the swelling of the intumescent coatings would have produced results with significant errors. Consequently, as in the TPS case, the experiments were performed for temperatures presumed to be below swelling conditions; hence, below 250℃.

4.2.5 Integrating Sphere System (ISS)

Integrating Sphere System (ISS) is an experimental equipment used for measuring the diffuse reflection and diffuse transmission of a wide range of materials. The integrating sphere is a hollow sphere coated with highly reflective and optically diffuse material (e.g. gold). Inside the sphere light is often introduced by using a laser beam: light enters the sphere and it is reflected several times by the wall of the sphere, resulting in ideal uniform illumination. Test samples are mounted behind an aperture, usually along the radius of the sphere, and they are illuminated by the reflected light. In order to determine the sample reflectance, the radiance inside the sphere measured by a detector is compared to the radiance obtained when the sample is replaced by a reflectance standard illuminated with the same light source at the same intensity. In this way, the diffuse reflection and diffuse transmission of solid and liquid materials can be measured [51-52].
The optical properties of the intumescent coating were studied using an Integrating Sphere System (ISS) apparatus (PIKE Upward IntegratIR) coupled with an FTIR (Fourier-Transform Infrared Spectroscopy) apparatus (Figure 4.5). All the experiments were performed at ambient temperature in open environment (air) and they were arranged according to the following groups:

- *Experiments on dry intumescent coating*. Thin sheets or small solid prisms of dry intumescent coating were tested by placing them on the sample port of the integrating sphere apparatus.

- *Experiments on swelled porous chars of the intumescent coating* obtained from the H-TRIS experiments. The measurements were carried out by placing the swelled porous char of the intumescent coating on the sample port of the integrating sphere apparatus. The tested surface was always the one exposed to the thermal radiation in the H-TRIS experiments. These experiments were conducted in order to evaluate the residual reflectivity of the intumescent coating with different degrees of degradation due to thermal exposure.

The reflectivity of the virgin and degraded intumescent coating was measured in a range of wavelengths included between 2 and 20 μm. This range covers most of the total thermal radiation emitted by a typical building fire, usually characterised by high soot content. This range is commonly included in the near-infrared and mid-infrared radiations [53-54].

Figure 4.4: NETZSCH Laser Flash Apparatus LFA 467 HyperFlash.

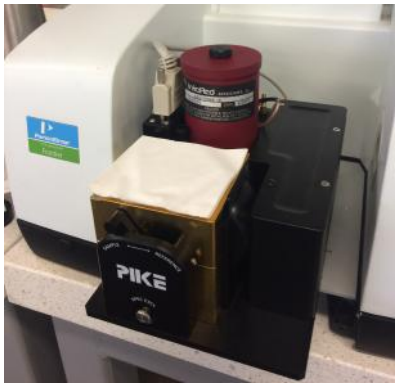

Figure 4.5: Integrating Sphere System (ISS) apparatus (PIKE Upward IntegratIR).

4.3 Experimental results

4.3.1 Material characterisation (TGA and DSC)

Figure 4.6 and Figure 4.7 present the results obtained from the TGA experiments in terms of normalised mass and its derivative (DTG curve) in reducing (nitrogen) and oxidising (air) atmosphere respectively. According to the available literature, the TGA results highlight that the product tested in this experimental study has similar characteristics to typical intumescent formulations [27, 32, 38, 55-59]. The most common intumescent formulations

are typically composed of a combination of *ammonium polyphosphate (APP)* as carbonisation catalyst, *pentaerythritol (PER)* as carbonisation agent, *melamine (MEL)* as blowing agent and acrylic resin as carbonic agent and binder. Based on the TGA results, the tested intumescent coating behaves like a APP–PER–MEL system, which typically decomposes according to the following stages:

- *"Thermal decomposition zone"* or *"melting zone"* - the carbonisation catalyst (e.g. APP) and carbonisation agent (e.g. PER) transform their crystalline structure and melt at temperatures between 200 and 300℃, increasing the coating viscosity and releasing volatiles. This reaction can be associated with the first peak in the DTG curves, which produces a mass loss of about 20%.

- *"Reaction zone"* or *"swelling zone"* - the further decomposition and interaction of the different chemical compounds lead to the formation of the expanded char structure by esterification. The blowing agent (e.g. MEL) is activated and it releases large quantities of non-flammable gases (e.g. NH_3 and CO_2), which are trapped within the coating to cause the molten matrix to swell into a "honeycomb" char structure. The second peak in the DTG curves denotes this process at temperatures between 300 and 400℃, producing a mass loss of about 20-25%.

- *"Char degradation zone"* or *Char structural changes zone* - at temperatures above 550℃, the expanded carbonaceous char further degrades and starts to decompose. The carbon in the porous char structure is oxidised, CO_2 is formed and released from the system. The decomposition of the intumescent char can be associated with the two small peaks in the DTG curves in oxidising atmosphere: a first reaction was detected at about 650℃ and a second reaction at about 750℃. The oxidation reactions usually produce a minor mass loss (about 5-10%). At the end of this stage, only the inorganic content of the coating remain, about 40-45% of the initial mass.

The single reactions of the different compounds are often difficult to outline because of the synergic effect of blowing agent, carbonization catalyst and agent due to their similar decomposition and reaction temperatures. However, the effectiveness of intumescent coatings mainly depends on the formation of swelled porous char, which is triggered by reactions among ammonium polyphosphate, pentaerythritol and melamine.

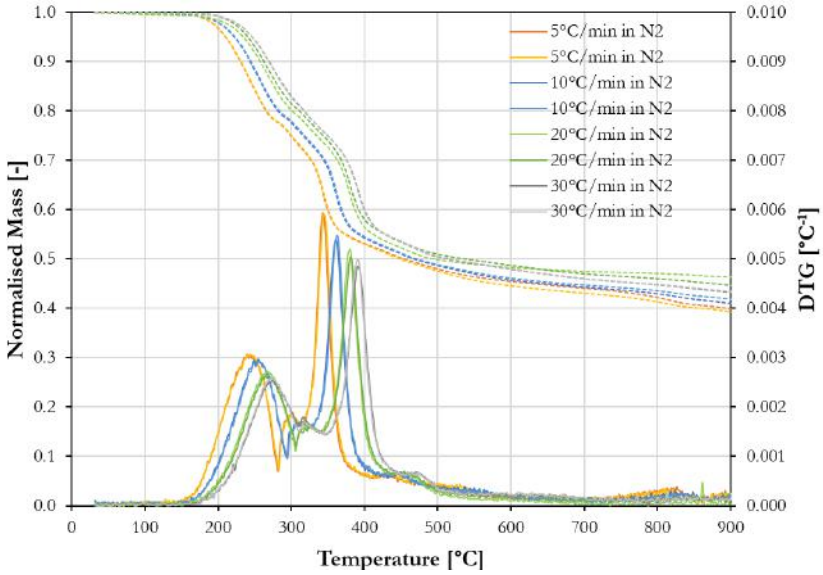

Figure 4.6: TGA experiments in reducing atmosphere (nitrogen) under different heating rates.

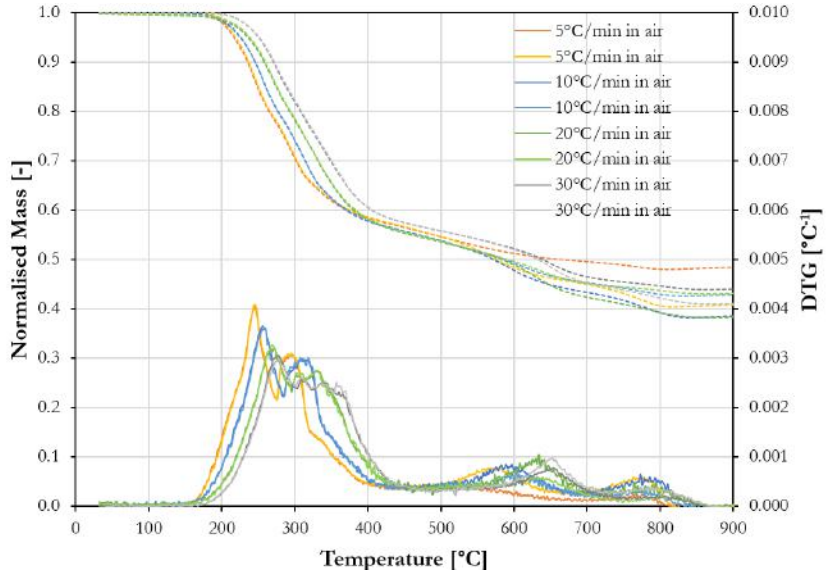

Figure 4.7: TGA experiments in oxidising atmosphere (air) under different heating rates.

In general, it is important to underline that the intumescent swelling reaction (second DTG peak) typically occurs at temperatures between 300 and 400℃ and the main reactions of the intumescent coating can be considered to be completed at about 400-450℃. At that temperature the main decomposing and swelling reactions are completed: the majority of the mass has been lost (about 40%), seeing the significant amount of inorganic compounds (about 40-45%). The different atmospheres do not affect the temperature range for the main reactions ($\sim$200-400℃). However, an oxidising atmosphere results in reactions shifting to-

wards lower temperatures with a lower reaction rate compared to a reducing atmosphere. In addition, as expected, the oxidation stage of the intumescent char is only detected in air atmosphere for coating temperatures above 550 ℃. Lastly, higher heating rates cause reactions to shift to higher temperatures: this effect is minor for onset temperatures, but it is more pronounced for peak temperatures [44].

Aside from the decomposition processes detected through the TGA results, the DSC experiments help to better understand the thermal degradation and phase changes of the intumescent coating from a calorimetric aspect. Figure 4.8 compares the results obtained from the TGA experiments to the ones obtained from the DSC experiments, carried out in reducing atmosphere (nitrogen), under an heating rate of 10 ℃/min and in the temperature interval 30-500 ℃. The DSC results are presented in terms of heat flow, namely the heat absorbed by the test sample to increase its temperature, divided by its own mass.

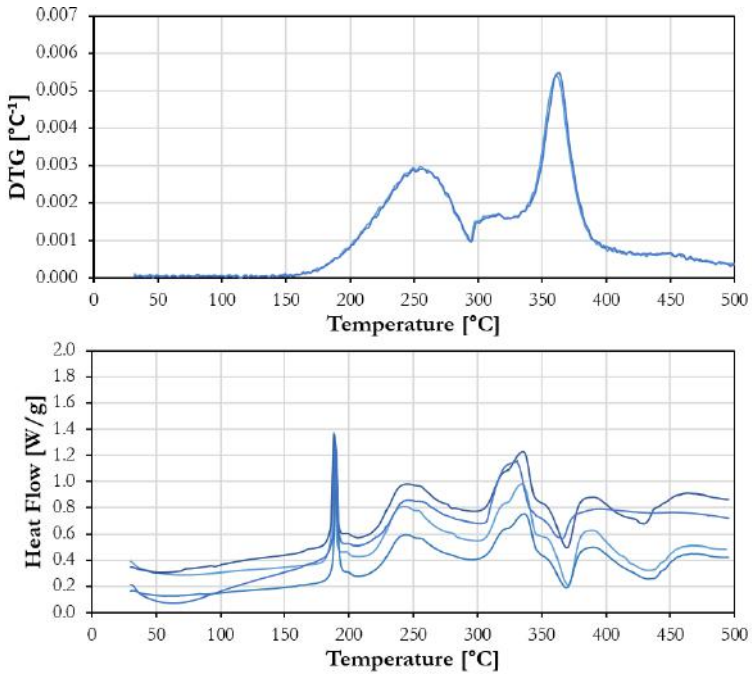

Figure 4.8: Comparison between the DTG curve (above) and DSC curve (below, endothermic reaction ↑) in reducing atmosphere (nitrogen) under 10 ℃/min.

Firstly, conversely to the TGA experiments, the DSC results highlight a scarce repeatability and reliability, likely due to an incorrect calibration of the equipment. Therefore, no assessment of the enthalpy of the different reactions is presented. However, the DSC curves are

useful to understand the general calorimetric characteristics of the different reactions occurring within the tested intumescent coating.

The DSC experiments evidence a first endothermic reaction happening in the intumescent coating at about 190 °C. This peak defines the beginning of the first reaction detected from the TGA experiments ("melting zone"). The reaction represents the melting of the acrylic resin, the carbonisation agent and the carbonisation catalyst: these compounds are subjected to a phase change (no mass loss) as they transform their crystal structure [55, 60]. Since the reaction occurs for each experiment at a specific temperature (around 190 °C), it appears thermally stable.

The second (about 250 °C) and third endothermic peaks (about 330 °C) are dominated by the decomposition of the blowing agent, the release of gaseous products and the formation of the expanded char structure by esterification. This process is triggered by endothermic reactions among ammonium polyphosphate, pentaerythritol, melamine and acrylic resin [2, 55, 61]. At similar temperature, about 370 °C, an exothermic peak is also recorded, but the available literature does not provide sufficient information regarding this reaction. In general, the main intumescent reactions occurring at the temperature range 200-400 °C are typically endothermic.

Above 400 °C, the performed DSC experiments does not provide a clear understanding of the reaction occurring in the intumescent coating. However, in oxygen-rich atmosphere, oxidation reactions are expected to happen above 550 °C, as confirmed by the TGA experiments. These reactions are typically characterized by exothermic peaks due to the oxidation of the swelled porous char and the release of carbon dioxide [55].

4.3.2 Thermal and physical properties (TPS and LFA)

Prior to swelling

The final average values of thermal conductivity, thermal diffusivity and specific heat capacity of the intumescent coating measured for temperatures up to 250 °C using the TPS and LFA test methods are collected in Table 4.2 and shown in Figure 4.9. This research study constitutes the first application of the LFA method to intumescent coatings, while a few researchers has already measured the thermal properties of intumescent coatings using the

TPS method [5, 22-23].

The experimental outcomes obtained from the two test methods produced results with good agreement. In the available literature, similar values were evaluated on different intumescent products following the TPS method [5, 22-23]. These results also confirm the small influence of temperature on the thermal properties of the coatings prior to swelling: at 250℃ the main degradation processes have not started yet or they are at a preliminary stage [23]. In particular, the thermal conductivity slightly decreases for higher temperatures, starting from about 0.50 W/mK at ambient temperature to about 0.30 W/mK at 250℃.

In addition, the density of the virgin dry intumescent coating at ambient temperature was evaluated by simple mass/volume measurements: ρ_c = 1500 $\pm$ 100 kg/m^3. According to its characterisation, the intumescent coating is expected to maintain this density until the temperature that triggers the first degradation reaction (about 200℃) is reached.

Table 4.2: Pre-swelling thermal and physical properties of the tested intumescent coating according to TPS and LFA methodologies.

	T[℃]	λ_c [W/mK]	α_c [mm^2/s]	$c_{p,c}$ [J/kgK]	ρ_c[kg/m^3]
	25	0.501	0.25	1293	1500
	50	0.494	0.235	1364	1500
TPS	100	0.484	0.207	1540	1500
	150	0.458	0.181	1692	1500
	200	0.336	0.124	1860	-
	30	0.503	0.245	1375	1500
	44	0.496	0.235	1410	1500
	66	0.495	0.236	1402	1500
	87	0.465	0.188	1667	1500
	109	0.452	0.173	1762	1500
LFA	131	0.440	0.172	1724	1500
	154	0.433	0.156	1855	1500
	178	0.354	0.129	1829	1500
	201	0.326	0.124	1759	-
	224	0.308	0.119	1736	-
	245	0.304	0.120	1686	-

Swelled coating char

The influence of elevated temperatures on the thermal properties of intumescent coatings have been previously evidenced by a few research studies involving the TPS method [5, 22-23]. These experiments showed how temperatures below onset of swelling (200-250℃) only

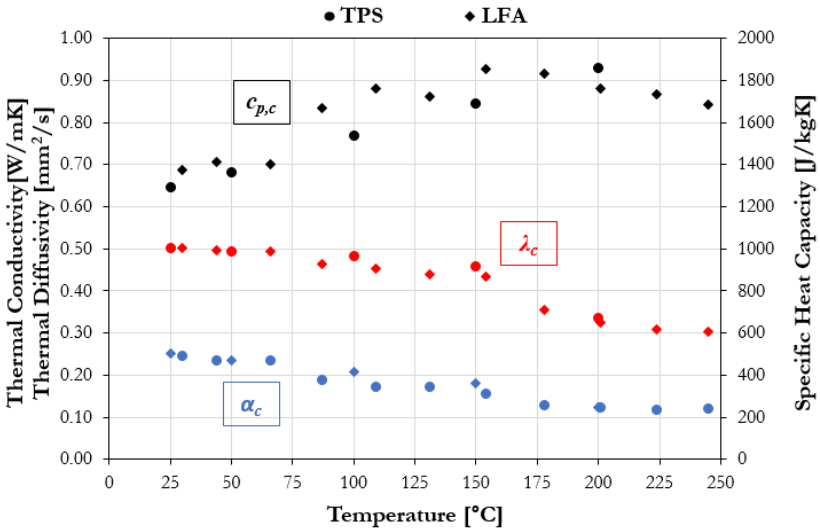

Figure 4.9: Average values of thermal conductivity, thermal diffusivity and specific heat capacity of the tested intumescent coating obtained from the TPS and LFA experiments.

slightly affect the thermal properties of intumescent coatings, such as the thermal conductivity. Above these temperatures, the material starts the swelling process and, consequently, the material properties change. For instance, the thermal conductivity is usually around 0.40-0.50 W/mK at ambient temperature, then start decisively decreasing around 200℃ (0.20-0.40 W/mK) and it reaches minimum values around 400℃ (0.05-0.15 W/mK), when the swelling process is expected to be completed. Above 400℃, the porous char structure does not change significantly, but the thermal conductivity typically starts increasing due to conduction phenomena in the solid part and radiation within the voids of the char [31].

The experimental results presented herein estimate the residual thermal properties of the intumescent coating exposed to different heating conditions. Surprisingly, it was found that the thermal conductivity, the thermal diffusivity and the specific heat capacity are included in small numerical ranges and they do not appear to be affected by the heating conditions imposed by the H-TRIS test method (refer to Table 4.3). These experimental results highlight the substantial similarity between the porous char structures obtained from experiments performed under different heating conditions. This finding contradicts the experimental outcomes previously presented, but the measured values are comparable to the ones available in the literature for swelled intumescent coatings (above 400℃) [5, 22-23]. Unfortunately, the resulting thermal properties can not be associated with a certain temperature because during the experiments the intumescent coating experienced different temperature ranges,

which varied in time and according to the imposed heating regime.
Similarly to ambient temperature, the density of the swelled coating char was evaluated by simple mass/volume measurements. As in the case of the thermal properties, the density of the swelled coating char was found to be very similar for all the swelled porous chars obtained from the H-TRIS experiments, regardless of the heating condition or the initial thickness.

Table 4.3: Thermal and physical properties of the intumescent coating porous char according to the TPS methodology.

λ_c **[W/mK]**	α_c **[mm^2/s]**	$c_{p,c}$ **[J/kgK]**	ρ_c**[kg/m^3]**
0.043 $\pm$ 0.008	0.588 $\pm$ 0.295	1550 $\pm$ 300	50 $\pm$ 8

4.3.3 Optical properties (ISS)

Measuring the reflectivity and absorptivity of solid materials at elevated temperatures is technically challenging and only a few research studies have been published regarding this topic [52, 62]. In the experimental study presented herein, all the measurements were conducted on the coating samples at ambient temperature and the influence of different degradation levels at the coating surface was investigated. As in the case of the TPS experiments on swelled coating chars, the residual properties were evaluated at ambient temperature and the results assume that the coating reflectivity is mainly affected by the the level of degradation due to thermal exposure. This constitutes the first attempt to measure the optical properties of virgin and degraded intumescent coatings using an integrating sphere.
Figure 4.10 shows the reflectivity measurements for different wavelengths for the virgin intumescent coating at ambient temperature. On the other hand, Figure 4.11 reports the residual reflectivity measurements for the intumescent coatings obtained from the experiments involving the H-TRIS test method. Over the wavelength spectrum 2-20 μm, the samples obtained from the H-TRIS experiments highlighted different reflectivity curves, affected by the thermal exposure. In particular, the influence of the thermal degradation on the reflectivity of intumescent coating chars appeared more relevant at low wavelengths (2-6 μm). Nevertheless, all the reflectivity curves fluctuate around 10%, both for ambient and elevated temperatures.

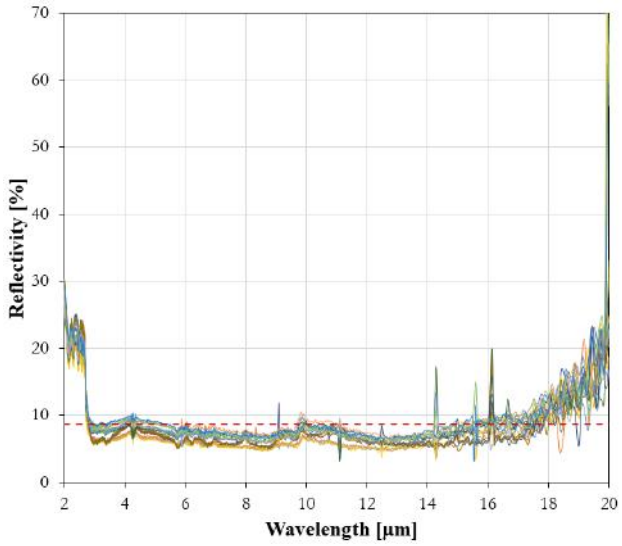

Figure 4.10: Reflectivity values as function of wavelength and average value for virgin intumescent coating (ambient temperature).

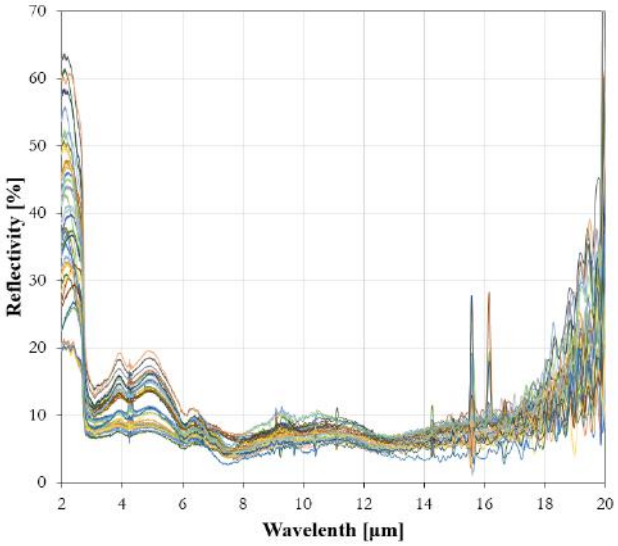

Figure 4.11: Reflectivity values as function of wavelength for intumescent coatings tested using H-TRIS (elevated temperatures).

In order to quantify the optical properties of the tested material, the intumescent coating was assumed to be an opaque material (i.e. null transmissivity) and to behave as grey body (i.e. emissivity equal to absorptivity) [63]. Consequently, the radiation balance at the surface of the tested material can be simplified as follow:

$$\rho + \alpha + \tau = 1 \quad \Rightarrow \quad \rho + \alpha = 1 \quad \Rightarrow \quad \alpha = \varepsilon = 1 - \rho \tag{4.1}$$

where ρ is the material reflectivity [-], α is the material absorptivity [-], τ is the material transmissivity [-] and ε is the material emissivity [-]. Following Equation 4.1, it is possible to calculate the average values of reflectivity ρ_c, absorptivity α_c and emissivity ε_c of the tested intumescent coating. The variation of the coating reflectivity ρ_c and the coating absorptivity α_c with different levels of degradations due to exposure to various constant incident radiant heat fluxes are shown in Figure 4.12.

At ambient temperature, the reflectivity of the intumescent coating is only slightly affected by the radiation wavelength and the measured average emissivity and absorptivity values are in line with the ones available in the literature (0.92-0.95) [37, 40]. On the other hand, as regards degraded coatings, the exposure to thermal radiation changed the superficial structure and characteristics of the intumescent coating, yielding to a change in the residual optical properties. In particular, exposures to higher heat fluxes produced higher reflectivity

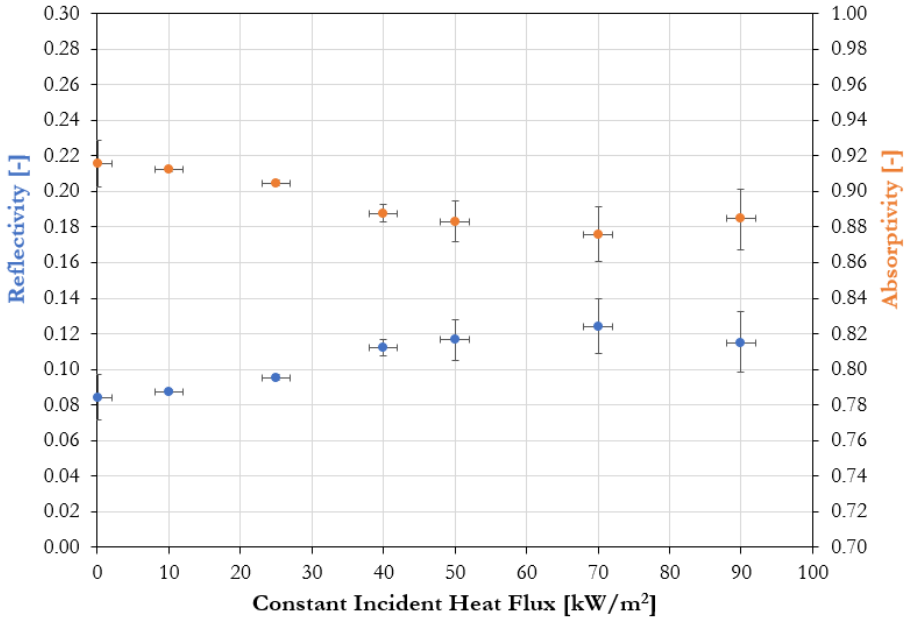

Figure 4.12: Average values of the residual reflectivity and absorptivity of the tested intumescent coating exposed to different constant incident radiant heat fluxes using the H-TRIS test method.

and lower absorptivity. Generally, the values of reflectivity and absorptivity of the tested intumescent coating varies within specific ranges:

- Intumescent coating reflectivity - ρ_c = 0.07- 0.14
- Intumescent coating absorptivity/emissivity - α_c = ε_c = 0.86 - 0.93

4.4 Conclusions

The current chapter presents a set of complementary studies carried out on the intumescent coating using standard experimental methodologies. The main aim of these experiments is to characterised the selected intumescent coating and quantify the physical, thermal and optical properties of the tested intumescent coating at ambient and elevated temperatures. Through the results obtained from the TGA and DSC experiments, it was found that the tested product has similar characteristics to typical intumescent formulations (e.g. APP-PER-MEL). In these typical formulations, the main thermal decomposition reactions occur at temperature included between 200 and 400℃. These reactions are typically endothermic. In particular, the intumescent swelling reaction typically happens at temperatures between 300 and 400℃ and the main reactions of the intumescent coating can be considered to

be completed at about 400-450℃. Above 550℃ and in a oxygen-rich environment, the expanded carbonaceous char further degrades and is subjected to exothermic oxidation, releasing carbon dioxide and producing a minor mass loss. Above 800℃, all the reactions are completed and a significant amount of inorganic compound is left (about 40-45% the initial mass).

The experiments conducted using the TPS and LFA equipment estimated the thermal and physical properties of the intumescent coating. The two set of experiments adopted two different methodologies, but they produced similar results. The thermal properties of the intumescent coating prior to swelling are in good agreement with the values available in the literature and they are only slightly influenced by temperature. As regards the experiments carried out on the swelled porous chars, the residual thermal properties of the intumescent coating did not appear to be directly affected by the heating conditions imposed by the H-TRIS test method.

The optical properties of the intumescent coating were measured using an integrating sphere system. Over the wavelength 2-20 μm, the reflectivity of the intumescent coating appeared to be more affected at low wavelengths. In general, the average absorptivity and emissivity values of the tested intumescent coating vary within the range 0.86-0.93, depending on the heating conditions imposed at the coating surface.

In conclusion, the complementary studies described herein provided a preliminary understanding of the material characterisation and thermo-physical properties of the intumescent coating, a starting point for modelling any heat transfer process through the tested material.

Bibliography

[1] Comité Europeén de Normalization (CEN). "EN 13381-8:2013 Test methods for determining the contribution to the fire resistance of structural members - Part 8: Applied reactive protection to steel members". Brussels, Belgium, 2013.

[2] Weisheim W., Schaumann P., Sander L. and Zehfuß J. "Numerical model for the fire protection performance and the design of intumescent coatings on structural steel exposed to natural fires". Journal of Structural Fire Engineering, vol. 11, no. 1, pp. 33-50, 2019.

[3] de Silva, Bilotta A. and Nigro E. "Experimental investigation on steel elements protected with intumescent coating". Construction and Building Materials, vol. 205, pp. 232-244, 2019.

[4] Wang L., Chen B., Zhang C. and Li G. "Experimental study on insulative properties of intumescent coating exposed to standard and nonstandard furnace curves". Fire and Materials, vol. 43, no. 7, pp. 782-793, 2019.

[5] Luangtriratana P., Kandola B.K., Duquesne S. and Bourbigot S. "Quantification of Thermal Barrier Efficiency of Intumescent Coatings on Glass Fibre-Reinforced Epoxy Composites". Coatings, vol. 8, no. 10, pp. 347-365, 2018.

[6] Kang J., Takahashi F. and T'ien J.S. "In situ thermal-conductivity measurements and morphological characterization of intumescent coatings for fire protection". Journal of Fire Sciences, vol. 36, no. 1, pp. 1–19, 2018.

[7] Bozzoli F., Mocerino A., Ranieri S. and Vocale P. "Inverse heat transfer modeling applied to the estimation of the apparent thermal conductivity of an intumescent fire retardant paint". Experimental Thermal and Fluid Science, vol. 90, pp. 143-152, 2018.

[8] Lucherini A., Giuliani L. and Jomaas G. "Experimental study of the performance of intumescent coatings exposed to standard and non-standard fire conditions". Fire Safety Journal, vol. 95, pp. 42-50, 2018.

[9] Lucherini A. "Experimental study of the behaviour of steel structures protected by different intumescent coatings and exposed to various fire scenarios". MSc thesis, Civil Engineering, Technical University of Denmark, 2016.

[10] Xu Q., Li G.-Q., Jiang J. and Wang Y.C. "Experimental study of the influence of topcoat on insulation performance of intumescent coatings for steel structures". Fire Safety Journal, vol. 101, pp. 25-38, 2018.

[11] Kang S., Choi S. and Choi J.Y. "Coupled thermo-physical behaviour of an inorganic intumescent system in cone calorimeter testing". Journal of Fire Sciences, vol. 35, no. 3, pp. 207-234, 2017.

[12] Li G.Q., Han J. and Wang Y.C. "Constant effective thermal conductivity of intumescent coatings: Analysis of experimental results". Journal of Fire Sceinces, vol 35, no. 2, pp. 132.155, 2017.

[13] Cirpici B.K., Wang Y.C. and Rogers B. "Assessment of the thermal conductivity of intumescent coatings in fire". Fire Safety Journal, vol. 81, pp. 74-84, 2016.

[14] Li G.Q., Han J., Lou G.B. and Wang Y.C. "Predicting intumescent coating protected steel temperature in fire using constant thermal conductivity". Thin-Walled Structures, vol. 98, pp. 177-184, 2016.

[15] Nadjai A., Petrou K., Han S. and Ali F. "Performance of unprotected and protected cellular beams in fire conditions". Construction and Building Materials, vol. 105, pp. 579-588, 2016.

[16] Bilotta A., De Silva D. and Nigro E. "Tests on intumescent paints for fire protection of existing steel structures". Construction and Building Materials, vol. 121, pp. 410-422, 2016.

[17] Bilotta A., De Silva D. and Nigro E. "General approach for the assessment of the fire vulnerability of existing steel and composite steel-concrete structures". Journal of Building Engineering, vol. 8, pp. 198-207, 2016.

[18] Kolsek J. and Cesarek P. "Performance-based fire modelling of intumescent painted steel structures and comparison to EC3". Journal of Constructional Steel Research, vol. 104, pp. 91-103, 2015.

[19] Wang L., Dong Y., Zhang D., Zhang D. and Zhang C. "Experimental study of heat transfer in intumescent coatings exposed to non-standard furnace curves". Fire Technology, vol. 51, no. 1, pp. 627-643, 2015.

[20] Elliott A., Temple A., Maluk C. and Bisby L. "Novel testing to study the performance of intumescent coatings under non-standard heating regimes". Fire Safety Science – Proceedings of the 11th International Symposium, University of Canterbury, New Zealand, pp. 652-665, 2014.

[21] Rush D., Bisby L., Gillie M., Jowsey A. and Lane B. "Design of intumescent fire protection for concrete filled structural hollow sections". Fire Safety Journal, vol. 67, pp. 13-23, 2014.

[22] Gardelle B., Duquesne S., Vandereecken P. and Bourbigot S. "Characterization of the carbonization process of expandable graphite/silicone formulations in a simulated fire". Polymer Degradation and Stability, vol. 98, pp. 1052-1063, 2013.

[23] Muller M., Bourbigot S., Duquesne S., Klein R., Giannini G., Lindsay C. and Vlassenbroeck J. "Investigation of the synergy in intumescent polyurethane by 3D computed tomography". Polymer Degradation and Stability, vol. 98, pp. 1638-1647, 2013.

[24] Wang L.L., Wang Y.C. and Li G.Q. "Experimental study of hydrothermal aging effects on insulative properties of intumescent coating for steel elements". Fire Safety Journal, vol. 55, pp.

168-181, 2013.

[25] Gardelle B., Duquesne S., Rerat V. and Bourbigot S. "Thermal degradation and fire performance of intumescent silicone-based coatings". Polymers for Advanced Technologies, vol. 24, no. 1, pp. 62-69, 2012.

[26] Zhang Y., Wang Y., Bailey C.G. and Taylor A.P. "Global modelling of fire protection performances of an intumescent coating under different furnace fire conditions". Journal of Fire Science, vol. 31, no.1, pp. 51-72, 2012.

[27] Zhang Y., Wang Y., Bailey C.G. and Taylor A.P. "Global modelling of fire protection performance of an intumescent coating under different cone calorimeter heating conditions". Fire Safety Journal, vol. 50, pp. 51-62, 2012.

[28] Li G.Q., Lou G.B., Zhang C., Wang L. and Wang Y. "Assess the fire resistance of intumescent coatings by equivalent constant thermal resistance". Fire Technology, vol. 48, pp. 529-546, 2012.

[29] Wang L.L., Wang Y.C., Yuan J.F. and Li G.Q. "Thermal conductivity of intumescent coating char after accelerated aging". Fire and Materials, vol. 37, pp. 440-456, 2012.

[30] Staggs J.E.J., Crewe R.J. and Butler R. "A theoretical and experimental investigation of intumescent behaviour in protective coatings for structural steel". Chemical Engineering Science, vol. 71, pp. 239-251, 2012.

[31] Staggs J.E.J. "Thermal conductivity estimates of intumescent chars by direct numerical simulation". Fire Safety Journal, vol. 45, pp. 228-237, 2010.

[32] Griffin G.J. "The modelling of heat transfer across intumescent polymer coatings". Journal of Fire Science, vol. 28, pp. 249-277, 2010.

[33] Dai X.H., Wang Y.C. and Bailey C. "A simple method to predict temperatures in steel joints with partial intumescent coating fire protection". Fire Technology, vol. 46, pp. 19-35, 2010.

[34] Opstad G.B.K. "Thermal properties of intumescent passive fire protection materials". Proceeding of 4th International Conference on Safety & Environment in Process Industry, vol. 19, 2010.

[35] Yuan J. "Intumescent coating performance on steel structures under realistic fire conditions". PhD thesis, School of Mechanical, Aerospace and Civil Engineering, University of Manchester, 2009.

[36] Bartholmai M. and Schartel B. "Assessing the performance of intumescent coatings using bench-scaled cone calorimeter and finite difference simulations". Fire and Materials, vol. 31, pp. 187-205, 2007.

[37] Omrane A., Wang Y.C., Goransson U., Holmstedt G. and Alden M. "Intumescent coating sur-

face temperature measurement in a cone calorimeter using laser-induced phosphorescence". Fire Safety Journal, vol. 42, pp. 68-74, 2007.

[38] Griffin G.J., Bicknell A.D. and Brown T.J. "Studies on the effect of atmospheric oxygen content on the thermal resistance of intumescent fire-retardant coatings". Journal of Fire Science, vol. 23, no. 4, 2005.

[39] Wang Y., Goransson U., Holmstedt G. and Omrane A. "A Model for prediction of temperature in steel structure protected by intumescent Coating, based on tests in the cone calorimeter". Fire Safety Science – Proceedings of the 8th International Symposium, Tsinghua University, Beijing, China, pp. 235-246, September 2005.

[40] Bartholmai M., Schriever R. and Schartel B. "Influence of external heat flux and coating thickness on the thermal insulation properties of two different intumescent coatings using cone calorimeter and numerical analysis". Journal of Fire Materials, vol. 27, pp. 151-162, 2003.

[41] Bourbigot S., Duquesne S. and Leroy J.-M. "Modeling of heat transfer of a polypropylene-based intumescent system during combustion". Journal of Fire Sciences, vol. 17, pp. 42-56, 1999.

[42] Henderson J.B. "A model for the thermal response of polymer composite materials with experimental verification". Journal of Composite Materials, vol. 19, pp. 579-595, 1985.

[43] Anderson C.E., Dziuk J. and Mallow W.A. "Intumescent reaction mechanisms". Journal of Fire Sciences, vol.3, pp. 161-194, 1985.

[44] Wagner M. "Thermal Analysis in Practice, Collected Applications". Mettler Toledo, 2009.

[45] Coats A.W. and Refern J.P. "Thermogravimetric analysis. A review". Analyst, vol. 88, pp. 906-924, 1963.

[46] O'Neill M.J. "Measurement of specific heat functions by Differential Scanning Calorimetry". Analytical Chemistry, vol. 38, pp. 1331–1336, 1966.

[47] International Organization for Standardization (ISO). "ISO 22007-2:2015 Plastics - Determination of thermal conductivity and thermal diffusivity - Part 2: Transient plane heat source (hot disc) method". Geneva, Switzerland, 2015.

[48] Gustafsson S.E. "Transient plane source techniques for thermal conductivity and thermal diffusivity measurements of solid materials". Review of Scientific Instruments, vol. 62, no. 3, pp. 797-804, 1991.

[49] International Organization for Standardization (ISO). "ISO 22007-4:2008 Plastics - Determination of thermal conductivity and thermal diffusivity - Part 4: Laser flash method". Geneva, Switzerland, 2008.

[50] Parker W.J., Jenkins R.J., Butler C.P. and Abbott G.L. "Flash Method of Determining Thermal

Diffusivity, Heat Capacity, and Thermal Conductivity". Journal of Applied Physics, vol. 32, no. 1679, 1961.

[51] Seifter A., Grover M., Holtkamp D.B., Iverson A.J., Stevens G.D., Turley W.D., Veeser L.R., Wilke M.D. and Young J.A. "Emissivity measurements of shocked tin using a multi-wavelength integrating sphere". Journal of Applied Physics, vol. 110, no. 093508, 2011.

[52] Boulet P., Brissinger D., Collin A., Acem Z. and Parent G. "On the influence of the sample absorptivity when studying the thermal degradation of materials". Materials, vol. 8, pp. 5398-5413, 2015.

[53] International Organization for Standardization (ISO). "ISO 20473:2007 Optics and photonics - Spectral bands". Geneva, Switzerland, 2007.

[54] Society of Fire Protection Engineers (SFPE). "SFPE Handbook of Fire Protection Engineering". Springer, 5th Edition, 2016.

[55] Wang Z., Han E. and Ke W. "Effects of nanoparticles on the improvement in fire-resistant and anti-ageing properties of flame-retardant coating". Surface & Coatings Technology, vol. 200, pp. 5706-5716, 2006.

[56] Bourbigot S., Le Bras M., Duquesne S. and Rochery M. "Recent Advances for Intumescent Polymers". Macromolecular Materials and Engineering, vol. 289, pp. 499–511, 2004.

[57] Puri R.G and Khanna A.S. "Influence of heat-stable filler on the thermal shielding performance of water-based intumescent fire-resistive coating for structural steel applications". Journal of Coatings Technology and Research, vol. 14, no. 2, pp. 323–331, 2017.

[58] Pimenta J.T., Goncalves C., Hiliou L., Coelho J.F.J. and Magalhaes F.D. "Effect of binder on performance of intumescent coatings". Journal of Coatings Technology and Research, vol. 13, no. 2, pp. 227-238, 2016.

[59] Morys M., Illerhaus B., Sturm H. and Schartel B. "Size is not all that matters: Residue thickness and protection performance of intumescent coatings made from different binders". Journal of Fire Sciences, vol. 35, no. 4, pp. 1-19, 2017.

[60] Vandersall H.L. "Intumescent coating systems, their development and chemistry", Journal of Fire and Flammability, vol. 2, pp. 97-140, 1971.

[61] Camino G., Costa L. and Martinasso G. "Intumescent fire-retardant systems". Polymer Degradation and Stability, vol. 23, no. 4, pp. 359-376, 1989.

[62] Acem Z., Brissinger D., Collin A., Parent G., Boulet P., Quach T.H.Y., Batiot B., Richard F. and Rogaume T. "Surface temperature of carbon composite samples during thermal degradation". International Journal of Thermal Sciences, vol. 11, pp. 427-438, 2017.

[63] Incropera F.P., DeWitt D.P., Bergman T.L. and Lavine A.S. "Fundamental of heat and mass transfer". John Wiley & Sons, 6th Edition, 2006.

5

Onset of swelling

5.1 Introduction and background

The literature review have emphasised the influence of heating conditions on the overall performance of thin intumescent coatings [1-5]. Particularly, some researchers have found out that slow growing fires may be a potential cause of vulnerability by producing incomplete swelling or melting/delamination of thin intumescent coatings prior to char formation [3-4].

The onset (or initiation) of swelling is key for assuring the effectiveness of thin intumescent coatings for providing thermal insulation to the substrate material during fire. The onset of swelling can be defined as the stage that the intumescent coating undergoes at the end of the melting phase and the initiation of the intumescent swelling process. Past experimental studies have shown that thin intumescent coatings usually start the swelling process at temperatures in the range of 200-300℃ [6-9]. While the fire performance of thin intumescent coatings has been extensively studied at medium and large scales using different fire testing methodologies (e.g. varied furnace and cone calorimeter), the onset of swelling has been mainly studied at a small scale. Thermo-Gravimetric Analysis (TGA) represents the main testing methodology to understanding the degradation processes of thin intumescent coatings and to engineer effective intumescent formulations [10-11]. However, in TGA testing, test samples are in the order of milligrams and the heating rate is relatively low; hence, the influence of heat transfer is marginalised. Consequently, there is limited research studies that have performed detailed analysis of the swelling processes for real-scale samples protected with thin intumescent coatings.

The study presented herein investigates the onset of swelling for a commercially available thin intumescent coating applied on steel plates and exposed to a wide range of heating conditions. Experiments were performed using an array of radiant panels for controlling incident radiant heat flux at the exposed surface of coated steel samples. This experimental technique allows for the direct and precise control of the thermal boundary conditions at the exposed surface of tested samples. Within the scope of this research study, the onset of swelling was defined based on two conditions: (1) visual observation of swelling during heating or (2) time-history of the steel temperature. Research outcomes derived from this work defined a threshold for the onset of swelling in terms of steel and coating temperatures and it concluded that the onset of swelling is directly influenced by the heating conditions at

the exposed surface and the applied initial DFT.

5.2 Experimental investigation

5.2.1 Experimental methodology

The test method used for this study aims at performing an accurate control of the heating conditions imposed on the test samples, ensuring high repeatability between tests. The Heat-Transfer Rate Inducing System (H-TRIS) test method was chosen for this purpose [12]. This test method controls the relative position between the target exposed surface of the test sample and an array of radiant panels, controlled with a computer-controlled linear motion system (see Figure 5.1). Within the limits of the minimum proximity to the exposed surface, test samples can be exposed to any specified time-history of incident radiant heat flux. The test setup used within the scope of this work was assembled by combining four high-performance natural-gas-fired radiant heater mounted on a supporting frame, forming a 300 x 400 mm^2 radiant heat source (see Figure 5.1). This setup enables a high and stable heating system with outstanding thermal homogeneity of the emitting surface. In the configuration used within the scope of this study, the H-TRIS test method imposes incident radiant heat fluxes between 5 and 100 kW/m^2. In the pre-test calibration of the test setup, the range of deviation of the incident radiant heat flux at the target surface of test samples was measured and estimated equal to $\pm$ 10% [12]. In addition, the experimental methodology enables the visual inspection of the test samples during testing (e.g. for gauging the rate of coating swelling), technically challenging during a conventional standard furnace test.

5.2.2 Experimental campaign (test samples)

The test samples used in this experimental study were 200 x 200 mm^2 mild carbon steel plates, 10 mm thick, resulting in a section factor A_p/V (i.e. ratio between exposed surface and volume of steel) equal to 100 m^{-1}. Samples were coated with a commercially available solvent-based thin intumescent coating. The product is designed for structural steel used in the build environment for internal, semi-exposed or external use and suitable for off-site and on-site application. It is a fast-track and self-priming coating. The steel plates were prepared

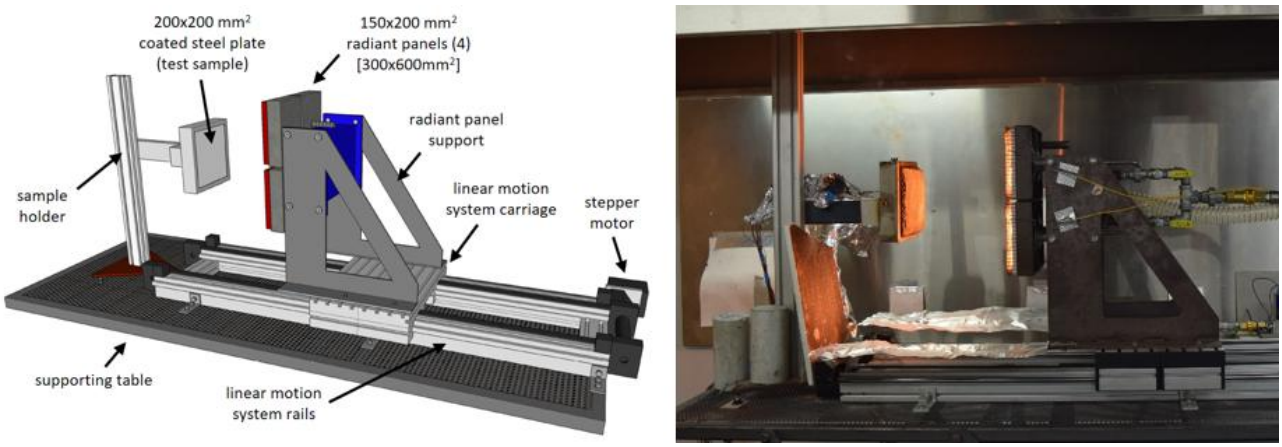

Figure 5.1: Illustration of the experimental setup based on the H-TRIS test method (*Bench-scale H-TRIS 2.0*).

at a *"Sa2.5 - Near white metal"* surface preparation grade and coated by a registered professional contractor using airless spray equipment [13]. Based on the average applied DFT measured with a non-destructive film thickness gauge, test samples were categorised into three groups (Table 5.1):

1. *"Low DFT"* – 1.00 mm ($\pm$ 0.20 mm)
2. *"Medium DFT"* – 1.80 mm ($\pm$ 0.20 mm)
3. *"High DFT"* – 2.80 mm ($\pm$ 0.20 mm)

Individual uncoated and coated test samples were tested using H-TRIS test method. Test samples were fire tested for 30 minutes to different levels of constant incident radiant heat flux, varying between 10 and 90 kW/m^2 (Table 5.1). During testing, a custom-built sample holder frame was used (see Figure 5.1). In order to aim for adiabatic thermal conditions at the back (unexposed surface) of the test sample and therefore minimise heat losses, the unexposed surface of test samples were insulated using a layer of 20 mm thick mineral wool and 13 mm thick plaster board.

5.2.3 Instrumentation

Up to three K-type thermocouples were attached to unexposed surface of the test samples in order to record the evolution of the steel temperature during testing. The transient rate of swelling of the coating was measured by image processing of videos taken using a high-resolution camera placed at the side of the test sample, aligned with the surface of the test

Table 5.1: Test matrix of the experimental study.

	Heating conditions	Number of repeat tests	DFT_{mean} [mm]
"Low DFT"	10 kW/m^2	1	0.887
	25 kW/m^2	2	1.062, 1.204
	40 kW/m^2	2	0.996, 1.069
	50 kW/m^2	2	1.194, 1.196
	70 kW/m^2	2	1.162, 1.198
	90 kW/m^2	3	1.134, 1.146, 1.146
"Medium DFT"	10 kW/m^2	2	1.620, 1.712
	16 kW/m^2	1	1.622
	20 kW/m^2	2	1.568, 1.869
	23 kW/m^2	2	1.732, 1.842
	25 kW/m^2	2	1.638, 1.786
	27 kW/m^2	2	1.690, 1.823
	35 kW/m^2	2	1.605, 1.906
	40 kW/m^2	2	1.680, 1.816
	50 kW/m^2	2	1.794, 1.920
	55 kW/m^2	2	1.772, 1.914
	70 kW/m^2	2	1.712, 1.898
	90 kW/m^2	3	1.630, 1.770, 1.870
"High DFT"	10 kW/m^2	1	2.716
	25 kW/m^2	2	2.714, 2.902
	40 kW/m^2	2	2.750, 2.822
	50 kW/m^2	2	2.854, 2.866
	70 kW/m^2	2	2.878, 2.954
	90 kW/m^2	3	2.992, 3.038, 3.086

sample. The real-time measurement of the coating swelling was also used for continuously controlling the relative distance between the coating swelling front and the array of radiant panels during testing. This was done to assure that incident radiant heat flux at the exposed surface of test samples was maintained to the specified level during the full duration of the test. In addition, the temperature of the exposed surface of test samples was measured using an Infra-Red camera.

5.3 Heat transfer model

In order to investigate the thermal conditions that influence and yield onset of swelling of thin intumescent coatings, a heat transfer model was formulated for describing the thermal conditions of test samples prior to swelling. The finite-difference model is based on the

numerical method developed by Emmons and Dusinberre, presented in detail in Appendix C [14-15]. The model explicitly solves a one-dimensional heat conduction problem by resolving energy-balance equations in the main direction of the heat flow. The model is discretised in a two-layer material with a total thickness equal to $L_1 + L_2$, intumescent coating and steel respectively. The model is discretised into N nodes, corresponding to N elements having a thickness of Δx (Figure 5.2). Boundary elements (exposed surface and unexposed surface) have a thickness of $\Delta x/2$.

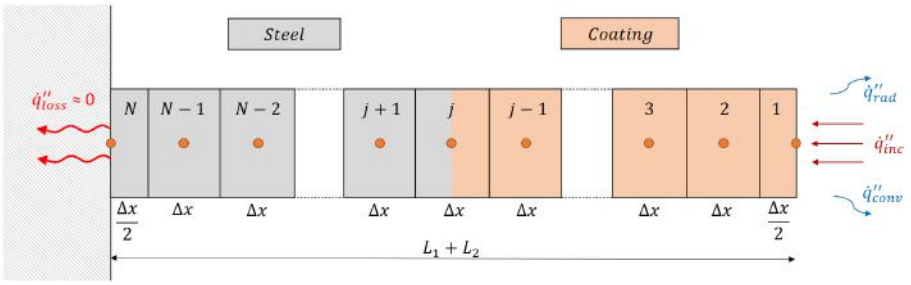

Figure 5.2: Schematic representation of the discretisation of the two-layers material heat transfer model.

The thermal boundary conditions at the exposed surface of test samples was experimentally controlled by a defining the incident radiant heat flux at the exposed surface. Hence, the model described herein was defined by equivalent conditions at the exposed surface using conventional correlations: incident radiant heat flux ($\dot{q}''_{inc}$) at the surface element with convective and radiative heat flux losses from the exposed surface ($\dot{q}''_{conv}$ and $\dot{q}''_{rad}$). Adiabatic conditions were assumed at the unexposed surface. In order to take into account the heat flux losses due to thermal processes in the coating, a volumetric heat source term $\dot{g}'''_c$ was introduced: positive for absorbed heat (endothermic reactions) and negative for generated heat (exothermic reaction). Energy-balance equations are formulated at each node, thus each element. The following formulas can be derived to calculate the evolution of the temperature of each node j for each time step i, according to the type of element (see Figure 5.2).

Surface element (coating)

$$T_1^{i+1} = T_1^i + \frac{2\Delta t}{\rho_c c_{p,c} \Delta x}\left[\alpha_c \dot{q}''_{inc} - \lambda_c \frac{T_1^i - T_2^i}{\Delta x} - h_{conv}\left(T_1^i - T_\infty\right) - \varepsilon_c \sigma\left(T_1^{i4} - T_\infty^4\right) - \frac{\dot{g}'''_c \Delta x}{2}\right] \tag{5.1}$$

Middle element (coating)

$$T_j^{i+1} = T_j^i + \frac{\lambda_c \Delta t}{\rho_c c_{p,c} \Delta x^2} \left[T_{j-1}^i - 2T_j^i + T_{j+1}^i - \frac{\dot{g}_c''' \Delta x^2}{2} \right] \tag{5.2}$$

Interface element (coating - steel)

$$T_j^{i+1} = T_j^i + \frac{\Delta t}{(\rho_c c_{p,c} + \rho_s c_{p,s}) \Delta x^2} \left[\lambda_c T_{j-1}^i - (\lambda_c + \lambda_s) T_j^i + \lambda_s T_{j+1}^i - \frac{\dot{g}_c''' \Delta x^2}{2} \right] \tag{5.3}$$

Middle element (steel)

$$T_j^{i+1} = T_j^i + \frac{\lambda_s \Delta t}{\rho_s c_{p,s} \Delta x^2} \left[T_{j-1}^i - 2T_j^i + T_{j+1}^i \right] \tag{5.4}$$

End element (steel)

$$T_N^{i+1} = T_N^i + \frac{2\lambda_s \Delta t}{\rho_s c_{p,s} \Delta x^2} \left[T_{N-1}^i - T_N^i \right] \tag{5.5}$$

where T_j^i is the temperature of the node j at time i [K], Δt is the time increment [sec], Δx is the space discretisation [m], $\dot{q}_{inc}''$ is the incident heat flux [W/m^2], $\dot{g}_c'''$ is the volumetric generated/absorbed heat flux [W/m^3], ρ_c / ρ_s is the density of coating / steel [kg/m^3], $c_{p,c}$ / $c_{p,s}$ is the specific heat capacity of coating / steel [J/kgK], λ_c / λ_s is the thermal conductivity of coating / steel [W/mK], α_c is the absorptivity of coating [-], ε_c is the emissivity of coating [-], h_{conv} is the convective heat transfer coefficient [W/m^{2}K], T_∞ is the ambient temperature [K] and σ is the Stefan-Boltzmann constant [$5.67 \cdot 10^{-8}$ W/m^{2}K^4].

Since explicit finite-element methods can be unconditionally stable and they can diverge from reaching a steady state solution, a stability criterion has to be introduced. According to Dusinberre, the time step of iteration Δt must be lower than the following limits [15]:

$$\Delta t \leq \frac{\rho c_p \Delta x^2}{2\lambda} \qquad\qquad \Delta t \leq \frac{\rho c_p \Delta x^2}{2(h_{tot} \Delta x + \lambda)} \tag{5.6}$$

The stability criterion was solved for different combinations of the thermal properties of the intumescent coating and steel. On the other hand, the convective h_{conv} and total h_{tot} heat transfer coefficients were estimated using empirical correlations found in the literature [16].

5.4 Criteria for onset of swelling

As above-mentioned, the onset of swelling for a thin intumescent coating is usually defined as the completion of the melting phase and the initiation of the reaction phase, which results in the intumescent swelling process. However, to the authors' knowledge, there is no consensus on describing the threshold for onset of swelling for thin intumescent coatings during heating. Within the scope of the work described herein, the experimental setup described in Section 5.2 was conceived in order to capture the onset of swelling for thin intumescent coatings exposed to various heating conditions. Particularly, the onset of swelling for thin intumescent coatings was described in accordance with the two following criteria:

1. *Swelling criterion*. The onset of swelling occurs upon a minimum measured coating swelling. According to the minimum thickness that could be accurately measured in the described experimental setup, a threshold of 3 mm was set (Figure 5.3).

$$t_{swell} \quad \Rightarrow \quad d_c \geq 3mm \tag{5.7}$$

2. *Steel temperature criterion*. The onset of swelling occurs at the moment when the second derivative of the evolution in time of the coated steel temperature is at its global minimum value. Physically, this moment in time represents a rapid drop in the rate of steel temperature increment, which is caused by the initiation of the coating swelling (Figure 5.3). The finite-difference derivation was performed according to different time increments, from 10 to 60 seconds, and the final time for onset of swelling was defined as the average between all of them.

$$t_{swell} \quad \Rightarrow \quad min\frac{\partial^2 T_s}{\partial t^2} \tag{5.8}$$

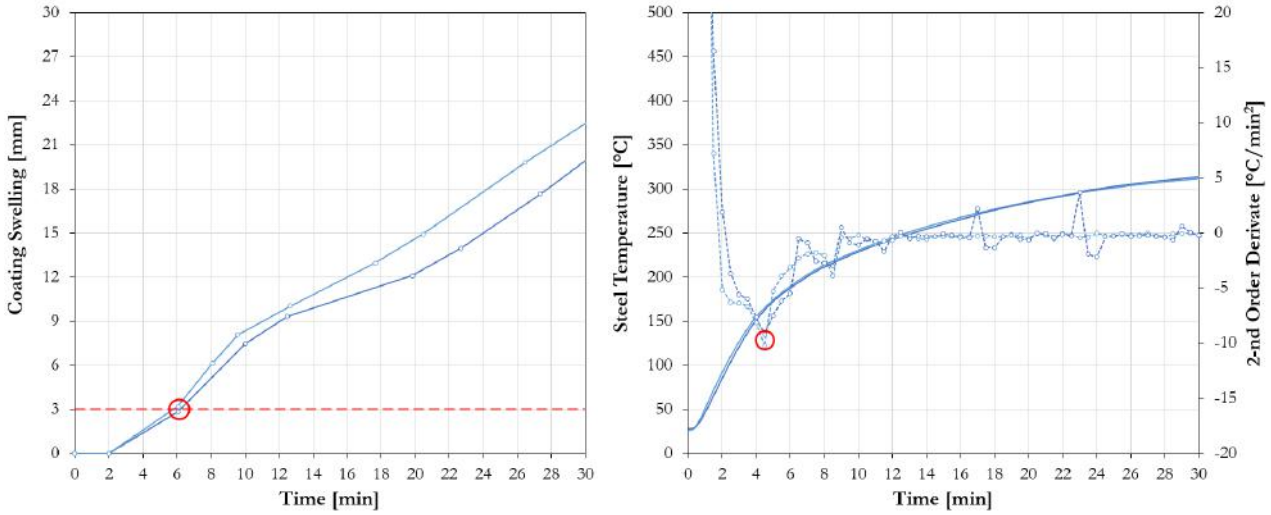

Figure 5.3: Swelling and steel temperature criteria for onset of swelling applied to the experimental data of two coated test samples exposed to a constant incident radiant heat flux of 40 kW/m^2 (*"Medium DFT"*).

5.5 Analysis and results

5.5.1 Experimental validation of the heat transfer model

In order to solve the heat transfer model described in Section 5.3, the thermal and physical properties of the thin intumescent coating and steel were defined. Regarding the steel, the thermal and physical properties of carbon steel were defined according to Eurocode 3 [17]:

- Density: ρ_s = 7850 kg/m^3
- Absorptivity: α_s = 0.75
- Specific heat capacity: $c_{p,s}(T)$ according to clause 3.4.1.2
- Thermal conductivity: $\lambda_s(T)$ according to clause 3.4.1.3

The values of thermal conductivity, thermal diffusivity and specific heat capacity of the intumescent coating as measured using the TPS, LFA and ISS methodologies have been presented in Section 4.3.2 (prior to swelling) and Section 4.3.3:

- Density: ρ_c = 1500 kg/m^3
- Absorptivity: α_c = 0.92
- Specific heat capacity: $c_{p,c}(T)$ according to Table 4.2 and Figure 4.9.

- Thermal conductivity: $\lambda_c(T)$ according to Table 4.2 and Figure 4.9.

In order to verify the validity of the model and measured physical and thermal properties, the heat transfer model described herein was experimentally validated using data related to steel temperatures during fire testing. The model was validated for the conditions of uncoated steel samples and the case of steel samples coated with a 2 mm thin intumescent coating. The following equations were used for defining the specific heat capacity, the thermal conductivity and the volumetric absorbed heat due to endothermic reaction of the intumescent coating that eventually results in swelling:

$$c_{p,c} = -0.0243 \cdot T_c^2 + 8.3602 \cdot T_c + 1089.3 \tag{5.9}$$

$$\lambda_c = -2 \cdot 10^{-6} \cdot T_c^2 - 0.0004 \cdot T_c + 0.5214 \tag{5.10}$$

$$\dot{g}_c''' = 2.4 \cdot 10^4 \cdot T_c \quad \text{for} \quad 200^oC \leq T_c \leq 300^oC \tag{5.11}$$

The graphs in Figure 5.4 and Figure 5.5 show good agreement between the experimental measurements and the heat transfer model. Regarding the uncoated tests (at 25, 40 and 70 kW/m^2), the agreement between the experimental measurements and the heat transfer model verified the validity of the assumption of adiabatic conditions at the unexposed surface and proved the accuracy of the calibration of the test method. Since no swelling was recorded due to the low temperatures, the case of 10 kW/m^2 was selected for validating the heat transfer model replicating the thermal conditions of steel samples with thin intumescent coating prior to swelling. The good agreement between the experimental and modelling data confirms the accuracy of the thermal and physical properties of the thin intumescent coating prior to swelling and of the thermal boundary conditions during fire testing. The thermal properties of the intumescent coating and the corresponding formulations (refer to Equations 5.9, 5.10 and 5.11) are accurate and have been validated only for the tested intumescent coating prior to swelling – tested at an incident heat flux of 10 kW/m^2 and up to a temperature of the coating of 250°C. In the case of higher heat fluxes, the temperature at the coating surface and within the coating itself rapidly increases and the coating initiates the swelling reaction at different rates based on the imposed heating conditions. Due to swelling occurring during testing and the model not accounting for this physical/chemical change of the intumescent coating, the heat transfer model diverges from the experimental data and it

is no longer valid. Particularly, due to the swelling process of the intumescent coating, the thermal conductivity is expected to decrease and the specific heat capacity is expected to increase due to the endothermic intumescent reaction.

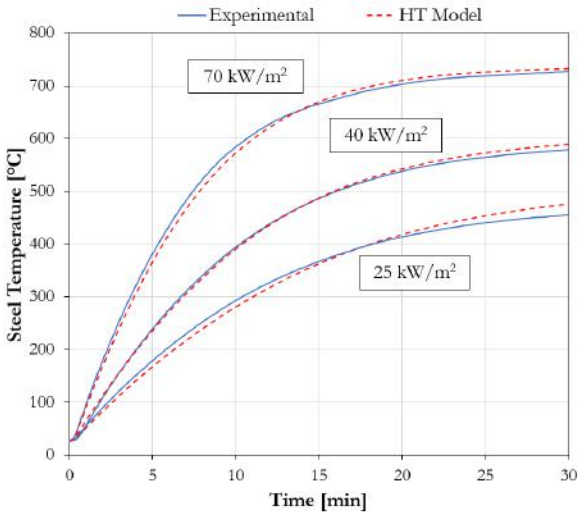

Figure 5.4: Steel temperatures comparison between experimental measurements and values computed using the described heat transfer model: uncoated steel plates exposed to 25, 40 and 70 kW/m^2.

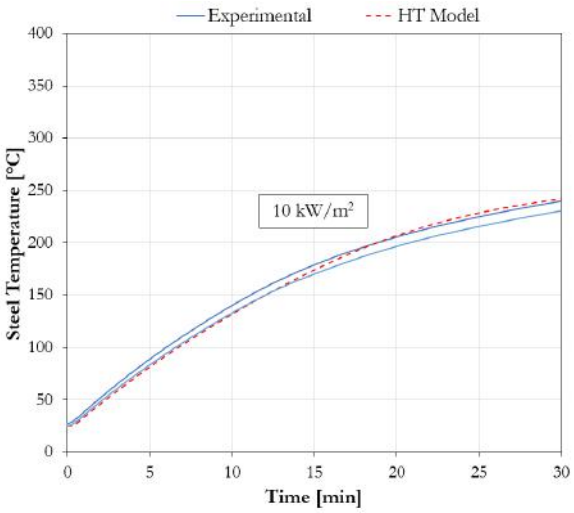

Figure 5.5: Steel temperatures comparison between experimental measurements and values computed using the described heat transfer model: steel plates coated with a 2 mm thin intumescent coating and exposed to 10 kW/m^2.

5.5.2 Onset of swelling

According to the two previous criteria, the time to onset of swelling under different incident radiant heat fluxes was evaluated for all the test samples coated with a *"Medium DFT"* of thin intumescent coating. Figure 5.6 shows how time to onset of swelling decreases with increasing heat fluxes and how the two criteria are fully comparable. Particularly, the minimum incident heat flux to reach onset of swelling during the fire testing was found to be equal to 23 kW/m^2 and no onset of swelling was recorded for samples below 20 kW/m^2. Similarly, to the concept of critical heat flux for ignition, the critical incident heat flux for swelling to occur for the tested thin intumescent coating was found to be included between 20 and 23 kW/m^2.

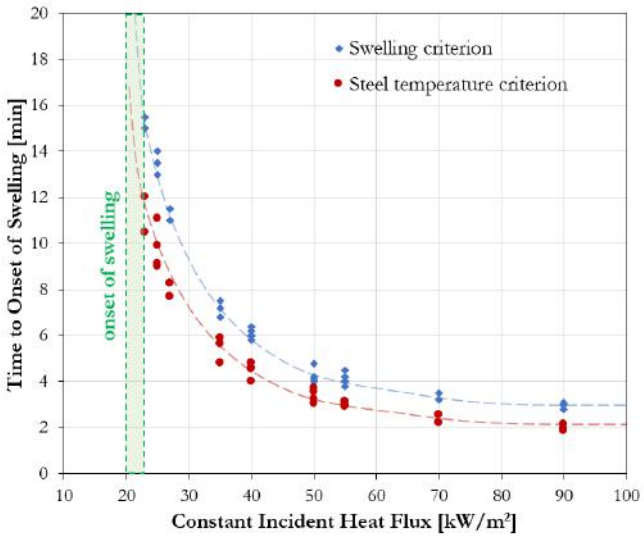

Figure 5.6: Time to onset of swelling for different incident constant heat fluxes, according to the two criteria (*"Medium DFT"*).

5.5.3 Net heat flux and accumulated thermal energy flux at onset of swelling

The evolution of the onset of swelling under different heat fluxes confirmed that the heating conditions experienced by the coated test samples during fire testing have a key role in this problem. Accordingly, using the heat transfer model described in Section 5.3, the time-history of net heat flux at the exposed surface was investigated. The net heat flux $\dot{q}''_{net}$ was calculated by subtracting the estimated heat losses $\dot{q}''_{loss,tot}$ (sum of the convective $\dot{q}''_{loss,conv}$ and radiative $\dot{q}''_{loss,rad}$ components) from the incident heat flux $\dot{q}''_{inc}$. From this, the accumulative thermal energy flux E''_{th} absorbed by the test sample at onset of swelling was evaluated as the area underneath the net heat flux curve (Figure 5.7):

$$E''_{th} = \int_0^{t_{swell}} \dot{q}''_{net} dt \tag{5.12}$$

The adopted heat transfer model enabled to calculate the accumulative thermal energy flux at onset of swelling for all the test samples coated with a *"Medium DFT"* of thin intumescent coating. Figure 5.8 shows how the tested thin intumescent coating required higher energy for reaching onset of swelling at low and high heat fluxes, while heat fluxes around 50 kW/m^2 represented an optimal point of minimum energy. In addition, it was found that onset of

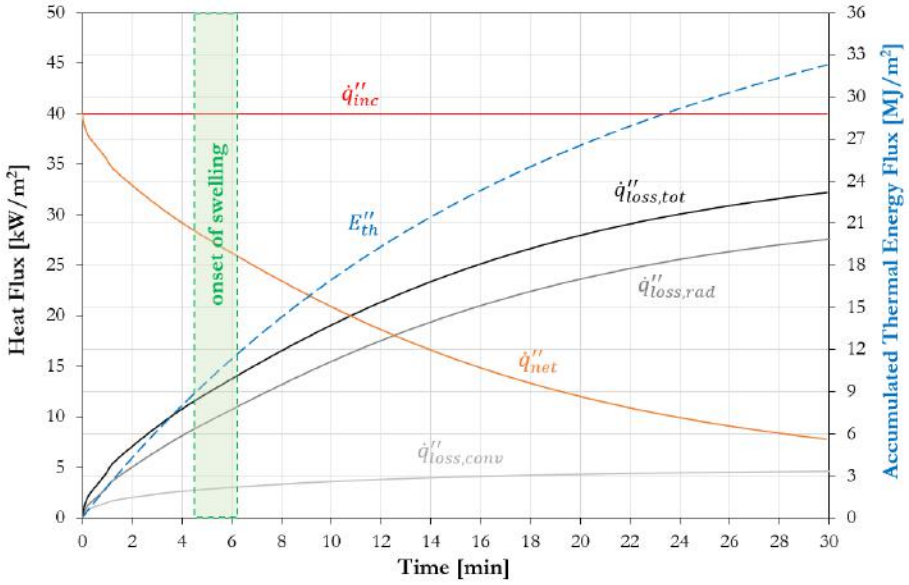

Figure 5.7: Incident radiant heat flux, heat losses (convective, radiative and total) and accumulative thermal energy flux for a typical test sample coated with a 2 mm thin intumescent coating and exposed to a constant incident radiant heat flux of 40 kW/m^2.

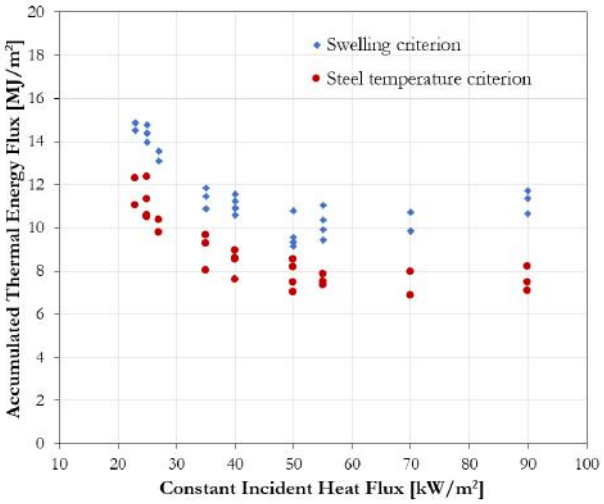

Figure 5.8: Accumulated net thermal energy flux at onset of swelling for different incident constant heat fluxes, according to the two criteria (*"Medium DFT"*).

swelling only occurred above a minimum net thermal energy flux equal 9 MJ/m^2 according to the swelling criterion, while 7 MJ/m^2 according to the steel temperature criterion.

5.5.4 Steel and coating temperatures at onset of swelling

The steel temperature at the time when the onset of swelling was achieved was evaluated for all the test samples coated with a *"Medium DFT"* of thin intumescent coating in accordance with the two criteria. Once again, the compatibility of the two criteria was confirmed. The tested thin intumescent coating initiated the swelling process for steel temperatures included between 100 and 260℃ and it required higher steel temperatures at lower heat fluxes (see Figure 5.9). The error bars in Figure 5.9 represent the accuracy of the steel temperatures within the same experiment, measured with different K-type thermocouples.

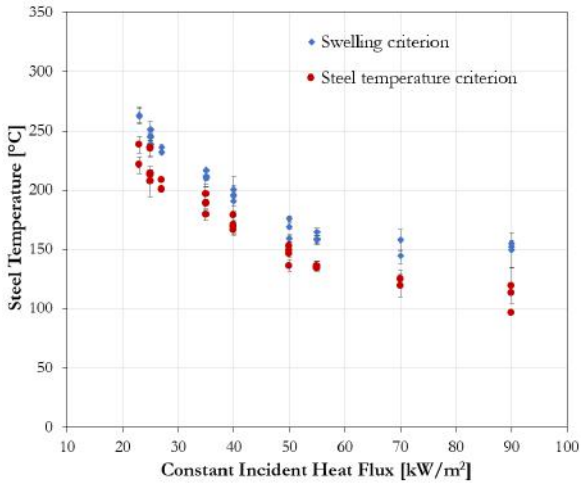

Figure 5.9: Steel temperature at onset of swelling for different incident constant heat fluxes, according to the two criteria (*"Medium DFT"*).

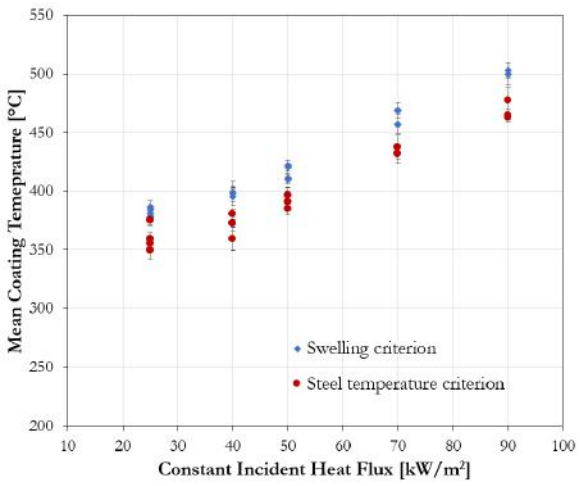

Figure 5.10: Mean coating temperature at onset of swelling for different incident constant heat fluxes, according to the two criteria (*"Medium DFT"*).

For samples tested at constant incident heat fluxes of 25, 40, 50, 70 and 90 kW/m^2, the surface temperature of the thin intumescent coating was measured using an Infra-Red camera. In the post-test analysis, the coating surface temperature was evaluated by setting a constant coating emissivity ε_c equal to 0.92 and averaging the coating temperature over a 50 x 50 mm^2 area, placed at the centre of the test sample (Figure 5.11). Subsequently, "mean coating temperature" was calculated as the average between the coating surface temperature and the steel temperature. Figure 5.10 shows the "mean coating temperature" at the onset of swelling for all the test samples coated with a *"Medium DFT"* of thin intumescent coating. The "mean coating temperature" varies between 350 and 500℃ and results evid-

ence the increase of the "mean coating temperature" at higher heat fluxes. The error bars in Figure 5.10 represent the accuracy of the measured temperatures, obtained as average between the error of the steel temperature (due to different K-type thermocouples) and the error of the coating surface temperature (maximum and minimum values over the control area).

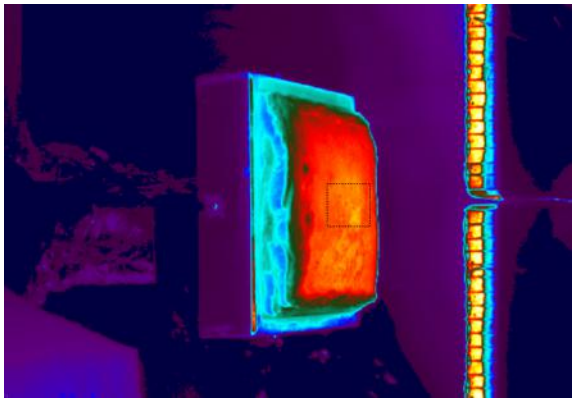

Figure 5.11: Post-test analysis of the coating surface temperatures using an Infra-Red camera.

5.5.5 Influence of the applied initial DFT

All the previous results were obtained by analysing the experiments carried out for all the test samples coated with a *"Medium DFT"* of thin intumescent coating. Secondly, the same analyses were performed for the two other groups of test samples, *"Low DFT"* and *"High DFT"*. Regarding the time to onset of swelling and the accumulated thermal energy flux at onset of swelling, similar graphs to the ones in Figure 5.9 and Figure 5.10 were obtained. No significant differences to the conclusions drawn for the *"Medium DFT"* test samples were outlined. On the contrary, the applied initial DFT significantly influenced the steel temperature and "mean coating temperature" at onset of swelling. Figure 5.12 and Figure 5.13 show this concept, according to the swelling criterion. Compared to the *"Medium DFT"* case, the onset of swelling occurred at higher ranges of steel temperatures (170-260℃) and "mean coating temperatures" (360-510℃) for all the test samples coated with a *"Low DFT"*, while at lower ranges of steel temperatures (90-200℃) and "mean coating temperatures" (370-480℃) for all the test samples coated with a *"High DFT"*. This difference was more obvious for the steel temperatures, rather than the "mean coating temperatures".

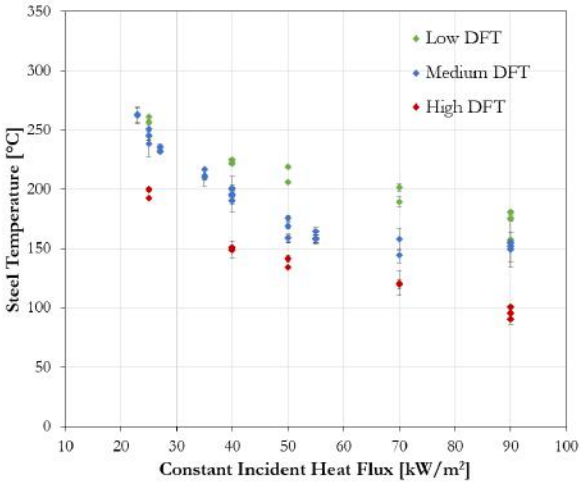

Figure 5.12: Influence of the applied initial DFT on the steel temperature at onset of swelling for different incident constant heat fluxes, according to the swelling criterion.

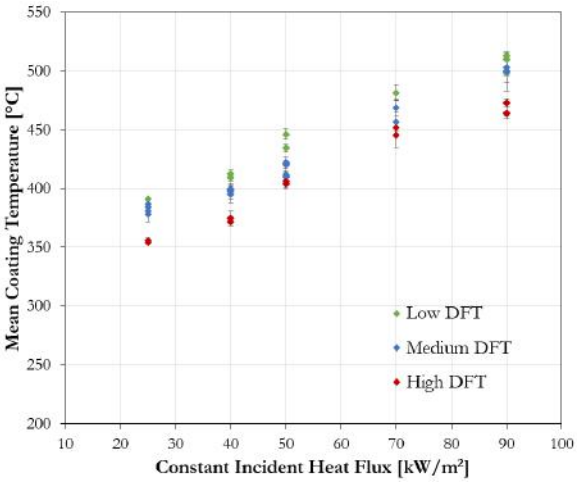

Figure 5.13: Influence of the applied initial DFT on the coating temperature at onset of swelling for different incident constant heat fluxes, according to the swelling criterion.

5.6 Conclusions

The current study presented a systematic investigation on the onset of swelling for thin intumescent coatings applied on steel plates. Tests samples coated with three different DFTs of a commercially available thin intumescent coating were fire tested under varied levels of incident radiant heat flux. From the results analysed herein, the following concluding remarks can be drawn:

- The finite-difference model shown herein is capable of simulating the temperature increase of coated steel plates prior to swelling.
- The onset of swelling for thin intumescent coatings can be assessed according to two criteria, one related to the minimum coating swelling and one related to the time-history of the coated steel temperatures.
- The critical incident heat flux for onset of swelling for the tested thin intumescent coating was found to be between 20 and 23 kW/m^2.
- For the occurrence of onset of swelling, the tested thin intumescent coating requires at least 7 MJ/m^2 of accumulative thermal energy flux, defined as the net heat flux absorbed by test samples during heating.

- This experimental study confirms that the onset of swelling of thin intumescent coatings is directly influenced by the heating conditions (or type of fire). For samples coated with *"Medium DFT"* (1.54 – 2.01 mm), the onset of swelling occurred for steel temperatures between 100 and 260°C and "mean coating temperatures" between 350 and 500°C.
- The onset of swelling of thin intumescent coatings is also influenced by the applied initial dry film thickness. For samples coated with a *"Low DFT"* (0.89 – 1.20 mm), the onset of swelling occurred for steel temperatures between 170 and 260°C and "mean coating temperatures" between 360 and 510°C. For samples coated with a *"High DFT"* (2.71 – 3.04 mm), the onset of swelling occurred for steel temperatures between 90 and 200°C, and a "mean coating temperatures" between 370 and 480°C.

The experimental study presented herein shows that the onset of swelling is a complex aspect of the behaviour of thin intumescent coatings exposed to fire. The problem appears to be governed by a combination of the time-history of the net heat flux, total net thermal energy, applied DFT and temperatures of the substrate and coating.

Bibliography

[1] Li G.Q., Lou G.B., Zhang C., Wang L. and Wang Y. "Assess the fire resistance of intumescent coatings by equivalent constant thermal resistance". Fire Technology, vol. 48, pp. 529-546, 2012.

[2] Wang L., Dong Y., Zhang D., Zhang D. and Zhang C. "Experimental study of heat transfer in intumescent coatings exposed to non-standard furnace curves". Fire Technology, vol. 51, no. 1, pp. 627-643, 2015.

[3] Elliott A., Temple A., Maluk C. and Bisby L. "Novel testing to study the performance of intumescent coatings under non-standard heating regimes". Fire Safety Science – Proceedings of the 11th International Symposium, University of Canterbury, New Zealand, pp. 652-665, 2014.

[4] Lucherini A., Giuliani L. and Jomaas G. "Experimental study of the performance of intumescent coatings exposed to standard and non-standard fire conditions". Fire Safety Journal, vol. 95, pp. 42-50, 2018.

[5] Zhang Y., Wang Y., Bailey C.G. and Taylor A.P. "Global modelling of fire protection performances of an intumescent coating under different furnace fire conditions". Journal of Fire Science, vol. 31, no.1, pp. 51-72, 2012.

[6] Bourbigot S., Duquesne S. and Leroy J.-M. "Modeling of heat transfer of a polypropylene-based intumescent system during combustion". Journal of Fire Sciences, vol. 17, pp. 42-56, 1999.

[7] Anna P., Marosi Gy., Bourbigot S., Le Bras M. and Delobel R. "Intumescent flame retardant systems of modified rheology". Polymer Degradation and Stability, vol. 77, pp. 243-247, 2002.

[8] Jimenez M., Duquesne S. and Bourbigot S. "Intumescent fire protective coating: toward a better understanding of their mechanism of action". Thermochimica Acta, vol. 449, pp. 16-26, 2006.

[9] Bourbigot S. and Duquesne S. "Fire retardant polymers: recent developments and opportunities". Journal of Materials Chemistry, vol. 17, pp. 2283-2300, 2007.

[10] Griffin G.J., Bicknell A.D. and Brown T.J. "Studies on the effect of atmospheric oxygen content on the thermal resistance of intumescent fire-retardant coatings". Journal of Fire Science, vol. 23, no. 4, pp. 303-328, 2005.

[11] Bourbigot S., Le Bras M., Delobel R. and Tremillon J.M. "Synergistic effect of zeolite in an intumescence process: Study of the interactions between the polymer and the additives". Journal of the Chemical Society, Faraday Transactions, vol. 92, no. 18, pp. 3435-3444, 1996.

[12] Maluk C., Bisby L., Krajcovic M. and Torero J.L. "A Heat-Transfer Inducing System (H-TRIS) Test Method". Fire Safety Journal, vol. 105, pp. 307-319, 2019.

[13] International Organization fro Standardization (ISO). "ISO 8501-1:2007 Preparation of steel substrates before application of paints and related products - Visual assessment of surface cleanliness - Part 1: Rust grades and preparation grades of uncoated steel substrates and of steel substrates after overall removal of previous coatings". Geneva, Switzerland, 2007.

[14] Emmons H.W. "The numerical solution of heat conduction problems". Transactions of American Society of Mechanical Engineers (ASME), vol. 65(6), pp. 607-615, 1943.

[15] Dusinberre G.M. "Heat transfer calculations by finite differences". International Textbook Company, Pennsylvania, USA, 293 pp., 1961.

[16] Incropera F.P., DeWitt D.P., Bergman T.L. and Lavine A.S. "Fundamental of heat and mass transfer". John Wiley & Sons, 6th Edition, 2006.

[17] Comité Europeén de Normalization (CEN). "EN 1993-1-2:2005 Eurocode 3: Design of steel structures - Part 1-2: General rules - Structural fire design". Brussels, Belgium, 2005.

6

Influence of heating conditions and initial coating thickness

6.1 Introduction and background

Within the structural and fire safety engineering practice, the insulating capacity of intumescent coatings is commonly assessed using two simplified engineering design methods based on exposure to the standard temperature-time fire curve in a furnace [1-4]. These methods are developed based on experimentally-measured temperatures of coated steel samples tested in a standard fire resistance test. The first method consists of creating *tabulated fire ratings*, where manufacturers offer design tables that list the minimum DFTs required to ensure a certain level of fire protection (i.e. the steel temperature remains below a certain predefined critical value in the standard fire resistance furnace test). Alternatively, the European *effective thermal conductivity method* can be used to simulate the heat transfer from the fire into the steel using a lumped capacitance approximation of the transient heat conduction problem [4]. This method assumes that the intumescent coating does not expand, but it experiences a transient change of its thermal conductivity. The resulting temperature-dependent effective thermal conductivity of the intumescent coating estimates an equivalent thermal barrier to the protected structure and this method implicitly assumes that the thermo-physical properties of the intumescent coating only depend on the temperature. However, intumescent coatings are chemically reactive materials and numerous researchers have emphasised the influence of the heating conditions on the intumescent process and the overall insulating effectiveness [5-10]. In particular, slow-growing fires or low heating regimes may have a negative impact on the insulating performance of intumescent coatings by causing incomplete swelling or even melting and delamination [5, 9].

As a consequence, the current procedures do not represent a comprehensive design practice to ensure the fire safety of structures. They do not fully assess the effectiveness of intumescent coatings through a detailed characterisation of the heat transfer within the swelling coating. Most importantly, these simplified engineering methods simulate the temperature evolution of coated samples in furnaces exposed to a single heating scenario, not addressing the whole range of potential heating regimes occurring in a fire. In a world moving towards performance-based engineering solutions, there is a need for explicitly understanding how different factors may influence the effectiveness of intumescent coatings, e.g. heating conditions and applied initial thickness. By obtaining this scientific and practical knowledge, it will

be possible to formulate and validate models able to produce realistic and reliable predictions for the design of fire-safe structures.

The available literature presents limited research studies that have looked at assessing the effectiveness of intumescent coatings through their thermo-physical response (refer to Chapter 2). This progress is commonly inhibited by inadequate testing methodologies and experimental setups. In particular, standard fire resistance tests in furnaces have been questioned due to the poor repeatability and the uncertain thermal boundary conditions imposed on test samples [11-12]. In addition, the closed environment of standard furnaces does not allow for accurate visual inspection of test samples during the heating exposure, a key aspect to comprehend the thermo-physical response of intumescent coatings. A few researchers have proposed various approaches and methodologies to analyse the heat transfer within intumescent coatings by placing in-depth thermocouples within intumescent coatings [13-15]. However, this methodology has been adopted in only a few cases because of the experimental difficulties related to gauging accurate measurements of the in-depth temperature distributions without disturbing the swelling process.

The study presented herein shows an experimental methodology aimed at analysing the effectiveness of intumescent coatings through a detailed characterisation of their thermo-physical response. In particular, the influences of different heating conditions and the applied initial thickness were investigated. Steel plates coated with a commercial solvent-based thin intumescent coating were exposed to well-defined and highly-repeatable heating conditions using the Heat-Transfer Rate Inducing System (H-TRIS) test method. Test samples were thoroughly instrumented in order to measure the real-time swelled coating thickness, the exposed surface temperature, the substrate temperature and the in-depth transient temperature profile within the intumescent coating.

6.2 Experimental investigation

6.2.1 Experimental methodology

The experimental methodology was chosen in order to have direct control and quantification of the thermal boundary conditions imposed on the test samples, ensuring high repeatability

between experiments at low economic and temporal costs. The Heat-Transfer Rate Inducing System (H-TRIS) offers these advantages over conventional testing, therefore it was selected as the appropriate experimental methodology [12]. H-TRIS accurately controls the relative position between the target exposed surface of the test sample and the surface of an array of radiant panels, moving on a computer-controlled linear motion system (Figure 6.1). In this way, H-TRIS is able to impose a well-defined time-history of incident radiant heat flux on the exposed surface of the test sample. In addition, thanks to its open environment, H-TRIS allows for the visual inspection of the test samples during the heating exposure (e.g. measuring the swelled coating thickness). The H-TRIS assembled for this specific research study was composed of four high-performance natural-gas-fired radiant panels mounted on a supporting frame and creating a 300 x 400 mm^2 radiant heat source (Figure 6.1). In this configuration, the apparatus can impose a wide range of incident radiant heat fluxes included between 5 and 100 kW/m^2 (refer to Chapter 3).

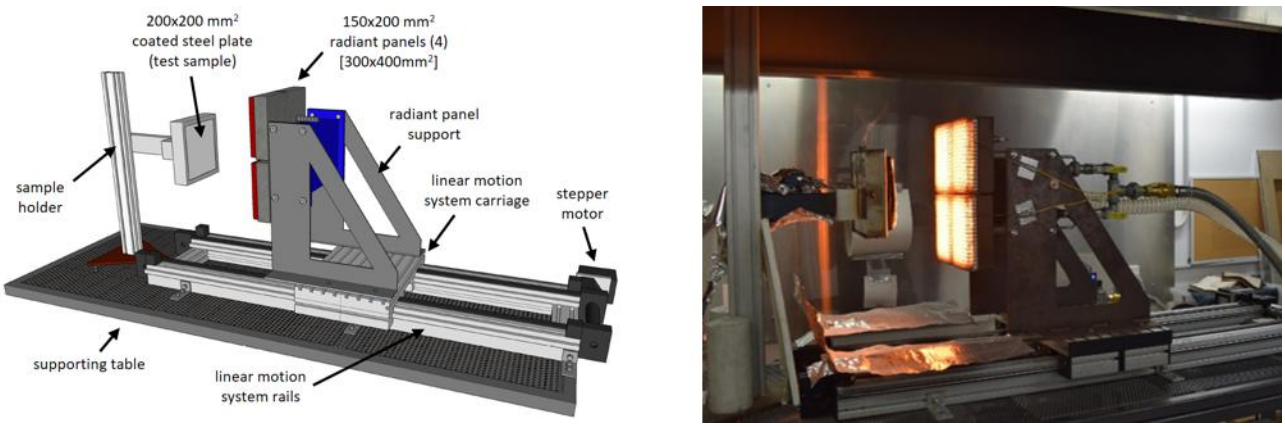

Figure 6.1: Illustration of the experimental setup based on the H-TRIS test method (*Bench-scale H-TRIS 2.0*).

6.2.2 Test samples and description of the experiments

The samples used in this experimental study are 200 x 200 mm^2, 10 mm thick mild carbon steel plates, resulting in a section factor A_p/V (i.e. ratio between exposed surface and volume of steel) equal to 100 m^{-1} (Figure 6.1). Based on the assembled H-TRIS, the sample dimensions were chosen in order to achieve a surface distribution of incident radiant heat flux on the sample surface with a deviation lower than 10%. The steel plates were professionally coated with a solvent-based thin intumescent coating. The product is commercialised world-

wide for providing up to 120 minutes fire resistance to universal steel sections and cellular beams. It is commonly used in the built environment for internal, semi-exposed or external use and it is suitable for off-site and on-site application. The coating is a fast-track and self-priming coating, therefore it was applied in one hand using airless spray equipment, without the use of any primer or topcoat. After one month of curing, the applied DFT was measured using a non-destructive film thickness gauge at five different locations (at each corner and the centre of each coated plate). Based on the mean DFT measured over the steel plate surface, the test samples were selected to be categorised into three groups:

1. *"Low DFT"* – 1.00 mm ($\pm$ 0.20 mm)
2. *"Medium DFT"* – 1.80 mm ($\pm$ 0.20 mm)
3. *"High DFT"* – 2.90 mm ($\pm$ 0.20 mm)

Table 6.1: Test matrix of the experimental study.

Sample group	Heating conditions	Number of repetitions	DFT_{mean} [mm]
"Low DFT"	10 kW/m^2	1	0.887
	25 kW/m^2	2	1.062, 1.204
	40 kW/m^2	2	0.996, 1.069
	50 kW/m^2	2	1.194, 1.1196
	70 kW/m^2	2	1.162, 1.198
	90 kW/m^2	3	1.134, 1.146, 1.146
"Medium DFT"	10 kW/m^2	2	1.620, 1.712
	25 kW/m^2	2	1.638, 1.786
	40 kW/m^2	2	1.680, 1.816
	50 kW/m^2	3	1.794, 1.920, 2.014
	70 kW/m^2	2	1.712, 1.898
	90 kW/m^2	3	1.630, 1.770, 1.870
"High DFT"	10 kW/m^2	1	2.716
	25 kW/m^2	2	2.714, 2.902
	40 kW/m^2	2	2.750, 2.822
	50 kW/m^2	2	2.854, 2.866
	70 kW/m^2	2	2.878, 2.954
	90 kW/m^2	3	2.992, 3.038, 3.086

Using the H-TRIS test method, coated samples were individually tested for 60 minutes under different levels of constant incident radiant heat flux: 10, 25, 40, 50, 70 and 90 kW/m^2 (Table 6.1). The heating conditions were explicitly chosen in order to subject the intumescent coating to various ranges of temperatures and heating rates, triggering the swelling reaction in

different ways. Particularly, based on a previous research study, a constant incident radiant heat flux of 10 kW/m^2 was expected not to initiate the swelling process of the intumescent coating (refer to Chapter 5). During the heating exposure, a custom-built steel frame was used in order to hold the test sample aligned with the centre-point of the array of radiant panels, in a vertical orientation (Figure 6.1). In order to replicate repeatable thermal boundary conditions, heat losses at the back of the test sample were minimised by insulating the unexposed surface of test samples using a layer of 20 mm thick ceramic wool (ISOLITE ISOWOOL blanket) and 13 mm thick plasterboard (Knauf FireShield).

6.2.3 Instrumentation

The experimental setup was instrumented in order to systematically gauge all the possible information necessary to describe the thermo-physical response of the intumescent coating during the heating exposure.

1. The *thickness of the swelled intumescent coating* was measured by image processing of video footages taken using a high-resolution camera placed at the side of the test sample, aligned with the surface of the test sample (Figure 6.2). The swelled coating thickness was estimated in correspondence of the central area of test samples, therefore disregarding edge effects at the sample boundaries. The real-time measurement of the coating thickness was also used for continuously adjusting the relative distance between the intumescent coating surface and the array of radiant panels. In this way, the incident radiant heat flux at the exposed surface of the test sample was maintained to the specified value during the full duration of experiments.

2. Up to seven K-type thermocouples (1.5 mm diameter) were installed in the test sample in order to measure the *transient temperature profile within the intumescent coating*. Prior to testing, 1.8 mm holes were drilled through the steel plate in order to allow the insertion of the in-depth thermocouples from the rear of the test sample (Figure 6.2). Preliminary tests evidenced that, if the thermocouples were placed at the beginning of the heating exposure, they would have perturbed the swelling process and the development of the intumescent char. Therefore, the thermocouples were inserted at specific locations within the swelling coating during the heating exposure. The

real-time measurement of the swelled coating thickness was used to understand when a thermocouple could be inserted at a certain depth. The thermocouples were positioned at depths multiple of 5 mm from the interface between the coating and the steel plate: 5, 10, 15, 20, 25, 30, 35 mm. Particular care was taken in order not to damage the surface crust developed by the intumescent coating, which represents a key feature for the development of an effective thermal barrier [9].

3. The *temperature of the steel plate* was measured using up to three K-type thermocouples attached to the unexposed surface of the test samples (Figure 6.2).
4. The *exposed surface temperature of the intumescent coating* was measured using an Infra-Red camera (model FLIR SC655: 16-bit 640 x 480 pixel resolution at 50 Hz, spectral range 7.5 - 14 μm, temperature range up to 2000°C) (Figure 6.2).

Figure 6.2: Different aspects of the experimental setup designed to gauge the thermo-physical response of intumescent coatings during heating exposure.

6.3 Experimental results

6.3.1 Steel temperatures and swelled coating thickness

The performance of intumescent coatings was firstly characterised according to the evolution of the steel temperatures and the swelled coating thicknesses during the thermal ex-

posure. Figure 6.3 shows the evolution of the steel temperatures and the swelled coating thicknesses for all the different experiments carried out on coated samples. The good repeatability between experiments was confirmed by the agreement of the temperature readings and the estimations of the swelled coating thickness. Throughout all the experiments, the steel temperatures measured using thermocouples had deviations lower than 10%, the central area of the test samples swelled rather homogeneously and the swelled coating thicknesses were measured with an accuracy of ± 2 mm. For simplicity and neatness of graphical visualisation, only the average values are displayed in this manuscript. In the graphs, the same colour collects all the experiments with the same heating conditions, while continuous, dashed and dotted lines report single experimental repetitions.

As regards the steel temperatures, most of the coated steel plates reached a steady-state temperature by the end of the heating exposure. However, in a few cases, the steel never reached a quasi-steady state temperature and the temperature kept increasing during the heating exposure, such as 50, 70 and 90 kW/m^2 for *"Low DFT"* and 70 and 90 kW/m^2 for *"Medium DFT"*. This aspect can be directly associated with the completion of the swelling process of the intumescent coating: in these cases, the coating completed the swelling process before the end of the experiment. In other cases, where the coating continuously swelled during the experiments, the steel plates tended to a similar range of steady-state temperatures, included between 300 and 350°C. The external incident heat flux had a minor influence. On the other hand, a higher applied initial DFT foreseeably produced a lower steady-state steel temperature due to the thicker porous char.

With regards to the swelled coating thicknesses, right after the application of the incident heat flux, the intumescent coating quickly started swelling with different rates depending on the heating conditions, i.e. the slope/derivative of the thickness-time curve (Figure 6.3). As expected, the samples exposed to 10 kW/m^2 did not practically swell, regardless of the applied initial DFT. For the higher heat fluxes, the swelling rate of the intumescent coating appeared to be directly influenced by the external incident heat flux, while independent on the applied initial DFT. On the contrary, the applied initial DFT governed the maximum thickness that the coating could have reachedd during the thermal exposure. In particular, test samples coated with *"Low DFT"*, *"Medium DFT"* and *"High DFT"* swelled up to about 30 mm, 40 mm and 65 mm, respectively. Figure 6.4 shows the typical porous chars developed

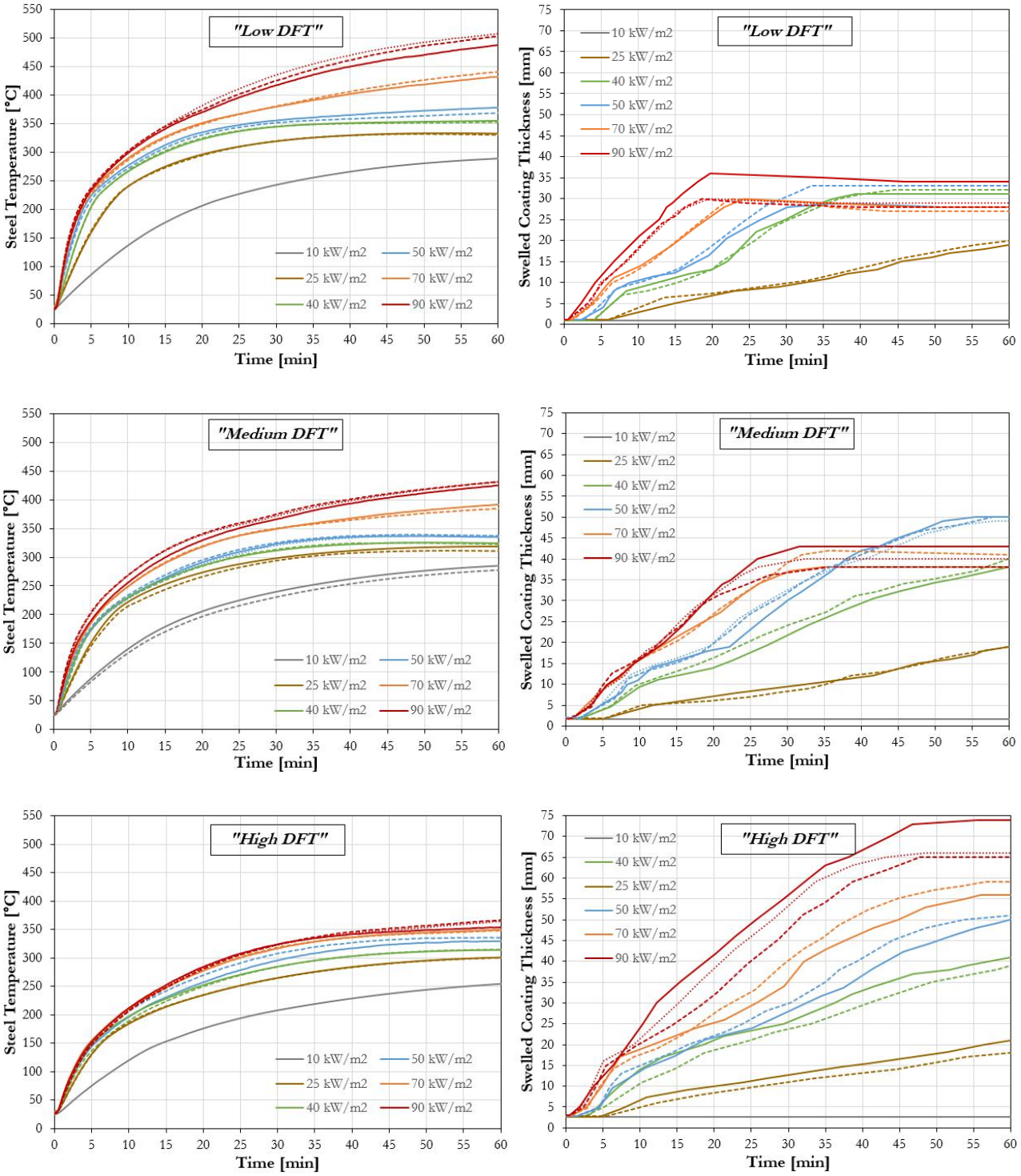

Figure 6.3: Comparison of the evolution of the coated steel temperatures and the swelled coating thickness for different applied initial DFTs and different constant incident heat fluxes.

by the intumescent coating at the end of the thermal exposure (more pictures are available in Appendix B): as shown in Figure 6.3, a thicker intumescent porous char was produced for a higher constant incident heat flux. In order to emphasise the difference between differ-

ent heating conditions, Figure 6.4 reports the test samples coated with *"High DFT"*: in this case, the intumescent coating was able to swell throughout the whole duration of the heating exposure and develop the thickest porous chars (within the limits of this experimental study). For high heat fluxes, Figure 6.4 also highlights the oxidation reactions occurring at the surface of the intumescent coating: the char turned into ash at the coating surface crust, characterised by a white/grey colour. This phenomenon can be clearly observed for constant incident heat fluxes of 70 and 90 kW/m^2, partially for 50 kW/m^2. Figire 6.4 also shows that typical porous chars formed into a dome-like shape, in some cases (40 kW/m^2) more than others. However, the char shape had a minor influence on the experimental outcomes of this research study because all the temperature and swelling measurements were concentrated in the central area of the test sample, where even temperature and homogenous swelling were observed. In addition, the one-dimensional heat transfer was ensured due to the small view factor of the sample edges compared to the exposed surface of the intumescent coating.

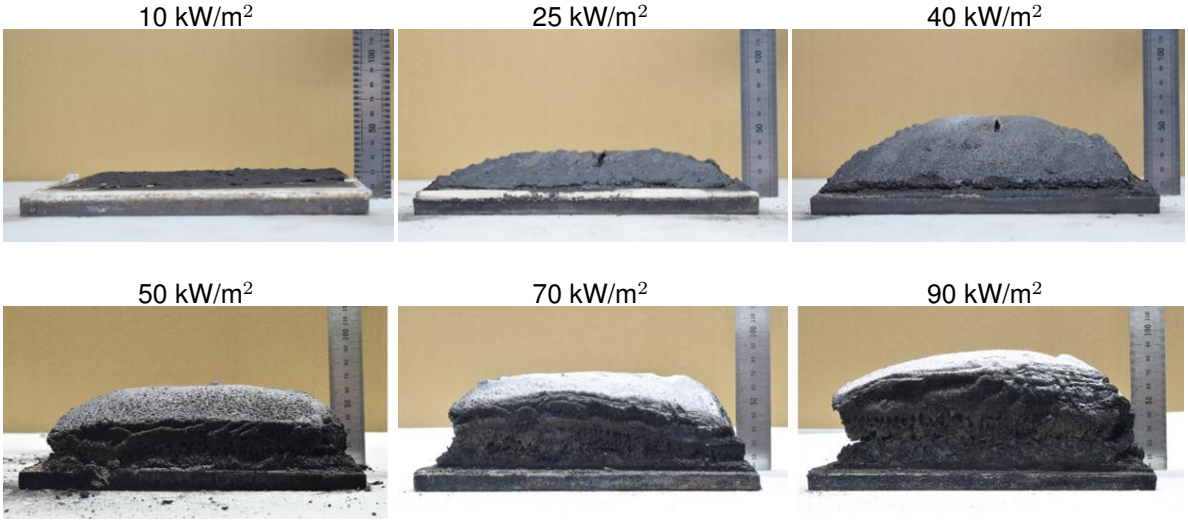

Figure 6.4: Typical porous chars developed by the intumescent coating at the end of the thermal exposure for different constant incident heat fluxes (*"High DFT"*).

6.3.2 Coating surface temperature

In a post-test analysis, the temperature evolution at the exposed surface of the intumescent coating was evaluated by processing the data obtained by the Infra-Red camera. The coating emissivity value was set equal to 0.90 and the coating temperature was averaged over

a 50 x 50 mm^2 area, placed at the centre of the test sample (refer to Figure 5.11). The emissivity value has a key role in this process and it can significantly influence the results. Consequently, a sensitivity analysis of the surface emissivity value of the intumescent coating was performed: the same procedure was repeated for varying coating emissivity 0.90 $\pm$ 0.05, accordingly to the average values found in a previous research study (spectral range 2 - 20 μm) (refer to Chapter 4). Figure 6.5 shows the envelopes of the measured temperatures at the coating surface in all the experiments carried out under different heating conditions and applied initial DFTs: all the different temperature curves are available in Appendix A. The continuous lines report the average temperatures calculated with an emissivity equal to 0.90, while the dotted lines define the envelopes obtained from the sensitivity analysis (maximum values: ε = 0.85; minimum values: ε = 0.95).

During the different experiments, the coating behaved like a low thermal inertia material by quickly reaching a specific surface temperature depending on the external heat flux and keeping a quasi-constant temperature during the rest of the heating exposure (thermally thick material characterised by a high Biot number). As expected, higher coating surface temperatures were measured for higher external constant incident heat fluxes. The applied initial DFT did not significantly influence the evolution of the coating surface temperature. In the second part of the heating exposure, the measured temperature gradually decreased, particularly for higher heat fluxes. This aspect could be related to the reduction in the emissivity due to the oxidation of the coating surface, which can be visually assessed through the colour change (white/grey). Another reason could be related to the migration of the oxidation front within the intumescent porous char: once the oxidation reaction (exothermic) is completed, the surface temperature decreases. Without any doubt, the lower surface temperatures measured in the cases of 70 and 90 kW/m^2 can be directly associated with oxidation processes taking place at the coating surface. For heat fluxes higher than 50 kW/m^2, the measured surface temperatures were above 700°C: at this temperature range, oxidation is expected. This aspect is confirmed by the TGA results in oxidising atmosphere and photographs of the intumescent porous chars (Figure 6.4), but it certainly needs further investigation to clarify the effects of the surface oxidation on the emissivity of swelling intumescent coatings.

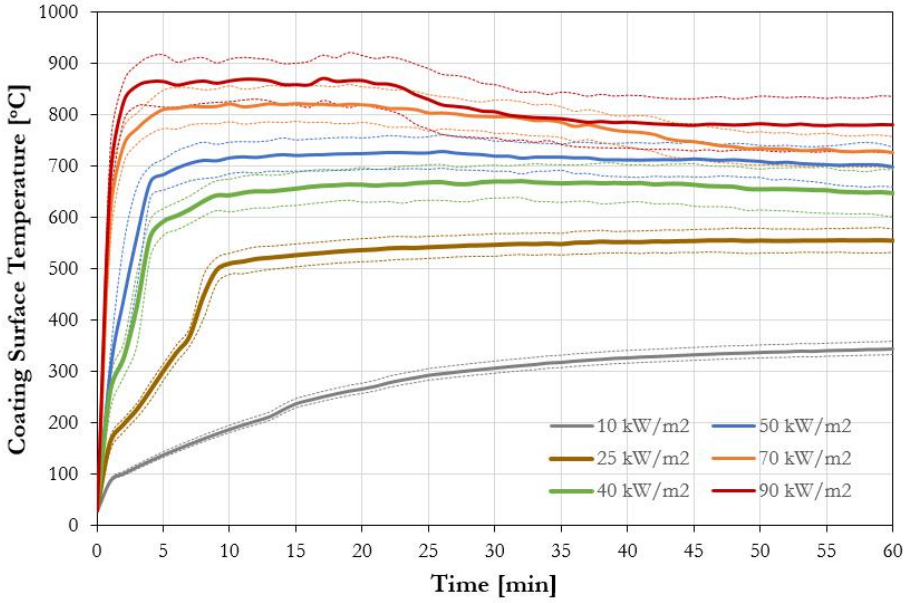

Figure 6.5: Envelopes of the temperature evolution at the coating surface for the different external constant incident heat fluxes (all experiments with different applied initial DFTs are included).

6.3.3 In-depth temperature profiles

The heat transfer within swelling intumescent coatings was then investigated analysing the evolution of the in-depth temperature profiles: all the different temperature curves are available in Appendix A. First, the agreement of the temperature readings between different experimental repetitions confirmed the good repeatability. In addition, the results highlighted the success of the designed experimental methodology able to accurately gauge the thermo-physical response of intumescent coatings. Comparisons between experiments with and without in-depth thermocouples also confirmed the minor interference of the installed instrumentation.

Figure 6.6 shows the temperature profiles measured at the end of the heating exposure for all the different experiments on coated samples. The temperature profiles can be assumed as steady-state if the swelling process of the intumescent coating was completed. The in-depth temperatures at different depths within the intumescent coating are reported with the average surface temperatures (ε = 0.90). For visualisation purposes, the error bars were omitted from the graphs. However, the in-depth thermocouples were placed within the intumescent coating with an accuracy $\pm$ 2 mm and the measured in-depth temperatures had a

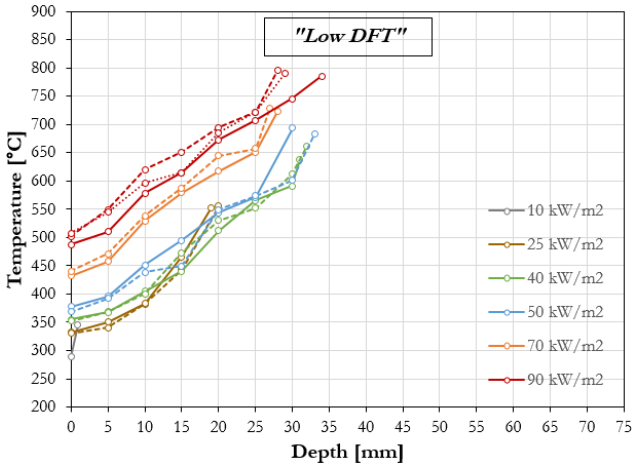

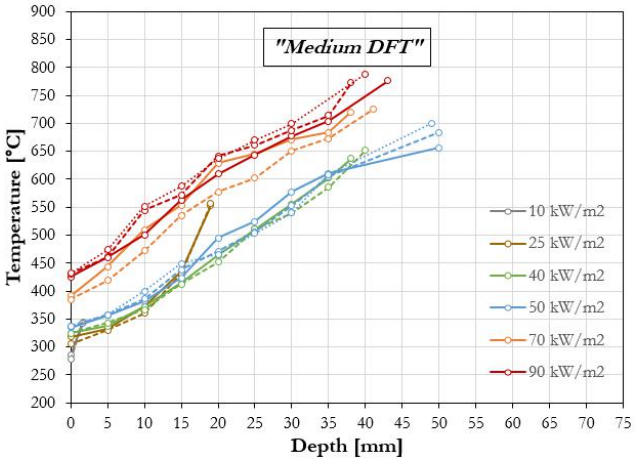

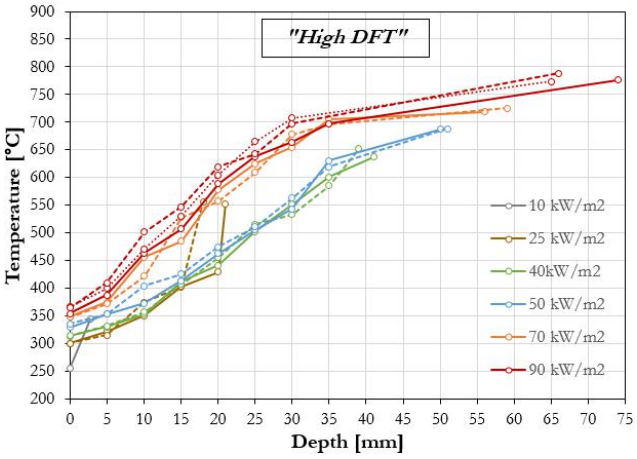

Figure 6.6: Comparison of the measured temperature profiles at the end of the heating exposure for different applied initial DFTs and different constant incident heat fluxes.

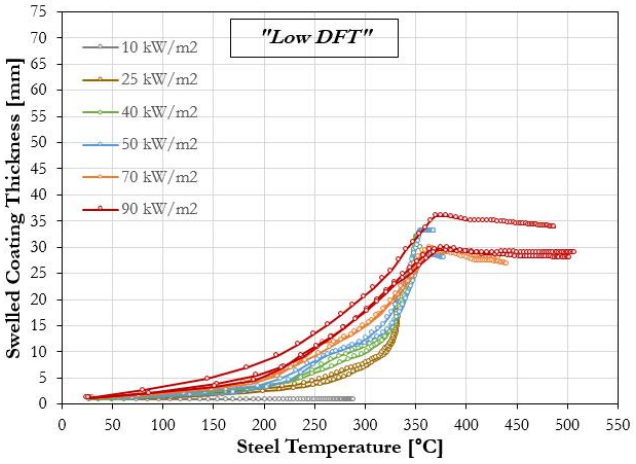

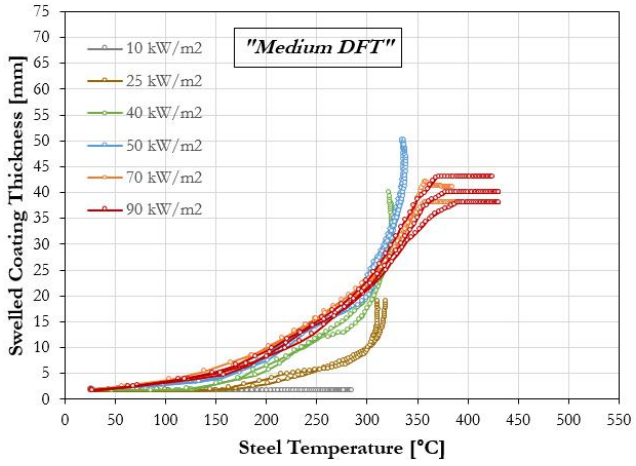

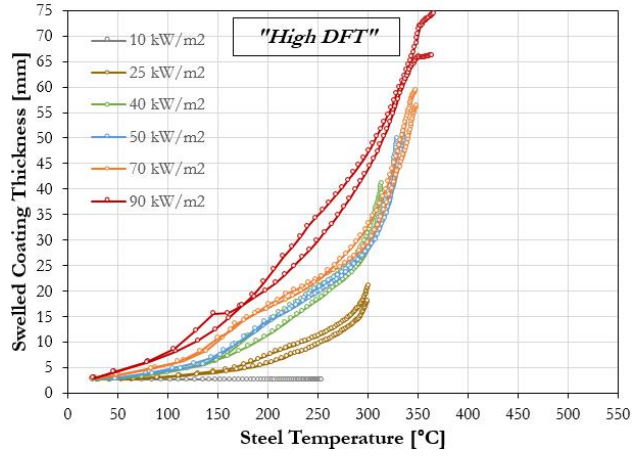

Figure 6.7: Swelled coating thicknesses as a function of the coated steel temperature for different applied initial DFTs and different constant incident heat fluxes.

deviation lower than 10%. The steady-state temperature profiles shown in Figure 6.6 had similar thermal gradients (slope of the in-depth temperature profile) within the intumescent coating. This aspect suggested that the intumescent porous char had similar thermal and physical properties, regardless of the imposed heating conditions. As already explained in the previous section, after the first transient period, the coating surface temperature can be considered as constant and it can be directly related to the external constant incident heat flux. Regarding the steel substrate, if the coating underwent continuous swelling, the steel temperature remained within a similar range (300-350℃). Consequently, the thermal gradient with the intumescent coating was governed by the swelled coating thickness. Since the extremes of the intumescent coating can be considered to have a quasi-constant temperature, further swelling resulted in stretching the thermal gradient between the steel substrate and the coating surface. This aspect is highlighted in Figure 6.8 at 50 kW/m^2, a steel plate coated with *"High DFT"* continuously swelled during the heating exposure and the steel temperature did not overcome 350℃. On the other hand, at 50 kW/m^2, a steel plate coated with *"Low DFT"* completed the swelling reaction after about 30-35 minutes of heating exposure and, beginning from that moment, the steel temperature started increasing above 350℃.

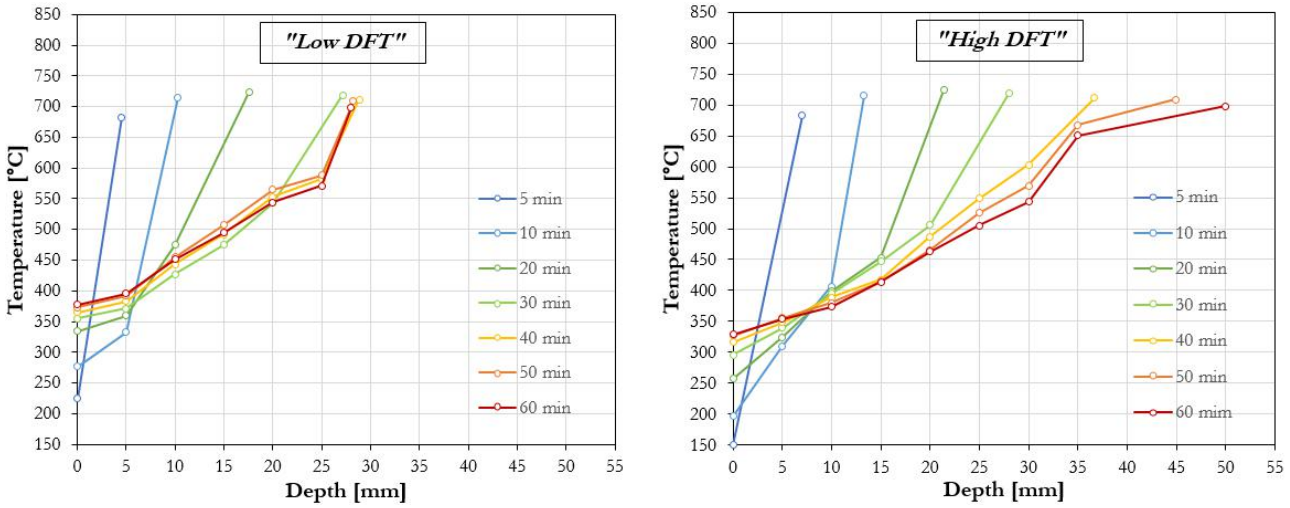

Figure 6.8: Comparison of the evolution of the temperature profiles (in-depth and surface) at different instants during the heating exposure with different applied initial DFTs exposed to 50 kW/m^2.

6.4 Analysis and discussion

So far, the experimental investigation has underlined how the evolutions of the substrate temperature and the swelled coating thickness are closely related and they have key roles in the understanding and the assessment of the effectiveness of intumescent coatings. Figure 6.7 reports the evolution of the swelled coating thicknesses as a function of the coated steel temperature for different applied initial DFTs and heating conditions. The experimental results confirmed how, in case of continuous swelling, the coated steel plates asymptotically tended to a similar temperature range included between 300 and 350 °C, regardless of the heating condition or the applied initial DFT. Contrarily, when the coating completed the swelling process, the steel temperatures increased above this threshold. This aspect is supported by the results obtained by TGA: the intumescent swelling reaction occurs at temperatures between 350 and 400 °C and it can be considered to be completed at about 400 °C.

The evolution of coated steel temperatures provides a first assessment of the coating effectiveness: i.e. the colder the steel, the better thermal insulation. In turn, as shown in Figure 6.7, the coated steel temperatures can be directly linked to the coating swelling process. Therefore, it can be concluded that the swelling process and the resulting swelled thickness govern the thermo-physical response of intumescent coatings, thus their effectiveness. In particular, the coated steel temperature acts as an indicator of the swelling process of intumescent coatings: if the steel temperature overcomes 350 °C, the swelling reaction is completed. This aspect has been verified also by a close investigation of the recorded video footage. This experimental outcome suggests that the swelling reaction takes place close to the steel substrate: particularly, about the interface between the steel and the applied intumescent coating. The intumescent coating swells and insulates the steel substrate by displacing the already-swelled coating towards the direction of the heat source. The swelling reaction continues at the virgin coating located behind the swelled porous char and in the proximity to the steel substrate. This process lasts until the intumescent coating is fully consumed, which can be directly related to the applied initial DFT. As a conclusion, the steel temperature can be directly associated with the swelling process because it defines the temperature experienced by the virgin coating, which is located behind the swelled porous char and sustains the swelling reaction.

The non-unique relationship between the steel temperature and the swelled coating thickness shown in Figure 6.7 may be explained by the direct influence of the heating conditions. In particular, experimental results highlighted that higher external incident heat fluxes produced higher coating thicknesses while the steel remains at the same temperature. Assuming similar thermal and physical properties of the intumescent porous char (as discussed in Section 6.3.3), a higher net heat flux to the virgin coating, which sustains the swelling reaction, is expected. Consequently, a higher incident heat flux at the coating surface provides higher net heat flux to the swelling reaction, thus it governs the swelling rate. For instance, an incident heat flux of 10 kW/m^2 did not trigger the swelling reaction due to the low steel temperatures (below 300℃) and the low net heat flux received by the virgin coating.

Nevertheless, the experimental study presented herein emphasised how the swelling process and the resulting swelled thickness govern the thermo-physical response of intumescent coatings, thus their effectiveness. In particular, the influence of heating conditions and the applied initial DFT can be clearly outlined and empirical correlations can be derived. First, the applied initial DFT governs the maximum swelled thickness that the intumescent coating could have reached during the thermal exposure. The applied initial DFT provides a quantification of the intumescent material that can potentially swell and hence produces porous char. Figure 6.9 defines a possible linear correlation between the applied initial DFT and the maximum swelled thickness of the intumescent coating after the completion of the swelling process. Regarding the heating conditions, the external incident heat flux at the coating surface governs the swelling rate of intumescent coatings. Figure 6.10 defines a possible linear correlation between the constant incident heat flux and the swelling rate of the intumescent coating. In this calculation, the swelling rate of the intumescent coating was linearised from the onset of swelling until the instant when the maximum swelled thickness was reached. Theoretically, it should be possible to correlate the swelling rate to more fundamental parameters, such as the net flux through the swelled porous char and received by the virgin coating that sustains the swelling reaction. The process would be possible only by formulating a heat transfer model. However, the thermal and physical properties of intumescent porous chars should be defined in order to estimate such parameters. This aspect is outside the scope of the current manuscript, but future studies will focus on that. As a conclusion, this experimental investigation presented how the swelling of intumescent

coatings, which is the main factor that governs their thermos-physical response and their effectiveness, can be predicted starting from well-defined thermal boundary conditions at the coating surface and applied initial DFT.

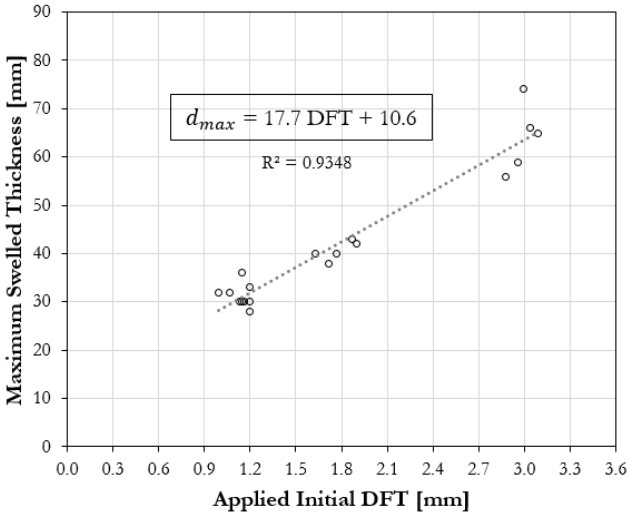

Figure 6.9: Empirical correlation between the applied initial DFT and the maximum swelled thickness of the intumescent coating.

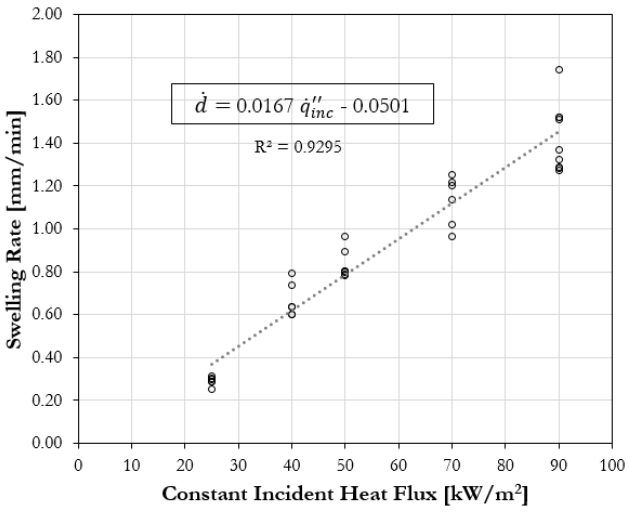

Figure 6.10: Empirical correlation between the external incident constant heat flux and the swelling rate of the intumescent coating.

6.5 Conclusions

The current practice of designing steel structures protected with intumescent coatings offers simplified engineering methods able to simulate the temperature evolution of coated steel samples tested in furnaces and exposed a single heating scenario. However, in a world moving towards performance-based solutions, there is a need for explicitly understanding how different factors may influence the effectiveness of intumescent coatings. The study presented herein shows an experimental methodology aimed at analysing the effectiveness of intumescent coatings through a detailed characterisation of their thermo-physical response for a range of heating conditions and applied initial Dry Film Thickness (DFT). Steel plates coated with a commercial solvent-based thin intumescent coating were exposed to well-defined and highly-repeatable heating conditions using radiant panels and in accordance with the Heat-Transfer Rate Inducing System (H-TRIS) test method. Experimental results demonstrate high repeatability between experiments and the ability to measure real-time swelled coating

thickness, the exposed surface temperature, the steel temperature and the in-depth transient temperature profile within the intumescent coating. From the experimental results, the following concluding remarks can be drawn:

- The swelling process and the resulting swelled thickness govern the thermo-physical response of intumescent coatings, thus their effectiveness. During swelling, the temperature of coated steel plates asymptotically tends to a temperature range between 300 and 350 ℃, regardless of the heating condition or the applied initial DFT. When the coating completes its swelling process, the steel temperature increases above 350 ℃. This aspect is supported by the material characterisation obtained by TGA experiments: the swelling reaction occurs at temperatures between 350 and 400 ℃ and it can be considered to be completed at about 400 ℃.
- The swelling reaction occurs in the proximity to the steel-coating interface. The intumescent coating swells and insulates the steel substrate by displacing the already-swelled coating towards the direction of the heat source. This explains why coated steel temperature acts as an indicator of the swelling process of intumescent coatings.
- The measured in-depth temperature profiles within the swelling coating suggest that the intumescent porous char has similar thermal and physical properties, regardless of the heating conditions or the applied initial DFT. The thermal gradient within the intumescent coating is governed by the swelled coating thickness.
- The heating conditions and the initial thickness differently influence the swelling process of intumescent coatings: the applied initial DFT governs the maximum swelled thickness, while the external incident heat flux at the coating surface governs the swelling rate. Using the empirical correlations derived based on the experimental results, the swelling of the tested intumescent coating can be predicted.

Future studies should focus on quantifying the thermal and physical properties of the intumescent porous char and implementing heat transfer models able to simulate the response of intumescent coatings. In particular, it would be interesting to understand if the net heat flux to the virgin coating, which is located behind the swelled porous char and sustains the swelling reaction, may be correlated to the swelling rate. Finally, the authors believe that the product tested in this experimental study represents a common behaviour of typical thin

intumescent coatings commercially available in the market. However, other products with different formulations should be investigated before generalising research outcomes.

Bibliography

[1] International Organization for Standardization (ISO). "ISO834-1:1999 Fire resistance tests - Elements of building construction - Part 1: General requirements for fire resistance testing". Geneva, Switzerland, 1999.

[2] Comité Europeén de Normalization (CEN). "EN 1363-1:2012 Fire resistance tests - Part 1: General Requirements". Brussels, Belgium, 2012.

[3] Comité Europeén de Normalization (CEN). "EN 1363-2:2012 Fire resistance tests - Part 2: Alternative and additional procedures". Brussels, Belgium, 1999.

[4] Comité Europeén de Normalization (CEN). "EN 13381-8:2013 Test methods for determining the contribution to the fire resistance of structural members - Part 8: Applied reactive protection to steel members". Brussels, Belgium, 2013.

[5] Elliott A., Temple A., Maluk C. and Bisby L. "Novel testing to study the performance of intumescent coatings under non-standard heating regimes". Fire Safety Science – Proceedings of the 11th International Symposium, University of Canterbury, New Zealand, pp. 652-665, 2014.

[6] Li G.Q., Lou G.B., Zhang C., Wang L. and Wang Y. "Assess the fire resistance of intumescent coatings by equivalent constant thermal resistance". Fire Technology, vol. 48, pp. 529-546, 2012.

[7] Wang L., Dong Y., Zhang D., Zhang D. and Zhang C. "Experimental study of heat transfer in intumescent coatings exposed to non-standard furnace curves". Fire Technology, vol. 51, no. 1, pp. 627-643, 2015.

[8] Zhang Y., Wang Y., Bailey C.G. and Taylor A.P. "Global modelling of fire protection performances of an intumescent coating under different furnace re conditions". Journal of Fire Science, vol. 31, no.1, pp. 51-72, 2012.

[9] Lucherini A., Giuliani L. and Jomaas G. "Experimental study of the performance of intumescent coatings exposed to standard and non-standard fire conditions". Fire Safety Journal, vol. 95, pp. 42-50, 2018.

[10] de Silva D., Bilotta A and Nigro E. "Experimental investigation on steel elements protected with intumescent coating". Construction and Building Materials, vol. 205, pp. 232-244, 2019.

[11] Maluk C., Bisby L., Terrasi G., Krajcovic M., Torero J.L. "Novel fire testing methodology: why, how and what now?". Proceedings of the Mini Symposium on Performance-based Fire Safety Engineering of Structures as part of the 1st International Conference on Performance Based land Life Cycle Structural Engineering, pp. 448-458, 2012.

[12] Maluk C., Bisby L., Krajcovic M. and Torero J.L. "A Heat-Transfer Inducing System (H-TRIS) Test Method". Fire Safety Journal, vol. 105, pp. 307-319, 2019.

[13] Bozzoli F., Mocerino A., Ranieri S. and Vocale P. "Inverse heat transfer modeling applied to the estimation of the apparent thermal conductivity of an intumescent fire retardant paint". Experimental Thermal and Fluid Science, vol. 90, pp. 143-152, 2018.

[14] Hsu S.Y. "Modeling of heat transfer in intumescent fire-retardant coating under high radiant heat source and parametric study on coating thermal response". Journal of Heat Transfer, vol. 140, no. 3, 2017.

[15] Kang J., Takahashi F. and T'ien J.S. "In situ thermal-conductivity measurements and morphological characterization of intumescent coatings for fire protection". Journal of Fire Sciences, vol. 36, no. 5, pp. 419-437, 2018.

7

Influence of substrate thermal conditions

7.1 Introduction and background

The majority of the research studies related to intumescent coatings can be generally divided into two main categories. The first category, led by chemists and chemical engineers, focuses on the development and invention of new formulations and ingredients for more effective and reliable intumescent coatings [1-4]. The second category, led by fire safety engineers, focuses on investigating the overall insulating effectiveness of intumescent coatings as thermal barrier for different structural elements and materials (refer to Chapter 2). Based on the research goal, the *swelling of intumescent coatings* is studied and assessed in different manners. Researchers focused on intumescent formulations usually investigate the coating swelling at a small scale. New ingredients and compounds are added and the swelling reaction is analysed in terms of mass loss (Thermo-Gravimetric Analysis, TGA), calorimetry (Differential Scanning Calorimetry, DSC) or spectroscopy (Fourier-Transform Infrared spectroscopy) [4-7]. On the contrary, within fire safety engineering practice, the insulating performance of intumescent coatings is usually assessed at medium and large scales using furnaces of various sizes [8-13]. These experiments mainly focus on measuring the temperature evolution of coated samples and this parameter is adopted as main performance criteria (i.e. failure is defined as a critical temperature for each specific case). For instance, according to the European method based on the concept of effective thermal conductivity, the complex thermal-physical response of intumescent coatings is simplified in an effective parameter [14-15]. The temperature-dependent effective thermal conductivity defines an equivalent thermal barrier provided by the intumescent coating to the substrate material under a certain heating regime [16-19]. This parameter incorporates several phenomena that occur in the intumescent coating, such as the swelling process, endo- and exothermic reactions [12]. In this way, the swelling of intumescent coatings is indirectly assessed in terms of a lower temperature rise in the protected material.

In general, the available literature presents limited research studies that have performed detailed analysis of the swelling process of intumescent coatings for real-scale coated samples. Research studies have highlighted the complexities in comprehensively gauging the swelling process of intumescent coatings, both from the physical and thermal aspects. In particular, several challenges are usually experienced in experimentally measuring the actual swelled

coating thickness and defining the triggering conditions for the swelling reaction. The research study presented in Chapter 5 investigated how the thermal conditions at the surface of coated steel plates affect the onset of swelling for thin intumescent coatings. Research outcomes defined the temperature ranges for which the swelling reaction was initiated, in terms of temperature experienced by the coating and the steel substrate. However, this research only reported the temperature thresholds for onset of swelling, but the swelling mechanism for medium-scale coated samples was not generally comprehended. In particular, how different thermal conditions at the exposed or unexposed side of the intumescent coating would influence the coating swelling was not fully understood. For example, within the research and regulatory community, ideal adiabatic boundary conditions in all surfaces deemed unexposed usually represent the target conditions, e.g. in standard fire resistance furnace tests [14-15]. Structural elements coated with intumescent coatings are commonly tested in configurations where samples are exposed from all surfaces/sides (e.g. I-profiles) or one-side exposure (e.g. plates). In the two testing configurations, the unexposed surface(s) are usually kept under adiabatic (or close to adiabatic) conditions by placing insulation material in direct contact with the unexposed surface(s) of the test sample. Since the swelling mechanism is still not fully understood, there is limited understanding on how imposing different thermal conditions at the coating boundaries may influence the swelling process and, in general, the effectiveness of intumescent coatings.

The experimental study presented herein aimed at investigating the influence of the substrate thermal conditions and the effects that this can have on the behaviour of intumescent coatings. Within the scope of this work, steel plates coated with a commercial solvent-based thin intumescent coating were tested using high-performance radiant panels in accordance with the Heat-Transfer Rate Inducing System (H-TRIS) test method. Firstly, the influence of different thermal conditions of steel substrates was investigated using different sample holders that simulate different thermal boundary conditions at the unexposed surface of the test sample. Secondly, the response of the intumescent coating applied on timber substrate and exposed to the same heating conditions was analysed. The described experimental results give a better understanding of the swelling process of intumescent coatings and the influence of the substrate thermal conditions. In particular, they evidence the direct influence of the substrate temperature on the coating swelling, thus the effectiveness of intumescent

coatings. Substrate thermal conditions that do not enable the rise of the substrate temperature can limit the coating swelling and therefore its effectiveness.

7.2 Experimental investigation

7.2.1 Experimental methodology

The methodology adopted in this experimental study is based on the Heat-Transfer Rate Inducing System (H-TRIS) proposed by Maluk et al., a well-established test method adopted in research-driven and product development projects for investigating the thermal behaviour of different materials at elevated temperatures [20]. The methodology utilises high-performance radiant panels and it enables the accurate control of the thermal boundary conditions imposed on the test samples with high repeatability and low costs compared with traditional furnace testing. Using a computer-controlled linear motion system, H-TRIS controls the relative position between the target exposed surface of the test sample and an array of radiant panels. In this way, within the limits of minimum and maximum proximities to the exposed surface, test samples can be exposed to any specified time-history of incident radiant heat flux. The experimental setup used within the scope of this work was assembled by combining four high-performance natural-gas-fired radiant heater mounted on a supporting frame, forming a 300 x 400 mm^2 radiant heat source and able to impose incident radiant heat fluxes up to 100 kW/m^2 (see Figure 7.1). Moreover, the experimental methodology enables the visual inspection of the test samples during the thermal exposure (e.g. measuring the swelled coating thickness), technically challenging during conventional standard furnace tests [16].

7.2.2 Test samples

The test samples used in this experimental study were 200 x 200 mm^2 mild carbon steel plates with a thickness of 10 mm, resulting in a section factor A_p/V (i.e. ratio between the exposed surface and volume of steel) equal to 100 m^{-1}. Based on the assembled array of radiant panels and a theoretical study on view factors of radiant surfaces, the sample dimensions were chosen in order to achieve a surface distribution of incident radiant heat flux

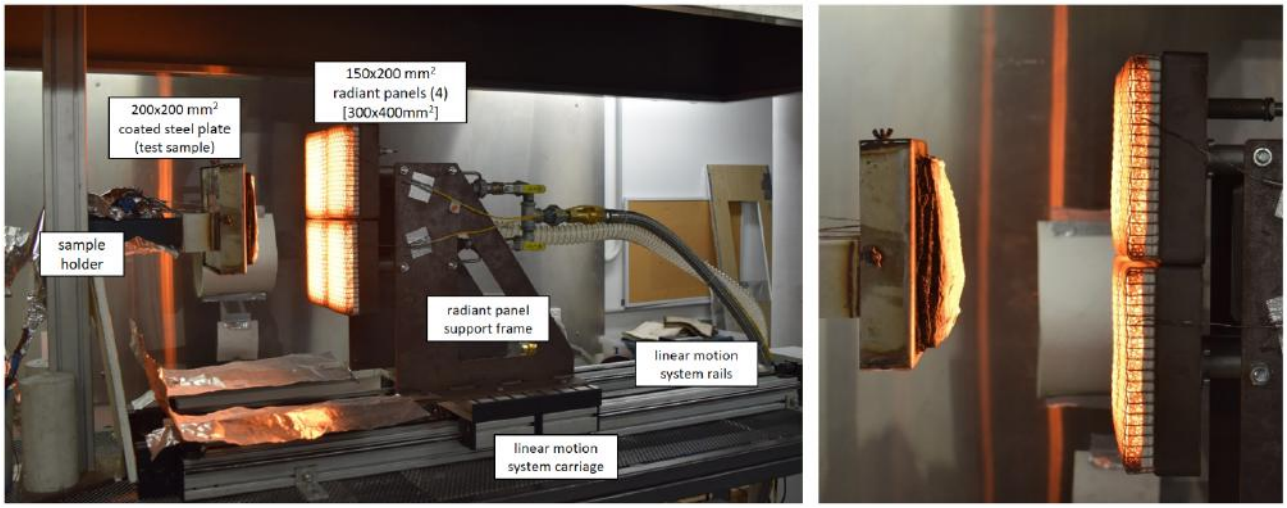

Figure 7.1: Experimental setup based on the H-TRIS test method (*Bench-scale 2.0*, *"Sample holder A"*).

Table 7.1: Test matrix of the experimental study.

Sample ID	Substrate thermal conditions	DFT_{mean} [mm]
CP-ISP-01	Insulating	1.920
CP-ISP-02		2.074
CP-ISP-03		2.014
CP-HSC1-01	Heat sink, low rate	2.140
CP-HSC1-02		2.216
CP-HSC1-03		2.226
CP-HSC2-01	Heat sink, medium rate	2.230
CP-HSC2-02		2.130
CP-HSC2-03		2.256
CP-HSC3-01	Heat sink, high rate	2.162
CP-HSC3-02		2.300
CP-HSC3-03		2.300

on the sample surface with a deviation lower than 10%. Steel samples were prepared and coated with a thin layer of a commercial solvent-based intumescent coating by a registered professional contractor using airless spray equipment. The product is available in the world-wide market and it is commonly designed for providing up to 120 minutes fire resistance to universal steel sections and cellular beams. It is used for internal, semi-exposed or external applications and it is suitable for off-site and on-site application. The coating was applied in one hand without the use of any primer or topcoat in accordance to the manufacturer guidelines (fast-track coating). After 1 month of curing, the DFT applied on test samples were measured using a non-destructive film thickness gauge at five different locations. The

samples were selected in order to have a mean applied DFT in the range 2.10 $\pm$ 0.20 mm: the measured values are listed in Table 7.1.

7.2.3 Experimental setup

The coated steel samples were individually tested using the described H-TRIS test method. Test samples were exposed for 60 minutes to a constant incident radiant heat flux of 50 kW/m^2 at the coated surface. Based on previous research, the heating condition was chosen to ensure a range of temperatures and heating rates higher than the thresholds for onset of swelling of typical thin intumescent coatings (refer to Chapter 5). During the thermal exposure, custom-built sample holders were used in order to hold the test sample aligned with the centre-point of the array of radiant panels, in vertical orientation (Figure 7.1). In particular, two different sample holders were used in order to control the thermal boundary conditions at the unexposed surface of the test sample:

1. *Sample holder A – Insulating conditions* (Figure 7.2a). This setup aims at reproducing adiabatic thermal boundary conditions at the unexposed surface of the test sample. In order to minimise the heat losses, the test sample was insulated at the back using a layer of 20 mm thick ceramic wool (ISOLITE ISOWOOL 1000 BLANKET 100, bulk density 96 kg/m^3) and 13 mm thick plasterboard (Knauf FireShield). The sample position was secured using a squared stainless steel frame around the sample edges.
2. *Sample holder B – Heat sink conditions* (Figure 7.2b). A heat sink was in contact with the unexposed surface of the test sample. The heat sink was a 20 mm thick mild carbon steel plate adjacent to a 10 mm thick cavity. This cavity was designed to allow for the circulation of chilled water (about 20°C). The water cavity was included between the heat sink and the 8 mm thick back mild carbon steel plate and contained by a 10 mm steel board frame. Water circulated inside the cavity thanks to a 1/4" inlet and 1/4" outlet. The water flow into the water cavity was controlled using a volumetric water flow meter. The test sample was secured in place using four steel clamps, two at the bottom and two at the lateral sides of the test sample.

Using the two described sample holders, the experimental investigation was carried out by imposing four different thermal boundary conditions at the unexposed surface of the test

sample (refer to Table 7.1):

1. *Insulated steel plate (ISP)* – Heat losses at the unexposed surface of the test sample were minimised by using *Sample holder A*.
2. *Steel plate with heat sink, low rate (HSC1)* – The thermal mass represented by the heat sink was added using the *Sample holder B*. No water circulated inside the cavity.
3. *Steel plate with heat sink, medium rate (HSC2)* – The heat sink was cooled by a minor water flow, controlled at 0.5 litres per minute (*Sample holder B*).
4. *Steel plate with heat sink, high rate (HSC3)* – The heat sink was kept cold by a significant continuous water flow, controlled at 10 litres per minute (*Sample holder B*).

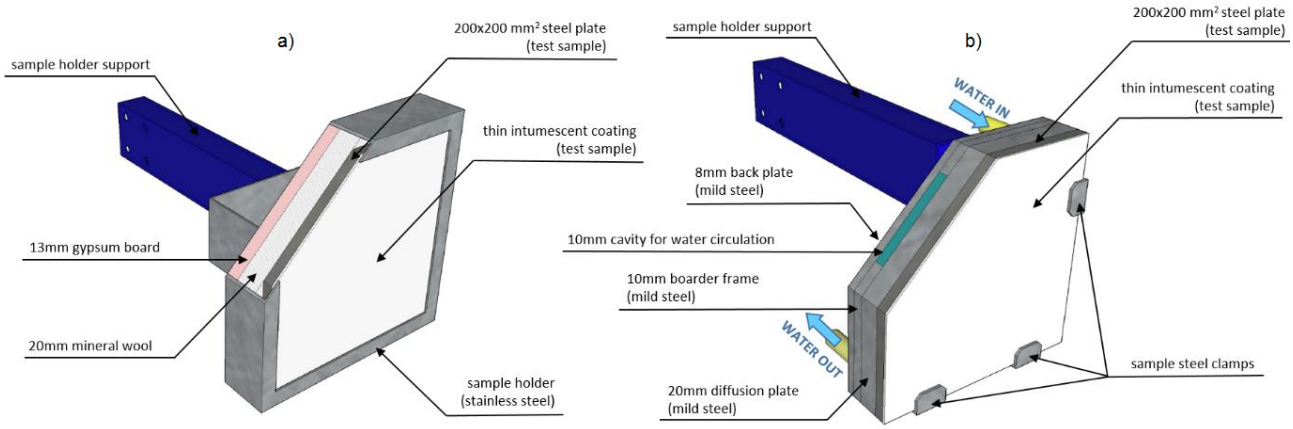

Figure 7.2: Detailed schematisation of sample holders: a) *Sample holder A* reproducing insulating conditions; b) *Sample holder B* reproducing different levels of heat exchange at the unexposed surface of the test sample.

7.2.4 Instrumentation

Up to three K-type thermocouples were attached to the unexposed surface of the test samples in order to measure the evolution of the steel temperature during the thermal exposure. In the cases of experiments with the *Sample holder B*, two K-type thermocouples were placed inside the heat sink at mid-depth by drilling 1.5 mm holes from the lateral side. The thickness of the swelling intumescent coating was measured by image processing of video footages taken using a high-resolution video camera placed at the side of the test sample, aligned with the surface of the test sample (Figure 7.3). The real-time measurement of the swelled coating thickness was also used for continuously adjusting the relative

distance between the intumescent coating surface and the array of radiant panels during the heating exposure. This was done to assure that incident radiant heat flux at the exposed surface of test samples was maintained to the specified value during the full duration of the experiments. In addition, the exposed surface temperature of the intumescent coating was measured using an Infra-Red camera (model DLIR SC655: 16-bit 640 x 480 pixel resolution at 50 Hz, spectral range 7.5 – 14 μm, temperature range up to 2000℃) (Figure 7.3).

Figure 7.3: Experimental setup designed to gauge the swelled coating thickness and the surface temperature of intumescent coatings during heating exposure (*Sample holder B*).

7.3 Preliminary investigations

Before running the main experimental investigation, a few preliminary studies were conducted in order to understand the robustness of the proposed methodology. Following the experimental setup described above, uncoated steel plates were exposed to a constant incident radiant heat flux of 50 kW/m^2 for 30 minutes. The aim of these studies was to understand if the four different thermal boundary conditions would have exposed the steel to a good variety of temperatures, ranging between two extreme cases: insulating conditions and heat sink cooled by a significant continuous water flow. Figure 7.4 shows the temperature evolution of uncoated steel samples for the four different thermal boundary conditions at the unexposed surface. The four different conditions leaded to a four distinctive quasi-steady state steel temperatures: about 640℃ for insulating conditions and about 430℃, 300℃ and 240℃ for

conditions involving the heat sink, respectively. This aspect proved the good definition of the different experimental conditions.

In addition, the experimental results were compared to the solution of a lumped capacitance approximation of transient heat conduction problem for an uncoated steel plate subjected to well-defined thermal boundary conditions [21]. The thermal boundary conditions at the exposed surface were defined by the imposed constant incident radiant heat flux ($\dot{q}''_{inc}$) and the resulting convective ($\dot{q}''_{conv}$) and radiative ($\dot{q}''_{rad}$) heat losses to the surrounding environment. The thermal boundary conditions at the unexposed surface were assumed as ideal adiabatic conditions. General correlations and thermal and physical material properties of carbon steel from the available literature were used [15, 21]. The good agreement between the heat transfer model and the experimental measurements of the steel substrate temperature supports the assumptions of the thermal conditions at the sample boundaries: minimised heat losses at the unexposed surface and the specified incident radiant heat flux (50 kW/m^2) imposed by the H-TRIS test method.

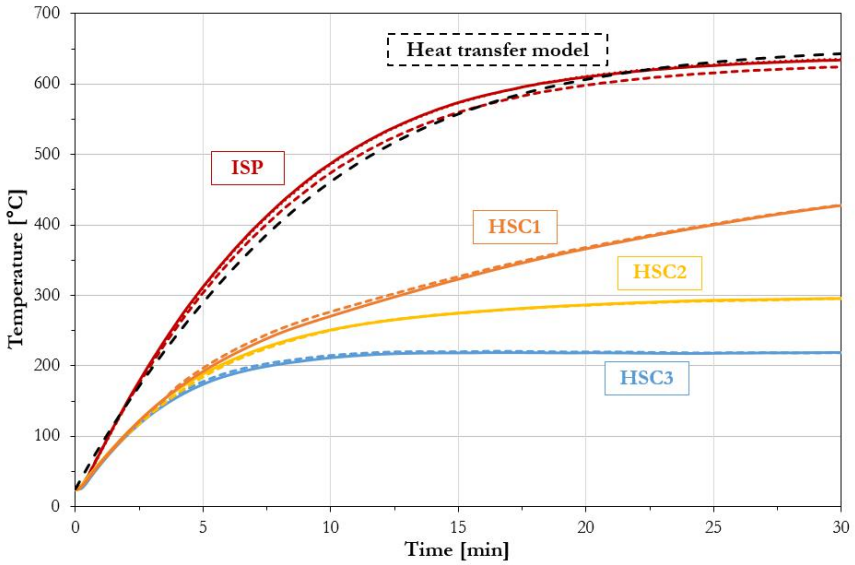

Figure 7.4: Comparison of the steel temperature evolution for the four different thermal conditions of the steel substrate.

7.4 Analysis and results

7.4.1 Visual observations

Thanks to its open environment, the experimental setup based on H-TRIS test method allowed for the visual inspection of the test samples during thermal exposure. As shown in Figure 7.5, upon heating, the coating underwent different phases, typical of intumescent reactions [22]. First, the virgin intumescent coating softens and gradually decompose: this can be observed by the change in colour from white to dark/black and the release of volatiles (*"Thermal decomposition zone"*). After that, the coating gradually swells (*"Swelling zone"*) and forms a carbonaceous porous char (*"Char formation zone"*). Finally, the oxidation reactions occur at the surface of the coating: the intumescent porous char progressively turns into a white/grey colour. In addition, during this final stage, the formation of cracks on the intumescent coating surface is observed: the cracks represent a key vulnerability for the thermal barrier provided by the intumescent coating (*"Char degradation zone"*) [22].

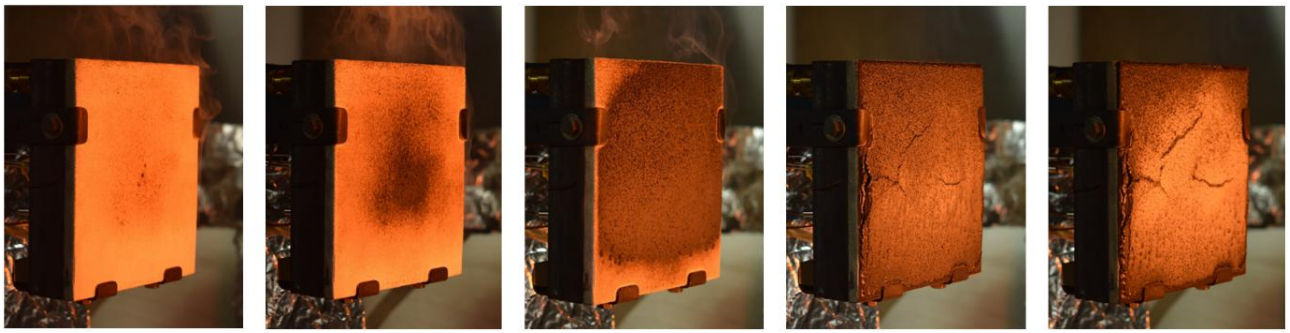

Figure 7.5: Different phases of the intumescent coating during thermal exposure (sample CP-HSC2-02).

7.4.2 Steel temperatures

The temperature evolution of coated steel samples for the four different thermal boundary conditions was recorded by using thermocouples positioned at the unexposed surface of the test samples. Figure 7.6 shows the evolution of the steel temperatures for all the experiments carried out on coated samples. The good repeatability between experiments was confirmed by the agreement of the different temperature readings. Throughout all the experiments, the steel temperatures measured using thermocouples has deviations lower than $\pm$ 20 ℃. Figure

7.6 reports the average values of the steel temperatures. In the graphs, the same colour collects all the experiments with the same substrate thermal conditions, while continuous, dashed and dotted lines report single experimental repetitions.

As predicted in the preliminary investigation on uncoated samples, the four different conditions leaded to a four distinctive quasi-steady state steel temperatures: about 340℃ for insulating conditions and about 250℃, 150℃ and 100℃ for the experiments involving the heat sink with low (HSC1), medium (HSC2) and high water-cooling rate (HSC3), respectively. This aspect confirmed the good definition of the different experimental conditions aiming at exposing the steel plates to a range of temperatures. However, test samples with different substrate thermal conditions achieved the quasi-steady state steel temperature at different instants during the thermal exposure.

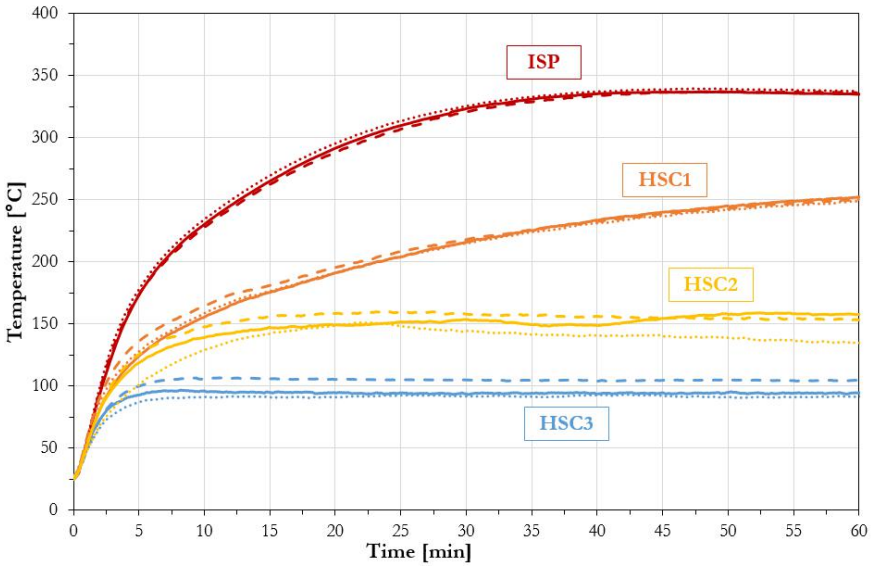

Figure 7.6: Comparison of the steel temperature evolution for the four different thermal conditions of the steel substrate.

7.4.3 Coating surface temperatures

The temperature evolution at the exposed surface of the intumescent coating was evaluated by post-processing the data obtained using the Infra-Red camera. The coating surface temperature was evaluated by setting a coating emissivity equal to 0.90 and the coating temperature was averaged over a 50 x 50 mm^2 area, placed at the centre of the test sample. The emissivity value has a key role in this process and experimental results can be signific-

antly influenced by this parameter. Therefore, a sensitivity analysis of the surface emissivity value of the intumescent coating was performed: the same procedure was repeated for varying coating emissivity 0.90 $\pm$ 0.02, according to the values found in the available literature [12, 23]. Figure 7.7 shows the envelope of the temperatures measured at the coating surface in all the experiments carried out on coated samples. During the different experiments, the coating behaved like a low thermal inertia material (thermally thick characterised by a high Biot number) by quickly reaching a certain surface temperature (650-700℃) and keeping a quasi-constant temperature during the rest of the heating exposure. The substrate thermal conditions did not have a significant effect on the evolution of the coating surface temperature. As expected, the surface temperature of the intumescent coating remained quasi-constant under the same imposed incident heat flux, after an initial transient period (first 5 minutes).

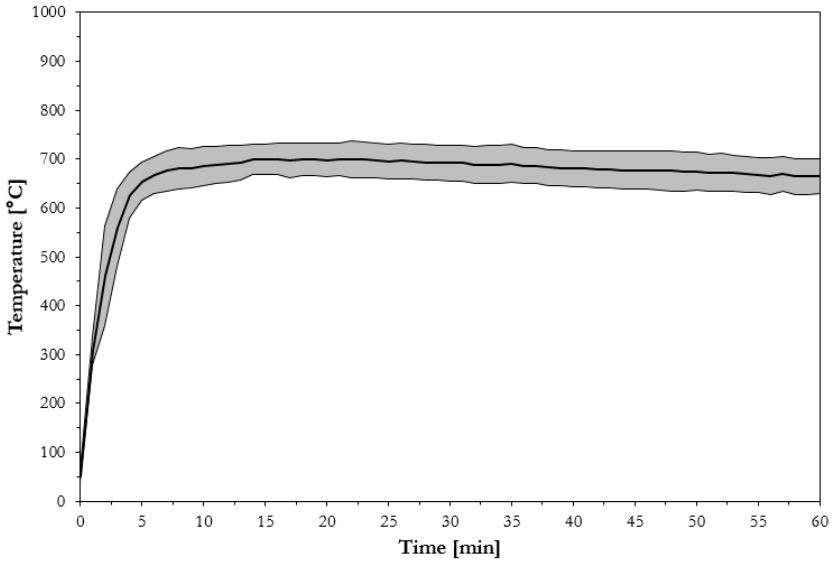

Figure 7.7: Envelope of the temperature evolution at the coating surface for the four different thermal conditions of the steel substrate.

7.4.4 Coating swelling

The time-history of coating swelling at the centre of each sample was estimated through image processing of high-resolution video footages. In most experiments, the central area of test samples swelled rather homogeneously and the swelled coating thickness was measured with an accuracy of $\pm$ 2 mm. Figure 7.8 shows the evolution of the swelled coating

thickness for all the experiments carried out on coated samples. Right after the application of the incident radiant heat flux, the intumescent coating started swelling with different rates depending on the substrate thermal conditions, i.e. the slope/derivative of the swelled coating thickness-time curve. In the case of insulating conditions at the unexposed surface of test samples (ISP), the intumescent coating continuously swelled during the thermal exposure, reaching a maximum thickness of about 50 mm. In the case of different thermal boundary conditions applied using the water-cooled heat sink, the swelling rate decreased for more extreme cooling conditions. In particular, the maximum thicknesses reached at the end of the thermal exposure were about 18 mm, 7 mm or 5 mm for the experiments involving the heat sink with low (HSC1), medium (HSC2) and high water-cooling rate (HSC3), respectively. As a result, the substrate thermal conditions appear to directly govern the swelling of intumescent coatings.

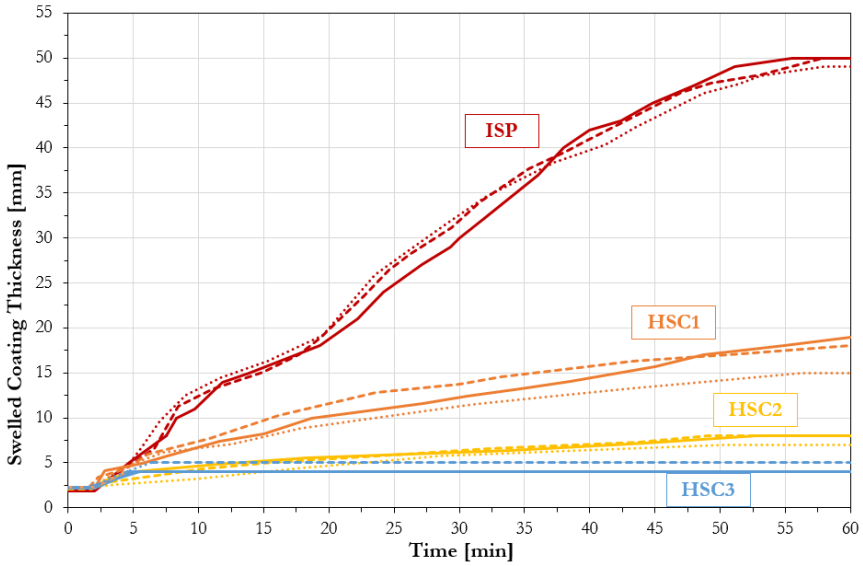

Figure 7.8: Comparison of the evolution of the swelled coating thickness for the four different thermal conditions of the steel substrate.

This aspect was also confirmed by the char structures produced by the intumescent coating at the end of the thermal exposure. Figure 7.9 shows photographs of typical porous char developed by the intumescent coating at the end of the thermal exposure. The char structures confirmed that the substrate thermal conditions can significantly influence the swelling of intumescent coatings. In the case of insulating conditions, the intumescent coating swelled homogenously and created a thick, dense and compact carbonaceous porous media able

to effectively protect the substrate material from the thermal exposure. On the other hand, for conditions involving the heat sink, the intumescent coating scarcely swelled and formed a thin carbonaceous layer. In these cases, a large amount of virgin un-reacted coating was observed in the final intumescent char. Figure 7.10 shows how only the portion of the intumescent coating close to the surface reacted, recognisable by colour changes. On the contrary, the portion of intumescent coating close to the steel did not react due to the significant thermal losses due to conduction through the coating and towards the heat sink. In all experiments, in the proximity of the coating surface, it is possible to observe char oxidation: the carbonaceous char turned into ash at the coating crust, characterised by a white-grey colour compared to the dark/black colour of the coating char. Since the surface temperatures exceeded 600℃, oxidation was expected to occur at the coating surface due to the H-TRIS oxygen-rich environment. Based on previous research, it is important to underline that the oxygen content of the exposing atmosphere can have affected the mode and rate of char formation and degradation [24].

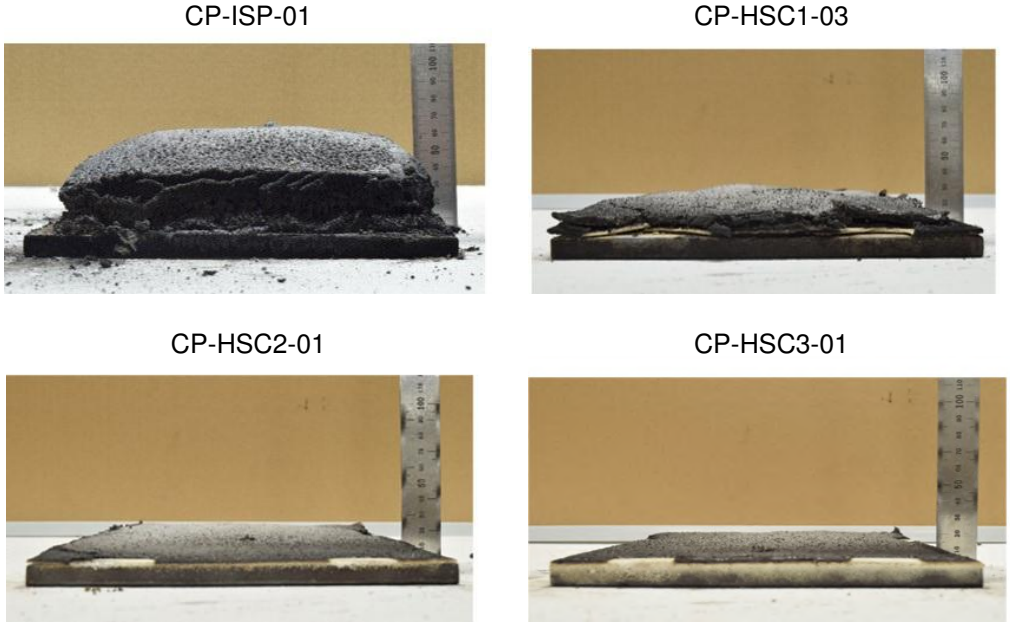

Figure 7.9: Comparison of typical char sections produced by the intumescent coating at the end of the thermal exposure.

Figure 7.10: Details of the final intumescent char (sample CP-HSC3-01).

7.5 Analysis and discussion

As underlined in the previous paragraphs, the thermal boundary conditions at the unexposed surface of the test sample appear to directly govern the swelling of intumescent coatings. In particular, each thermal condition of the steel substrate can be associated with a certain evolution of the steel substrate temperature and the swelled coating thickness. Figure 7.11 shows the swelled coating thickness as a function of the steel substrate temperature for the four different experimental setups conducted on coated samples. The plot highlights a direct relationship between the substrate temperature and the swelled coating thickness under the same thermal exposure (50 kW/m^2). At the same steel temperature, the swelled coating had a very similar thickness for all the different thermal conditions of steel. Particularly, in the experiments involving the water-cooled heat sink, the reduced coating swelling can be related to the low temperature experienced by the steel plates.

The described experimental results give a better understanding of the swelling process of intumescent coatings and the influence of the substrate thermal conditions. Figure 7.12 shows a simplified schematisation of the thermal conditions of tested samples. Upon heating, the swelled intumescent char, characterised by low thermal conductivity and low density (thermally thick characterised by a high Biot number), quickly reaches a quasi-steady state temperature at the surface (T_{surf}) and experiences a steep thermal gradient within its thickness. Within the depth of the intumescent coating, the unreacted virgin coating is located behind the swelled porous char and close to the interface between the steel and the applied coating. At this specific interface, the swelling reaction typically take place. When the virgin coating is above a certain temperature range, the material degrades and chemical

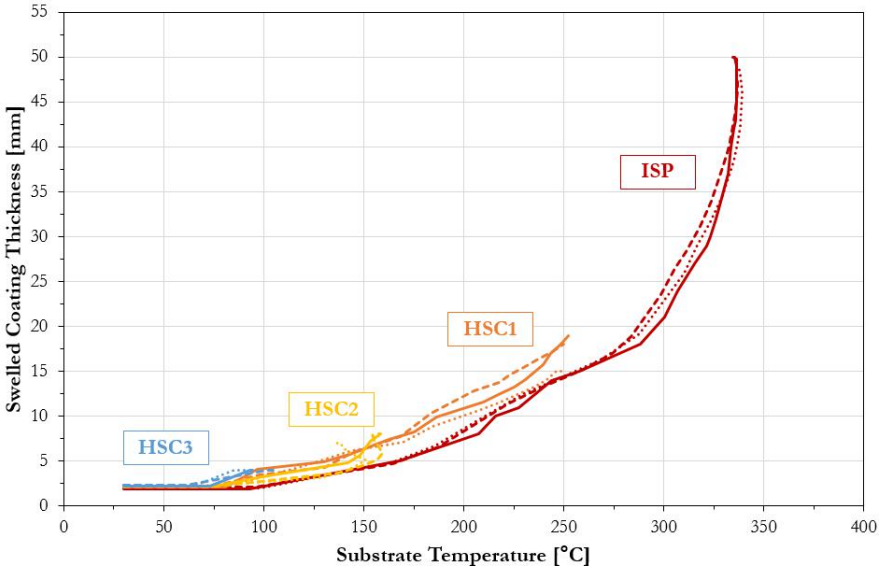

Figure 7.11: Comparison of the evolution of the swelled coating thickness as a function of the substrate temperature for the four different thermal conditions of the steel substrate.

reactions occur. In these processes, a large amount of gases are usually produced by the activation of the blowing agent, key compound contained in typical intumescent formulations. The released gases are trapped within the coating thanks to the distinctive physical and mechanical properties (e.g. density and viscosity). The entrapment of gases represent a fundamental process during intumescence in order to optimise the coating swelling. Several researchers have highlighted how the order and the matching of the chemical and physical processes are essential, as they must happen in an appropriate sequence, as the temperature is raised [4-5].

The reacting virgin coating located next to the steel-coating interface is characterised by a low Biot number due to the relatively high thermal conductivity (compared to the swelled intumescent char) and the limited physical thickness. Consequently, the virgin intumescent coating behaves as a thermally thin material and its temperature can be approximated with the temperature of the steel substrate (T_s). Accordingly, the substrate temperature can be directly related to the swelling process because it defines the temperature experienced by the reacting virgin coating, which is located behind the swelled porous char and sustains the swelling process. In particular, the intumescent coating swells and insulates the substrate by displacing the already-swelled coating towards the direction of the heat source. This aspect was also verified by a close investigation of the recorded video footages. As a conclusion, the

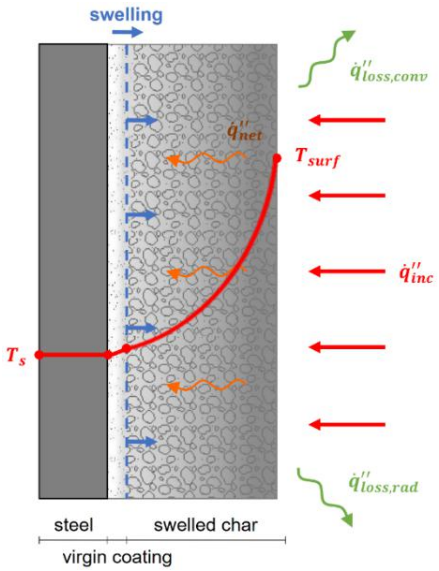

Figure 7.12: Schematisation of the mechanism of coating swelling.

substrate temperature governs the swelling of intumescent coatings and thermal conditions that do not enable the temperature rise in the substrate material can limit the coating swelling and therefore its effectiveness.

7.6 Application to different substrate material: timber

The research community is currently looking into the possibility of applying intumescent coatings to protect substrate materials different from steel. For instance, researchers are exploring the advantages of applying intumescent coatings on concrete elements to mitigate the destructive effects of fire-induced spalling and reduce the heat penetration thought the concrete into the steel reinforcements [25-26]. In addition, other recent studies have shown that intumescent coatings can be efficiently applied on timber to prevent the occurrence of surface ignition, reduce the flame spread, delay the onset of timber charring and decrease the charring rate within wooden elements [27]. In particular, a research study focused on the application of intumescent coatings on timber elements was recently published [28]. The exploratory investigation adopted the same experimental methodology based on the H-TRIS test method to study the behaviour of coated Cross-Laminated Timber (CLT) blocks subjected to the same heating conditions: a constant incident radiant heat flux of 50 kW/m^2 for 60 minutes. The test samples had also identical dimensions of the exposed surface, 200

x 200 mm^2. Test samples were 100 mm thick, composed of 5 lamellae (20 mm thick each) of Australian softwood. The tested product was the same commercially available solvent-based thin intumescent coating, applied to a mean Dry Film Thickness (DFT) in a similar range: 2.10 $\pm$ 0.20 mm (samples series S21). This research study provides the perfect ground to apply the experimental outcomes presented herein to the case of coated timber samples.

Analogously to this experimental study, the time-history of the coating swelling at the centre of each sample was estimated through image processing of high-resolution video footages. Figure 7.13 compares the evolution of the swelled coating thickness for all the experiments carried out on coated samples with different substrate thermal conditions, including timber. Contrarily, regarding the evolution of the substrate temperatures, it is difficult to produce a similar plot to the one presented in Figure 7.6 for the timber case. This is related to the difficulties of estimating the temperature evolution in the proximity of the coating-timber interface and the uncertainties related to measuring in-depth temperatures within a low conductivity material like timber [28-29]. Consequently, for the timber case, it is not possible to produce similar plots to the ones shown in Figure 7.6 and Figure 7.11. Finally, considering the identical heating conditions, the application of different substrate conditions using timber is expected to have a minor influence on the temperature evolution of the exposed coating surface.

Figure 7.13 highlights how the timber sample defined another substrate thermal condition for the intumescent coating, fundamentally different to the ones involving steel plates. The comparison of the evolution of the swelled coating thickness confirms that the substrate thermal conditions influence the swelling of intumescent coatings. In the timber case, right after the application of the incident radiant heat flux, the intumescent coating rapidly swelled with a high rate (i.e. slope/derivative of the thickness-time curve), even greater than the one measured for coated steel plates with insulating conditions. In addition, the swelling process quickly concluded during the thermal exposure (at about 25 minutes), while in the other cases the intumescent coating continuously swelled during whole duration of the experiment. The main explanation of the different behaviour of the swelling intumescent coating can be directly associated with the thermal conditions produced by the timber substrate. Timber is a low thermal inertia material: when exposed to a heat flux, timber tends to conduct less heat through its thickness and increase its temperature in the proximity of its surface. On the

contrary, steel is commonly a thermally thin material due to its high thermal conductivity. As a consequence, the temperature evolution at the substrate-coating interface is expected to increase more rapidly than the steel cases. Following the principles explained in the previous section, the substrate thermal conditions influenced the swelling of the intumescent coating and, in particular, the timber substrate accelerated the swelling process: it created a faster rise of the temperature experienced by the reacting virgin coating, which is located behind the swelled porous char and sustains the swelling process.

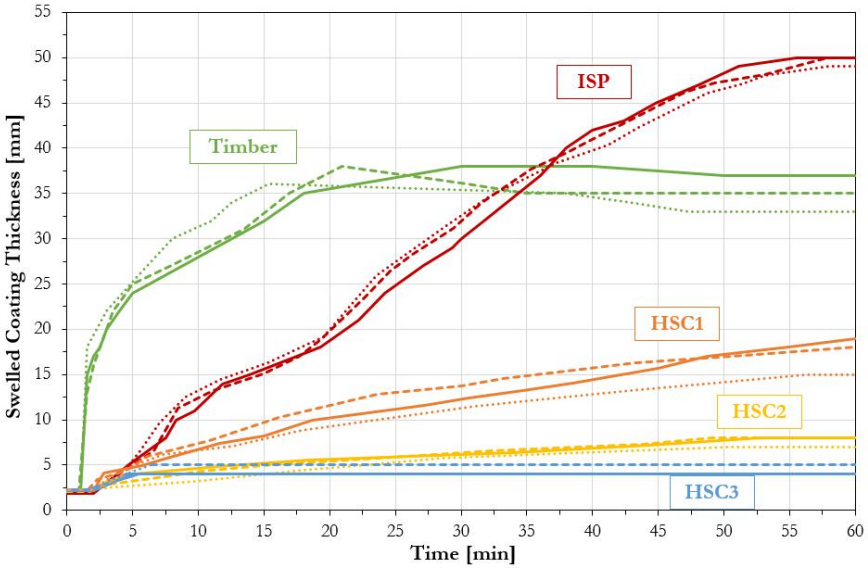

Figure 7.13: Comparison of the evolution of the swelled coating thickness for the different substrate thermal conditions.

In general, the swelling of intumescent coatings and therefore their effectiveness are governed by the thermal conditions of the substrate and, in particular, by the physical and thermal properties of substrate system. These characteristics control the temperature evolution at the substrate-coating interface, hence the virgin intumescent coating which regulates the swelling reaction. Within the scope of this experimental study, the heating conditions at the exposed surface of the intumescent coating were fixed to a constant incident radiant heat flux of 50 kW/m^2. From this surface thermal exposure, the tested intumescent coating was expected to receive a similar amount of energy for the different substrate thermal conditions. However, the different substrate thermal conditions controlled the capacity of the system to concentrate and dissipate heat in the proximity of the substrate-coating interface. In this way, the substrate thermal conditions controlled the temperature evolution of the re-

acting intumescent coating and they consequently governed the swelling process. Figure 7.14 offers a schematic explanation of the different substrate thermal conditions. The use of steel plates, insulated or in contact with the water-cooled heat sink, or timber blocks control the net heat flux into the reacting intumescent coating, defined as control volume within the scope of this experimental study. From the case that allowed faster coating swelling to the case that essentially prevented coating swelling, the different substrate thermal conditions can be explained as in the following (refer to Figure 7.14):

1. *Timber*. The low thermal inertia of timber limits the conduction through its thickness ($\dot{q}''_{back}$) and it enables fast temperature rise in the proximity of its surface. Consequently, the intumescent coating quickly reaches onset of swelling and it has a high swelling rate.

2. *Insulated steel plate*. The steel plate behaves as a thermally thin material due to the high thermal conductivity of steel and the limited physical thickness of the plate. Accordingly, no thermal gradient is expected to develop within the plate thickness. The heat losses at the unexposed surface of the test sample are minimised by the insulation material ($\dot{q}''_{back}$). The steel plate quickly increases its temperature, but it is damped by the relatively high thermal mass of the steel plate ($\dot{q}''_{s}$), compared to the coating. Consequently, the intumescent coating swells with a lower rate compared to the timber case.

3. Steel plate with water-cooled heat sink. As in the insulated case, the steel plate behaves as a thermally thin material and it increases its temperature according to the thermal mass of the steel plate ($\dot{q}''_{s}$). However, in this case, significant heat losses are caused by the water-cooled heat sink in contact with the unexposed surface of the test sample ($\dot{q}''_{back}$). The steel temperature rise is directly governed by the heat losses induced by the heat sink. Consequently, the intumescent coating swells with lower rates compared to the insulated steel plate case and the swelling rate decreases with higher cooling due to greater water flows.

1.

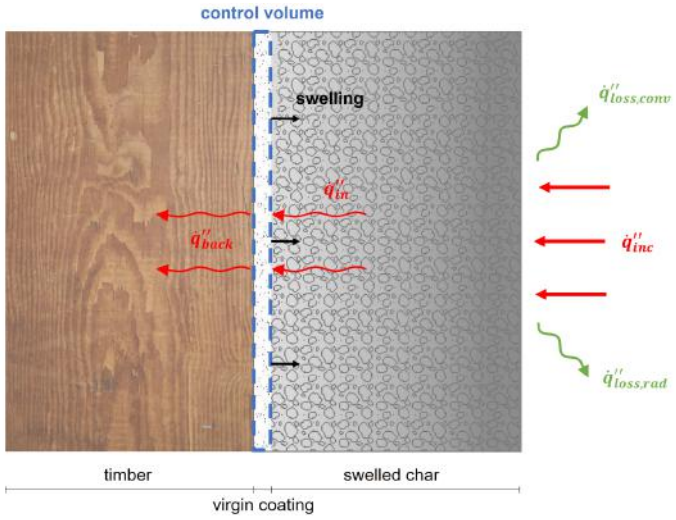

2.

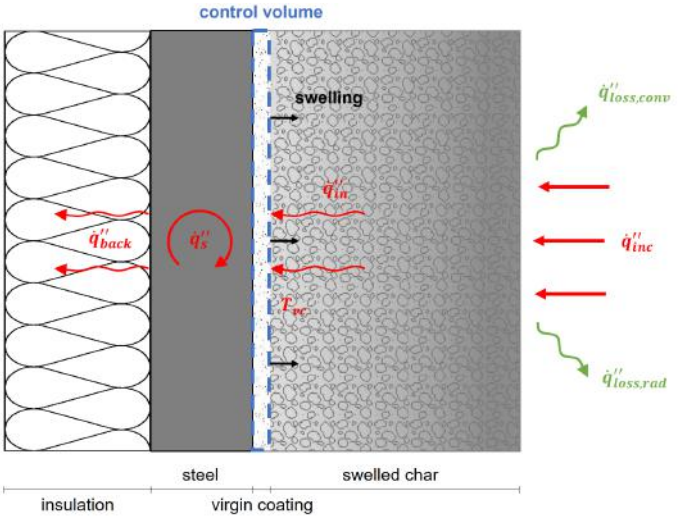

3.

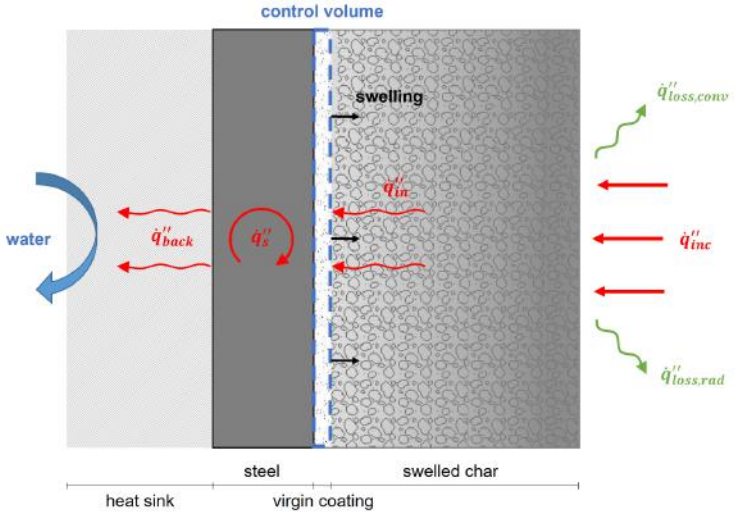

Figure 7.14: Schematisation of the different substrate thermal conditions.

Similar concepts could be extended for different substrate materials and steel/timber substrates with different characteristics. For instance, in the case of a thinner steel plate with insulating conditions at the unexposed surface, the temperature of the coated steel plate is expected to rise faster than the case of a thicker steel plate due to the lower thermal mass. Consequently, the swelling rate of the intumescent coating is expected to be included between the one measured for the timber substrate (upper bound) and the one measured for the insulating conditions of a thicker steel plate (lower bound). Similarly, in the case of a concrete substrate, the swelling rate of the intumescent coating is expected to be slightly lower to the timber case because of the higher thermal inertia of concrete, compared to timber. Nevertheless, it is important to underline that this experimental study did not investigate the potential consequences of adhesion issues between the steel/timber substrate and the tested intumescent coating. The experimental outcomes highlighted within this research assumed good adhesion at the substrate-coating interface. In the case of different materials or intumescent product, particular attention should be paid for ensuring the good adhesion between the substrate and the protection materials. For instance, in the cited research, the timber charring was avoided by applying a thick intumescent coating (samples series S21) and keeping the temperature within the timber samples below 300 ℃. Future studies should aim at inspecting this specific aspect.

Unfortunately, within the scope of this experimental study, the substrate thermal conditions can be only explained and analysed in a qualitative manner. The quantification of the thermal conditions obtained involving different substrate systems would be possible only by formulating detailed and complex heat transfer models. However, the problem is characterised by many uncertainties and unknown variables (e.g. thermal and physical properties of the intumescent coating) that make it too complicated and prevent any experimental validation. Overall, future performance-based designs of different systems protected with intumescent coatings should involve the selection of accurate thermal conditions. This experimental study highlighted how the substrate thermal conditions can influence the swelling of intumescent coatings, therefore their effectiveness. At the testing and design stages, the thermal boundary conditions at the exposed and back surfaces of the intumescent coating should be defined with great care. Specifically, the thermal boundary conditions should be as close as possible to the design scenario or they should target the closest critical scenario in order

to ensure the safe design of intumescent coatings applied on different substrate materials.

7.7 Conclusions

The designed experimental setup and the systematic testing of coated test samples under controlled and highly repeatable heating conditions (at the heated and unheated surface of test samples) enabled the careful investigation of the influence of the substrate thermal conditions and the effects that this can have on the behaviour of thin intumescent coatings. Within the scope of this work, steel plates coated with a commercial solvent-based thin intumescent coating were exposed to a constant incident radiant heat flux of 50 kW/m^2 using high-performance radiant panels in accordance with the Heat-Transfer Rate Inducing System (H-TRIS) test method. Firstly, the influence of different thermal conditions of steel substrates was investigated using different sample holders that simulate four different thermal boundary conditions at the unexposed surface of the test sample. Secondly, the response of the intumescent coating applied on timber substrate and exposed to the same heating conditions was analysed.
From the experimental results described herein, the following concluding remarks can be drawn:

- The thermal boundary conditions at the unexposed surface of the test sample directly govern the swelling of intumescent coatings, thus their effectiveness. In particular, under the same thermal exposure (50 kW/m^2), a direct relationship can be established between the substrate temperature and the swelled coating thickness.

- The described experimental results give a better understanding of the swelling process of intumescent coatings. The swelling reaction takes place at the virgin coating located behind the swelled porous char and close to the interface between the applied coating and the substrate material. The intumescent coating swells and insulates the substrate by displacing the already-swelled coating towards the direction of the heat source.

- The evolution of the substrate temperature governs the swelling of intumescent coatings because it defines the temperature experienced by the reacting virgin coating located close to the substrate-coating interface.

- The physical and thermal conditions of the substrate control the capacity of the system to concentrate and dissipate heat in the proximity of the substrate-coating interface. In this way, the substrate thermal conditions govern the temperature evolution of the reacting intumescent coating and consequently the swelling process. Accordingly, the highest swelling rate was recorded for the timber substrate (low thermal inertia), while the lowest swelling rate was recorded for the water-cooled heat sink with the highest cooling rate (high heat losses).

In general, this experimental investigation highlighted the importance of selecting accurate thermal conditions for the performance-based design of different systems protected with intumescent coatings. The thermal boundary conditions affect the swelling of intumescent coatings, therefore this needs to be considered when extrapolating test results used to characterise performance. As regards the section factor, different section geometries are usually tested within a certain range (e.g. 25-350 m^{-1}) and it is accepted that it is a conservative practice to extend the results to lower values. While this is correct if a colder section is assumed to have better performance, if the desired outcome was the prediction of the temperature, then the results of this experimental study show that it is necessary to consider a different level of swelling. This will also apply to extrapolation to smaller sections. As a conclusion, the thermal boundary conditions at the exposed and back surfaces of the intumescent coating should be defined and analysed with great care, as close as possible to the design scenario in order to ensure a robust and safe design.

Bibliography

[1] Mariappan T. "Recent developments of intumescent fire protection coatings for structural steel: A review". Journal of Fire Sciences, vol. 34, no. 2, pp. 1-44, 2016.

[2] Puri E.G., Khanna A.S. "Intumescent coatings: a review on recent progress". Journal of Coatings Technology and Research, vol. 14, pp.1-20, 2017.

[3] Weil E.D. "Fire-protective and flame-retardant coatings – A state-of-the-arte review". Journal of Fire Science, vol. 29, pp. 259-296, 2011.

[4] Bourbigot S. and Duquesne S. "Fire retardant polymers: recent developments and opportunities". Journal of Material Chemistry, vol. 17, pp.2283-2300, 2007.

[5] Jimenez M., Duquesne S. and Bourbigot S. "Intumescent fire protective coating: toward a better understanding of their mechanism of action". Thermochimica Acta, vol. 449, no. 1-2, pp. 16-26, 2006.

[6] Yan L., Xu Z. and Wang X. "Influence of nano-silica on the flame retardancy and smoke suppression properties of transparent intumescent flame-retardant coatings". Process in Organic Coatings, vol. 112, pp. 319-329, 2017.

[7] de Sa S.C., de Souza M.M., Peres R.S., Zmozinski A.V., Braga R.M., de Araujo Melo D.M. and Ferreira C.A. "Environmentally friendly intumescent coatings formulated with vegetable compounds". Process in Organic Coatings, vol. 113, pp. 47-59, 2017.

[8] Weisheim W., Schaumann P., Sander L. and Zehfuß J. "Numerical model for the fire protection performance and the design of intumescent coatings on structural steel exposed to natural fires". Journal of Structural Fire Engineering, vol. 11, no. 1, pp. 33-50, 2019.

[9] Wang L., Dong Y., Zhang D., Zhang D. and Zhang C. "Experimental study of heat transfer in intumescent coatings exposed to non-standard furnace curves". Fire Technology, vol. 51, no. 1, pp. 627-643, 2015.

[10] Zhang Y., Wang Y., Bailey C.G. and Taylor A.P. "Global modelling of fire protection performance of an intumescent coating under different cone calorimeter heating conditions". Fire Safety Journal, vol. 50, pp. 51-62, 2012.

[11] Li G.Q., Lou G.B., Zhang C., Wang L. and Wang Y. "Assess the fire resistance of intumescent coatings by equivalent constant thermal resistance". Fire Technology, vol. 48, pp. 529-546, 2012.

[12] Bartholomai M., Schriever R. and Schartel B. "Influence of external heat flux and coating thickness on the thermal insulation properties of two different intumescent coatings using cone

calorimeter and numerical analysis". Journal of Fire Materials, vol. 27, pp. 151-162, 2003.

[13] Morys M., Illerhaus B., Sturm H. and Schartel B. "Revealing the inner secrets of intumescence: Advanced standard time temperature oven (STT Mufu+) - μ-computed tomography approach". Fire and Materials, vol. 41, pp. 927-939, 2017.

[14] Comité Europeén de Normalization (CEN). "EN 13381-8, Test methods for determining the contribution to the fire resistance of structural members - Part 8: Applied reactive protection to steel members". Brussel, Belgium, 2013.

[15] Comité Europeén de Normalization (CEN). "EN 1993-1-2:2005 Eurocode 3: Design of steel structures - Part 1-2: General rules - Structural fire design". Brussels, Belgium, 2005.

[16] Elliott A., Temple A., Maluk C. and Bisby L. "Novel testing to study the performance of intumescent coatings under non-standard heating regimes". Fire Safety Science – Proceedings of the 11th International Symposium, University of Canterbury, New Zealand, pp. 652-665, 2014.

[17] de Silva D., Bilotta A. and Nigro E. "Experimental investigation on steel elements protected with intumescent coating". Construction and Building Materials, vol. 205, pp. 232-244, 2019.

[18] Cirpici B.K., Wang Y.C. and Rogers B. "Assessment of the thermal conductivity of intumescent coatings in fire". Fire Safety Journal, vol. 81, pp. 74-84, 2016.

[19] Xu Q., Li G.-Q., Jiang J. and Wang Y.C. "Experimental study of the influence of topcoat on insulation performance of intumescent coatings for steel structures". Fire Safety Journal, vol. 101, pp. 25-38, 2018.

[20] Maluk C., Bisby L., Krajcovic M. and Torero J.L. "A Heat-Transfer Inducting System (H-TRIS) test method". Fire Safety Journal, vol. 105, pp. 307-319, 2019.

[21] Incropera F.P., DeWitt D.P., Bergman T.L. and Lavine A.S. "Fundamental of heat and mass transfer". John Wiley & Sons, 6th Edition, 2006.

[22] Lucherini A., Giuliani L. and Jomaas G. "Experimental study of the performance of intumescent coatings exposed to standard and non-standard fire conditions". Fire Safety Journal, vol. 95, pp. 42-50, 2018.

[23] Omrane A., Wang Y.C., Goransson U., Holmstedt G. and Alden M. "Intumescent coating surface temperature measurement in a cone calorimeter using laser-induced phosphorescence". Fire Safety Journal, vol. 42, pp. 68-74, 2007.

[24] Griffin G.J., Bicknell A.D. and Brown T.J. "Studies on the effect of atmospheric oxygen content on the thermal resistance of intumescent, fire-retardant coatings". Journal of Fire Sciences, vol. 23, pp. 303-328, 2005.

[25] Krivenko P.V., Guzii S.G., Bodnarova L., Valek J., Hela R., and Zach J. "Effect of thickness of the

intumescent alkali aluminosilicate coating on temperature distribution in reinforced concrete". Journal of Building Engineering, vol. 8, pp. 14–19, 2016.

[26] Lu F. and Fontana M. "Intumescent coating against explosive spalling of HPC in fire". Proceedings of 5th International Workshop on Concrete Spalling due to Fire Exposure, Borås, Sweden, pp. 365-374, 2017.

[27] Yan L., Xu Z. and Liu D. "Synthesis and application of novel magnesium phosphate ester flame retardants for transparent intumescent fire-retardant coatings applied on wood substrates". Progress in Organic Coatings, vol. 129, pp. 327–337, 2019.

[28] Lucherini A., Razzaque Q.S. and Maluk C. "Exploring the fire behaviour of thin intumescent coatings used on timber". Fire Safety Journal, vol. 109, pp. 102887, 2019.

[29] Beck J.V. "Thermocouple temperature disturbances in low conductivity materials". Journal of Heat Transfer, vol. 84, pp. 124-132, 1962.

8

Heat transfer modelling

8.1 Introduction and background

The literature review has highlighted how several researchers have proposed different numerical and mathematical models of various complexities in order to simulate the behaviour of swelling intumescent coatings under thermal exposure (refer to Chapter 2). However, these models and design tools have not been universally generalised or internationally regulated because of their limited application, the high complexity or the contrasting results, considering the wide range of products available in the market. Within the structural fire safety practice, these methods are particularly focused on the accurate prediction of the temperature evolution of the substrate material protected by the intumescent coating. This problem is usually solved by treating the coating as inert material (no swelling) and estimating its temperature-dependent thermal and physical properties as equivalent thermal barrier to the protected substrate (e.g. effective thermal conductivity method) [1].

The research studies presented in Chapter 5, Chapter 6 and Chapter 7 proposed an experimental methodology aimed at analysing the effectiveness of thin intumescent coatings through a detailed characterisation of their thermo-physical response adopting the Heat-Transfer Rate Inducing System (H-TRIS) test method [2]. The experimental outcomes showed how the heating conditions, the substrate thermal conditions and the applied initial coating thickness affect the behaviour of the tested commercial solvent-based thin intumescent coating. In particular, the research studies demonstrated that the effectiveness of thin intumescent coatings is primarily controlled by the swelling process and the resulting swelled coating thickness. Accordingly, the swelling of thin intumescent coatings is influenced by several factors in different manners: for example, it was found that the heating conditions govern the swelling rate of the intumescent coating, while the applied initial thickness governs the maximum thickness that the coating can potentially achieve during the thermal exposure.

Based on these experimental outcomes, the research study presented herein investigates the development of a simplified heat transfer model that allows to simulate the thermal and physical response of swelling intumescent coatings for a range of conditions and scenarios (e.g. heating conditions and applied initial coating thickness). This chapter analyses the assumptions and simplifications that are introduced in the formulation of the heat

transfer model and assesses the validity of the proposed approach for the potential use in performance-based design engineering methods.

8.2 Modelling approach

The development of a numerical model able to simulate the heat transfer through swelling intumescent coatings represents a crucial aspect for design purposes because it aims at quantifying the thermal and physical properties of thermal barriers developed by thin intumescent coatings to protect substrate materials. In contrast to the experimental methodologies presented in Chapter 4 that evaluate several material properties in specific conditions (e.g. TPS and LFA), this model aims at providing good predictions of the thermal and physical response of thin intumescent coatings during the thermal exposure (see Figure 8.1). Following this approach, the main aim of the heat transfer model is to simulate and evaluate the effectiveness of thin intumescent coatings in order to define performance-based design engineering methods.

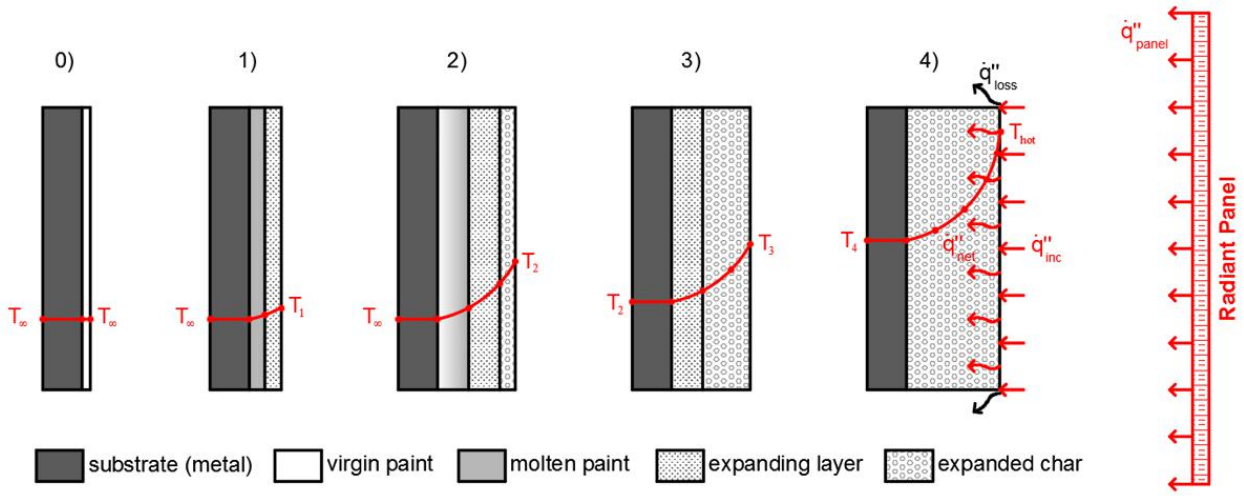

Figure 8.1: Simplified schematic illustration of the heat transfer problem within swelling intumescent coatings exposed to an incident heat flux imposed by a radiant panel.

The proposed heat transfer model is based and validated on the experimental campaign carried out on 10mm-thick steel plates coated with a commercial solvent-based thin intumescent coating presented in Chapter 6. Particularly, the experimental study focused on analysing the effectiveness of thin intumescent coatings through a detailed characterisation

of their thermo-physical response and investigated the influence of different heating conditions and applied initial coating thicknesses.

The phenomenon of intumescence is very challenging to model due to the complex thermo-psysical response of reactive coatings that may be influenced by various factors (e.g. heating conditions). Due to the complex nature of the problem, the heat transfer model involves several assumptions and simplifications which are derived following the experimental campaigns and their outcomes:

- The model focuses on solving the *one-dimensional heat conduction problem* by resolving energy-balance equations based on fundamental physical principles. All the experimental setups and testing campaigns were initially conceived and designed to simplify the heat transfer to a one-dimensional problem following the main direction of the heat flow, starting from the coating surface, through the swelling intumescent coating and towards the protected substrate material.

- The model discretises the intumescent coating in finite elements and corresponding nodes. The *swelling of thin intumescent coatings* is modelled by adding finite elements in the proximity to the substrate-coating interface where the virgin coating is located and sustains the swelling reaction. Empirical correlations are introduced to predict the evolution of the swelled coating thickness during the thermal exposure.

- The model assumes that the effectiveness of the thermal barrier provided by the intumescent coating is mainly dependent on the ability of developing *swelled porous char*. The intumescent coating is approximated as swelled porous char with specific constant material properties. The resulting material properties do not correspond to exact values, but they are lumped into *effective properties* that enable an accurate prediction of the thermal and physical evolution of the tested samples under specific conditions. In particular, the thermal conductivity of the swelled porous char undergoes an optimisation process to increase the model fitting using multiple scenarios.

- The model relies on the accurate definition of the *thermal conditions at the coating boundaries* (surface and substrate). The thermal boundary conditions at the exposed coating surface were defined by the time-history of incident heat flux imposed by the H-TRIS test method and the corresponding convective and radiative heat flux losses with

the surrounding environment. On the other hand, the substrate thermal conditions at the unexposed coating surface were defined by a steel plate treated as thermally-thin thermal mass with adiabatic thermal boundary conditions.

Starting from the inputs and assumptions described above, the heat transfer model aims at quantifying the effectiveness of thin intumescent coatings for a wide range of potential conditions, in terms of heating exposure and applied initial coating thickness. The insulating performance is analysed by defining the thermal and physical response of swelling intumescent coatings during the thermal exposure. In particular, the objective of the heat transfer model is to predict the thermal gradient within swelling intumescent coatings by simulating the evolution of the surface and substrate temperatures and the swelled coating thickness. This enables a fundamental understanding on the effectiveness of the thermal barrier provided by thin intumescent coatings to various substrate materials. Also, it provides an estimation of the evolution of the substrate temperature during thermal exposure, which is the key aspect to study the behaviour of structural elements protected with thin intumescent coatings.

8.3 Derivation of the heat transfer model

Starting from the model formulation presented in Chapter 5 (used for assessing the thermal behaviour prior to swelling), the heat transfer model was similarly defined as a finite-difference numerical model based on the *Crank-Nicolson method*, a finite-difference method able to solve the one-dimensional heat conduction equation [3-4]. Contrarily to the explicit numerical method developed by Emmons and Dusinberre, the Crank-Nicolson method is a second-order method in time, and implicit in time and numerically stable. Consequently, it does not require stability criteria. The formulation is based on building a system of N linear equations and N variables (i.e. temperatures of each node at the step $i+1$), based on the following governing equation:

$$T_j^{i+1} = T_j^i + \frac{\Delta t}{2}\left(\left.\frac{dT}{dt}\right|_j^i + \left.\frac{dT}{dt}\right|_j^{i+1}\right) \tag{8.1}$$

where T_j^i is the temperature of the node j at time i [K], $\left.\frac{dT}{dt}\right|_j^i$ is the temperature variation of the node j at time i [K/sec] and Δt is the time increment [sec]. The Crank-Nicolson method requires the derivation of the temperature variation over time $\frac{dT}{dt}$ for each element j of the

discretisation at time steps i and $i+1$. The defined system of equations forms a tridiagonal matrix system, which simplifies and significantly reduces the computational cost of the model [3-4].

The main aim of the heat transfer model is to simulate and evaluate the effectiveness of thin intumescent coatings. For this reason and differently to the previous case, the model is discretised in a *single-layer material* (intumescent coating only) with a total thickness equal to L, which corresponds to the actual coating thickness d_c. The material discretisation is organised in finite N elements, similarly for the case of the explicit heat transfer model. All the N elements are represented by N nodes. The interior elements have the node placed in the element's centre and they have a thickness of Δx. On the other hand, the boundary elements (surface element and end element) have the node placed at the element's edge and they have a thickness of $\Delta x/2$. No interface elements are considered.

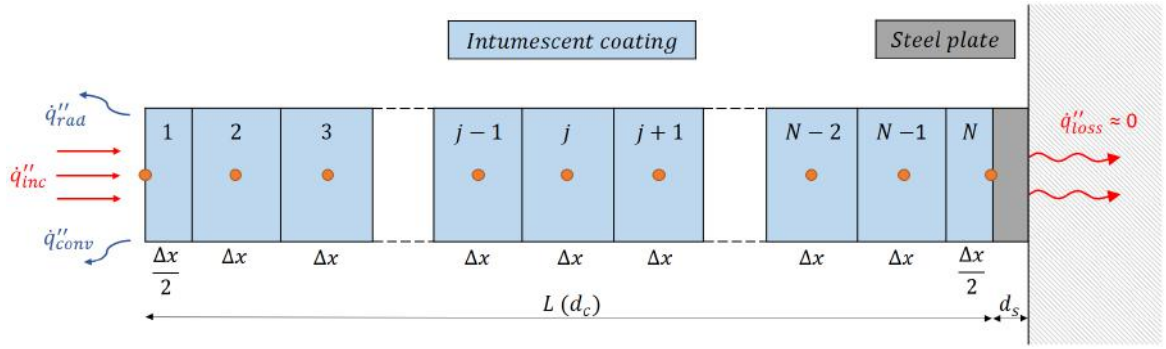

Figure 8.2: Schematic illustration of the single-layer material heat transfer model including the thermal boundary conditions.

Analogously to the previous model, equivalent assumptions, boundary conditions and material properties were defined in order to represent the problem defined in the different thermal experiments. Generally, the thermal boundary conditions at the exposed surface of test samples were defined by the time-history of incident heat flux imposed by the H-TRIS test method ($\dot{q}''_{inc}$) with convective and radiative heat flux losses ($\dot{q}''_{conv}$ and $\dot{q}''_{rad}$) with the surrounding environment. These thermal boundary conditions were modelled using conventional correlations available in the literature (refer to Appendix C) [5]. Adiabatic conditions were assumed at the unexposed surface. Due to thermally-thin nature of the substrate steel plate (high thermal conductivity and low physical thickness, low Biot number), it was lumped into a thermal mass connected to the coating end element and characterised by no thermal

gradient and a single temperature, which corresponds to the same temperature of the steel-coating interface. Figure 8.2 illustrates the heat transfer model based on the single-layer material space domain discretisation and the described thermal boundary conditions, generally adopted in the current research study.

Starting from energy-balance equations at each node, thus each element, the following formulas for surface, middle and end elements (thus nodes) were derived. The obtained formulas allow to build and solve the tridiagonal matrix system aimed at calculating the temperature evolution of each node j for each time step i, depending on the type of element (either surface, middle or end). The various governing equations were systematically organised into a specific order: unknown variables (T_j^{i+1}) and their parameters on the left-hand side, known parameters on the right side. The derivation and assumptions of each of the following formulas is presented in detail in Appendix D.

Surface element: know time-history of incident heat flux.

$$\begin{gathered} T_1^{i+1}\left[1+Fo_1^i+\frac{h_{tot}\Delta t}{\rho_c c_{p,c}\Delta x}\right]+T_2^{i+1}\left[-Fo_1^i\right]= \\ T_1^i+Fo_1^i\left(T_2^i-T_1^i\right)+\frac{\alpha_c\Delta t}{\rho_c c_{p,c}\Delta x}\left(\dot{q}_{inc}^{''i}+\dot{q}_{inc}^{''i+1}\right)+\frac{h_{tot}\Delta t}{\rho_c c_{p,c}\Delta x}\left(2T_\infty-T_1^i\right) \end{gathered} \tag{8.2}$$

Middle element: pure conduction.

$$\begin{gathered} T_{j-1}^{i+1}\left[-\frac{Fo_j^i}{2}\right]+T_j^{i+1}\left[1+Fo_j^i\right]+T_{j+1}^{i+1}\left[-\frac{Fo_j^i}{2}\right]= \\ T_j^i+\frac{Fo_j^i}{2}\left(T_{j-1}^i-2T_j^i+T_{j+1}^i\right)+dFo_j^i\left(T_{j+1}^i-T_{j-1}^i\right)^2 \end{gathered} \tag{8.3}$$

End element: thermally thin material with adiabatic thermal boundary conditions.

$$T_{N-1}^{i+1}\left[-Fon_N^i\right]+T_N^{i+1}\left[1+Fon_N^i\right]=T_N^i+Fon_N^i\left(T_{N-1}^i-T_N^i\right) \tag{8.4}$$

where T_j^i is the temperature of the node j at time i [K], Δt is the time increment [sec], Δx is the space discretisation thickness [m], $\dot{q}_{inc}^{''i}$ is the incident heat flux [W/m^2] at time i, ρ_c is the density of the intumescent coating [kg/m^3], $c_{p,c}$ is the specific heat capacity of the intumescent coating [J/kgK], λ_c is the thermal conductivity of the intumescent coating [W/mK], α_c is the absorptivity of the intumescent coating [-] and T_∞ is the ambient temperature [K].

Within the derivation of the heat transfer model, different parameters are obtained and they have a key role in the mathematical formulation. First, a simplified formulation of the *Fourier*

number Fo_j^i [-] for each node j at time i can be expressed as:

$$Fo_j^i = \frac{\lambda_c \Delta t}{\rho_c c_{p,c} \Delta x^2} \tag{8.5}$$

If the thermal conductivity is not constant (first-derivative different from zero), the *Fourier number derivative* dFo_j^i [K^{-1}] can be expressed as:

$$dFo_j^i = \frac{d\lambda_c}{dT} \cdot \frac{\Delta t}{4\rho_c c_{p,c} \Delta x^2} \tag{8.6}$$

where $\frac{d\lambda}{dT}$ is the derivative of the temperature-dependent thermal conductivity of the node j at time i.

In the specific case of an end element connected to a thermally-thin thermal mass (steel plate), the *Fourier number* Fon_N^i [-] for the end node N at time i can be expressed as:

$$Fon_N^i = \frac{\lambda_c \Delta t}{\Delta x \left[\Delta x \rho_c c_{p,c} + 2 d_s \rho_s c_{p,s}\right]} \tag{8.7}$$

where d_s is the steel plate thickness [m], ρ_s is the density of steel [kg/m^3] and $c_{p,s}$ is the specific heat capacity of steel [J/kgK].

Finally, the radiative and convective losses were lumped into a unique heat transfer coefficient, known as *total heat transfer coefficient* h_{tot} [W/m^{2}K], which can be expressed as:

$$h_{tot}(T_1^i) = h_{conv}(T_1^i) + \varepsilon_c \sigma \frac{(T_1^i)^4 - T_\infty^4}{T_1^i - T_\infty} = h_{conv}(T_1^i) + \varepsilon_c \sigma \left[(T_1^i)^2 + T_\infty^2\right]\left(T_1^i + T_\infty\right) \tag{8.8}$$

where h_{conv} is the convective heat transfer coefficient [W/m^{2}K], ε_c is the emissivity of the intumescent coating [-] and σ is the Stefan-Boltzmann constant ($5.67 \cdot 10^{-8}$ W/m^{2}K^4).

Throughout the development of the current project, other heat transfer models were formulated in order to comprehend the influence of different factors in the physical and thermal problem. For completeness, the heat transfer models with different assumptions and thermal boundary conditions are presented in the Appendix D.

8.3.1 Heat transfer model prior to swelling

As already presented in Chapter 5, the finite-difference heat transfer model described in Section 5.3 is capable of simulating the temperature increase of uncoated and coated steel plated prior to onset of swelling. This model is based on the numerical method developed by Emmons and Dusinberre and it is presented in detail in Appendix C [6-7]. This model

is discretised in a *two-layer material* (intumescent coating and steel) and it solves the one-dimensional heat conduction problem in the main direction of the heat flow. A similar implicit heat transfer model was formulated based on the Crank-Nicolson method using equivalent boundary conditions, assumptions and material properties. However, prior to onset of swelling, the heat transfer problem is heavily transient and the thermal processes taking place in the intumescent coating (i.e. endo- and exo-thermic reactions) have a key importance. Consequently, they were considered in the problem by introducing a volumetric heat source term $\dot{g}_c'''$, analogous to the one presented in Section 5.5.

In order to solve the described heat transfer model, equivalent material properties were defined. Regarding the *steel*, the thermal and physical properties of carbon steel were defined in accordance with Eurocode 3 [8]:

- Thermal conductivity: $\lambda_s(T)$ [W/mK] according to clause 3.4.1.3
- Density: ρ_s = 7850 kg/m^3
- Specific heat capacity: $c_{p,s}(T)$ [J/kgK] according to clause 3.4.1.2
- Absorptivity/Emissivity: $\alpha_s = \varepsilon_s$ = 0.75

Regarding the *intumescent coating*, the thermal and physical properties prior to swelling were defined in accordance with the material characterisation presented in Chapter 4:

- Thermal conductivity: $\lambda_c = -2 \cdot 10^{-6} \cdot T_c^2 - 0.0004 \cdot T_c + 0.5214$ [W/mK]
- Density: ρ_c = 1500 kg/m^3
- Specific heat capacity: $c_{p,c} = -0.0243 \cdot T_c^2 + 8.3602 \cdot T_c + 1089.3$ [J/kgK]
- Absorptivity/Emissivity: $\alpha_c = \varepsilon_c$ = 0.92
- Volumetric heat source term: $\dot{g}_c''' = 2.4 \cdot 10^4 \cdot T_c$ [W/m^3] for $200^oC \leq T_c \leq 300^oC$

Similarly to what presented in Chapter 5, the heat transfer model was validated for coated steel plates exposed to a constant incident heat flux of 10 kW/m^2 and uncoated steel plates exposed to various constant incident heat fluxes. The model was benchmarked based on the temperature evolution of coated or uncoated steel plates. Similar graphs to Figure 5.4 and Figure 5.5 were produced. The good agreement between the experimental and the predicted temperatures verified the validity of the assumption of adiabatic conditions at the

unexposed surface, the accuracy of the heat flux calibration of the H-TRIS test method and the adopted material properties (steel and intumescent coating prior to swelling).

8.3.2 Heat transfer model including swelling

In Chapter 6 and Chapter 7, the current research study has emphasised how the effectiveness of thin intumescent coatings is mainly influenced by the swelling process and the resulting swelled coating thickness. In particular, the swelling reaction occurs in the proximity to the steel-coating interface where the virgin coating is located and sustains the process. In this way, the swelling intumescent coating insulates the protected substrate by displacing the already-swelled coating toward the direction of the heat source. This explains why the swelling of intumescent coatings and the substrate temperature are strictly related. Following these experimental outcomes, the previous heat transfer model (prior to swelling) is extended in order to include the swelling of thin intumescent coatings. First of all, the swelling reaction is modelled by adding finite elements of the same thickness Δx at the steel-coating interface, in particular next to the coating end element. The new added element is introduced at the same temperature of the previous coating end element and the temperature of the new second-last coating element is calculated as the average value between the temperatures of the two adjacent elements. In this way, the protective thermal barrier developed by the intumescent coating increases its thickness during the thermal exposure following certain empirical correlations presented in the section below. In accordance with this approach, the size of the tridiagonal matrix system continuously increases following the swelling of the intumescent coating. Figure 8.3 offers a schematic illustration of the modelling approach described herein.

Definition of the swelled coating thickness

Chapter 6 has outlined how the heating conditions and the applied initial thickness affect the swelling of the tested intumescent coating: the external incident heat flux governs the swelling rate of the intumescent coating, while the applied initial DFT governs the maximum swelled coating thickness that the intumescent coating could reach during the thermal exposure. Figure 6.9 and Figure 6.10 proposed empirical correlations to predict the evolution of the swelled coating thickness during the thermal exposure, starting from well-defined

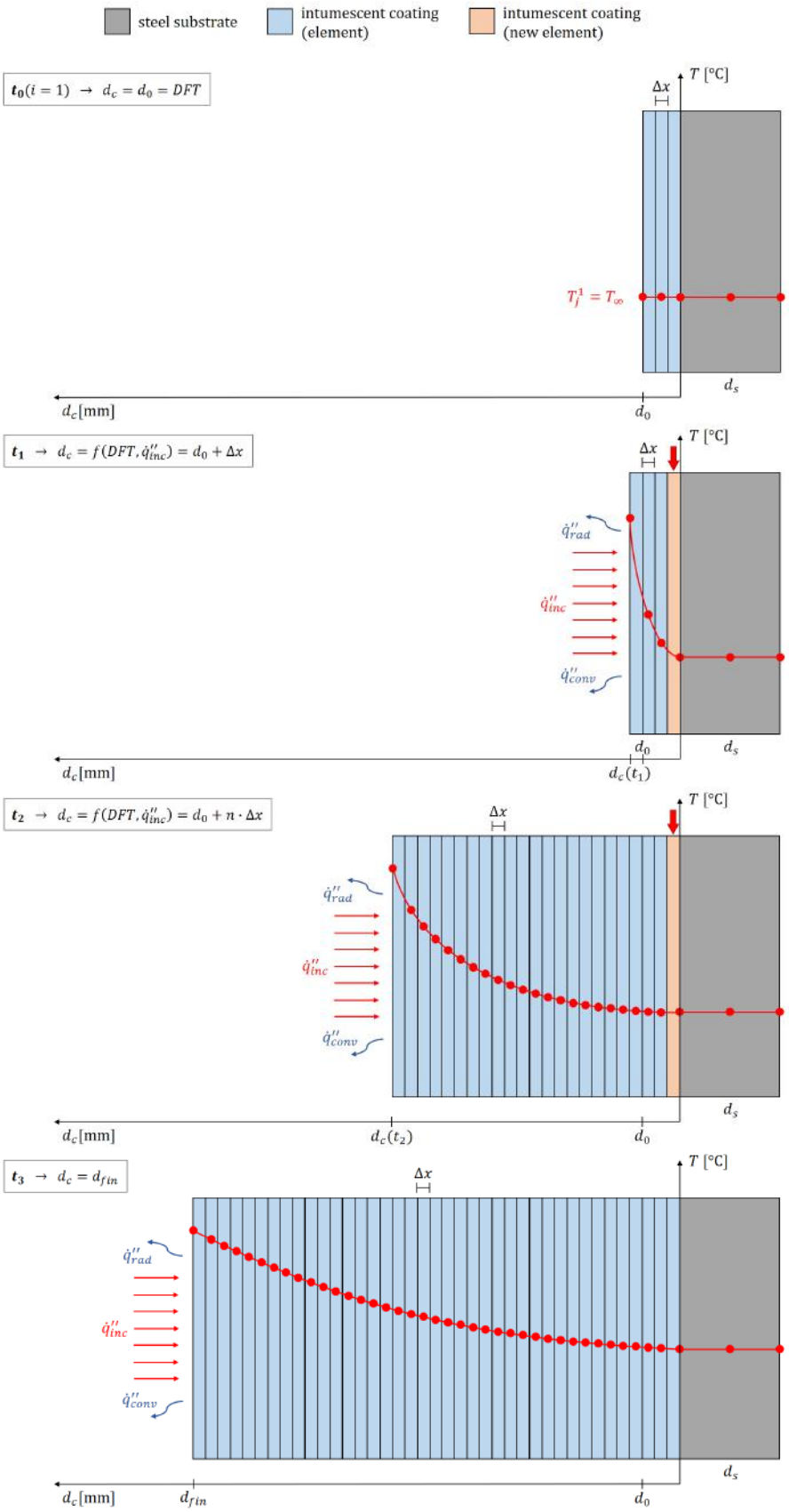

Figure 8.3: Schematic illustration of the heat transfer model formulated for swelling intumescent coatings.

thermal boundary conditions at the coating surface and the applied initial coating thickness. In particular, the maximum swelled coating thickness of the intumescent coating d_{max} [mm] can be expressed as a function of the applied initial DFT [mm]:

$$d_{max} = 17.7 \cdot DFT + 10.6 \tag{8.9}$$

On the other hand, starting from the linear formulation presented in Figure 6.10, the fitting of the empirical correlation between the constant incident heat flux and the swelling rate of the intumescent coating was improved by introducing a second-order polynomial equation and increasing the R-squared value (refer to Figure 8.4). In addition, considering the outcomes presented in Chapter 5, the swelling rate of the intumescent coating was assumed null for external heat fluxes lower than the critical incident heat flux for onset of swelling (20-23 kW/m^2). As a result, the swelling rate of the intumescent coating $\dot{d}_c$ [mm/min] can be expressed as a function of the incident heat flux:

$$\dot{d}_c = \begin{cases} 0 & \text{if} \quad \dot{q}''_{inc} < 20kW/m^2 \\ -0.0001 \cdot \left(\dot{q}''_{inc}\right)^2 + 0.0280 \cdot \dot{q}''_{inc} - 0.3320 & \text{if} \quad \dot{q}''_{inc} \geq 20kW/m^2 \end{cases} \tag{8.10}$$

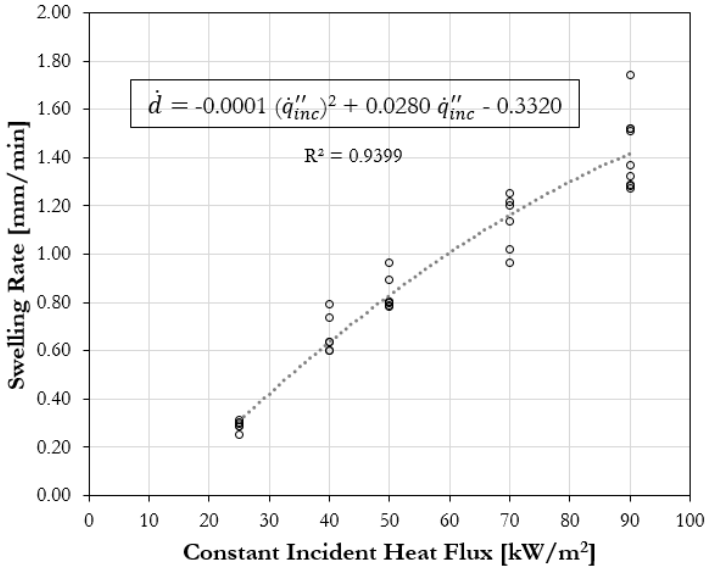

Figure 8.4: Improved empirical correlation for predicting the swelling rate of the intumescent coating as a function of the external incident constant heat flux.

Accordingly, the evolution of the swelled thickness of the intumescent coating $d_c(t)$ [mm]

during thermal exposure can be predicted using the following expression:

$$d_c(t) = \begin{cases} DFT + \dot{d}_c \Delta t & \text{if} \quad DFT + \dot{d}_c \Delta t \leq d_{max} \\ d_{max} \end{cases} \tag{8.11}$$

where d_{max} is the maximum swelled coating thickness [mm], DFT is the applied initial dry film thickness [mm], $d_c(\Delta t)$ is the swelled coating thickness at the time increment Δt [mm], Δt is the time increment (from the beginning of the thermal exposure) [min] and $\dot{q}''_{inc}$ is the constant incident heat flux [kW/m^2]. It is important to underline that, for simplicity, the swelling rate was linearised during the whole thermal exposure: the onset of swelling was considered at time zero, at the application of the external heat flux. The time to onset of swelling was not included due to its minor influence on the whole heat transfer problem (only a few minutes in the cases which registered relevant swelling).

Employing Equation 8.9, Equation 8.10 and Equation 8.11, the evolution of the swelled thickness of the tested intumescent coating during thermal exposure can be calculated for all the experimental cases presented in Chapter 6: six different constant incident heat fluxes (10, 25, 40, 50, 70 and 90 kW/m^2) and three different applied initial DFTs (*"Low DFT"*, *"Medium DFT"* and *"High DFT"*). In accordance with the measured mean DFTs, the initial thickness of the intumescent coating was set equal to 1.0 mm, 1.8 mm or 2.9 mm for *"Low DFT"*, *"Medium DFT"* or *"High DFT"*, respectively. Figure 8.5 compares the experimentally-measured swelled coating thickness and the one predicted using the described empirical correlations. The empirical model occasionally under- or over-estimates the swelled coating thickness, especially for extreme cases (e.g. 90 kW/m^2, *"High DFT"*). However, the overall trend for predicting the evolution of the swelled coating thickness for different applied initial DFTs and different constant incident heat fluxes is captured by using the described correlations. The implications of adopting these empirical models will be faced in the sensitivity analysis presented in Section 8.4.3.

Definition of the intumescent coating's properties

As highlighted in Chapter 6, the measured in-depth temperature profiles showed how the intumescent porous chars obtained from different heating conditions have similar properties and the thermal gradient within the swelling intumescent coating is mainly governed by the

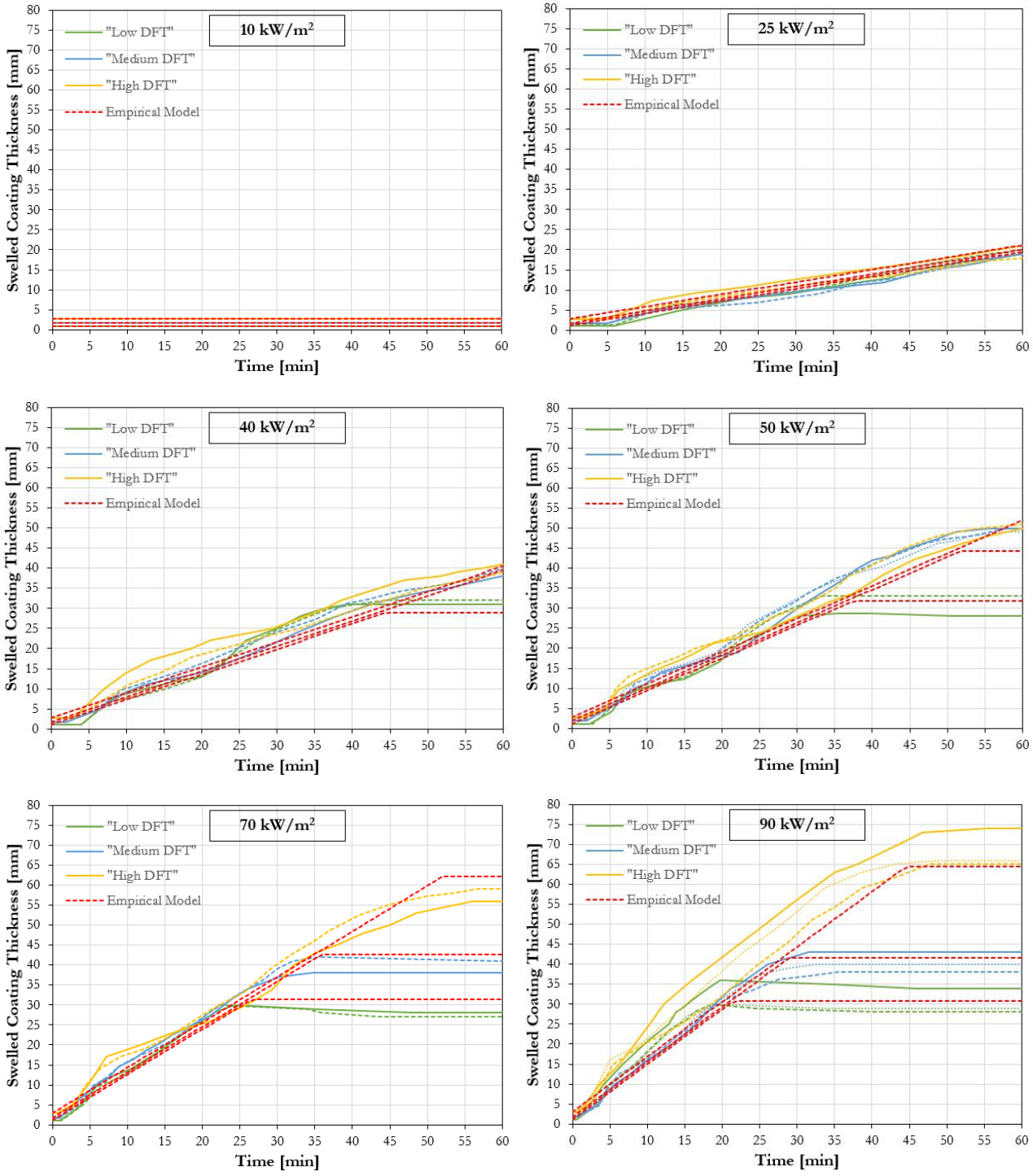

Figure 8.5: Comparison between the experimentally-measured swelled coating thickness and the one predicted using empirical correlations for different applied initial DFTs and different constant incident heat fluxes.

swelled coating thickness. This was also confirmed by the TPS experiments on intumescent porous chars presented in Chapter 4. Thus, the material properties involved in the current

heat transfer model were defined in accordance with these experimental outcomes.
Since the heat transfer problem is governed by an accurate prediction of the swelling process and the swelled coating thickness, the model is based on the assumption that the effectiveness of the thermal barrier provided by the intumescent coating is mainly dependent on the ability of developing porous char. For simplicity, the swelling intumescent coating is directly approximated as porous char with specific constant material properties. Defining precise temperature-dependent material properties would have increased the accuracy of the heat transfer model. However, since the problem is primarily controlled by the swelling process, the heat transfer model is approximated in order to offer a simplified solution characterised by a few governing parameters.
In order to understand the relevance of each single thermal and physical property in the heat transfer problem, a sensitivity analysis was carried out starting from the material properties of coating porous chars estimated in Chapter 4. The model accuracy was evaluated based on the the *Root-Mean-Square Error (RMSE)* between the experimentally-measured temperature evolution of coated steel plates ($T_{s,exp}$) compared to the predicted temperature evolution using the described heat transfer model ($T_{s,mod}$), evaluated at 1 min time-intervals:

$$RMSE(T_s) = \sqrt{\frac{\Sigma(T_{s,exp} - T_{s,mod})^2}{N}} \tag{8.12}$$

The model was benchmarked against the temperature evolution of the coated steel plate because the substrate temperature represents the main performance criteria for most applications in structural fire safety engineering. In each case, a sign was given to the Root-Mean-Square Error (RMSE): positive RMSE represents a over-prediction of the steel temperature, while a negative RMSE represents a under-prediction of the steel temperature. Figure 8.6 reports the results obtained from the sensitivity analysis with respect to the thermal conductivity, density, specific heat capacity and absorptivity/emissivity of the intumescent coating. The sensitivity analysis revealed clear trends. The density, the specific heat capacity and the absorptivity/emissivity of the intumescent coating have a minor influence on the accuracy of the heat transfer model, while the thermal conductivity plays a key role in the problem. This outcome was quite predictable due to the nature of the heat transfer problem. Following this approach, the modelling of swelling intumescent coatings becomes a physical problem, largely driven by an accurate prediction of the swelled coating thickness. The

heat transfer problem turns into *quasi steady-state* due to the highly-insulating properties of the intumescent coating (high Biot number), the applied constant incident heat flux and the relatively-high swelling speed, compared to the penetration speed of the heat wave within the swelling intumescent coating. In this way, the thermal transient state is disregarded and the model focuses on solving a quasi steady-state heat transfer problem. This assumption is more valid for high heat fluxes because at low heat fluxes the thermal transient phenomena (change in density, specific heat capacity...) control the problem. For instance, the heating condition that did not trigger swelling (10 kW/m^2) underlined a minor dependency on the thermal conductivity of the intumescent coating: this case is fundamentally different to the swelling cases because it is governed by transient phenomena, which are neglected in the proposed model.

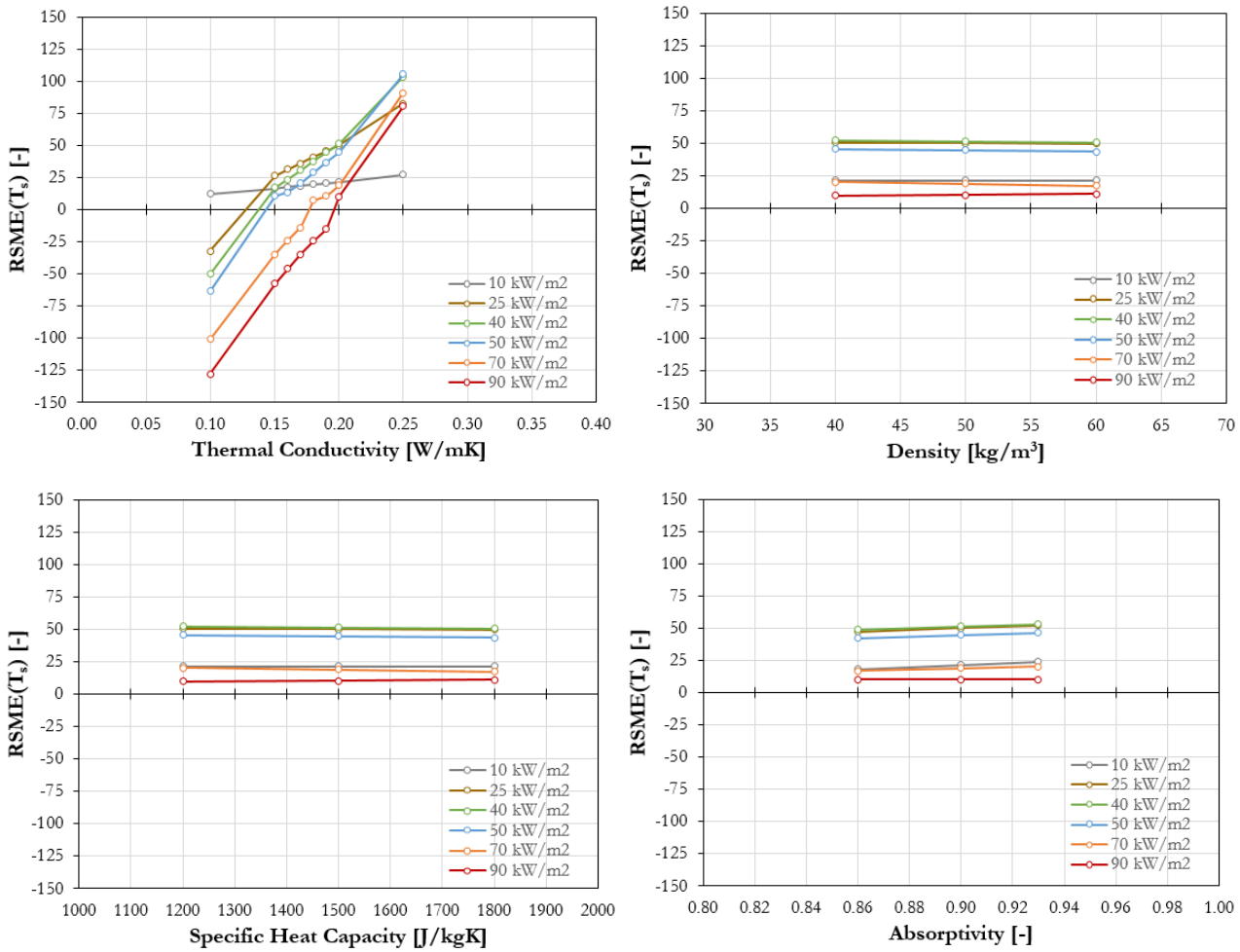

Figure 8.6: Sensitivity analysis with respect to the thermal conductivity, density, specific heat capacity and absorptivity/emissivity of the intumescent coating (*"Medium DFT"*).

Following the outcomes from the material characterisation presented in Chapter 4 and the sensitivity analysis, the thermal and physical properties of the intumescent coating were defined as:

- Density: ρ_c = 50 kg/m^3
- Specific heat capacity: $c_{p,c}$ = 1550 J/kgK
- Absorptivity/Emissivity: α_c = ε_c = 0.90 (average value within the 0.86-0.93 range evaluated using the Integrating Sphere System (ISS) in Section 4.3.3)

It is noteworthy that, due to the definition of a quasi steady-state thermal problem and the omission of transient phenomena, the heat source term (volumetric heat source term $\dot{g}_c^{'''}$) introduced for the heat transfer model prior to swelling was removed. As highlighted by the sensitivity analysis, transient phenomena (e.g. endothermic or exothermic reactions) become secondary within the defined thermo-physical problem.
On the contrary, in order to obtain an accurate prediction of the thermal and physical behaviour of the tested intumescent coating, the thermal conductivity was lumped into an effective value and subjected to an optimisation process. As highlighted in the sensitivity analysis shown in Figure 8.6, no specific value of the thermal conductivity is able to eliminate the discrepancy (zero deviation) between the model and the experimental measurements for all the different heating conditions. A similar trend was also detected for different initial thicknesses, *"Low DFT"* and *"High DFT"*. Consequently, the thermal conductivity of the intumescent coating was chosen based on the minimum total Root-Mean-Square Error (RMSE) between the experimentally-measured and predicted temperature evolutions of coated steel plates, summed for all the different heating conditions (RMSE absolute values). Figure 8.7 displays the results obtained from this analysis, carried out for all the different DFTs. The values of thermal conductivity that produced the minimum total errors were 0.16 W/mK for *"Medium DFT"* and *"High DFT"*, and 0.17 W/mK for *"Low DFT"*. Therefore, the thermal conductivity of the intumescent coating λ_c was set equal to 0.16 W/mK. Adding or removing the deviation related to the case of 10 kW/m^2 was marginal due to the different fundamental nature of the problem (no swelling): anyway, it has been included for completeness.

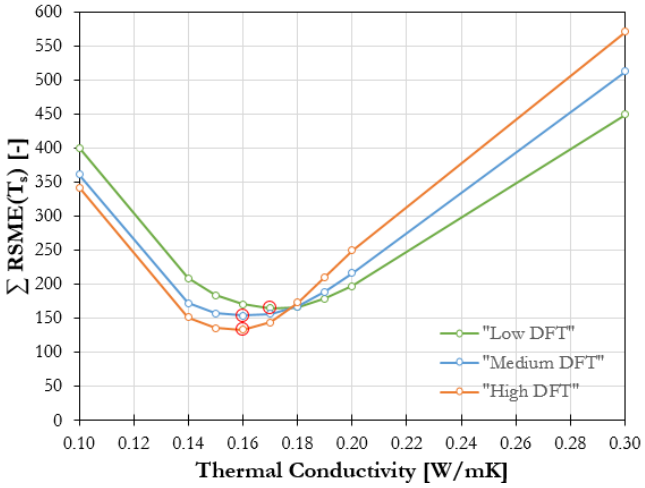

Figure 8.7: Total Root-Mean-Square Error (RMSE) for different thermal conductivity values of the intumescent coating (*"Medium DFT"*).

8.4 Modelling results and validation

8.4.1 Steel and coating surface temperatures

Employing the described empirical correlations, assumptions and material properties, the numerical model was implemented in order to solve the heat transfer problem for all the experimental cases presented in Chapter 6. Figure 8.8, Figure 8.9 and Figure 8.10 show the modelling results for the six different constant incident heat fluxes and three different applied initial DFTs. In particular, the reported plots compare the evolution of the experimentally-measured coating surface and steel temperatures to the ones predicted using the described heat transfer model.

The modelling results highlight the ability of the numerical model to characterise the heat transfer problem within the swelling intumescent coating. Regarding the steel temperatures, the prediction accuracy varies for different cases. In general, for low heat fluxes, the steel temperatures are over-predicted and the model accuracy increases for higher heat fluxes. For very high heat fluxes (e.g. 70 and 90 kW/m^2), the steel temperatures are under-predicted. A similar trend is detected for the various applied initial DFTs, but more accurate predictions are usually obtained for higher values (e.g. *"High DFT"*). This aspect is emphasised in Figure 8.11 and it is the result of the optimisation process carried out on the thermal conductivity of the intumescent coating. The error throughout the whole problem

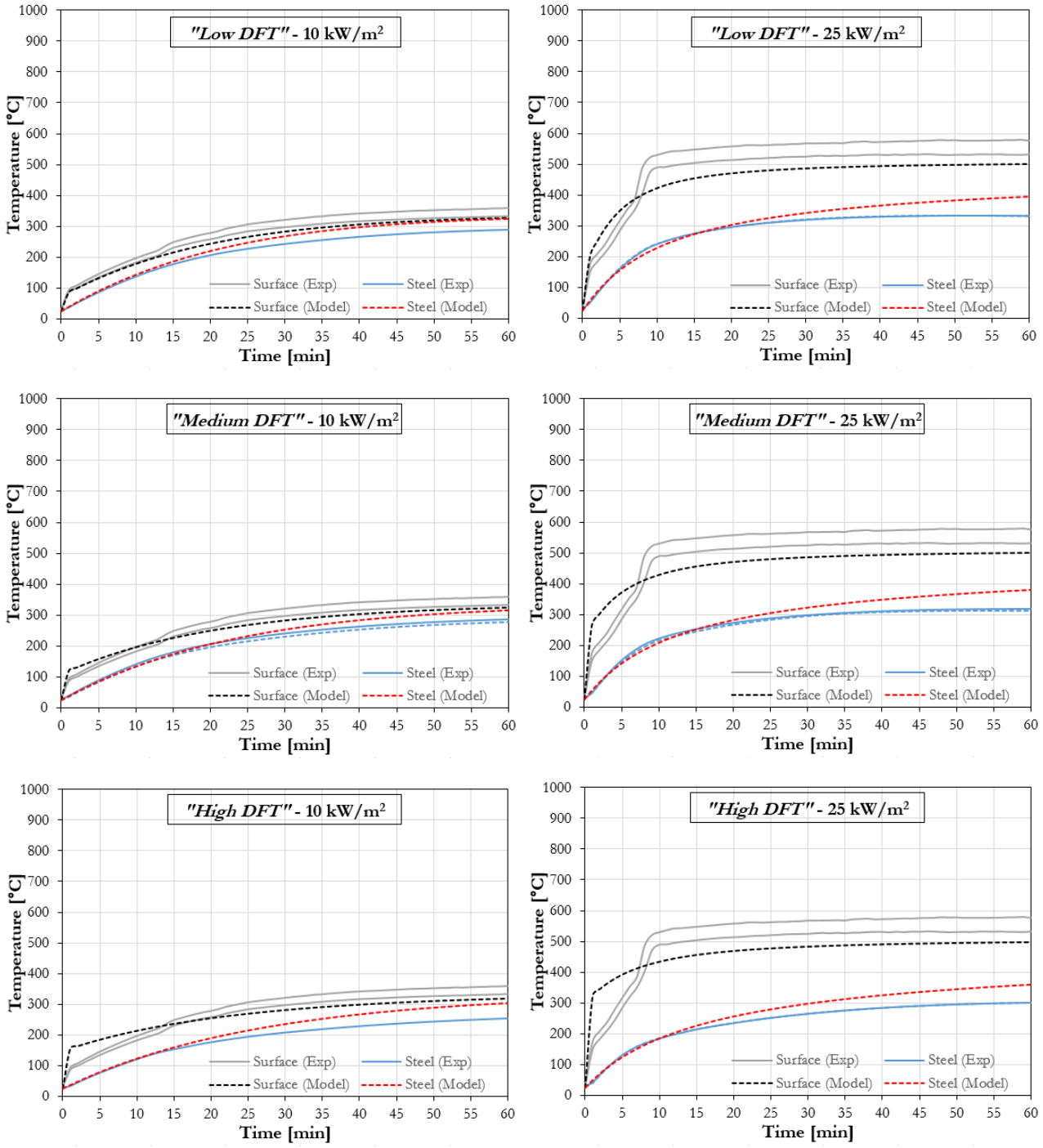

Figure 8.8: Comparison between the experimentally-measured coating surface and steel temperatures and the ones predicted using the described heat transfer model (10 and 25 kW/m^2).

is minimised and it has been balanced between over-predicted cases (positive RMSE) and under-predicted cases (negative RMSE). However, within the structural fire safety engineering practice, an under-estimation of the steel temperatures may imply a potential failure on the unsafe side. Optimisation processes for the definition of the thermal conductivity of

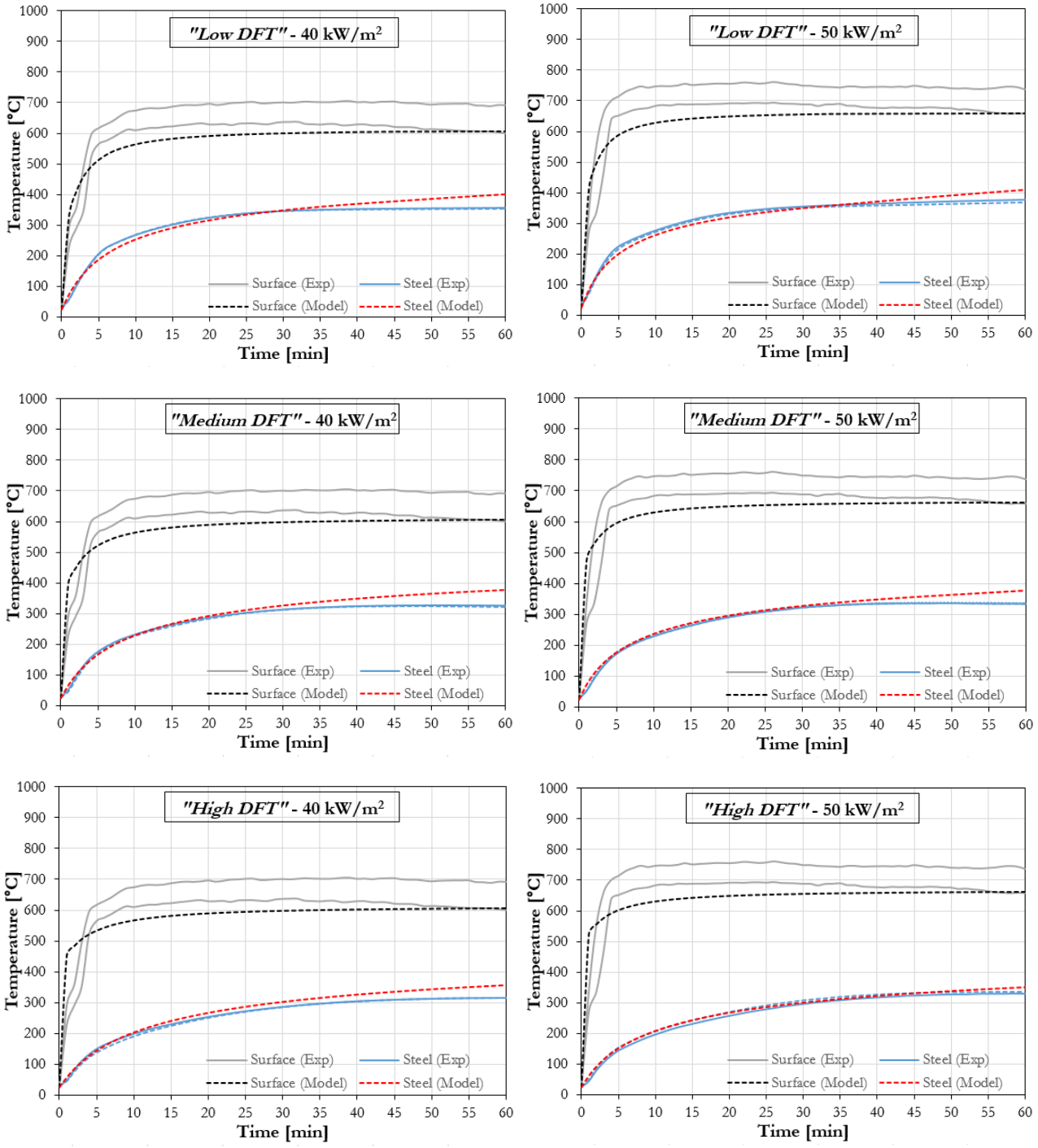

Figure 8.9: Comparison between the experimentally-measured coating surface and steel temperatures and the ones predicted using the described heat transfer model (40 and 50 kW/m^2).

the intumescent coating, similar to the on presented herein, could be implemented in order to consistently predict the steel temperatures on the safe side (over-prediction, positive RMSE). For instance, this process was repeated for a value of thermal conductivity equal to 0.20 W/mK and the model deviations are reported in Figure 8.12.

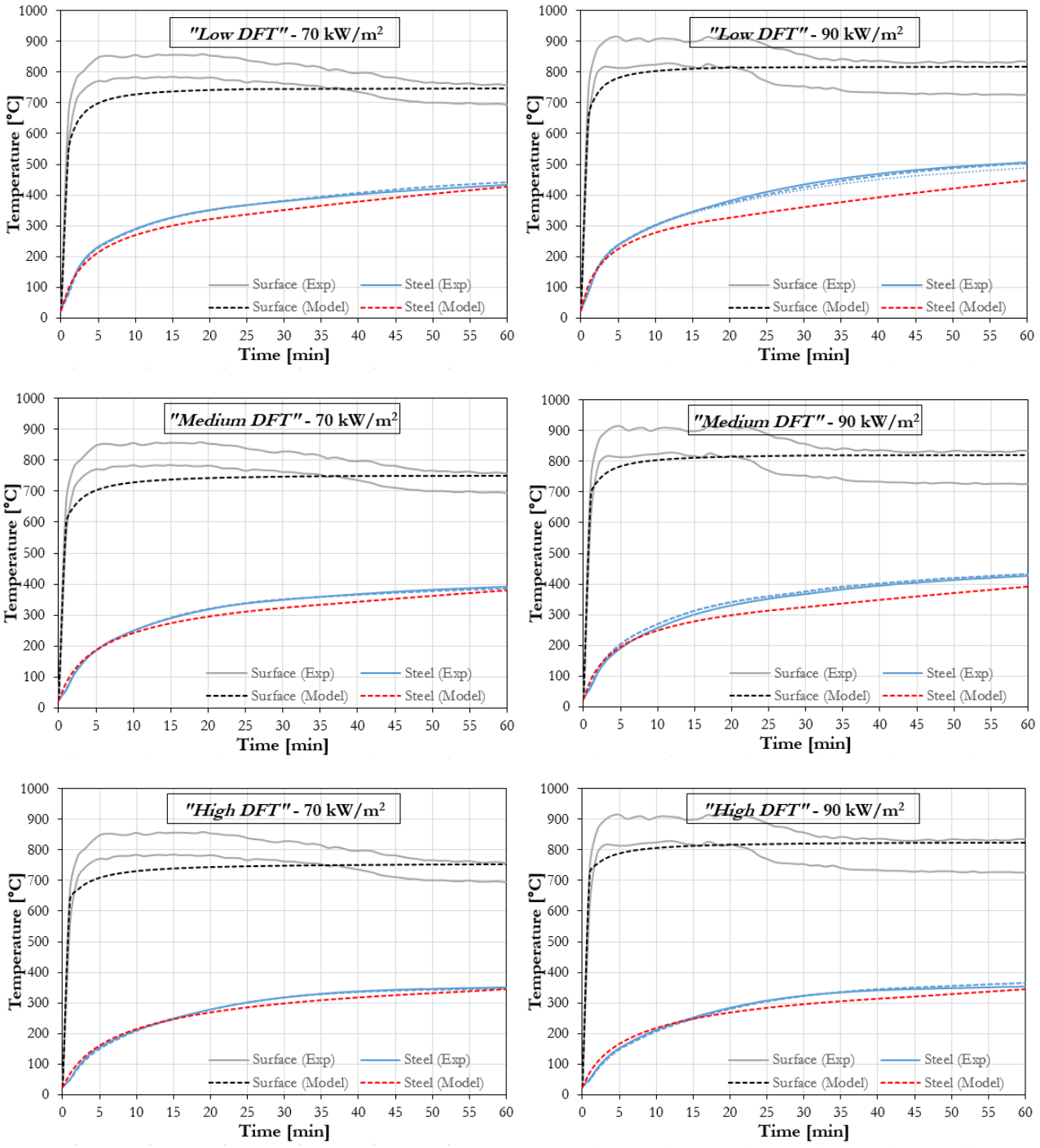

Figure 8.10: Comparison between the experimentally-measured coating surface and steel temperatures and the ones predicted using the described heat transfer model (70 and 90 kW/m^2).

Figure 8.8, Figure 8.9 and Figure 8.10 also compare the temperature evolution at the coating surface. The general trend is captured, but the surface temperatures are generally underestimated. This could be related to different aspects. The first reason could be related to oxidation taking place at the coating surface in the oxygen-rich environment of the H-

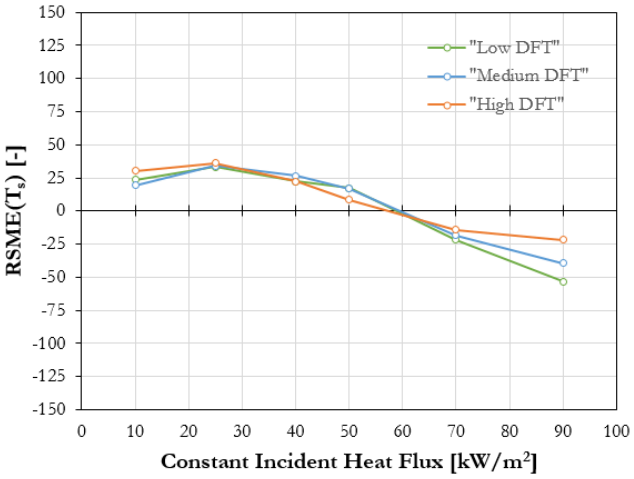

Figure 8.11: Root-Mean-Square Error (RMSE) for different constant incident heat fluxes and applied initial DFTs (λ_c = 0.16 W/mK).

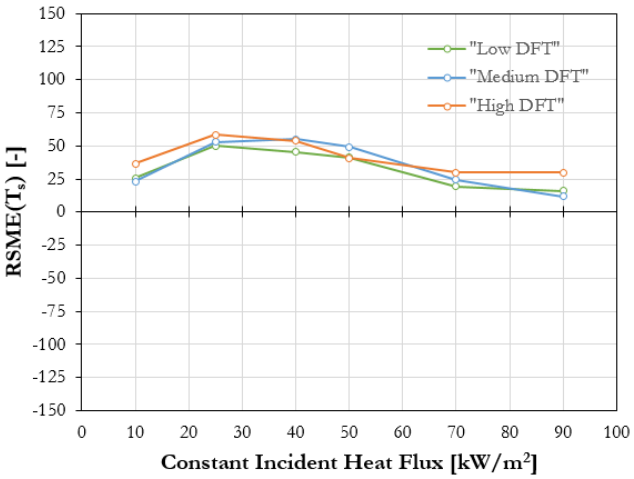

Figure 8.12: Root-Mean-Square Error (RMSE) for different constant incident heat fluxes and applied initial DFTs (λ_c = 0.20 W/mK).

TRIS test method. The TGA experiments presented in Section 4.3.1 underlined how, in the presence of oxygen and for temperatures above 550 ℃, the intumescent coating undergoes oxidation reactions. Since the proposed model does not consider any oxidation process, the surface temperature may be under-estimated. Another reason could be related to the accuracy of the imposed thermal boundary conditions: the constant incident heat flux at the sample surface was applied with an accuracy of $\pm$ 10%. Finally, the predicted surface temperature and the surface temperature measured using the IR camera strongly rely on a correct definition of the surface properties of the intumescent coating, especially absorptivity and emissivity. These parameters control the net heat flux received by the test samples by defining the absorbed heat by the intumescent coating and the radiation losses at the coating surface. However, as shown in Figure 8.6, absorptivity and emissivity have a minor influence in the calculation of the protected steel temperatures. The current model employs a constant average value, independent of the material temperature and the radiation wavelength: this assumption may be another potential cause of deviation between the experimental and the modelled cases. Moreover, due to its quasi steady-state nature, the proposed model poorly predicts the initial transient phase of the heat transfer problem: this aspect is more obvious for low heat fluxes, while for high heat fluxes is less evident.

In general, the heat transfer model is capable of describing the heat transfer within the swelling intumescent coating because it is able to restrict the problem by defining the two edges

of the thermal gradient. As already discussed, the thermal gradient within the intumescent coating is mainly governed by the swelled coating thickness and the thermal boundary conditions at the coating surface. The surface coating temperature depends on the heating conditions and the coating swelling results in stretching the thermal gradient between the steel substrate and the coating surface. It is noteworthy that the application of the numerical model to the case of 10 kW/m^2, along with all the cases that do not trigger the swelling of the intumescent coating, loses significance. In these cases, the heat transfer problem is primarily transient and other models as the one presented for prior to swelling represent a preferable option.

8.4.2 In-depth temperature profiles

Using the experimental measurements and adopting the described heat transfer model, it is also possible to investigate the evolution of the in-depth temperature profiles within the swelling coating during the thermal exposure. Figure 8.13 reports the comparison between the experimentally-measured and predicted in-depth temperature profiles. For neatness of graphical visualisation, three instants during the thermal exposure were selected and plotted: 10, 30 and 60 minutes. Furthermore, the graphs only report the average in-depth temperature profile, evaluated between different experimental repetitions: all the different temperature curves are available in Appendix A. In Figure 8.13, the accuracy of each experimental measurement was provided using error bars at the last data point (coating surface). The horizontal error bars represent the accuracy of the location of the in-depth thermocouple and the evaluation of the swelled thickness of the intumescent coating ($\pm$ 2 mm). On the contrary, the vertical error bars represent the accuracy of the surface coating temperature and the maximum temperature discrepancy between different experimental repetitions. The case of *"Medium DFT"* was chosen as example: similar conclusions can be drawn from different initial applied DFTs.

The first significant characteristic of the in-depth temperature profiles obtained from the numerical model is their linearity. Common heat transfer problems of insulation materials (high Biot number) with well-defined thermal properties and constant geometrical dimensions (e.g. thickness) are usually constituted by a transient phase and a steady-state phase [5]. At the beginning of any thermal exposure, the transient phase is generally characterised by

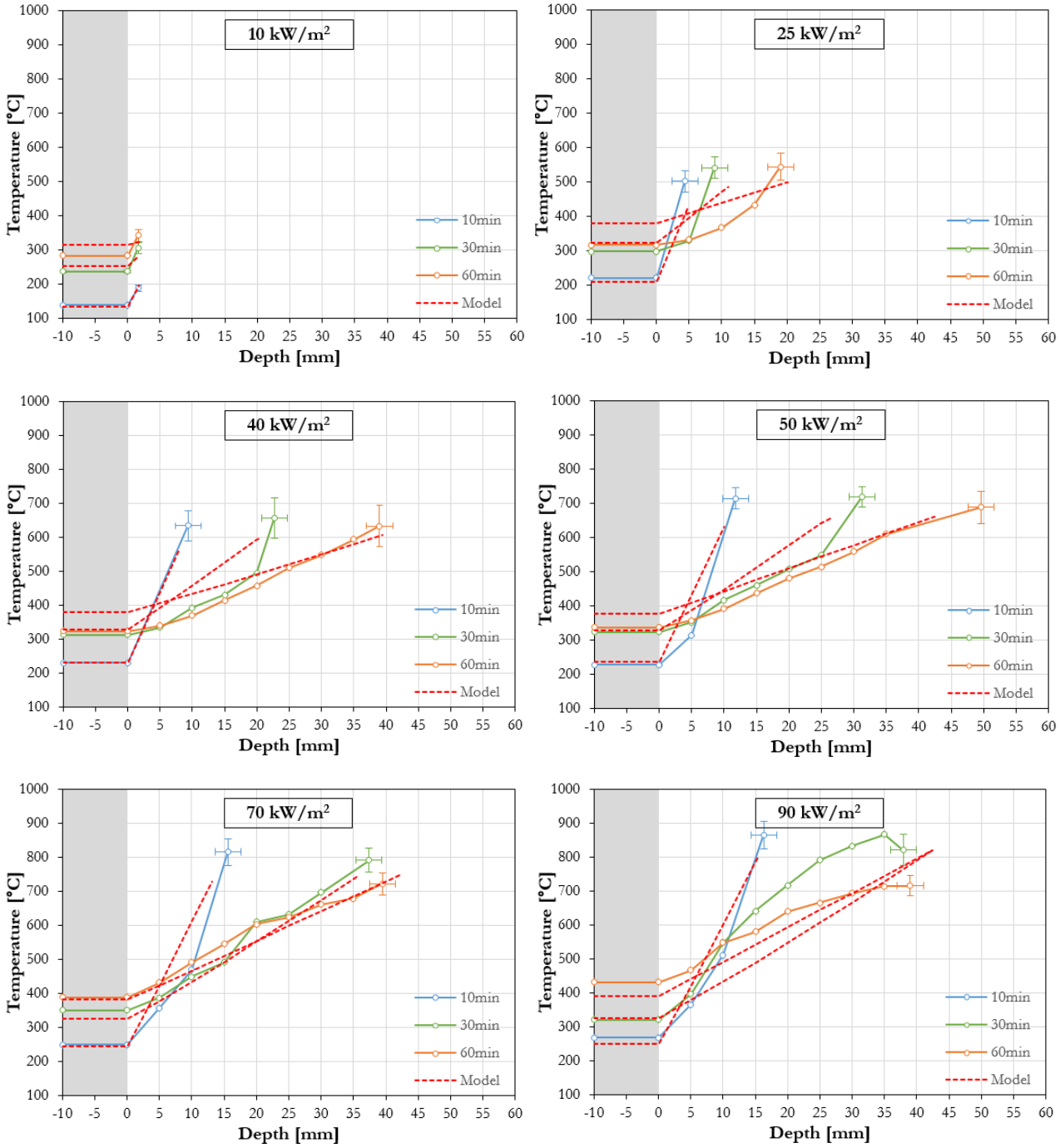

Figure 8.13: Comparison between the experimentally-measured in-depth temperature profiles (steel and coating) and the ones predicted using the described heat transfer model at different instants during the heating exposure (*"Medium DFT"*).

a curved in-depth thermal profile due to transient phenomena (e.g. heat capacitance vs. thermal conduction) occurring within the insulation material. Successively, the in-depth temperature profile gradually tends to equilibrium, characterised by a linear gradient according

to the thermo-physical properties and the thermal boundary conditions of the insulation material. However, based on the assumptions and the definition of the heat transfer problem, this case is essentially different. As highlighted in the definition of the coating properties, within the current study the modelling of swelling intumescent coatings becomes a physical problem, mainly driven by the definition of the swelled coating thickness. The heat transfer problem is actually *quasi steady-state* due to the highly-insulating material properties, the applied constant incident heat flux and the relatively-high swelling rate, compared to the penetration speed of the heat wave within the intumescent coating. Following these assumptions, the duration of the transient phase is minimal and a quasi steady-state linear thermal gradient within the intumescent coating is obtained based on its swelled thickness.

The plots in Figure 8.13 underline this discrepancy between the experimentally-measured and predicted in-depth temperature profiles. The difference is foreseeably more significant in the first part of the thermal exposure (e.g. 10 min) and for lower constant incident heat fluxes (e.g. 25 kW/m^2): the cases in which transient phenomena are more relevant. Despite the shape, the thermal gradient within the intumescent coating is generally captured: this is the direct consequence of a good prediction of the temperature evolutions at the coating surface and steel substrate.

In addition, it is important to stress the fact the in-depth temperatures obtained using K-type thermocouples are subjected to significant errors because of the measurement characteristics. Several researchers have highlighted how the in-depth measurements within a low-conductivity material may be significantly affected by the measuring methodology. In particular, the relatively-big size of the used K-type thermocouples (1.5 mm diameter), the positioning of the in-depth thermocouples in parallel to the main direction of the heat transfer (from the rear of test samples) and the possible creation of an air-gap around the thermocouple head may have introduced considerable errors to the in-depth temperature measurements [9-11]. The magnitude of the error is difficult to quantify, but it is important to acknowledge it for different applications or future studies.

Another important point regarding the evolution of the in-depth temperature profiles is the presence of *in-depth oxidation* within the swelling intumescent coating. This aspect can be noticed in the experimentally-measured thermal profile for 90 kW/m^2, especially for the 30 minutes instant (Figure 8.13), and the evolution of the in-depth temperatures for high heat

fluxes (reported in Appendix A). As already discussed, the adopted heat transfer model disregards this phenomenon due to its high complexity and this topic is outside the scope of this research study.

8.4.3 Sensitivity and uncertainty analysis

After checking the modelling results with respect to the surface and steel temperatures and the in-depth thermal profiles, the accuracy of the numerical model was verified through a sensitivity analysis with respect to some key governing factors embedded in the model assumptions and simplifications. As discussed in Section 8.3.2 and shown in Figure 8.6, the density, the specific heat capacity and the absorptivity/emissivity of the intumescent coating have a minor influence on the accuracy of the heat transfer model, while the thermal conductivity plays a key role in the problem. The model discrepancy and convergence in regards to the thermal conductivity have been already confronted in Section 8.3.2. The sensitivity analysis presented herein investigates the influence of the accurate definition of certain key parameters on the modelling results. In particular, this analysis focuses on the implications of the accuracy of the constant incident heat flux, the initial applied dry film thickness and the adopted empirical correlation for the calculation of the swelling rate of the intumescent coating. The heating conditions of a constant incident heat flux of 50 kW/m^2 and an applied initial thickness *"Medium DFT"* were chosen as exemplar case.

The first sensitivity parameter is the incident heat flux. The section describing the experimental setup based on the radiant exposure of the H-TRIS test method reports that the distribution of the incident heat flux on the sample surface had an accuracy and of $\pm$ 10%: in the case of 50 kW/m^2, an accuracy of $\pm$ 5 kW/m^2. Within the heat transfer model, the incident heat flux has a key role in the definition of the heating conditions and the prediction of the swelling rate of the intumescent coating during the thermal exposure. Figure 8.14 shows how the evolution of the swelled coating thickness slightly changes, but the resulting steel temperatures are practically identical. As a conclusion, the numerical model appears to be robust with respect to the incident heat flux.

The second sensitivity parameters is the applied initial Dry Film Thickness (DFT). In the H-TRIS experiments, the coated steel plated were categorised into three DFT groups (*"Low DFT"*, *"Medium DFT"* and *"High DFT"*) with an accuracy of $\pm$ 0.20 mm. In the case of

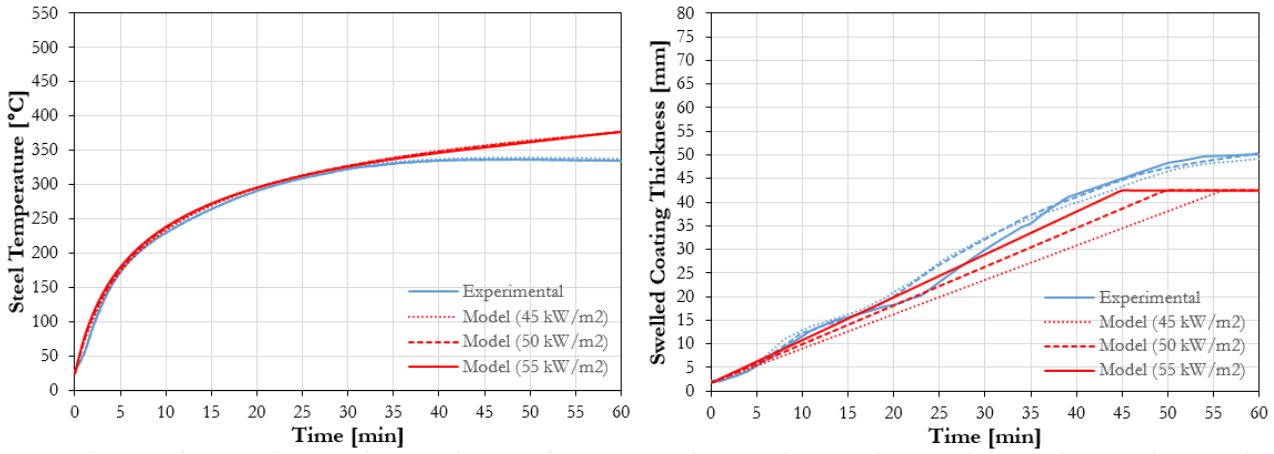

Figure 8.14: Sensitivity analysis with respect to the incident heat flux (50 kW/m^2, *"Medium DFT"*).

"Medium DFT" (1.80 mm), the average DFT of the test samples was included in the range between 1.60 mm and 2.00 mm. Within the heat transfer model, the initial thickness has a key role in the determination of the maximum swelled thickness that the intumescent coating can achieve during the thermal exposure. Figure 8.15 shows how the maximum swelled coating thickness sightly changes, but the resulting steel temperatures are very similar. As a conclusion, the numerical model appears to be robust with respect to the applied initial DFT.

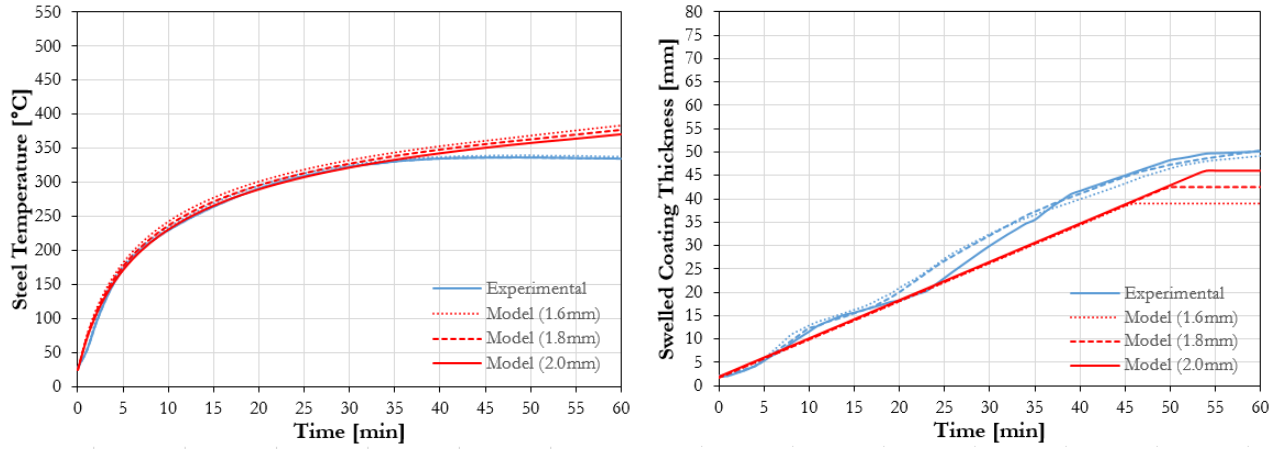

Figure 8.15: Sensitivity analysis with respect to the applied initial DFT (50 kW/m^2, *"Medium DFT"*).

The third and final sensitivity parameters is the swelling rate of the intumescent coating and, in particular, the empirical correlation defined based on Figure 8.4 and Equation 8.4 which evaluates the coating swelling rate based on the external incident heat flux. However, within the same heating conditions, the experimental values were included between an upper and lower bound. In the case of 50 kW/m^2, Equation 8.4 estimates a coating swelling rate

equal to 0.82 mm/min. However, throughout all the experimental repetitions, this value was included between 0.78 mm/min (lower bound) and 0.96 mm/min (upper bound). Figure 8.16 shows how the modelling results are influenced by the definition of the coating swelling rate. The evolution of the swelled coating thickness slightly changes, but the resulting steel temperatures are affected as well. As a conclusion, the sensitivity analysis underlined how the heat transfer model is particularly sensitive to the coating swelling rate and it requires a careful definition of it.

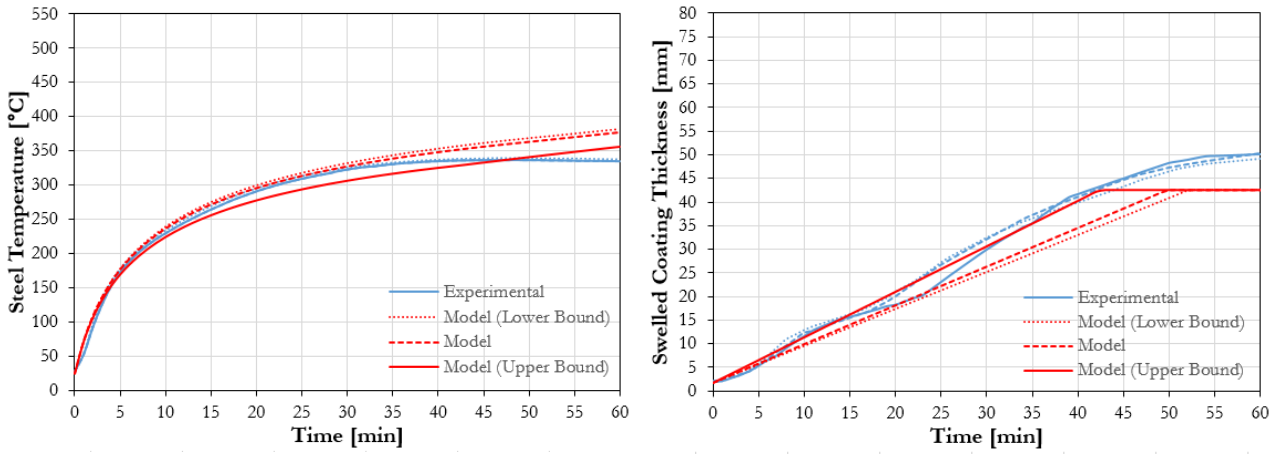

Figure 8.16: Sensitivity analysis with respect to the swelling rate (50 kW/m^2, *"Medium DFT"*).

In order to obtain a better understanding of the influence of these parameters on the heat transfer problem, the sensitivity analysis with respect to the incident heat flux, the applied initial DFT and the swelling rate of the intumescent coating was extended for all the different experimental heating conditions. Figure 8.17 offers an overview on how the model convergence is affected by the three parameters. The plots confirm that the accuracy of the constant incident heat flux ($\pm$ 10%) and the the applied initial DFT ($\pm$ 0.20 mm) has a minor effect. On the contrary, Figure 8.17 underlines how the heat transfer model is especially sensitive to the coating swelling rate: the discrepancy increases for higher incident heat fluxes, where a bigger scattering of the experimental swelling rates was registered (refer to Figure 8.4). As a conclusion, the sensitivity analysis stresses the importance of carefully predicting the swelling rate and swelled coating thickness, which are the main governing factors of the effectiveness of thin intumescent coatings.

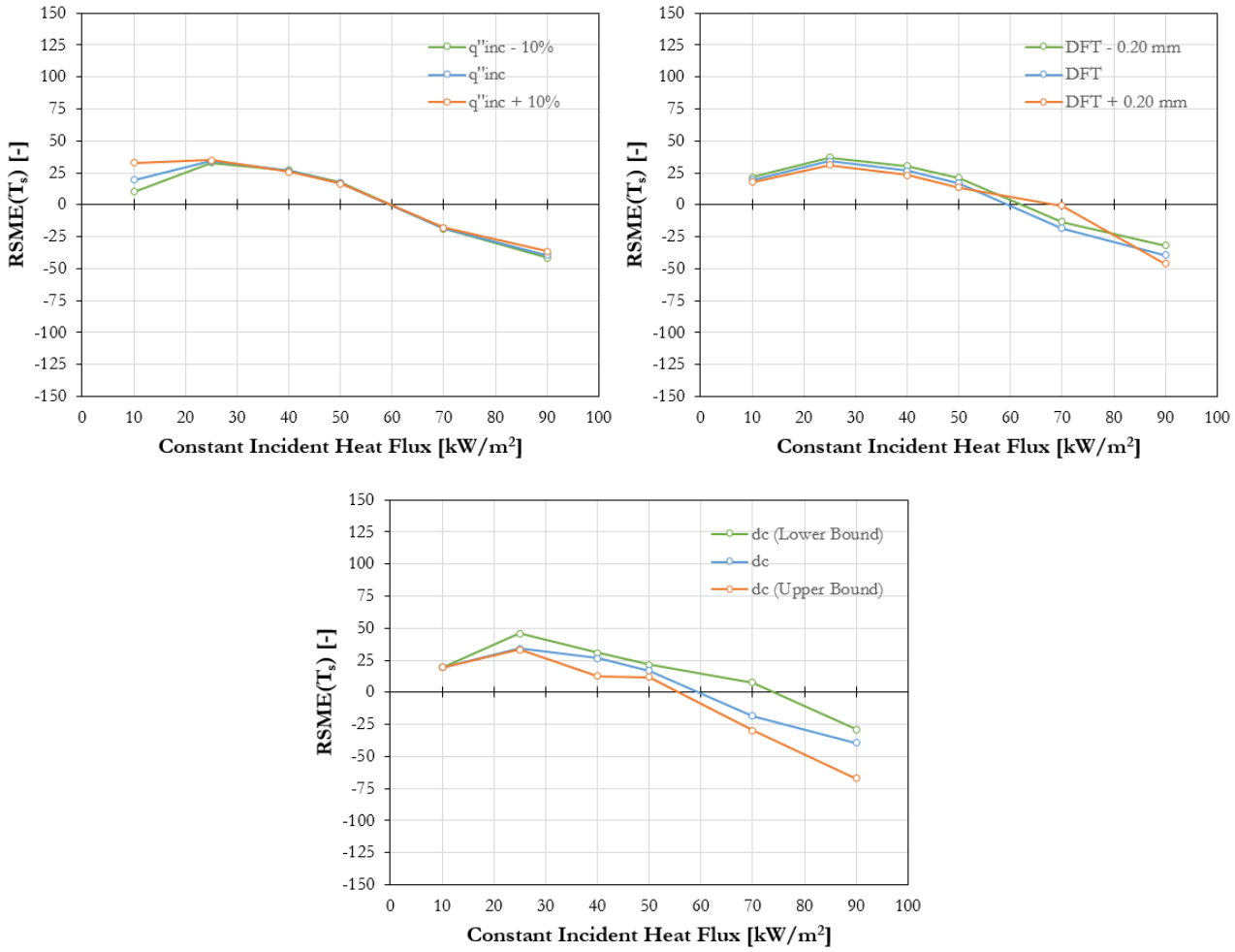

Figure 8.17: Sensitivity analysis with respect to the incident heat flux, the applied initial DFT and the swelling rate of the intumescent coating for different constant incident heat fluxes (*"Medium DFT"*).

8.5 External validation of the heat transfer model for different time-histories of incident heat flux

The proposed heat transfer model has been formulated based on experiments involving coated steel plates exposed to different levels of constant incident radiant heat fluxes using the Heat-Transfer Rate Inducing System (H-TRIS) test method. Subsequently, a new set of experiments based on different time-histories of incident heat flux was carried out in order to extend the knowledge related to the performance of intumescent coatings under non-standard heating conditions and validate the applicability of the proposed model.

8.5.1 Experimental methodology, test samples and description of the experiments

Similarly to the previous experimental campaign described in Section 6.2, steel plates were prepared and coated with the same commercially available solvent-based thin intumescent coating following the procedure explained in Chapter 3. The test samples were selected to have a mean applied DFT in the range 1.80 $\pm$ 0.20 mm and be part of the *"Medium DFT"* group. In accordance with the Heat-Transfer Rate Inducing System (H-TRIS) test method, individual coated test samples were exposed to different time-histories of incident radiant heat flux for 60 minutes as shown in Figure 8.18. The heating conditions were characterised by different linear-increasing time-histories of incident heat flux. Particularly, in the first 30 minutes, the rate of heat flux rise was 3.000, 0.917, 1.833 and 0.667 kW/m^{2}min for *"Linear 1"*, *"Linear 2"*, *"Linear 3"* and *"Linear 4"*, respectively. The heating conditions were chosen in order to expose the intumescent coating to various ranges of temperature and heating rate, essentially different from the ones imposed by the constant incident heat fluxes. The same sample holder and instrumentations as in the experiments described in Section 6.2 were used.

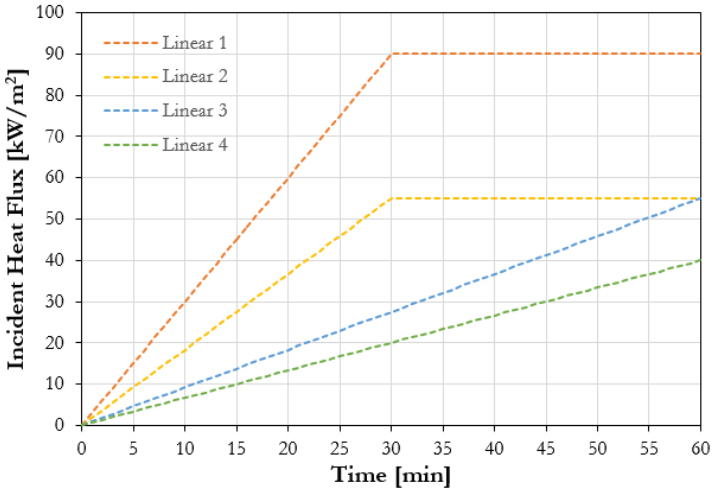

Figure 8.18: Time-histories of linear-increasing incident heat flux.

8.5.2 Experimental results

As analogously presented in Section 6.3, the evolutions of the average steel temperatures and the swelled coating thickness during the thermal exposure for different heating conditions are shown in Figure 8.19: as in previous chapters, the same colour collects all the experiments with the same heating conditions, while continuous and dashed lines report single experimental repetitions.

The H-TRIS test method and the designed experimental setup offered great repeatability between experiments and, in general, similar conclusions to the one discussed in Chapter 6 can be drawn. For instance, the experiments confirmed that during continuous swelling the steel plates tended to the similar temperature range included between 300 and 350 °C. Only in the case of *"Linear 1"*, the intumescent coating completed the swelling process after about 45 minutes of thermal exposure and then the steel temperature increased above 350 °C. The experiments confirmed that different heating conditions cause different swelling rates and swelled coating thicknesses. In particular, thicker coating thicknesses were registered for higher heat fluxes and generally for a higher amount of thermal energy provided to the reactive coating: pictures of typical porous chars developed by the intumescent coating at the end of the heating exposure can be found in Appendix B. In some experiments, due to the low heat fluxes in the first part of the thermal exposure, the onset of swelling was significantly delayed and only happened for incident heat fluxes about or above 20 kW/m^2.

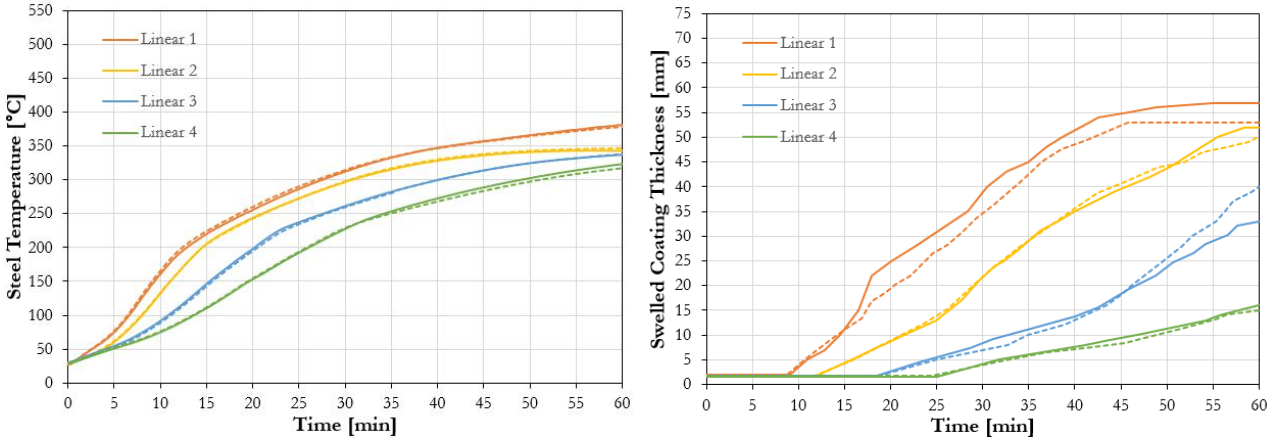

Figure 8.19: Comparison of the evolution of the coated steel temperatures and the swelled coating thickness for different linear-increasing incident heat fluxes (experimental, *"Medium DFT"*).

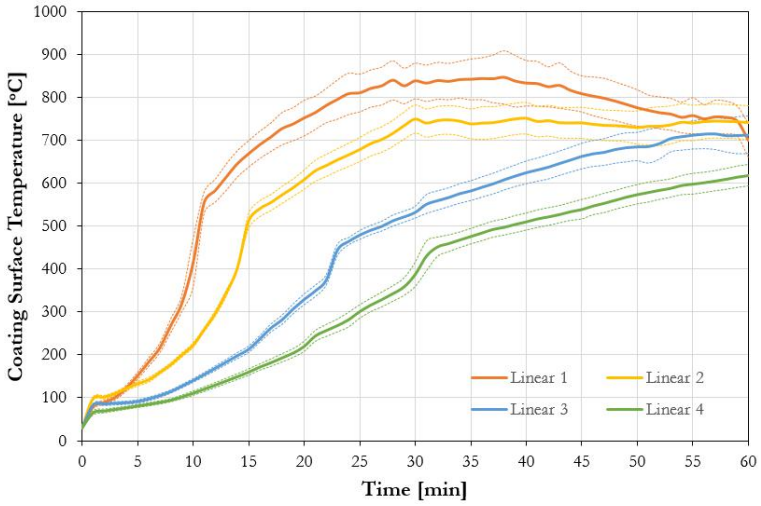

Figure 8.20: Envelopes of the temperature evolution at the coating surface for different linear-increasing incident heat fluxes (experimental, *"Medium DFT"*).

The evolution of the surface coating temperature was analysed in an equivalent way to the one presented in Section 6.3.2. Figure 8.20 reports the envelopes of the measured temperatures for all the experiments carries out under linear-increasing time-histories of incident heat flux: all the different temperature curves are available in Appendix A. Since the thermal surface conditions were mostly changing during the heating exposure, the coating surface reached quasi-constant temperatures only in a few cases (*"Linear 1"* and *"Linear 2"*) and each heating condition produced unique temperature curves. Similar outcomes to ones presented in Section 6.3.2 can be also inferred, as well as similar conclusions to Section 6.3.3 can be drawn in regards the evolution of the in-depth temperature profiles: all the different temperatures curves are available in Appendix A.

8.5.3 Modelling results and validation

Similarly to Section 8.4.1, the numerical model was implemented in order to solve the heat transfer problem for the experimental cases involving linear-increasing time-histories of incident heat flux, adopting the same assumptions and material properties. Figure 8.21 shows the modelling results for the four different heating conditions. In particular, the reported plots compare the evolution of the experimentally-measured coating surface and steel temperatures to the ones predicted using the described heat transfer model. Besides, the evolution of the swelled coating thickness is also compared: experimentally-measured against the

modelling curves obtained using the empirical correlations described in Section 8.3.2.

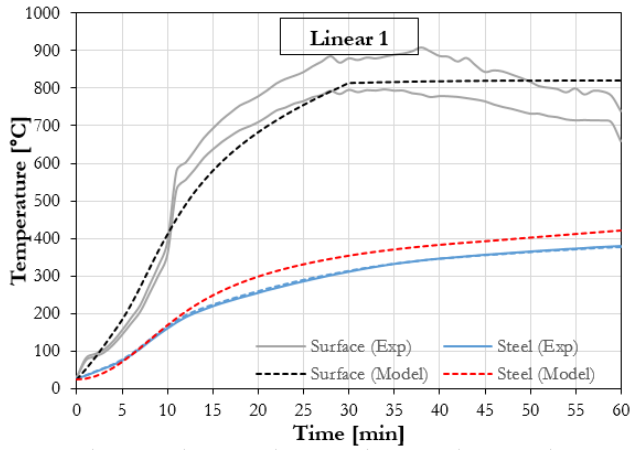

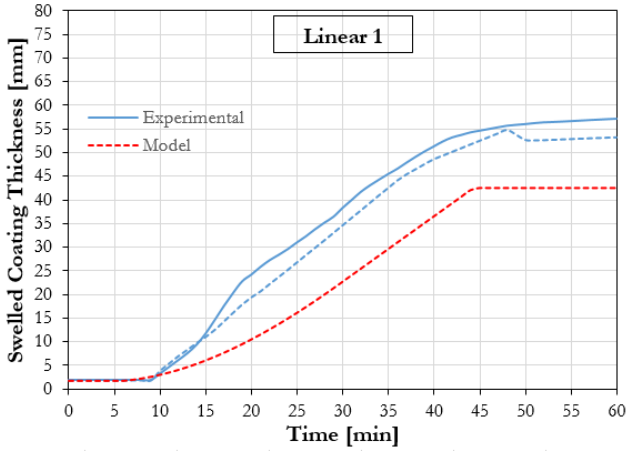

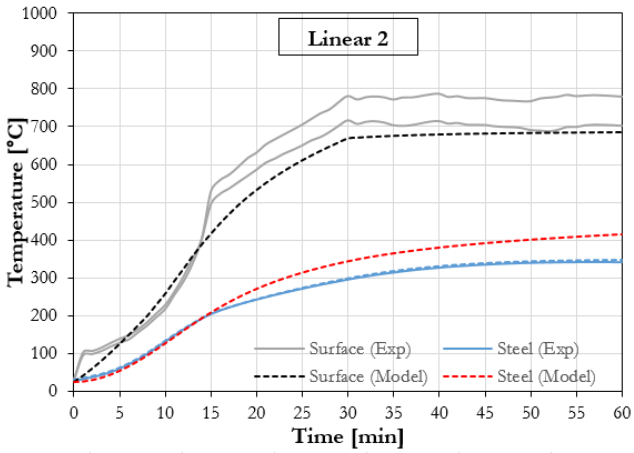

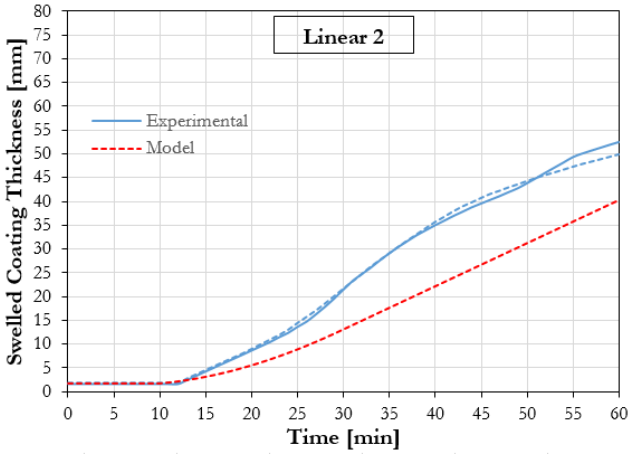

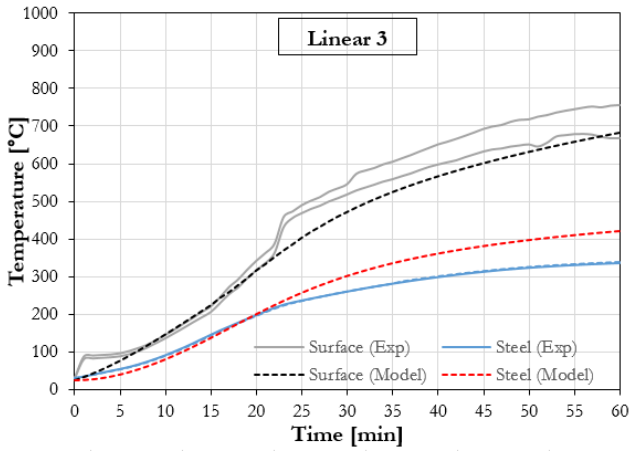

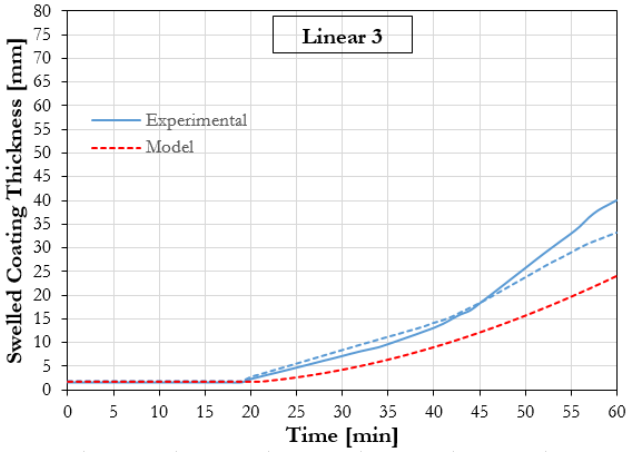

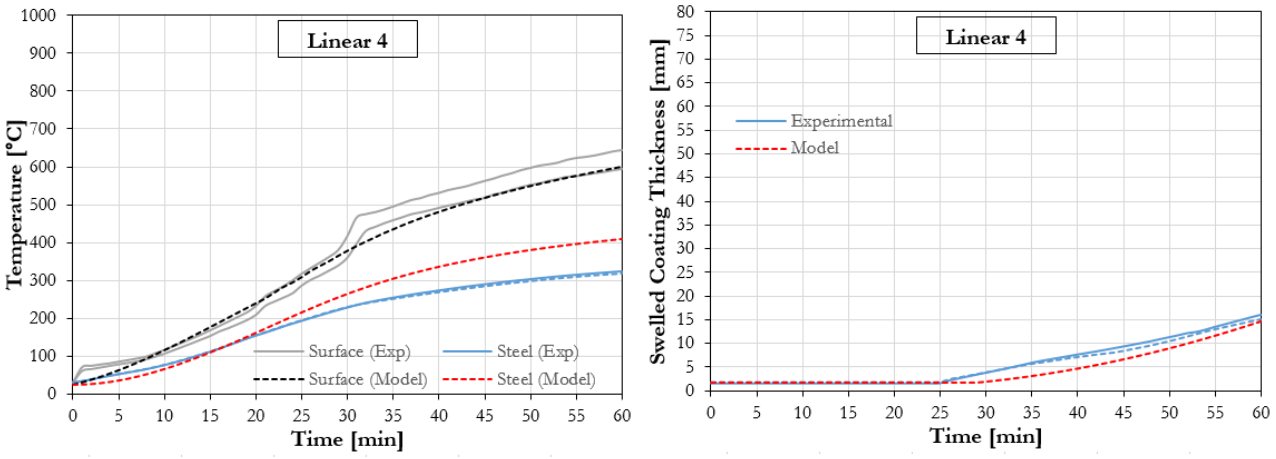

Figure 8.21: Comparison between the experimental and predicted coating surface and steel temperatures and swelled coating thicknesses for different linear-increasing incident heat fluxes (*"Medium DFT"*).

The presented modelling results highlight that, under heating conditions different to a constant incident heat flux, the numerical model is able to predict the thermal and physical behaviour of the intumescent coating in broad terms because only the general trends of the steel and coating surface temperatures are captured. Similar to the previous cases, the surface temperature at the coating surface is generally under-predicted due to analogous reasons explained in Section 8.4.1. However, the steel temperatures are always over-predicted, most likely due to the under-prediction of the swelled coating thickness. This is a direct consequence of the transient nature of the heating conditions based on linear-increasing incident heat fluxes. As previously discussed, the heat transfer model was conceived and validated based on constant incident heat fluxes. Consequently, the numerical model is more accurate for steady-state or quasi steady-state conditions. These are the cases in which the Biot number of the intumescent coating is high ($Bi \gg 10$): the swelled coating is thermally thick and it has reached its maximum temperature in equilibrium with the external sources of heat. This behaviour is more evident for high constant heat fluxes (shorter transient phase). On the other hand, the numerical model has limitations for thermal conditions involving transient phenomena. These are the cases in which the Biot number of the intumescent coating is low ($Bi \ll 1$): the swelled coating is thin (no relevant swelling) and this behaviour is more relevant for low constant heat fluxes (longer transient phase) or time-varying heat fluxes [12-13]. Consequently, due to transiently-varying nature of linear-increasing heat flux exposures, the model is not able to capture the behaviour of the intumescent coating, in particular

the coating swelling based on the proposed empirical correlations. This issue introduces a "delay" in the evolution of the swelled coating thickness: this can be noticed in Figure 8.21 where the experimental and predicted slopes of the swelled coating thickness curves are significantly different. However, in the periods of constant incident heat flux (second 30 minutes in the *"Linear 1"* and *"Linear 2"* exposures), the swelling rate is well predicted, but the model suffers the error introduced during the transient phase. These outcomes underline the model limitations and point out the aspects in which the model requires improvements.

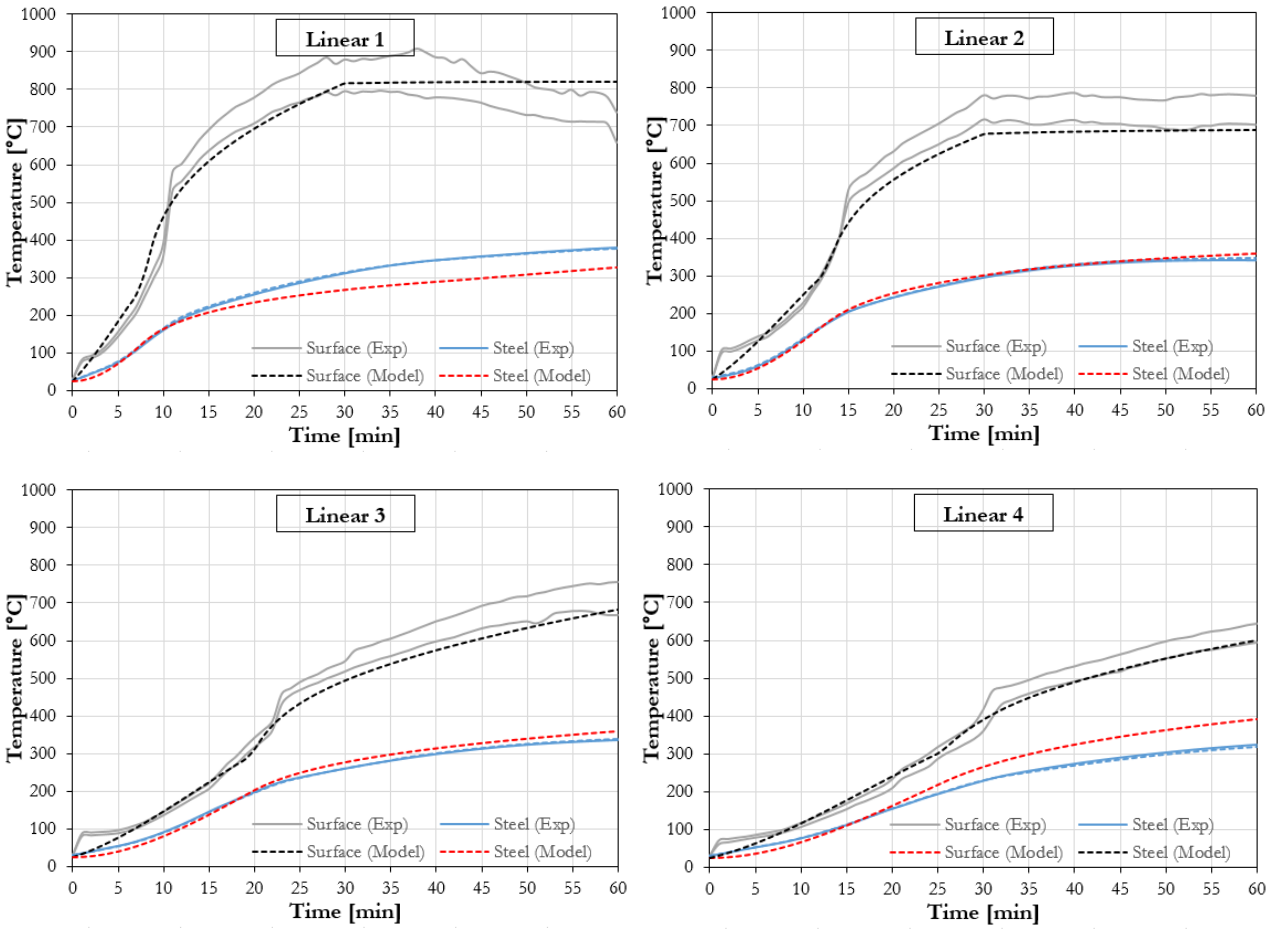

Figure 8.22: Comparison between the experimentally-measured coating surface and steel temperatures and the ones predicted using the described heat transfer model with experimental swelled coating thicknesses for different linear-increasing incident heat fluxes (*"Medium DFT"*).

Since the heat transfer problem is mainly governed by the swelling of the intumescent coating, the first way to improve the numerical model is by increasing the prediction accuracy of the swelled coating thickness. For example, Figure 8.22 reports the modelling results obtained using the experimentally-measured swelled coating thicknesses instead of using the

empirical correlations. The resulting coating surface temperatures are unchanged, but the evolution of the steel temperatures underwent a significant improvement. In particular, similar conclusions to the one presented in Section 8.4.1 can be drawn: adopting the defined thermal conductivity, the steel temperatures are under-predicted for high heat fluxes and over-predicted for low heat fluxes. Also in this case, the optimisation of the thermal conductivity value can be carried out in order to improve the results based on the analysis goals. Nevertheless, within the proposed heat transfer model, these outcomes confirm again the key importance of predicting the swelling process of the intumescent coating and the resulting swelled coating thickness.

8.6 Analysis and discussion

Applications and benefits of the model

In a world moving towards performance-based engineering solutions, the current study proposes a comprehensive heat transfer model for simulating the complex behaviour of thin intumescent coatings under a range of different potential conditions, in terms of heating conditions, applied initial thickness and substrate characteristics. In particular, the experimental studies have produced an explicit understanding about how different factors may influence the effectiveness of thin intumescent coatings thought a detailed characterisation of their thermal and physical response. The numerical model represents an engineering tool able to predict the temperature evolution within swelling intumescent coatings and it can be employed in order to investigate the temperature evolution within protected structural elements and the effects of material degradation, thermally-induced forces and displacements in complex structural systems. In addition, the research project has highlighted which aspects have a key role in the effectiveness of thin intumescent coatings and shall be considered for a rigorous and systematic design process. The heat transfer model, based on energy-balance equations and fundamental physical principles, can be potentially extended to many applications and adapted to be implemented in the main commercial finite-difference software (e.g. ABAQUS and SAFIR16). For examples, the material properties of the intumescent coating can be defined as in Section 8.3.2 and the coating swelling can be simulated using a coefficient of thermal expansion dependent on the heating conditions (e.g. incident-heat-flux

dependent).

Model shortcomings

The proposed heat transfer model carries a series of assumptions, simplifications and limitations based on the performed experimental studies and the model formulation. For instance, the numerical model was validated for a range of constant incident heat fluxes (10-90 kW/m^2) and applied initial DFTs (0.90 - 3.10 mm) and it would be interesting to investigate if the outcomes presented in this research can be extended to wider ranges. Moreover, the heat transfer model was formulated in accordance with the adopted experimental methodology, the Heat-Transfer Rate Inducing System (H-TRIS) test method. This allowed for accurate and direct control of the thermal boundary conditions imposed on test samples with high repeatability and low costs, but enforced one-dimensional heat transfer in a oxygen-rich environment, introducing additional simplifications and opening further research questions. For instance, additional experimental studies could have clarified the influence of oxygen and coating oxidation on the behaviour of thin intumescent coatings. In addition, the presented experimental investigations focused on one-dimensional heat transfer for coated samples and the research outcomes should be extended to real-scale coated structural elements, such as protected steel sections, in order to include large-scale effects (e.g. crack formation).

The tested thin intumescent coating as exemplar

Considering the wide variety of products available in the market, the experimental and modelling outcomes presented herein may change for different intumescent coatings. Within this research study, a solvent-based thin intumescent coating was chosen as product exemplar. Unfortunately, the commercial name and the specific components of the tested intumescent coating cannot be disclosed due to proprietary reasons, but it is important to underline the fundamental nature of this research. This research provides an essential assessment procedure applicable to any coating and the results are therefore useful examples of the key information that can be extracted. In that sense, this research study should remain product-independent and the specific coating just an example of application.
Nevertheless, Chapter 4 has presented the material characterisation of the tested intumes-

cent coating through various experimental methodologies, especially Thermo-Gravimetric Analysis (TGA) and Differential Scanning Calorimetry (DSC). These results uniquely identify the characteristics of the intumescent formulation by defining the chemical reactions and thermal decomposition processes that the material experiences at different temperatures and under different heating regimes. The results obtained by the material characterisation constitute a unique fingerprint against which other products can be compared. For example, the available literature offers a vast amount of TGA data to compare different intumescent products [14-33]. In particular, according to the extended literature review and the material characterisation, the behaviour of the tested intumescent coating was defined as "typical" because its composition was found alike the most common intumescent formulation based on the combination of ammonium polyphosphate (APP) as carbonisation catalyst, pentaerythritol (PER) as carbonisation agent, melamine (MEL) as blowing agent and acrylic resin as carbonic agent and binder. For example, in these formulations the intumescent swelling reaction typically occurs at temperatures between 300 and 400℃ and the main reactions can be considered completed above 400-450℃.

No doubt, extensive experimental and modelling campaigns should be performed on different commercially available products and formulations in order to comprehend if the presented research outcomes can be generalised. This understanding will increase the knowledge of the behaviour and effectiveness of intumescent coatings and enable the definition of systematic testing methodologies and performance-based engineering solutions for the fire-safe design of structures protected with intumescent coatings.

Future model improvements

The heat transfer model can be certainly improved under different aspects. As shown in Section 8.5, the heat transfer model requires improvements for the prediction of transient phases and phenomena. Furthermore, the empirical correlations proposed for the evaluation of the coating swelling rate and the resulting swelled coating thickness were based on heating conditions of constant incident heat fluxes: quasi-constant swelling rates were registered, most likely as a result of quasi-constant net heat fluxed provided to the swelling reaction. Accordingly, it should be possible to correlate the swelling process of thin intumescent coatings (e.g. swelling rate $\dot{d}_c$) to more fundamental parameters. An example is

the net heat flux received by the virgin coating ($\dot{q}''_{net}$), which is located in the proximity to the substrate-coating interface and sustains the swelling reaction. As shown in Figure 8.23, the virgin coating can act as control volume and a detailed heat transfer model may be able to evaluate the heat flux that penetrates the swelled porous char and reaches the swelling material, and the heat flux that dissipates at the substrate based on its thermal conditions. This concept can be expressed as:

$$\dot{d}_c = f\left(\dot{m}''\right) \qquad \Rightarrow \qquad \dot{m}'' = C\frac{\dot{q}''_{net}}{\Delta H_r} = C\frac{\dot{q}''_{in} - \dot{q}''_{back}}{\Delta H_r} \tag{8.13}$$

where $\dot{d}_c$ is the coating swelling rate [mm/min], $\dot{m}''$ is the mass reaction rate [kg/sm^2], C is a constant [-], $\dot{q}''_{net}$ is the net heat flux into the swelling reaction [kW/m^2], ΔH_r is the heat of reaction [J/kg], $\dot{q}''_{in}$ is the total heat flux into the swelling reaction [kW/m^2] and $\dot{q}''_{back}$ is the total heat flux leaving the swelling reaction [kW/m^2]. However, due to the complex nature of the behaviour of intumescent coatings, the presented heat transfer model was formulated with several assumptions and simplifications: it effectively predicts the coating and substrate temperatures, but it is not able to accurately describe the thermal and physical phenomena in detail and estimate $\dot{q}''_{net}$.

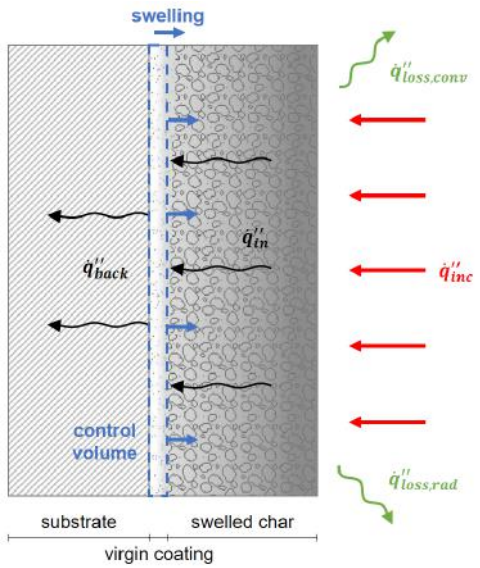

Figure 8.23: Schematisation of the swelling mechanism of thin intumescent coatings based on the concept of net heat flux received by the virgin coating.

The literature review also underlined that the substrate thermal conditions play a key role in the performance of thin intumescent coatings. In the case of steel structures, this aspect is

usually associated with the steel section factor A_p/V and it quantifies how rapidly the steel substrate increases its temperature, based on the evaluation of received heat (i.e. exposed surface area) and the steel thermal mass (i.e. volume). In this case, it is assumed that the steel element has no heat losses and all the heat is associated with the temperature rise of the steel thermal mass. A similar concept can be applied to other substrate materials, such as timber, by evaluating the heat received by the substrate ($\dot{q}''_{in}$) and the substrate thermal losses ($\dot{q}''_{back}$). This topic was investigated in Chapter 7 and extensively explained in Section 7.6. The experimental outcomes evidenced how the substrate thermal conditions govern the swelling of thin intumescent coatings, thus their effectiveness in protecting load-bearing structural elements. However, due to the high complexity, this aspect was not included in the heat transfer model, but it is discussed herein according to Figure 8.24 and Figure 8.25.

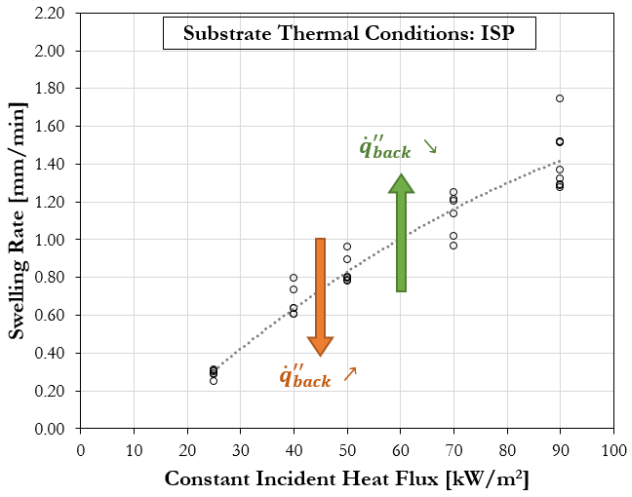

Figure 8.24: Influence of the constant incident heat flux on the swelling rate of the intumescent coating, under the same substrate thermal conditions (ISP: insulated steel plate).

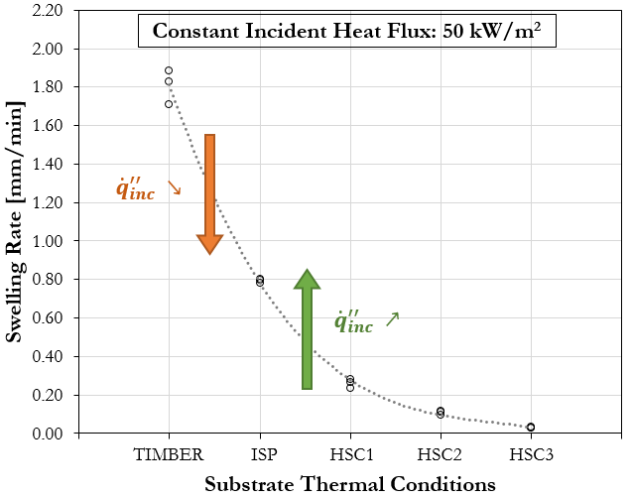

Figure 8.25: Influence of the substrate thermal conditions on the swelling rate of the intumescent coating, under the same constant incident heat flux (50 kW/m^2).

The two plots, obtained elaborating Figure 6.10 and Figure 7.13 respectively, highlight how the swelling rate of the intumescent coating is affected by the incident heat flux at the exposed surface of test samples ($\dot{q}''_{inc}$) and the substrate thermal conditions at the unexposed surface ($\dot{q}''_{back}$). The incident heat flux at the exposed surface controls the amount of heat that penetrates through the intumescent porous char and reaches the reacting virgin coating. On the other hand, the substrate thermal conditions control the capacity of the substrate to concentrate or dissipate heat in the proximity of the reacting virgin coating. Consequently,

these two parameters control the temperature evolution of the reacting virgin coating and they govern the swelling process of the intumescent coating. Unfortunately, within the scope of this research project, the extreme complexity of the heat transfer problem does not allow for the quantification of the net heat flux received by the reacting virgin coating ($\dot{q}''_{net}$) and this topic is analysed only in a qualitative manner. The problem is characterised by many uncertainties and unknown variables that complicate the problem and prevent any experimental validation. However, the current research have emphasised the importance of considering both the thermal boundary conditions at the exposed surface and at the protected substrate for a robust performance-based design of thin intumescent coatings.

Design principles for thin intumescent coatings

This study aims at contributing to build the principles for developing engineering methods for the performance-based design of structural elements protected with thin intumescent coatings, taking into account their effectiveness for a wide range of potential conditions (e.g. fire scenarios, applied initial DFT...). In particular, the current research have shown how the effectiveness of thin intumescent coatings is mainly governed by the coating swelling process and the resulting swelled coating thickness. This concept should be always taken into account for the definition of any design practice and the proposition of any testing environment. Any approach and methodology aimed at assessing the performance of thin intumescent coatings should focus on the evolution of the swelled coating thickness as explicit quantification of their effectiveness. In particular, a rigorous and systematic testing and design methodology should consider the conditions that promote the swelling of intumescenti coating and the conditions in which the reactive coating is ineffective. Theoretical or empirical correlations may be formulated in order to simulate the swelling process. In addition, based on the research outcomes of this study, the same methodologies should concentrate in carefully measuring the temperature evolution of the substrate material and defining/controlling the thermal conditions at the coating boundaries: for example, the surface conditions in terms of an incident heat flux and the substrate conditions in terms of thermal mass, heat losses or the thermo-physical properties of the coated substrate. Due to the extreme difficulty and the limited influence of the thermal and physical properties of the intumescent porous char, minor effort should be made to measure the in-depth temperature

profiles within swelling intumescent coatings. The research study has demonstrated how the thermal gradient is mainly controlled by the thermal conditions at the coating boundaries and the swelled coating thickness.

Within this research study, the experimental setup based on the Heat-Transfer Rate Inducing System (H-TRIS) test method offered considerable advantages to investigate the effectiveness of thin intumescent coatings. The H-TRIS open environment allowed for the real-time measurement of the swelled coating thickness and this enabled the continuous and direct control of the thermal boundary conditions at the exposed surface of the intumescent coating during the whole thermal experiment. In addition, the experimental results obtained by adopting the H-TRIS test method reported high reliability and repeatability between experiments at low economic and temporal costs compared to conventional furnace fire testing.

After carefully understanding the swelling process under different thermal (e.g. heating or substrate) and physical (e.g. initial thickness) conditions, more research should focus on other aspects that govern the performance of thin intumescent coatings. For example, experimental studies may investigate the stickability of the intumescent coating to the protected substrate, the mechanical strength of the intumescent porous char, the degradation and cracking of the intumescent porous char at elevated temperatures, or the performance of thin intumescent coatings exposed to degrading agents such as weathering and temperature fluctuations.

8.7 Conclusions

The heat transfer model presented herein aims at simulating the thermal and physical behaviour of thin intumescent coatings under thermal exposure for a wide range of potential conditions, in terms of heating exposure and applied initial coating thickness. The model solves the one-dimensional heat conduction problem by resolving energy-balanced equations using the finite-difference Crank-Nicolson method. The heat transfer model was formulated according to the experimental outcomes obtained by testing steel plates coated with a commercially available solvent-based thin intumescent coatings using the Heat-Transfer Inducing System (H-TRIS) test method. Accordingly, the swelling of the intumescent coating was implemented by adding finite elements in the proximity of the substrate-coating

interface, where the swelling process takes place and insulates the protected substrate by displacing the already-swelled coating char towards the direction of the heat source. The intumescent coating was modelled as swelled porous char with constant material properties obtained from complementary studies using standard experimental methodologies (TPS, LFA and ISS). Empirical correlations based on the influence of the heating conditions and the applied initial coating thickness were introduced to predict the evolution of the swelled coating thickness during the thermal exposure. Based on equivalent assumptions and simplifications, a similar heat transfer model was formulated in order to simulate the temperature increase of uncoated and coated samples prior to onset of swelling: for instance, the test samples subjected to constant incident heat fluxes less severe than the critical one for onset of swelling (10 kW/m^2).

From the results obtained from the heat transfer model, the following concluding remarks can be drawn:

- The insulating performance and effectiveness of thin intumescent coatings are mainly governed by the swelling process and ability of developing swelled porous char. Sensitivity analyses underlined how the heat transfer becomes a physical problem: the model accuracy is primarily dependent on the correct prediction of the coating swelling rate and the evolution of the swelled coating thickness during the thermal exposure. On the contrary, the thermal and physical properties of the swelled coating char affect the heat transfer model in a limited manner.

- The heat transfer model is capable of characterising the heat transfer through swelling intumescent coatings, especially by predicting the evolution of coating surface and steel temperatures. The prediction accuracy varied for different cases and the thermal conductivity of the intumescent coating was turned into an effective parameter in order to adjust the error between the model and the experiments. When the discrepancy is minimised, the surface temperatures are under-estimated, while the steel temperatures are over-estimated for low heat fluxes and under-estimated for high heat fluxes.

- Based on the model assumptions and simplifications, the formulated model defined a quasi steady-state thermal problem: the swelled coating achieves a quasi-steady surface temperature in equilibrium with external heat source due to its high Biot number.

The heating conditions based on constant incident heat fluxes, the material properties of the intumescent coating characterised by low thermal conductivity (high Biot number) and the relatively-high swelling rate compared to the penetration speed of the heat wave within the swelling coating reduced the impact of transient states and transient phenomena. Consequently, the model solves steady-state heat transfer problems and loses accuracy for the cases driven by transient phenomena: phases before onset of swelling (low Biot number), low heat fluxes (longer transient phase) and heating conditions characterise by varying incident heat flux.

- The evolution of the in-depth temperature profiles tends to steady-state conditions and they become linear: this aspect introduces additional error between the predicted and experimental results. However, since the model is able to accurately simulate the surface and steel temperatures, as well as the evolution of the swelled coating thickness, the thermal gradient within the swelling intumescent coating is correctly predicted, despite the profile shape and during transient phases.

After carefully understanding the swelling process under different thermal (e.g. heating or substrate) and physical (e.g. initial thickness) conditions, more research should focus on other aspects that govern the performance of thin intumescent coatings. For example, experimental studies may investigate the stickability of the intumescent coating to the protected substrate, the mechanical strength of the intumescent porous char, the degradation and cracking of the intumescent porous char at elevated temperatures, or the performance of thin intumescent coatings exposed to degrading agents such as weathering and temperature fluctuations.

Bibliography

[1] Comité Europeén de Normalization (CEN). "EN 13381-8:2013 Test methods for determining the contribution to the fire resistance of structural members - Part 8: Applied reactive protection to steel members". Brussels, Belgium, 2013.

[2] Maluk C., Bisby L., Krajcovic M. and Torero J.L. "A Heat-Transfer Inducing System (H-TRIS) Test Method". Fire Safety Journal, vol. 105, pp. 307-319, 2019.

[3] Crank J. and Nicolson P. "A practical method for numerical evaluation of solutions of partial differential equations of the heat-conduction type". Advances in Computational Mathematics, vol. 6, pp. 207-226, 1996.

[4] Hidalgo J.P. "Performance-based methodology for the fire safe design of insulation materials in energy efficient buildings". PhD thesis, School of Engineering, The University of Edinburgh, 2015.

[5] Incropera F.P., DeWitt D.P., Bergman T.L. and Lavine A.S. "Fundamental of heat and mass transfer". John Wiley & Sons, 6th Edition, 2006.

[6] Emmons H.W. "The numerical solution of heat conduction problems". Transactions of American Society of Mechanical Engineers (ASME), vol. 65(6), pp. 607-615, 1943.

[7] Dusinberre G.M. "Heat transfer calculations by finite differences". International Textbook Company, Pennsylvania, USA, 293 pp., 1961.

[8] Comité Europeén de Normalization (CEN). "EN 1993-1-2:2005 Eurocode 3: Design of steel structures - Part 1-2: General rules - Structural fire design". Brussels, Belgium, 2005.

[9] Beck J.V. "Thermocouple temperature disturbances in low conductivity materials". Journal of Heat Transfer, vol. 84, pp. 124-132, 1962.

[10] Pope I., Hidalgo J.P. and Torero J.L. "A correction method for thermal disturbances induced by thermocouples in a low-conductivity charring material". Fire Safety Journal, Article in press.

[11] Fahrni R., Schmid J., Klippel M. and Frangi A. "Investigation of different temperature measurement design and installations in timber members as low conductive material". Proceedings of the 10th International Conference on Structures in Fire (SiF), Ulster University, Belfast, UK, pp. 257–264, 2018.

[12] Drysdale D. "An introduction to fire dynamics". John Wiley & Sons, Ltd, 3rd Edition, 2011.

[13] Torero J.L, Law A. and Maluk C. "Defining the thermal boundary condition for protective structures in fire". Engineering Structures, vol. 149, pp. 104-112, 2017.

[14] Zhang Y., Wang Y., Bailey C.G. and Taylor A.P. "Global modelling of fire protection perform-

ances of an intumescent coating under different furnace fire conditions". Journal of Fire Science, vol. 31, no.1, pp. 51-72, 2012.

[15] Griffin G.J. "The modelling of heat transfer across intumescent polymer coatings". Journal of Fire Science, vol. 28, pp. 249-277, 2010.

[16] Griffin G.J., Bicknell A.D. and Brown T.J. "Studies on the effect of atmospheric oxygen content on the thermal resistance of intumescent fire-retardant coatings". Journal of Fire Science, vol. 23, no. 4, 2005.

[17] Wang Z., Han E. and Ke W. "Effects of nanoparticles on the improvement in fire-resistant and anti-ageing properties of flame-retardant coating". Surface & Coatings Technology, vol. 200, pp. 5706-5716, 2006.

[18] Bourbigot S., Le Bras M., Duquesne S. and Rochery M. "Recent Advances for Intumescent Polymers". Macromolecular Materials and Engineering, vol. 289, pp. 499–511, 2004.

[19] Jimenez M., Duquesne S. and Bourbigot S. "Intumescent fire protective coating: toward a better understanding of their mechanism of action". Thermochimica Acta, vol. 449, no. 1-2, pp. 16-26, 2006.

[20] Alongi J., Han Z. and Bourbigot S."Intumescence: Tradition versus novelty. A comprehensive review". Progress in Polymer Science, vol. 51, pp. 28–73, 2015.

[21] Puri R.G and Khanna A.S. "Influence of heat-stable filler on the thermal shielding performance of water-based intumescent fire-resistive coating for structural steel applications". Journal of Coatings Technology and Research, vol. 14, no. 2, pp. 323–331, 2017.

[22] Pimenta J.T., Goncalves C., Hiliou L., Coelho J.F.J. and Magalhaes F.D. "Effect of binder on performance of intumescent coatings". Journal of Coatings Technology and Research, vol. 13, no. 2, pp. 227-238, 2016.

[23] Morys M., Illerhaus B., Sturm H. and Schartel B. "Size is not all that matters: Residue thickness and protection performance of intumescent coatings made from different binders". Journal of Fire Sciences, vol. 35, no. 4, pp. 1-19, 2017.

[24] Weisheim W., Schaumann P., Sander L. and Zehfuß J. "Numerical model for the fire protection performance and the design of intumescent coatings on structural steel exposed to natural fires". Journal of Structural Fire Engineering, vol. 11, no. 1, pp. 33-50, 2019.

[25] Wang L.L., Wang Y.C. Li C.Q. and Zhang Q.Q. "An experimental study of the effects of topcoat on aging and fire protection properties of intumescent coatings for steel elements". Fire Safety Journal, vol. 111, no. 102931, 2020.

[26] Kang S., Choi S. and Choi J.Y. "Coupled thermo-physical behaviour of an inorganic intumescent

system in cone calorimeter testing". Journal of Fire Sciences, vol. 35, no. 3, pp. 207-234, 2017.

[27] Yuan J. "Intumescent coating performance on steel structures under realistic fire conditions". PhD thesis, School of Mechanical, Aerospace and Civil Engineering, University of Manchester, 2009.

[28] Ahmad F., Ullah S., Merican N.H., Oñate E., Al-Sehemi A.G. and Yeoh G.H. "An investigation on thermal performance of wollastonite and bentonite reinforced intumescent fire-retardant coating for steel structures". Construction and Building Materials, vol. 228, no. 116734, 2019.

[29] Fateh T., Guillaume E. and Joseph P. "An experimental study of the thermal performance of a novel intumescent fire protection coating". Fire Safety Journal, vol. 92, pp. 132–141, 2017.

[30] Tian N., Delichatsios M.A., Zhang J. and Fateh T. "A methodology and a simple engineering fire performance model for intumescent fire retardant coatings". Fire Safety Journal, vol. 98, pp. 120–129, 2018.

[31] Tranchard P., Samyn F., Duquesne S., Estèbe B. and Bourbigot S. "Modelling behaviour of a carbon epoxy composite exposed to fire: Part I -Characterisation of thermophysical properties". Materials, vol. 10, pp. 494, 2017.

[32] Mariappan T., Agarwal A. and Ray S. "Influence of titanium dioxide on the thermal insulation of waterborne intumescent fire protective paints to structural steel". Progress in Organic Coatings, vol. 111, pp. 67–74, 2017.

[33] Yasir M., Amir N., Ahmad F., Ullah S. and Jimenez M. "Effect of basalt fibers dispersion on steel fire protection performance of epoxy-based intumescent coatings". Progress in Organic Coatings, vol. 122, pp. 229–238, 2018.

9

Conclusions and recommendations for future research

9.1 Summary of the main conclusions

A number of conclusions can be drawn on the basis of the research studies presented and discussed within this thesis. The key summary points and conclusions are highlighted below:

- An experimental methodology was proposed to analyse the effectiveness of intumescent coatings through a detailed characterisation of their thermo-physical response. In particular, the influences of different heating conditions (constant incident heat flux 10-90 kW/m^2) and the applied initial thickness (dry film thickness 1-3 mm) were investigated. Steel plates coated with a commercial solvent-based thin intumescent coating were exposed to well-defined and highly-repeatable thermal conditions in accordance with the Heat-Transfer Rate Inducing System (H-TRIS) test method. The experimental setup was instrumented in order to gauge the thermo-physical response of the intumescent coating during the heating exposure: the real-time swelled coating thickness, the exposed surface temperature, the substrate temperature and the in-depth transient temperature profile within the intumescent coating.

- The Thermo-Gravimetric Analysis (TGA) and Differental Scanning Calorimetry (DSC) experiments were carried out in order to investigate the chemical reactions and thermal decomposition processes occurring in the intumescent coatings at different temperatures and under different heating regimes. It was found that the tested product has similar characteristics to "typical" intumescent formulations (e.g. APP-PER-MEL systems): the main thermal decomposition reactions occur at temperatures included between 200 and 400°C, including the swelling reaction which typically happens between 300 and 400°C.

- Experiments involving the Transient Plane Source (TPS) and the Laser Flash Analysis (LFA) equipment evaluated the physical and thermal properties of the intumescent coating. Prior to onset of swelling, thermal conductivity, specific heat capacity and density are only slightly influenced by temperature, but they drastically change for swelled intumescent porous chars. On the other hand, the Integrating Sphere System (ISS) enabled the evaluation of the optical surface properties: the average absorptivity and emissivity of the intumescent coating were found to be in the range 0.86-0.93,

depending on the heating conditions.

- The onset of swelling for thin intumescent coatings represents a key feature for providing thermal insulation to the protected substrate and this research study showed how it can defined based on the visual observation of swelled coating thickness and the temperature evolution of the steel plate. According to these criteria, the tested intumescent coating required a constant incident heat flux higher than 20-23 kW/m^2 for initiating the swelling process. Thresholds for the onset of swelling in terms of steel (100-250 ℃) and mean coating temperatures (350-500 ℃) were derived and it was found that the onset of swelling is directly influenced by the heating conditions and the applied initial coating thickness. A first simplified finite-difference heat transfer model was formulated and validated in order to simulate the temperature increase of uncoated and coated steel samples prior to onset of swelling (e.g. 10 kW/m^2).

- The H-TRIS experiments evidenced how the swelling process and the resulting swelled coating thickness govern the thermo-physical response of thin intumescent coatings, thus their effectiveness. This explains why the substrate temperature and the swelling process are closely related. The swelling reaction occurs at the virgin coating located behind the swelled porous char and close to the interface between the applied coating and the substrate material. The intumescent coating swells and insulates the protected substrate by displacing the already-swelled coating towards the direction of the heat source. In all the cases involving coated steel plates, during swelling, the steel temperature asymptotically tended to a temperature range between 300 and 350 ℃. When the coating completed its swelling process, the steel temperature increased above 350 ℃. This aspect is supported by the TGA experiments: the intumescent swelling reaction is typically completed for temperatures around 400 ℃.

- The heating conditions and the applied initial coating thickness differently influence the swelling process of thin intumescent coatings, therefore their effectiveness. The external incident heat flux at the coating surface governs the swelling rate, while the applied initial coating thickness governs the maximum swelled thickness that the intumescent coating can reach during the thermal exposure. Empirical correlations based on these experimental outcomes were derived to predict the evolution of the swelled

coating thickness during thermal exposure.

- The swelling and the effectiveness of thin intumescent coatings is also influenced by the substrate thermal conditions. The physical and thermal properties of the substrate controls the capacity of the system to concentrate or dissipate heat in the proximity of the coating-substrate interface. Consequently, the substrate temperature controls the swelling of intumescent coatings because it defines the temperature experienced by the reacting virgin coating located in the proximity to the substrate-coating interface. Accordingly, high swelling rates were recorded for insulating conditions (timber substrate), while low swelling rates for conditions characterised by significant heat losses (steel plate with water-cooled heat sink).

- Based on the experimental results, the finite-difference heat transfer model was expanded to simulate the thermal and physical response of swelling intumescent coatings for the tested ranges of constant incident heat flux and applied initial coating thickness. The swelling of thin intumescent coatings was implemented by adding finite elements in the proximity of the substrate-coating interface and the intumescent coating was modelled as swelled porous char with constant material properties. The described model is capable of generally describing the heat transfer through swelling intumescent coatings by predicting the evolution of the coating surface and steel temperatures. The model accuracy is primarily dependent on the correct prediction of the coating swelling rate and the evolution of the swelled coating thickness: in this case, empirical correlations were derived based on the experimental outcomes.

- The heating conditions based on constant incident heat fluxes, the highly-insulating material properties of the intumescent coating and the relatively-high swelling rate compared to the penetration speed of the heat wave within the swelling coating defined a quasi steady-state thermal problem which minimised the impact of transient states and transient phenomena. The model is mainly governed by the ability of the intumescent coating to develop porous char and the coating material properties have limited influence. Consequently, the model solves steady-state heat transfer problems (linear thermal gradients) and loses accuracy for the cases driven by transient phenomena, such as phases before onset of swelling and heating conditions characterise by varying

incident heat flux.

9.2 Recommendations for future research

Although the knowledge related to thin intumescent coatings has been increased by the research studies presented and discussed within this thesis, further research is required in order to achieve a general understanding of behaviour of thin intumescent coatings for the design of fire-safe structures. A number of recommendations to continue and extend the research presented in this thesis are highlighted below:

- The presented experimental and modelling outcomes have been analysed and validated within certain ranges of the problem variables, which can be directly associated to the definition of the experimental campaigns. For example, the experimental studies focused on a range of constant incident heat fluxes included between 10 and 90 kW/m^2, a range of applied initial Dry Film Thickness (DFT) included between 1 and 3 mm and a range of substrate thermal conditions defined by the two extremes: timber substrate and a 10mm-thick steel plate with a water-cooled heat sink. These ranges define the boundaries of the experimental and modelling outcomes obtained within this thesis. Future research should investigate if these results can be extended to wider ranges. However, researchers should always consider reasonable ranges of applications: for instance, the maximum and minimum applied initial Dry Film Thickness (DFT) of a certain product is usually prescribed by the manufacturer and fire safety engineers can suggest the range of potential heating regimes that an intumescent coating may be exposed in certain applications.

- This research project have highlighted how the swelling process and the ability of the intumescent coating to develop thick swelled porous char govern their effectiveness. As a consequence, any model aimed at simulating the response of intumescent coatings is primarily dependent on a correct prediction of the coating swelling rate and the evolution of the swelled coating thickness. The presented heat transfer model adopted empirical correlations obtained from experiments under constant incident heat fluxes and it was found that these outcomes can be poorly applied in different heating conditions (e.g. time-histories of varying incident heat fluxes). Future research should focus

on correlating the swelling process of thin intumescent coatings (e.g. swelling rate) to more fundamental parameters: for instance, the neat heat flux through the swelled porous char and received by the reacting virgin coating located in the proximity to substrate-coating interface. In this improvement, the influence of the substrate thermal conditions should also be included. This process would require a detailed and complex heat transfer model: an initial theoretical attempt is presented at the end of Chapter 8. If the problem becomes too complex and with too many uncertainties, fully-empirical correlations can be derived as in this research study.

- This research has been proposed as fundamental study on a solvent-based thin intumescent coating: it provides an essential assessment procedure applicable to any coating and the results are therefore useful examples of the key outcomes that can be extracted. Consequently, this research should remain product-independent and the specific coating just an example chosen from the vast range of worldwide commercially available products. However, in order to generalise the presented research outcomes, extensive experimental and modelling campaigns should be performed on different commercial products and formulations. The material characterisation of the intumescent coating (particularly TGA and DSC) constitutes a unique fingerprint against which other products can be compared. The available literature offers a vast amount of TGA data to compare different intumescent products: this resource may be used as first assessment criteria to understand if various intumescent coatings with similar material characteristics follow a certain performance trend.

- The definition of the experimental setup based on the H-TRIS test method offered several advantages compared to other experimental methodologies, but it did not consider certain factors that might have affected the behaviour of thin intumescent coatings and the research outcomes. The first aspect is the oxygen-rich environmental of the H-TRIS test method: further research should focus on understanding the influence of oxygen and the coating oxidation on the swelling of thin intumescent coatings. Moreover, the H-TRIS test method uses bench-scale test samples and simplifies the heat transfer problem to one-dimension. Once the one-dimensional behaviour is comprehended, experimental studies should investigate the behaviour of real-scale coated

structural elements, involving a multi-dimensional heat transfer. For example, the study of coated steel columns or beams with a 3-sided or 4-sided thermal exposure may facilitate the understanding of large scale effects, such as the presence of edges, crack formation, char detachment and coating melting/delamination.

- Many other aspects related to the performance of thin intumescent coatings are still not fully understood and require further research. As an example, since the swelling and the resulting swelled coating thickness has a key importance in the effectiveness of thin intumescent coatings, researchers should investigate how their performance is affected when the coating swelling is obstructed by the presence of a physical obstacles or barriers. Another crucial aspect is related to the long-term durability of the reactive coatings. Intumescent coatings suffer from solar radiation, moisture cycles, temperature fluctuations and atmospheric contaminants and their degradation should be taken into account in the design of effective coatings throughout the entire life of structures. Researchers should propose a methodology to quantify the "reactivity" of the degraded intumescent coatings, compared to the virgin one. All the above-mentioned aspects should be carefully investigated and analysed in order to achieve a fundamental understanding on how different factors may influence the effectiveness of intumescent coatings and should be considered in performance-based design methodologies.

A | Appendix A

Additional experimental results

This appendix collects all the additional experimental results (e.g. temporal evolution of steel, in-depth and surface temperatures...) that, due to space restrictions, have been omitted from the main body of the current document. The following experimental results are presented for completeness. In the following graphs, as in the other plots presented in the current document, the same colour collects all the experiments with the same heating conditions or applied initial DFT, while continuous, dashed and dotted lines reports single experimental repetitions.

Steel and in-depth coating temperatures

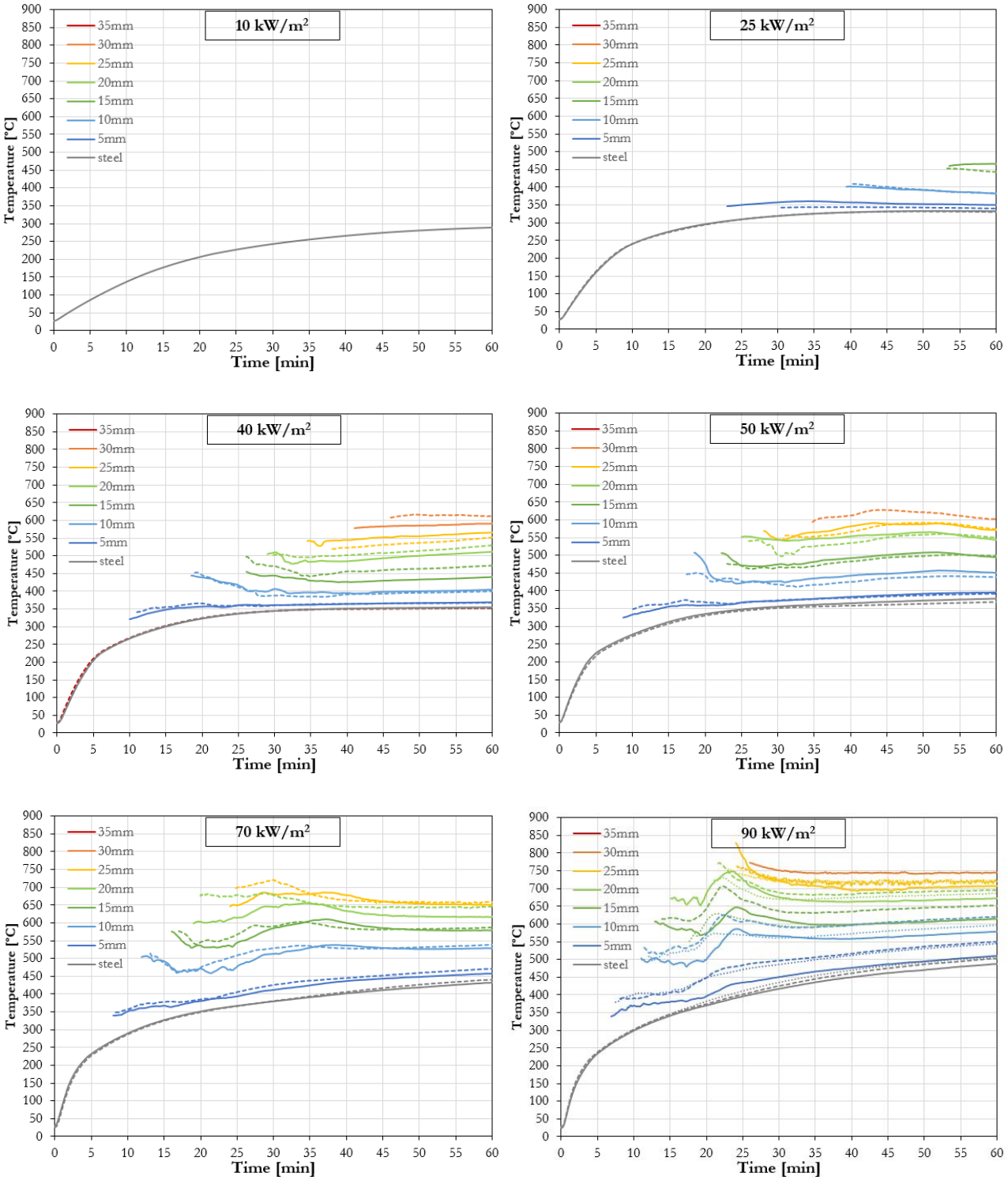

Figure A.1: Comparison of measured steel and in-depth coating temperatures for different constant incident heat fluxes (*"Low DFT"*).

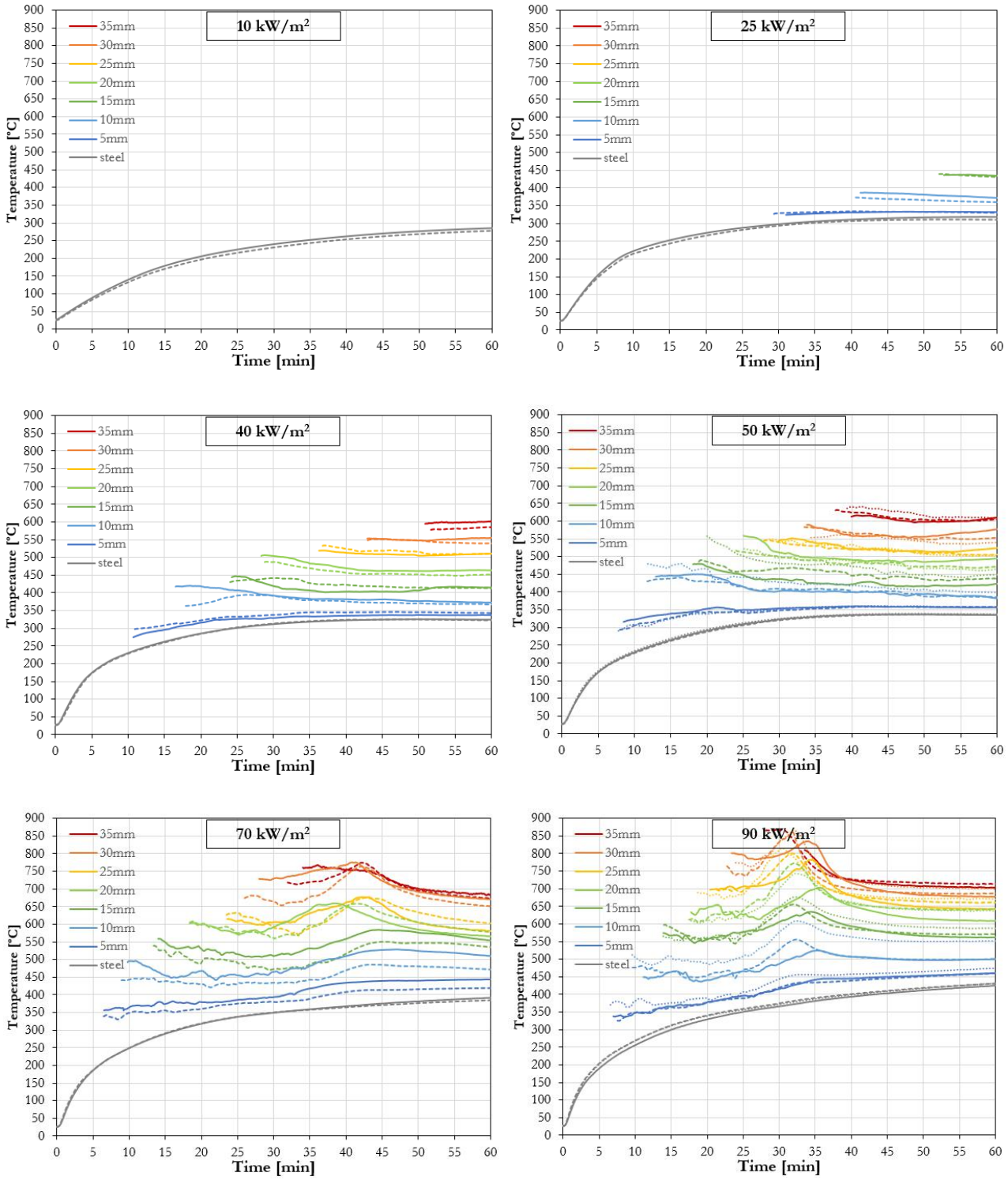

Figure A.2: Comparison of measured steel and in-depth coating temperatures for different constant incident heat fluxes (*"Medium DFT"*).

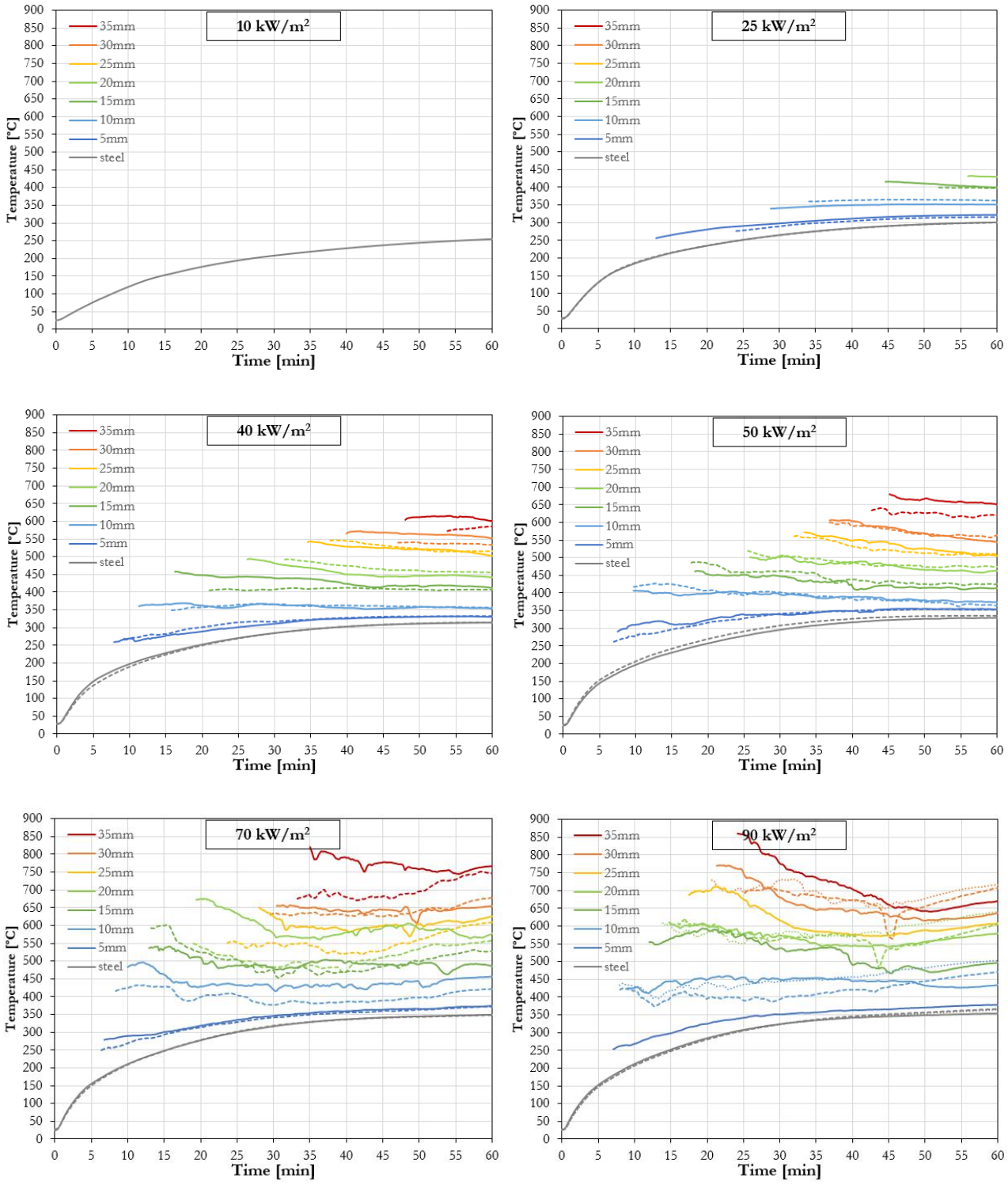

Figure A.3: Comparison of measured steel and in-depth coating temperatures for different constant incident heat fluxes (*"High DFT"*).

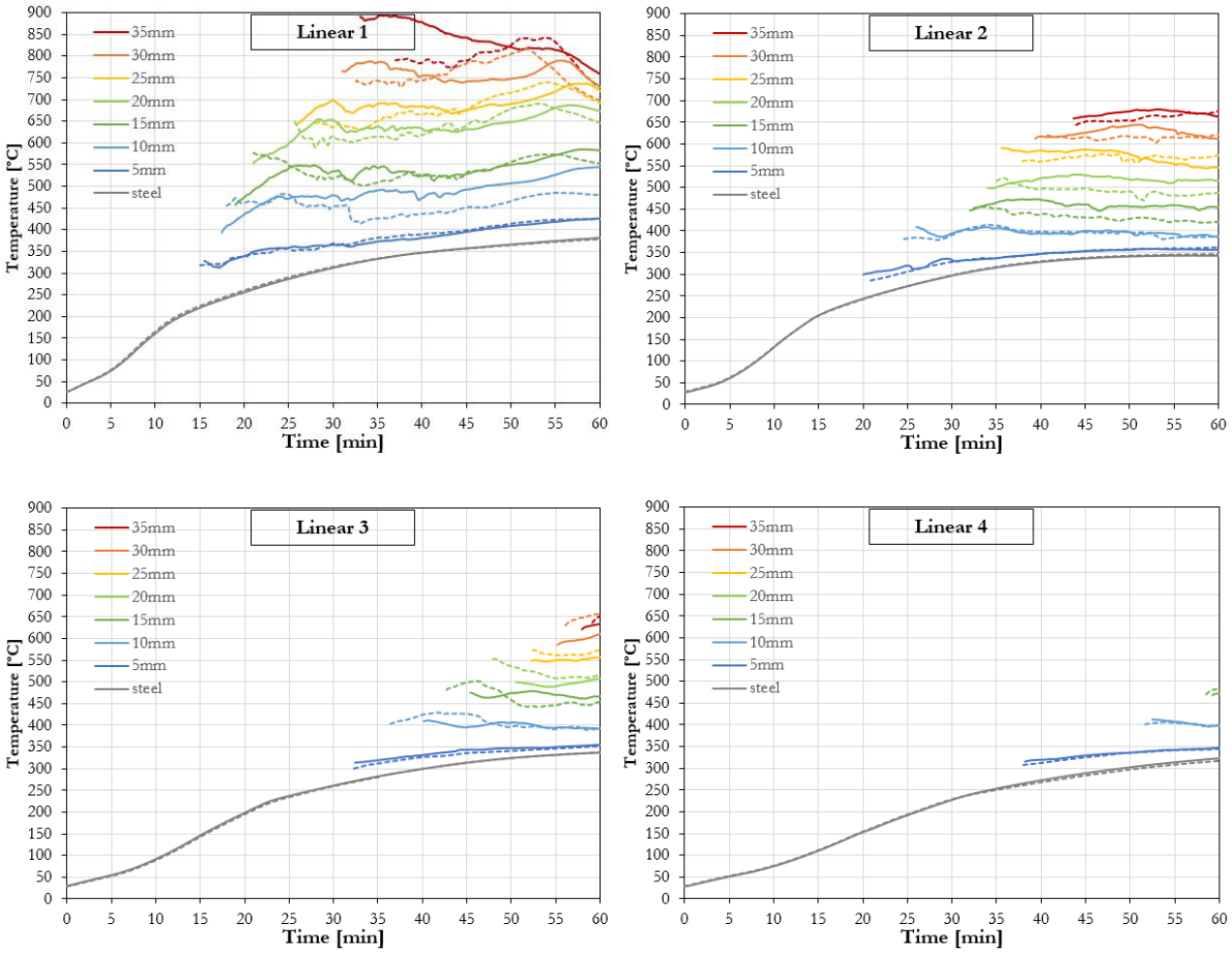

Figure A.4: Comparison of measured steel and in-depth coating temperatures for different linear-increasing incident heat fluxes (*"Medium DFT"*).

Coating surface temperatures (IR camera)

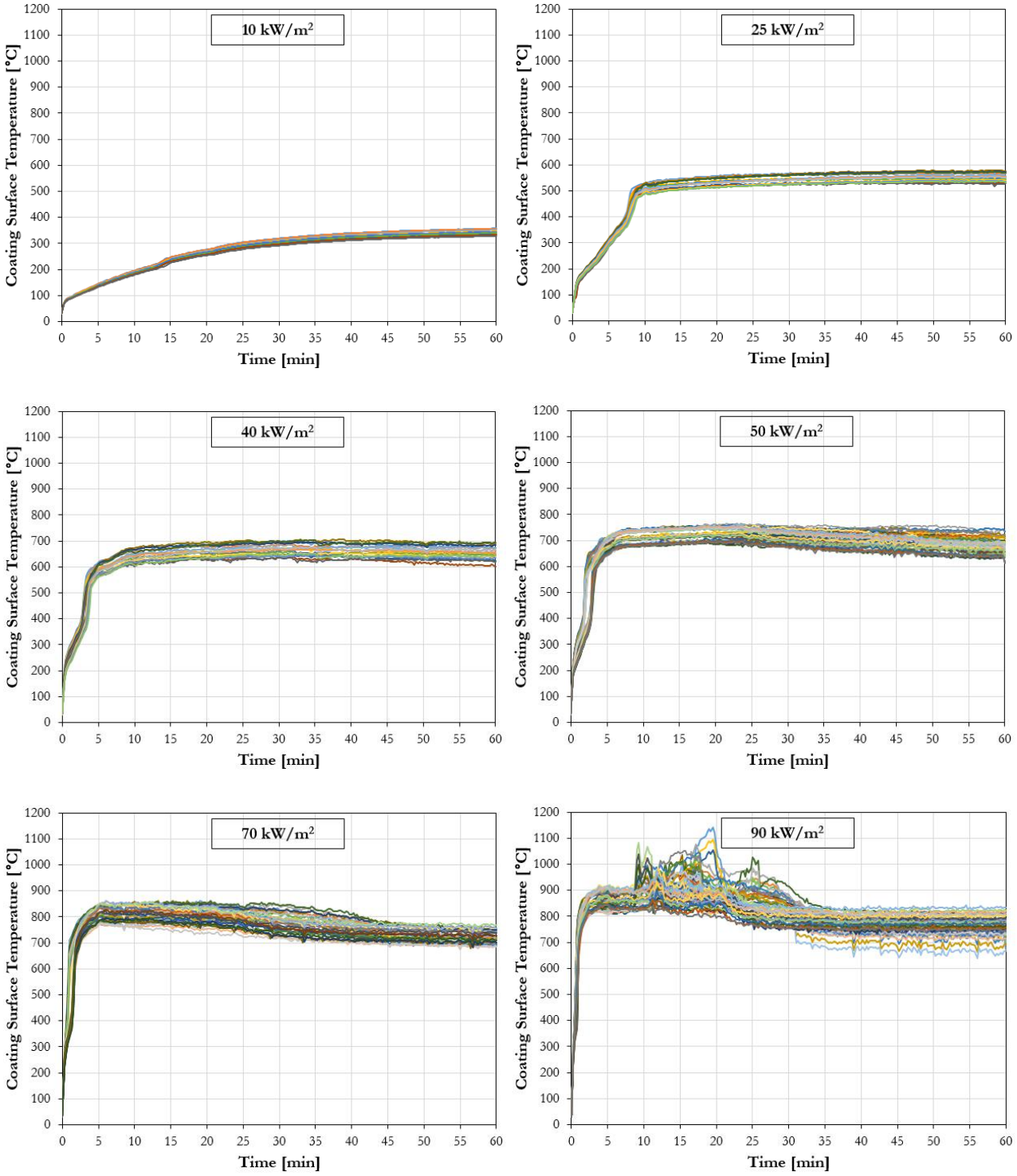

Figure A.5: Experimentally measured surface coating temperatures for different constant incident heat fluxes (IR camera post-processing).

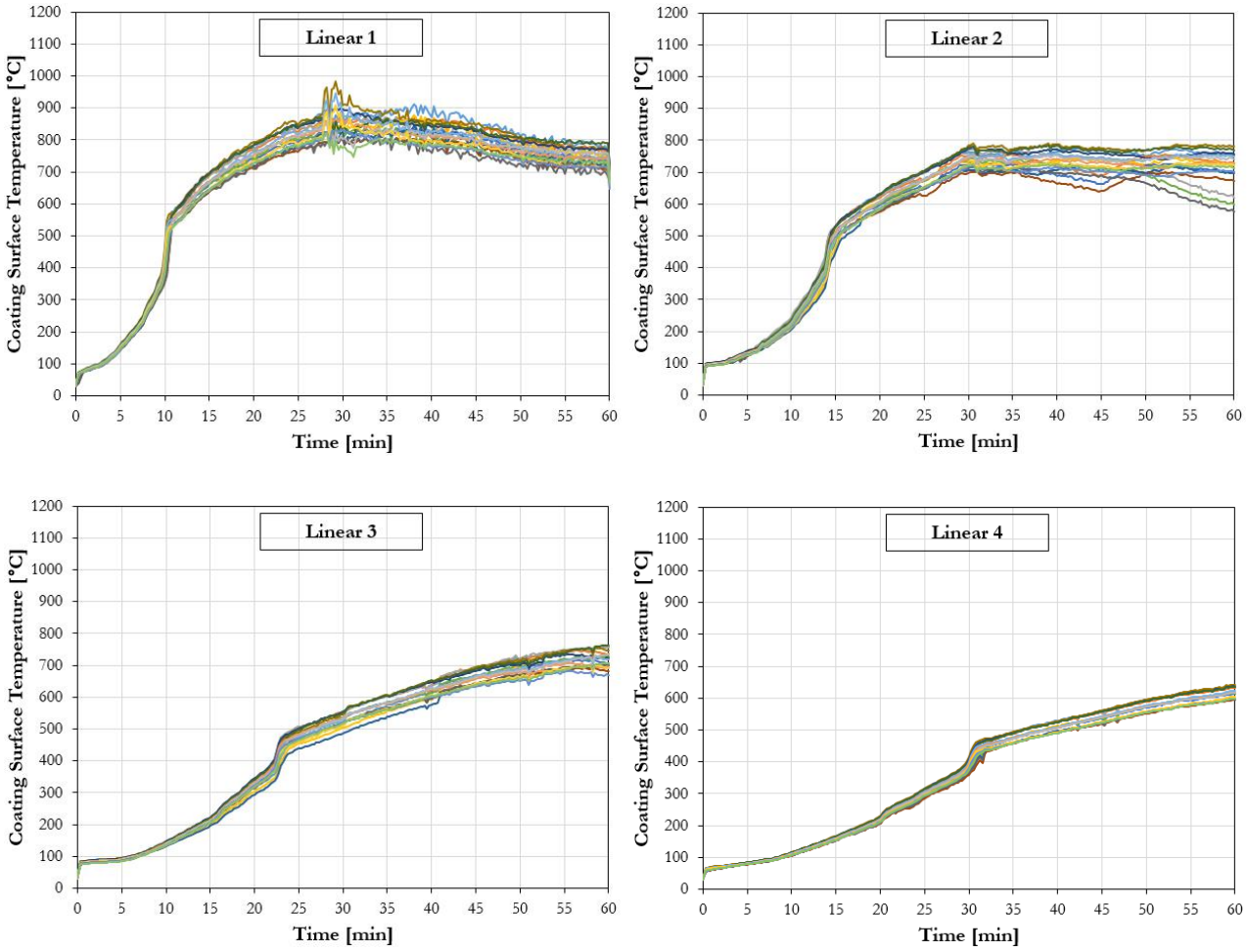

Figure A.6: Experimentally measured surface coating temperatures for different linear-increasing incident heat fluxes (IR camera post-processing).

B | Appendix B

Coating porous chars pictures

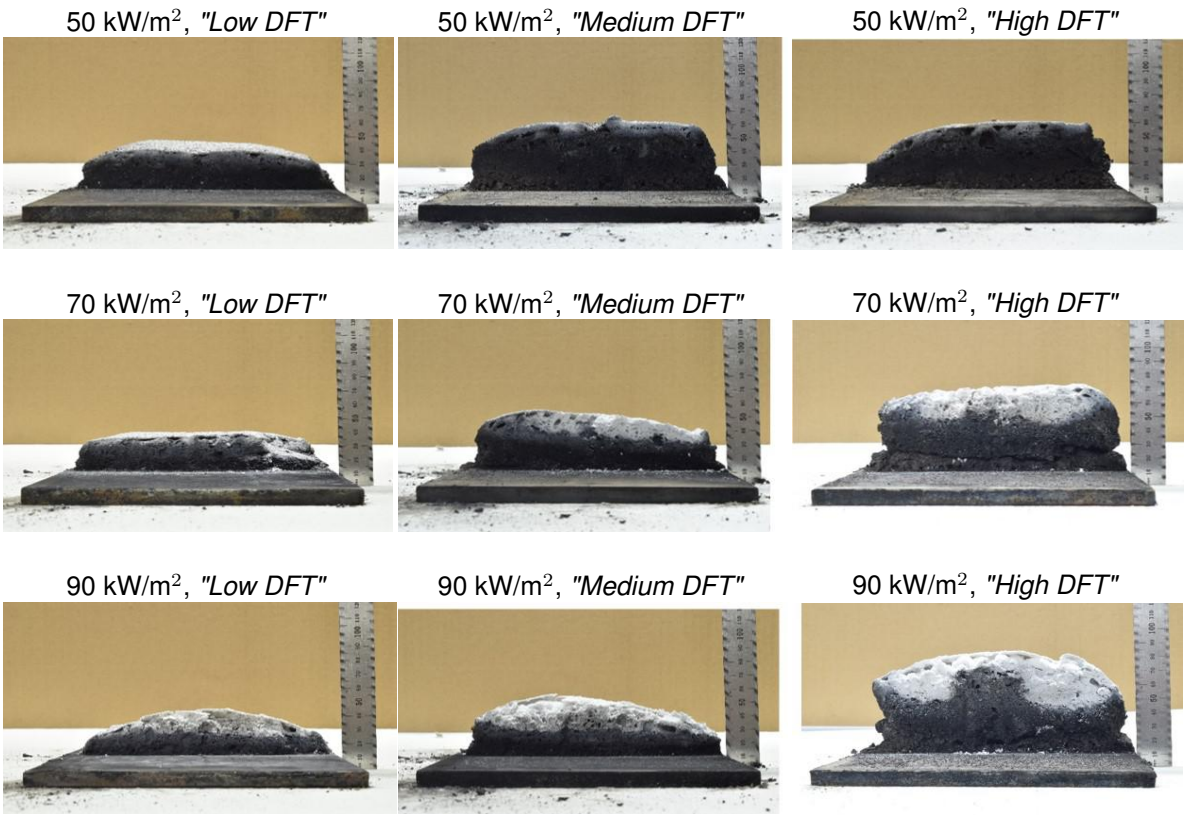

Figure B.1: Comparison between typical porous chars (sections) developed by the intumescent coating at the end of the thermal exposure for different constant incident heat fluxes and applied initial thickness.

Figure B.2: Comparison between typical porous chars (whole) developed by the intumescent coating at the end of the thermal exposure for different constant incident heat fluxes and applied initial thickness.

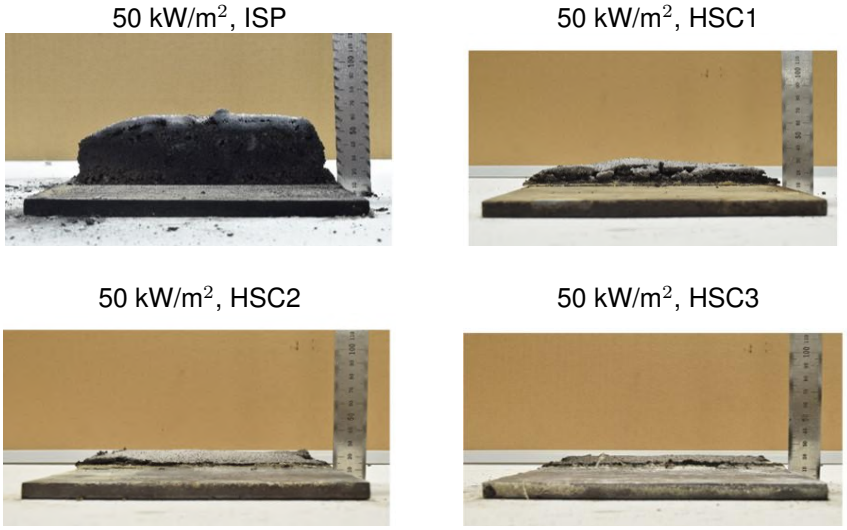

Figure B.3: Comparison between typical porous chars (sections) developed by the intumescent coating at the end of the thermal exposure with different substrate thermal conditions (*"Medium DFT"*).

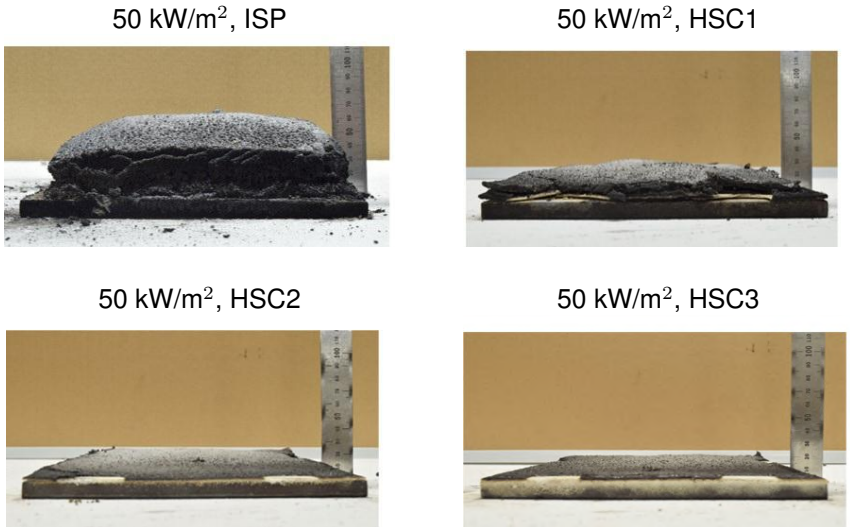

Figure B.4: Comparison between typical porous chars (whole) developed by the intumescent coating at the end of the thermal exposure with different substrate thermal conditions (*"Medium DFT"*).

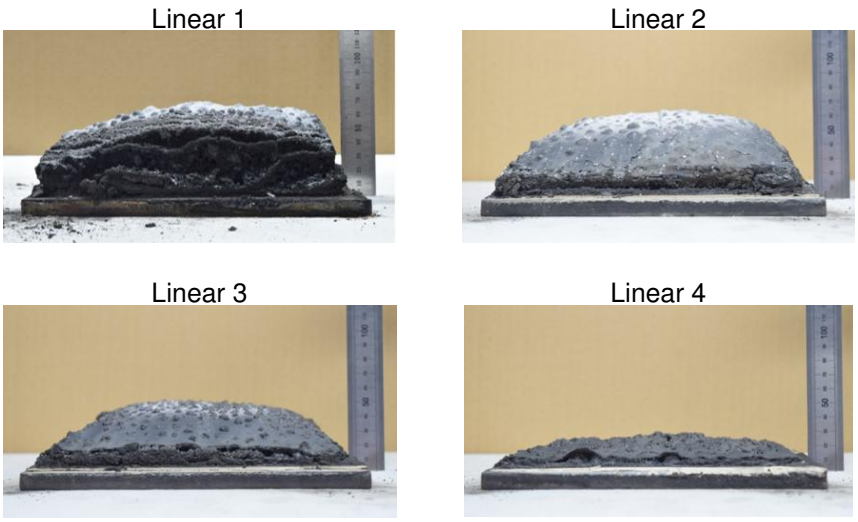

Figure B.5: Comparison between typical porous chars (whole) developed by the intumescent coating at the end of the thermal exposure for different linear-increasing incident heat fluxes (*"Medium DFT"*).

C | Appendix C

Explicit heat transfer modelling

An explicit one-dimensional heat transfer model is formulated in order to simulate and understand the thermal conditions and the heat transfer within the tested materials (steel plate only, intumescent coating only or coated steel plate). The model is based on the finite-difference method developed by Emmons and Dusinberre and it explicitly solves the heat conduction problem by resolving energy-balance equations in the main direction of the heat flow [1,2].

Material discretisation

Single-layer material

The discretisation of a *single-layer material* of thickness L is based on N elements. All the elements are represented by nodes. The interior elements have the node placed in the element's centre and they have a thickness of Δx. On the other hand, the boundary elements (surface element and end element) have the node placed at the element's edge and they have a thickness of $\Delta x/2$. A schematic representation of the single-layer material space domain discretisation is shown in Figure C.1.

Two-layers material

The discretisation of a *two-layers material* of thickness $L_1 + L_2$ is based on N elements. All the elements are represented by nodes. The interior elements have the node placed in the element's centre and they have a thickness of Δx. The interface element has the node placed on the interface surface between the two different layers and it has a thickness of

Δx. On the other hand, the boundary elements (surface element and end element) have the node placed at the element's edge and they have a thickness of $\Delta x/2$. For simplicity, Δx is the same in both materials. A schematic representation of the two-layers material space domain discretisation is shown in Figure C.2. The same approach considered for a two-layers material can be extended to any composite material composed of different materials and layers.

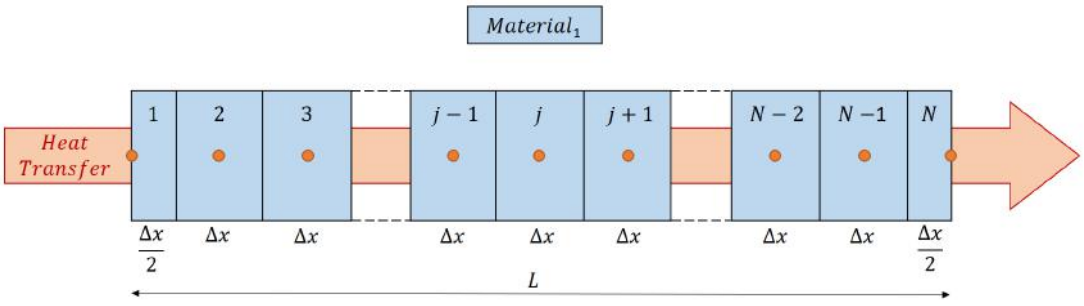

Figure C.1: Single-layer material space domain discretisation.

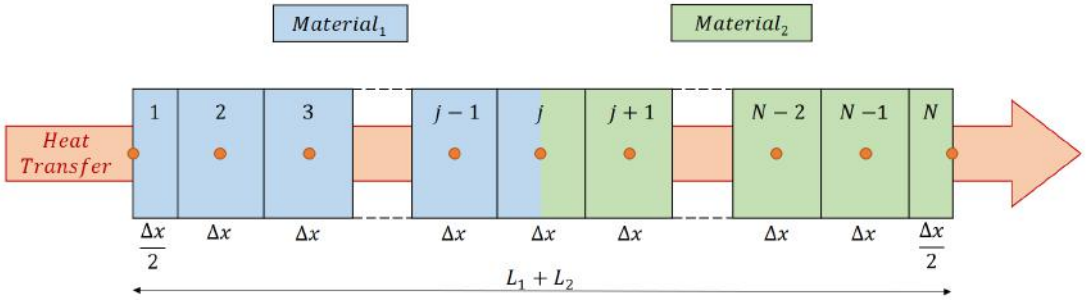

Figure C.2: Two-layers material space domain discretisation.

Thermal boundary conditions

The direction of the heat flow follows the increment of the element index j, which runs from 1 (surface element) to N (end element). The H-TRIS test method exposed the tested materials to a incident heat flux $\dot{q}''_{inc}$ at the surface element. Also, it has heat flux losses $\dot{q}''_{loss}$ at the surface elements due to radiation $\dot{q}''_{rad}$ and convection $\dot{q}''_{conv}$ with the surrounding environment. Adiabatic conductions are assumed at the back face of the tested material. Figure C.3 shows a schematic representation of the two-layers material space domain discretisation with the thermal boundary conditions at the surface and end elements.

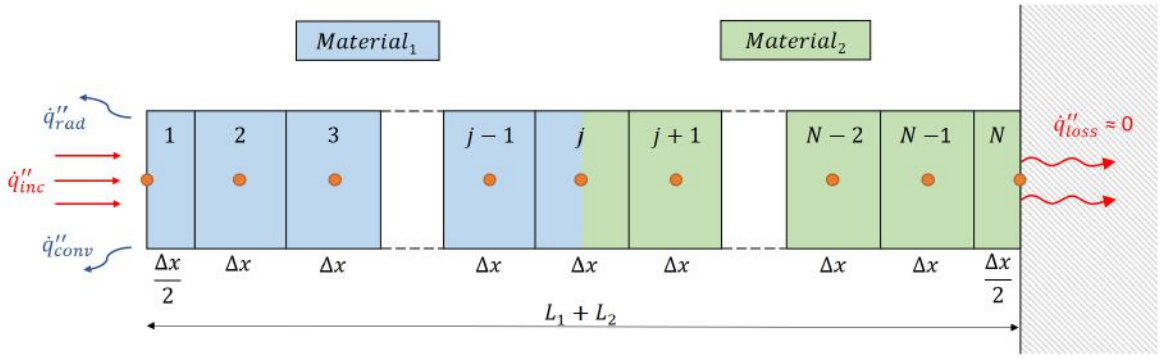

Figure C.3: Two-layers material space domain discretisation with a schematic representation of the thermal boundary conditions at the surface and end elements.

Heat transfer principles and fundamental laws

The heat transfer and the thermal boundary conditions are modelled using conventional correlations available in the literature [3].

Conduction

Heat transfer through *conduction* is governed by Fourier's law:

$$\dot{q}''_{cond} = -\lambda \frac{\Delta T}{\Delta x} = -\lambda \frac{T_{j+1} - T_j}{L} \tag{C.1}$$

where $\dot{q}''_{conv}$ is the conductive heat flux [W/m^2], λ is the thermal conductivity [W/mK], T_{j+1} is the temperature of the node $j+1$ [K], T_j is the temperature of the node j [K] and L is the characteristic length [m].

Radiation

Heat transfer through *radiation* is governed by the Stefan-Boltzmann's law:

$$\dot{q}''_{rad} = F_{12}\varepsilon\sigma(T^4_{surf} - T^4_{\infty}) \tag{C.2}$$

where $\dot{q}''_{rad}$ is the radiative heat flux [W/m^2], F_{12} is the view factor [-], ε is the emissivity [-], σ is the Stefan-Boltzmann constant ($5.67 \cdot 10^{-8}$ W/m^{2}K^4), T_{surf} is the surface temperature [K] and T_{∞} is the ambient (fluid) temperature [K].

Convection

Heat transfer through *convection* is governed by the Newton's law of cooling:

$$\dot{q}''_{conv} = h_{conv}(T_{surf} - T_{\infty}) \tag{C.3}$$

where $\dot{q}''_{conv}$ is the convective heat flux [W/m^2], h_{conv} is the convective heat transfer coefficient [W/m^{2}K], T_{surf} is the surface temperature [K] and T_{∞} is the ambient (fluid) temperature [K]. The *convective heat transfer coefficient* h_{conv} is the key parameter that empirically estimates the convection between a hot surface and a moving fluid. In the literature empirical correlations are available for most engineering applications [3]. The most common form to calculate the convective heat transfer coefficient h_{conv} of a vertical plate can expressed as:

$$h_{conv} = \frac{\overline{Nu}_L \, \lambda_{air}}{L} \tag{C.4}$$

where $\overline{Nu}_L$ is the Nusselt number [-], λ_{air} is the air thermal conductivity [W/mK] and L is the characteristic length of the geometry [m].
According to Churcill and Chu [4], the following correlations are suitable for evaluating the Nusselt number $\overline{Nu}_L$ (convection vs. conduction heat transfer) in the most engineering calculations:

$$\overline{Nu}_L = \begin{cases} 0.68 + \dfrac{0.670 Ra_L^{1/4}}{\left[1 + (0.492/Pr)^{9/16}\right]^{4/9}} & \text{if } Ra_L \leq 10^9 \\ \left[0.825 + \dfrac{0.387 Ra_L^{1/6}}{\left[1 + (0.492/Pr)^{9/16}\right]^{8/27}}\right]^2 & \text{if } Ra_L \geq 10^9 \end{cases} \tag{C.5}$$

$$Ra_L = \frac{g \beta_{air} (T_{surf} - T_{\infty}) L^3}{\nu_{air} \alpha_{air}} \tag{C.6}$$

$$Pr = \frac{\nu_{air}}{\alpha_{air}} \tag{C.7}$$

$$\beta_{air} = \frac{1}{T_{film}} \tag{C.8}$$

$$T_{film} = \frac{T_{surf} + T_{\infty}}{2} \tag{C.9}$$

where Ra_L is the Rayleigh number [-] (conduction vs. convection heat transfer), Pr is the Prandlt number [-] (momentum vs. thermal diffusivity), g is the gravitational acceleration

(9.81 m/s^2), ν_{air} is the air kinematic viscosity [m^2/s], α_{air} is the air thermal diffusivity [m^2/s], β_{air} is the air volumetric thermal expansion coefficient [K^{-1}, T_{film} is the film temperature [K] and T_{surf} is the surface temperature [K].

Using the temperature dependent tabulated values suggested by Incropera et al. [3], the following Lagrangian polynomial approximations can be used to calculate the air thermal conductivity λ_{air}, the air kinematic viscosity ν_{air} and the air thermal diffusivity α_{air}.

$$\begin{aligned}\lambda_{air} = &- 2.733 \cdot 10^{-3} + 1.240 \cdot 10^{-4} \cdot T_f - 1.363 \cdot 10^{-7} \cdot T_f^2 \\ &+ 2.112 \cdot 10^{-10} \cdot T_f^3 - 2.326 \cdot 10^{-13} \cdot T_f^4 \\ &+ 1.277 \cdot 10^{-16} \cdot T_f^5 - 2.471 \cdot 10^{-20} \cdot T_f^6\end{aligned} \tag{C.10}$$

$$\begin{aligned}\nu_{air} = &- 2.164 \cdot 10^{-5} + 2.172 \cdot 10^{-7} \cdot T_f - 6.066 \cdot 10^{-10} \cdot T_f^2 \\ &+ 1.359 \cdot 10^{-12} \cdot T_f^3 - 1.366 \cdot 10^{-15} \cdot T_f^4 \\ &+ 6.636 \cdot 10^{-19} \cdot T_f^5 - 1.236 \cdot 10^{-22} \cdot T_f^6\end{aligned} \tag{C.11}$$

$$\begin{aligned}\alpha_{air} = &- 1.601 \cdot 10^{-5} + 1.556 \cdot 10^{-7} \cdot T_f - 3.187 \cdot 10^{-10} \cdot T_f^2 \\ &+ 1.111 \cdot 10^{-12} \cdot T_f^3 - 1.373 \cdot 10^{-15} \cdot T_f^4 \\ &+ 7.581 \cdot 10^{-19} \cdot T_f^5 - 1.497 \cdot 10^{-22} \cdot T_f^6\end{aligned} \tag{C.12}$$

Numerical stability

Explicit finite-element methods can be unconditionally stable, therefore they can diverge from reaching a steady state solution if their stability is not ensured. A *stability criterion* has to be introduced. According to Dusinberre [2] the time step of iteration must be lower than the following limits:

$$\Delta t \leq \frac{\rho c_p \Delta x^2}{2\lambda} \qquad \Delta t \leq \frac{\rho c_p \Delta x^2}{2[h_{tot}\Delta x + \lambda]} \tag{C.13}$$

where h_{tot} is the total heat transfer coefficient [W/m^{2}K], which can be calculated as:

$$h_{tot} = \sigma\varepsilon(T_j^2 + T_\infty^2)(T_j + T_\infty) + h_{conv} \tag{C.14}$$

In case of a multi-layer heat transfer model, the values of ρ, c_p, λ and h_{tot} have to be defined in a way to obtain minimum values of Δt.

Derivation of governing equations (without heat source term)

Starting from energy-balance equations at each node, thus each element, the following formulas can be derived to calculate the temperature evolution of each node (surface, middle, interface and end) for each time step i.

Surface element

$$T_1^{i+1} = T_1^i + \frac{2\Delta t}{\rho c_p \Delta x}\left[\alpha \dot{q}''_{inc} - \lambda \frac{T_1^i - T_2^i}{\Delta x} - h_{conv}(T_1^i - T_\infty) - F_{12}\varepsilon\sigma(T_1^{i4} - T_\infty^4)\right] \tag{C.15}$$

Middle element

$$T_j^{i+1} = T_j^i + \frac{\lambda \Delta t}{\rho c_p \Delta x^2}\left[T_{j-1}^i - 2T_j^i + T_{j+1}^i\right] \tag{C.16}$$

End element

$$T_n^{i+1} = T_n^i + \frac{2\lambda \Delta t}{\rho c_p \Delta x^2}\left[T_{n-1}^i - T_n^i\right] \tag{C.17}$$

Interface element (multi-layer)

$$T_j^{i+1} = T_j^i + \frac{\Delta t}{(\rho_1 c_{p1} + \rho_2 c_{p2})\Delta x^2}\left[\lambda_1 T_{j-1}^i - (\lambda_1 + \lambda_2)T_j^i + \lambda_2 T_{j+1}^i\right] \tag{C.18}$$

where T_j^i is the temperature of node j at time i [K], Δt is the time step [sec], ρ_k is the density of material k [kg/m^3], $c_{p,k}$ is the specific heat capacity of material k [J/kgK], Δx is the discretisation thickness [m], α: surface absorptivity [-], $\dot{q}''_{inc}$ is the incident heat flux [W/m^2], λ_k is the thermal conductivity of material k [W/mK], h_{conv} is the convective heat transfer coefficient [W/m^{2}K], T_∞ is the ambient temperature [K], F_{12} is the view factor [-], ε is the surface material emissivity [-] and σ is the Stefan-Boltzmann constant ($5.67 \cdot 10^{-8}$ W/m^{2}K^4).

In this case, the problem assumes a pure conduction problem: all the heat received by a certain element is conducted through its own thickness or used for increasing its own temperature (specific heat capacity). In addition, as any other finite-difference method, the current model is depended on the definition of the model discretisation: a smaller spacial discretisation Δx (consequently smaller time step Δt following the numerical stability) usually produces more accurate results, but it requires and utilises a high computational power.

Derivation of governing equations (with heat source term)

In order to take into account the heat losses due to thermal processes occurring within the materials, a *volumetric heat source term* $\dot{g}'''$ [W/m^3] is introduced: positive for absorbed heat (endothermic reactions) and negative for generated heat (exothermic reaction). All the previous equations can be re-derived as:

Surface element

$$T_1^{i+1} = T_1^i + \frac{2\Delta t}{\rho c_p \Delta x}\left[\alpha \dot{q}''_{inc} - \lambda\frac{T_1^i - T_2^i}{\Delta x} - h_{conv}(T_1^i - T_\infty) - F_{12}\varepsilon\sigma(T_1^{i4} - T_\infty^4) - \dot{g}'''\frac{\Delta x}{2}\right] \quad \text{(C.19)}$$

Middle element

$$T_j^{i+1} = T_j^i + \frac{\Delta t}{\rho c_p \Delta x^2}\left[\lambda(T_{j-1}^i - 2T_j^i + T_{j+1}^i) - \dot{g}'''\Delta x^2\right] \quad \text{(C.20)}$$

End element

$$T_n^{i+1} = T_n^i + \frac{2\Delta t}{\rho c_p \Delta x^2}\left[\lambda(T_{n-1}^i - T_n^i) - \dot{g}'''\frac{\Delta x^2}{2}\right] \quad \text{(C.21)}$$

Interface element (multi-layer)

$$T_j^{i+1} = T_j^i + \frac{\Delta t}{(\rho_1 c_{p1} + \rho_2 c_{p2})\Delta x^2}\left[\lambda_1 T_{j-1}^i - (\lambda_1 + \lambda_2)T_j^i + \lambda_2 T_{j+1}^i - (\dot{g}_1''' + \dot{g}_2''')\frac{\Delta x^2}{2}\right] \quad \text{(C.22)}$$

where T_j^i is the temperature of node j at time i [K], Δt is the time step [sec], ρ_k is the density of material k [kg/m^3], $c_{p,k}$ is the specific heat capacity of material k [J/kgK], Δx is the discretisation thickness [m], α: surface absorptivity [-], $\dot{q}''_{inc}$ is the incident heat flux [W/m^2], λ_k is the thermal conductivity of material k [W/mK], h_{conv} is the convective heat transfer coefficient [W/m^{2}K], T_∞ is the ambient temperature [K], F_{12} is the view factor [-], ε is the surface material emissivity [-], σ is the Stefan-Boltzmann constant ($5.67 \cdot 10^{-8}$ W/m^{2}K^4) and $\dot{g}_k'''$ is the volumetric heat source term of material k [W/m^3].

Bibliography

[1] Emmons H.W. "The numerical solution of heat conduction problems". Transactions of American Society of Mechanical Engineers (ASME), vol. 65(6), pp. 607-615, 1943.

[2] Dusinberre G.M. "Heat transfer calculations by finite differences". International Textbook Company, Pennsylvania, USA, 293 pp., 1961.

[3] Incropera F.P., DeWitt D.P., Bergman T.L. and Lavine A.S. "Fundamental of heat and mass transfer". John Wiley & Sons, 6th Edition, 2006.

[4] Churcill S.W., and Chu H.H.S. "Correlating equations for laminar and turbulent free convection from a vertical plate". International Journal of Heat and Mass Transfer, vol. 18, pp. 1323-1329, 1975.

D | Appendix D

Implicit heat transfer modelling

Start from the first simplified explicit heat transfer model presented in Appendix C, an implicit one-dimensional heat transfer model is formulated in order to simulate and understand the thermal conditions and the heat transfer within the tested materials (steel plate only, intumescent coating only or coated steel plate). Contrarily to the previous one, this heat transfer model is based on the *Crank-Nicolson method*, a finite-difference method able to solve one-dimensional heat conduction equations [1,2]. The method is a second-order method in time and implicit in time and numerically stable. The formulation is based on building a system of N linear equations and N variables (i.e. temperatures of each node at the step $j+1$), based on the following equation:

$$T_j^{i+1} = T_j^i + \frac{\Delta t}{2}\left(\left.\frac{dT}{dt}\right|_j^i + \left.\frac{dT}{dt}\right|_j^{i+1}\right) \tag{D.1}$$

where T_j^i is the temperature of the node j at time i [K], $\left.\frac{dT}{dt}\right|_j^i$ is the temperature variation of the node j at time i [K/sec] and Δt is the time increment [sec].
The Crank-Nicolson method requires the derivation of the temperature variation over time $\frac{dT}{dt}$ for each element j of the discretisation at time steps i and $i+1$. The defined system of equations forms a tridiagonal matrix system, which simplifies and reduces the computational cost of the model significantly.

Material discretisation

The material discretisation is organised in finite elements, similarly for the case of the explicit heat transfer model. In this case, the discretisation is set as a *single-layer material* of thick-

ness L is based on N elements. All the elements are represented by nodes. The interior elements have the node placed in the element's centre and they have a thickness of Δx. On the other hand, the boundary elements (surface element and end element) have the node placed at the element's edge and they have a thickness of $\Delta x/2$. No interface elements are considered. A schematic representation of the space domain discretisation is shown in Figure D.1. As for the explicit model, a multi-layer material discretisation can be applied to any number of layers, but it will not be presented herein.

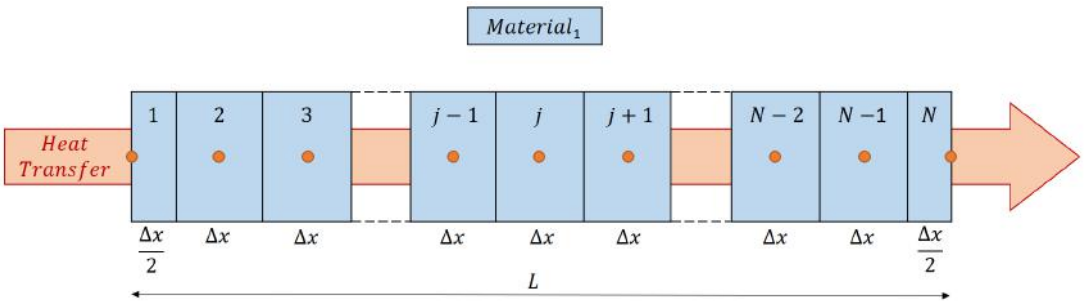

Figure D.1: Single-layer material space domain discretisation.

Derivation of governing equations

Similarly to the explicit case presented in Appendix C, the heat is transferred one-dimensionally following the increment of the element index j, starting from 1 (surface element) to N (end element). The heat transfer and the thermal boundary conditions are modelled using conventional correlations available in the literature, following the the principles and fundamental laws presented in Appendix C. However, in this case, the thermal boundary conditions at the surface and end elements of the tested material differ based on the specific problem. In particular, the thermal boundary conditions at the surface element can be described as:

- A known time-history of incident heat flux $\dot{q}''_{inc}$ with corresponding heat flux losses $\dot{q}''_{loss}$ due to radiation $\dot{q}''_{rad}$ and convection $\dot{q}''_{conv}$ with the surrounding environment.
- Known temperature $T_1(t)$.

On the contrary, the thermal boundary conditions at the end element can be described as:

- Adiabatic thermal boundary conditions.

- Thermally thin material (steel plate) with adiabatic thermal boundary conditions.
- Known temperature $T_N(t)$.

In order to simply the problem, the model assumes a pure conduction problem and it does not include any heat generation/absorption (heat source term) within the material elements. In addition, the thermal and physical material properties are lumped into effective properties in order to predict the thermal evolution of the tested samples.
Starting from energy-balance equations at each node, thus each element, different formulas are derived based on the specific problem, dependent on the definition of the thermal boundary conditions and material properties. The obtained formulas allow to build tridiagonal matrix systems in order to calculate the temperature evolution of each node (surface, middle and end) for each time step i. In order to build the tridiagonal matrix system, the equation are systematically organised in a specific order: unknown variables and their parameters on the left-hand side, known parameters on the right-hand side.
Also in this case, the model precision depends on the model discretisation, but there are no restictions on the definition of the spacial discretisation Δx and the time step Δt because the implicit method is numerically stable.

Within the derivation of the heat transfer model, different parameters are obtained and they have a key role in the mathematical formulation. First, a simplified formulation of the *Fourier number* Fo_j^i for each node j at time i can be expressed as:

$$Fo_j^i = \frac{\lambda(T_j^i)\Delta t}{\rho(T_j^i)c_p(T_j^i)\Delta x^2} \tag{D.2}$$

where $\lambda(T_j^i)$ [W/mK], $\rho(T_j^i)$ [kg/m^3] and $c_p(T_j^i)$ [J/kgK] are respectively the temperature-dependent thermal conductivity, density and specific heat capacity of the node j at time i, Δt is the time increment [sec] and Δx is the space discretisation thickness [m]. It should be noted that in this appendix the thermal and physical properties are described as temperature dependent.

Due to the non-linearity introduced by temperature dependence on the thermal conductivity, the *Fourier number derivative* dFo_j^i is defined as:

$$dFo_j^i = \frac{d\lambda(T_j^i)}{dT} \cdot \frac{\Delta t}{4\rho(T_j^i)c_p(T_j^i)\Delta x^2} \tag{D.3}$$

where $\frac{d\lambda(T_j^i)}{dT}$ is the derivative of the temperature-dependent thermal conductivity of the node j at time i.

Finally, the *total heat transfer coefficient* h_{tot} can be calculated as:

$$h_{tot}(T_1^i) = h_{conv}(T_1^i) + \varepsilon\sigma\frac{(T_1^i)^4 - T_\infty^4}{T_1^i - T_\infty} = h_{conv}(T_1^i) + \varepsilon\sigma\left[(T_1^i)^2 + T_\infty^2\right]\left(T_1^i + T_\infty\right) \tag{D.4}$$

where h_{conv} is the convective heat transfer coefficient [W/m^{2}K], ε is the emissivity [-], σ is the Stefan-Boltzmann constant ($5.67 \cdot 10^{-8}$ W/m^{2}K^4), T_1^i is the temperature of the surface element at time i [K] and T_∞ is the ambient temperature [K].

The following pages present the derivation of the heat transfer formulations, starting from simple energy-balance equations for each single element (surface, middle and end) towards obtaining the equations constituting the tridiagonal matrix system, organised as parameters matrix, unknowns vector and known parameters vector. Depending on the heat transfer problem, the initial assumptions are different, as well as the number of equations and number of variables.

Surface element

Known time-history of incident heat flux

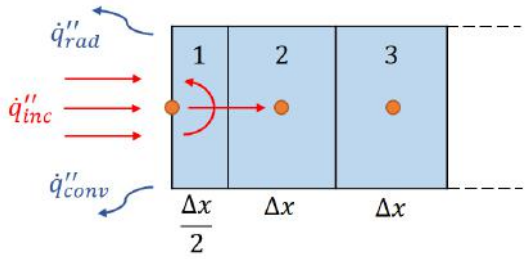

$$\alpha \dot{q}''_{inc} - h_{tot}\left(T_1 - T_\infty\right) = \rho c_p \frac{\Delta x}{2}\frac{\partial T_1}{\partial t} + \frac{\lambda(T_1 - T_2)}{\Delta x}$$

$$\frac{\partial T_1}{\partial t} = \frac{2\alpha \dot{q}''_{inc}}{\rho c_p \Delta x} + \frac{2h_{tot}}{\rho c_p \Delta x}\left(T_\infty - T_1\right) + \frac{2\lambda}{\rho c_p \Delta x^2}\left(T_2 - T_1\right)$$

Crank-Nicolson method $$T_1^{i+1} = T_1^i + \frac{\Delta t}{2}\left(\left.\frac{dT}{dt}\right|_1^i + \left.\frac{dT}{dt}\right|_1^{i+1}\right)$$

$$T_1^{i+1} = T_1^i + \frac{\Delta t}{2}\left[\frac{2\alpha \dot{q}''^i_{inc}}{\rho c_p \Delta x} + \frac{2h_{tot}}{\rho c_p \Delta x}\left(T_\infty - T_1^i\right) + \frac{2\lambda}{\rho c_p \Delta x^2}\left(T_2^i - T_1^i\right)\right]$$
$$+\frac{\Delta t}{2}\left[\frac{2\alpha \dot{q}''^{i+1}_{inc}}{\rho c_p \Delta x} + \frac{2h_{tot}}{\rho c_p \Delta x}\left(T_\infty - T_1^{i+1}\right) + \frac{2\lambda}{\rho c_p \Delta x^2}\left(T_2^{i+1} - T_1^{i+1}\right)\right]$$

Fourier number $$Fo_1^i = \frac{\lambda(T_1^i)\Delta t}{\rho(T_1^i)c_p(T_1^i)\Delta x^2}$$

$$T_1^{i+1} = T_1^i + Fo_1^i\left(T_2^i - T_1^i + T_2^{i+1} - T_1^{i+1}\right)$$
$$+\frac{\alpha \Delta t}{\rho c_p \Delta x}\left(\dot{q}''^i_{inc} + \dot{q}''^{i+1}_{inc}\right) + \frac{h_{tot}\Delta t}{\rho c_p \Delta x}\left(2T_\infty - T_1^i - T_1^{i+1}\right)$$

$$T_1^{i+1}\left[1 + Fo_1^i + \frac{h_{tot}(T_1^i)\Delta t}{\rho(T_1^i)c_p(T_1^i)\Delta x}\right] + T_2^{i+1}\left[-Fo_1^i\right] =$$
$$T_1^i + Fo_1^i\left(T_2^i - T_1^i\right) + \frac{\alpha \Delta t}{\rho(T_1^i)c_p(T_1^i)\Delta x}\left(\dot{q}''^i_{inc} + \dot{q}''^{i+1}_{inc}\right) + \frac{h_{tot}(T_1^i)\Delta t}{\rho(T_1^i)c_p(T_1^i)\Delta x}\left(2T_\infty - T_1^i\right) \quad \text{(D.5)}$$

Middle element

Known temperature at the surface

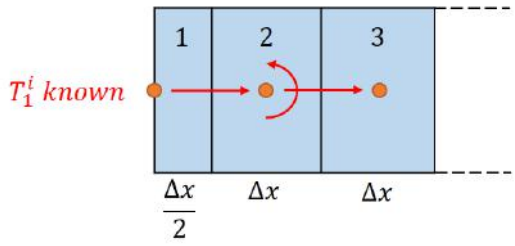

$$\frac{\lambda(T_1 - T_2)}{\Delta x} = \rho c_p \Delta x \frac{\partial T_2}{\partial t} + \frac{\lambda(T_2 - T_3)}{\Delta x}$$

$$\frac{\partial T_2}{\partial t} = \frac{\lambda}{\rho c_p \Delta x^2}(T_1 - 2T_2 + T_3)$$

Crank-Nicolson method $$T_2^{i+1} = T_2^i + \frac{\Delta t}{2}\left(\left.\frac{dT}{dt}\right|_2^i + \left.\frac{dT}{dt}\right|_2^{i+1}\right)$$

$$T_2^{i+1} = T_2^i + \frac{\Delta t}{2}\frac{\lambda}{\rho c_p \Delta x^2}\left[\left(T_1^i - 2T_2^i + T_3^i\right) + \left(T_1^{i+1} - 2T_2^{i+1} + T_3^{i+1}\right)\right]$$

Fourier number $$Fo_2^i = \frac{\lambda(T_2^i)\Delta t}{\rho(T_2^i)c_p(T_2^i)\Delta x^2}$$

$$T_2^{i+1} = T_2^i + \frac{Fo_2^i}{2}\left(T_1^i - 2T_2^i + T_3^i + T_1^{i+1} - 2T_2^{i+1} + T_3^{i+1}\right)$$

$$T_2^{i+1}\left[1 + Fo_2^i\right] + T_3^{i+1}\left[-\frac{Fo_2^i}{2}\right] = T_2^i + \frac{Fo_2^i}{2}\left(T_1^i - 2T_2^i + T_3^i + T_1^{i+1}\right) \tag{D.6}$$

Pure conduction

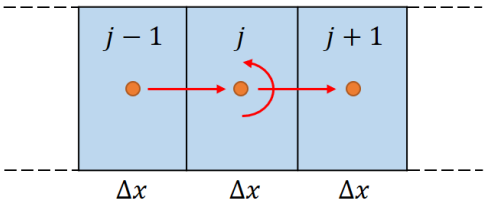

$$\frac{\partial\left(\lambda\cdot\partial T\right)}{\partial x^2}=\rho c_p\frac{\partial T}{\partial t}$$

$$\lambda(T)\frac{\partial^2 T}{\partial x^2}+\frac{\partial\lambda}{\partial x}\cdot\frac{\partial T}{\partial x}=\rho c_p\frac{\partial T}{\partial t}$$

$$\lambda(T)\frac{\partial^2 T}{\partial x^2}+\frac{\partial\lambda}{\partial T}\cdot\left(\frac{\partial T}{\partial x}\right)^2=\rho c_p\frac{\partial T}{\partial t}$$

Central difference method $$\frac{\partial^2 T}{\partial x^2}=\frac{T_{j-1}-2T_j+T_{j+1}}{\Delta x^2}$$

Differentiation $$\left(\frac{\partial T}{\partial x}\right)^2=\left(\frac{T_{j+1}-T_{j-1}}{2\Delta x}\right)^2$$

$$\frac{\partial T_j}{\partial t}=\frac{\lambda(T_{j-1}-2T_j+T_{j+1})}{\rho c_p\Delta x^2}+\frac{1}{\rho c_p}\cdot\frac{d\lambda}{dT}\cdot\left(\frac{T_{j+1}-T_{j-1}}{2\Delta x}\right)^2$$

Crank-Nicolson method $$T_j^{i+1}=T_j^i+\frac{\Delta t}{2}\left(\left.\frac{dT}{dt}\right|_j^i+\left.\frac{dT}{dt}\right|_j^{i+1}\right)$$

Fourier number $$Fo_j^i=\frac{\lambda(T_j^i)\Delta t}{\rho(T_j^i)c_p(T_j^i)\Delta x^2}$$

Fourier number derivative $$dFo_j^i=\frac{d\lambda(T_j^i)}{dT}\cdot\frac{\Delta t}{4\rho(T_j^i)c_p(T_j^i)\Delta x^2}$$

$$\begin{aligned}&T_{j-1}^{i+1}\left[-\frac{Fo_j^i}{2}\right]+T_j^{i+1}\left[1+Fo_j^i\right]+T_{j+1}^{i+1}\left[-\frac{Fo_j^i}{2}\right]=\\&T_j^i+\frac{Fo_j^i}{2}\left(T_{j-1}^i-2T_j^i+T_{j+1}^i\right)+dFo_j^i\left(T_{j+1}^i-T_{j-1}^i\right)^2\end{aligned}\tag{D.7}$$

Known temperature at the back face

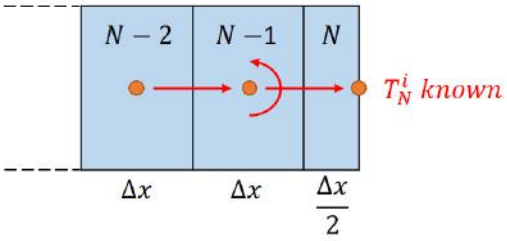

$$\frac{\lambda(T_{N-2}-T_{N-1})}{\Delta x}=\rho c_p \Delta x\frac{\partial T_{N-1}}{\partial t}+\frac{\lambda(T_{N-1}-T_N)}{\Delta x}$$

$$\frac{\partial T_{N-1}}{\partial t}=\frac{\lambda}{\rho c_p \Delta x^2}\left(T_{N-2}-2T_{N-1}+T_N\right)$$

Crank-Nicolson method $$T_{N-1}^{i+1}=T_{N-1}^{i}+\frac{\Delta t}{2}\left(\left.\frac{dT}{dt}\right|_{N-1}^{i}+\left.\frac{dT}{dt}\right|_{N-1}^{i+1}\right)$$

$$T_{N-1}^{i+1}=T_{N-1}^{i}+\frac{\Delta t}{2}\frac{\lambda}{\rho c_p \Delta x^2}\left[\left(T_{N-2}^{i}-2T_{N-1}^{i}+T_N^{i}\right)+\left(T_{N-2}^{i+1}-2T_{N-1}^{i+1}+T_N^{i+1}\right)\right]$$

Fourier number $$Fo_{N-1}^{i}=\frac{\lambda(T_{N-1}^{i})\Delta t}{\rho(T_{N-1}^{i})c_p(T_{N-1}^{i})\Delta x^2}$$

$$T_{N-1}^{i+1}=T_{N-1}^{i}+\frac{Fo_{N-1}^{i}}{2}\left(T_{N-2}^{i}-2T_{N-1}^{i}+T_N^{i}+T_{N-2}^{i+1}-2T_{N-1}^{i+1}+T_N^{i+1}\right)$$

$$T_{N-2}^{i+1}\left[-\frac{Fo_{N-1}^{i}}{2}\right]+T_{N-1}^{i+1}\left[1+Fo_{N-1}^{i}\right]=T_{N-1}^{i}+\frac{Fo_{N-1}^{i}}{2}\left(T_{N-2}^{i}-2T_{N-1}^{i}+T_N^{i}+T_N^{i+1}\right)\quad\text{(D.8)}$$

End element

Adiabatic thermal boundary conditions

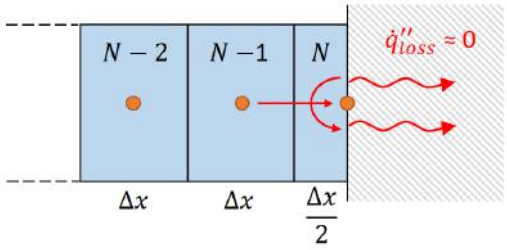

$$\frac{\lambda(T_{N-1} - T_N)}{\Delta x} = \rho c_p \frac{\Delta x}{2} \frac{\partial T_N}{\partial t}$$

$$\frac{\partial T_N}{\partial t} = \frac{2\lambda}{\rho c_p \Delta x^2} (T_{N-1} - T_N)$$

Crank-Nicolson method $$T_N^{i+1} = T_N^i + \frac{\Delta t}{2} \left(\frac{dT}{dt}\bigg|_N^i + \frac{dT}{dt}\bigg|_N^{i+1} \right)$$

$$T_N^{i+1} = T_N^i + \frac{\Delta t}{2} \left[\frac{2\lambda \left(T_{N-1}^i - T_N^i \right)}{\rho c_p \Delta x^2} + \frac{2\lambda \left(T_{N-1}^{i+1} - T_N^{i+1} \right)}{\rho c_p \Delta x^2} \right]$$

Fourier number $$Fo_N^i = \frac{\lambda(T_N^i)\Delta t}{\rho(T_N^i) c_p(T_N^i) \Delta x^2}$$

$$T_N^{i+1} = T_N^i + Fo_N^i \left(T_{N-1}^i - T_N^i + T_{N-1}^i - T_N^{i+1} \right)$$

$$T_{N-1}^{i+1} \left[-Fo_N^i \right] + T_N^{i+1} \left[1 + Fo_N^i \right] = T_N^i + Fo_N^i \left(T_{N-1}^i - T_N^i \right) \tag{D.9}$$

Thermally thin material with adiabatic thermal boundary conditions

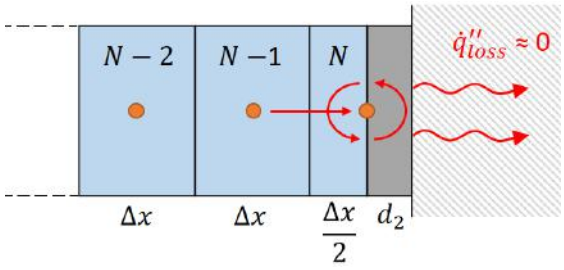

$$\frac{\lambda(T_{N-1}-T_N)}{\Delta x}=\rho c_p\frac{\Delta x}{2}\frac{\partial T_N}{\partial t}+\rho_2 c_{p,2}d_2\frac{\partial T_N}{\partial t}$$

$$\frac{\partial T_N}{\partial t}=\frac{\lambda\left(T_{N-1}-T_N\right)}{\Delta x}\cdot\frac{1}{\rho c_p\frac{\Delta x}{2}+\rho_2 c_{p,2}d_2}$$

Crank-Nicolson method $$T_N^{i+1}=T_N^i+\frac{\Delta t}{2}\left(\left.\frac{dT}{dt}\right|_N^i+\left.\frac{dT}{dt}\right|_N^{i+1}\right)$$

$$T_N^{i+1}=T_N^i+\frac{\Delta t}{2}\left[\frac{\lambda\left(T_{N-1}^i-T_N^i\right)}{\Delta x}+\frac{\lambda\left(T_{N-1}^{i+1}-T_N^{i+1}\right)}{\Delta x}\right]\cdot\frac{1}{\rho c_p\frac{\Delta x}{2}+\rho_2 c_{p,2}d_2}$$

Fourier number $$Fon_N^i=\frac{\lambda(T_N^i)\Delta t}{\Delta x\left[\Delta x\rho(T_N^i)c_p(T_N^i)+2d_2\rho_2(T_N^i)c_{p,2}(T_N^i)\right]}$$

$$T_N^{i+1}=T_N^i+Fon_N^i\left(T_{N-1}^i-T_N^i+T_{N-1}^i-T_N^{i+1}\right)$$

$$T_{N-1}^{i+1}\left[-Fon_N^i\right]+T_N^{i+1}\left[1+Fon_N^i\right]=T_N^i+Fon_N^i\left(T_{N-1}^i-T_N^i\right) \tag{D.10}$$

1. Single-layer material with known time-history of incident heat flux at the surface and adiabatic thermal boundary conditions at the back face

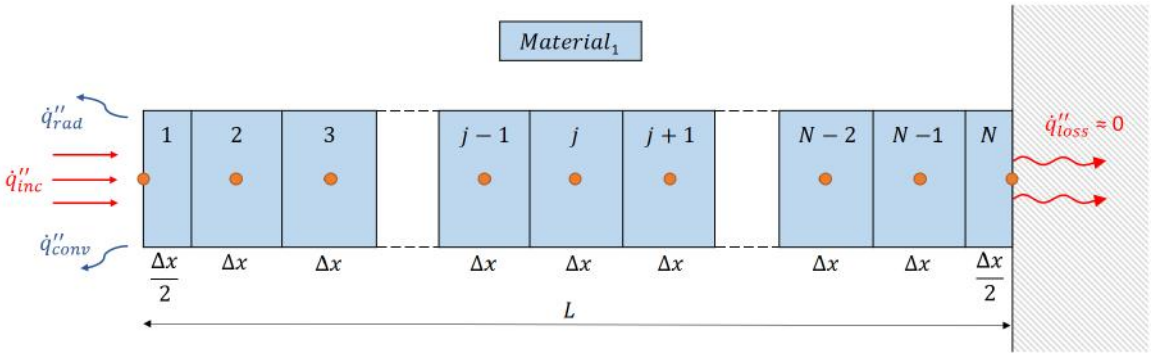

Surface element

$$T_1^{i+1}\left[1+Fo_1^i+\frac{h_{tot}(T_1^i)\Delta t}{\rho(T_1^i)c_p(T_1^i)\Delta x}\right]+T_2^{i+1}\left[-Fo_1^i\right]= T_1^i+Fo_1^i\left(T_2^i-T_1^i\right)+\frac{\alpha\Delta t}{\rho(T_1^i)c_p(T_1^i)\Delta x}\left(\dot{q}''^i_{inc}+\dot{q}''^{i+1}_{inc}\right)+\frac{h_{tot}(T_1^i)\Delta t}{\rho(T_1^i)c_p(T_1^i)\Delta x}\left(2T_\infty-T_1^i\right) \tag{D.11}$$

Middle element

$$T_{j-1}^{i+1}\left[-\frac{Fo_j^i}{2}\right]+T_j^{i+1}\left[1+Fo_j^i\right]+T_{j+1}^{i+1}\left[-\frac{Fo_j^i}{2}\right]= T_j^i+\frac{Fo_j^i}{2}\left(T_{j-1}^i-2T_j^i+T_{j+1}^i\right)+dFo_j^i\left(T_{j+1}^i-T_{j-1}^i\right)^2 \tag{D.12}$$

End element

$$T_{N-1}^{i+1}\left[-Fo_N^i\right]+T_N^{i+1}\left[1+Fo_N^i\right]=T_N^i+Fo_N^i\left(T_{N-1}^i-T_N^i\right) \tag{D.13}$$

$$\underset{[N\times N]}{\mathbf{A}} \cdot \underset{[N\times 1]}{\mathbf{x}} = \underset{[N\times 1]}{\mathbf{B}}$$

$$\begin{bmatrix} 1+Fo_1^i+\frac{h_{tot}(T_1^i)\Delta t}{\rho(T_1^i)c_p(T_1^i)\Delta x} & -Fo_1^i & & & & & & \\ & \ddots & & & & & & \\ & & \ddots & & & & & \\ & & & -\frac{Fo_j^i}{2} & 1+Fo_j^i & -\frac{Fo_j^i}{2} & & \\ & & & & \ddots & & & \\ & & & & & \ddots & & \\ & & & & & & \ddots & \\ & & & & & & -Fo_N^i & 1+Fo_N^i \end{bmatrix} \cdot \begin{bmatrix} T_1^{i+1} \\ \vdots \\ \vdots \\ \vdots \\ T_j^{i+1} \\ \vdots \\ \vdots \\ \vdots \\ T_N^{i+1} \end{bmatrix} = \begin{bmatrix} T_1^i + Fo_1^i(T_2^i - T_1^i) + \frac{\alpha\Delta t}{\rho(T_1^i)c_p(T_1^i)\Delta x}(\dot{q}_{inc}^{''i} + \dot{q}_{inc}^{''i+1}) \\ +\frac{h_{tot}(T_1^i)\Delta t}{\rho(T_1^i)c_p(T_1^i)\Delta x}(2T_\infty - T_1^i) \\ \vdots \\ \vdots \\ \vdots \\ T_j^i + \frac{Fo_j^i}{2}(T_{j-1}^i - 2T_j^i + T_{j+1}^i) + dFo_j^i(T_{j+1}^i - T_{j-1}^i)^2 \\ \vdots \\ \vdots \\ \vdots \\ T_N^i + Fo_N^i(T_{N-1}^i - T_N^i) \end{bmatrix} \tag{D.14}$$

2. Single-layer material with known time-history of incident heat flux at the surface and thermally thin material with adiabatic thermal boundary conditions at the back face

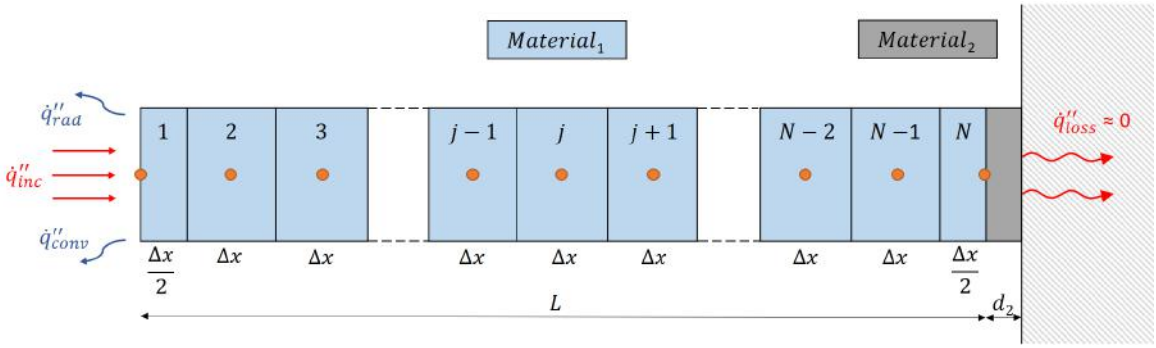

Surface element

$$T_1^{i+1}\left[1+Fo_1^i+\frac{h_{tot}(T_1^i)\Delta t}{\rho(T_1^i)c_p(T_1^i)\Delta x}\right]+T_2^{i+1}\left[-Fo_1^i\right]= T_1^i+Fo_1^i\left(T_2^i-T_1^i\right)+\frac{\alpha\Delta t}{\rho(T_1^i)c_p(T_1^i)\Delta x}\left(\dot{q}''^i_{inc}+\dot{q}''^{i+1}_{inc}\right)+\frac{h_{tot}(T_1^i)\Delta t}{\rho(T_1^i)c_p(T_1^i)\Delta x}\left(2T_\infty-T_1^i\right) \tag{D.15}$$

Middle element

$$T_{j-1}^{i+1}\left[-\frac{Fo_j^i}{2}\right]+T_j^{i+1}\left[1+Fo_j^i\right]+T_{j+1}^{i+1}\left[-\frac{Fo_j^i}{2}\right]= T_j^i+\frac{Fo_j^i}{2}\left(T_{j-1}^i-2T_j^i+T_{j+1}^i\right)+dFo_j^i\left(T_{j+1}^i-T_{j-1}^i\right)^2 \tag{D.16}$$

End element

$$T_{N-1}^{i+1}\left[-Fon_N^i\right]+T_N^{i+1}\left[1+Fon_N^i\right]=T_N^i+Fon_N^i\left(T_{N-1}^i-T_N^i\right) \tag{D.17}$$

$$Fon_N^i=\frac{\lambda(T_N^i)\Delta t}{\Delta x\left[\Delta x\rho(T_N^i)c_p(T_N^i)+2d_2\rho_2(T_N^i)c_{p,2}(T_N^i)\right]} \tag{D.18}$$

$$\mathbf{A} \cdot \mathbf{x} = \mathbf{B}$$
$$[\mathrm{N}\times\mathrm{N}] \quad [\mathrm{N}\times 1] \quad [\mathrm{N}\times 1]$$

$$\begin{bmatrix} 1+Fo_1^i+\frac{h_{tot}(T_1^i)\Delta t}{\rho(T_1^i)c_p(T_1^i)\Delta x} & -Fo_1^i & & & & & \\ & \ddots & & & & & \\ & & \ddots & & & & \\ & & -\frac{Fo_j^i}{2} & 1+Fo_j^i & -\frac{Fo_j^i}{2} & & \\ & & & & \ddots & & \\ & & & & & \ddots & \\ & & & & & -Fon_N^i & 1+Fon_N^i \end{bmatrix} \cdot \begin{bmatrix} T_1^{i+1} \\ \vdots \\ T_j^{i+1} \\ \vdots \\ T_N^{i+1} \end{bmatrix} = \begin{bmatrix} T_1^i + Fo_1^i(T_2^i - T_1^i) + \frac{\alpha\Delta t}{\rho(T_1^i)c_p(T_1^i)\Delta x}(\dot{q}_{inc}^{''i} + \dot{q}_{inc}^{''i+1}) \\ +\frac{h_{tot}(T_1^i)\Delta t}{\rho(T_1^i)c_p(T_1^i)\Delta x}(2T_\infty - T_1^i) \\ \vdots \\ T_j^i + \frac{Fo_j^i}{2}(T_{j-1}^i - 2T_j^i + T_{j+1}^i) + dFo_j^i(T_{j+1}^i - T_{j-1}^i)^2 \\ \vdots \\ T_N^i + Fon_N^i(T_{N-1}^i - T_N^i) \end{bmatrix} \tag{D.19}$$

3. Single-layer material with known time-history of incident heat flux at the surface and known temperature at the back face

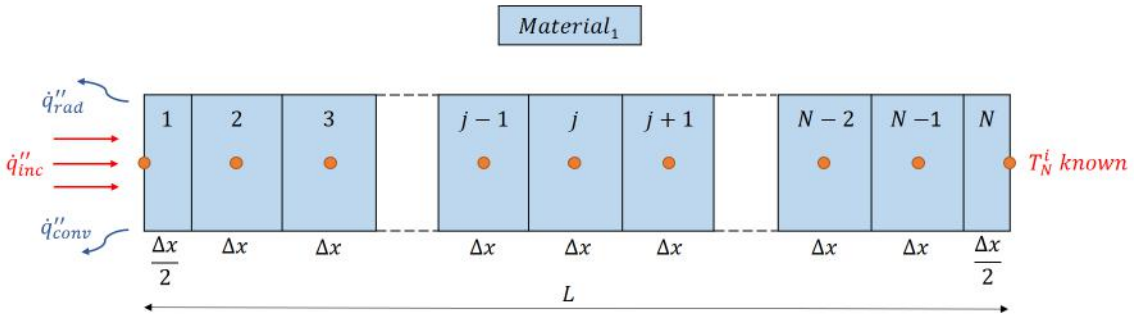

Surface element

$$T_1^{i+1}\left[1+Fo_1^i+\frac{h_{tot}(T_1^i)\Delta t}{\rho(T_1^i)c_p(T_1^i)\Delta x}\right]+T_2^{i+1}\left[-Fo_1^i\right]=$$
$$T_1^i+Fo_1^i\left(T_2^i-T_1^i\right)+\frac{\alpha\Delta t}{\rho(T_1^i)c_p(T_1^i)\Delta x}\left(\dot{q}''^i_{inc}+\dot{q}''^{i+1}_{inc}\right)+\frac{h_{tot}(T_1^i)\Delta t}{\rho(T_1^i)c_p(T_1^i)\Delta x}\left(2T_\infty-T_1^i\right) \tag{D.20}$$

Middle element

$$T_{j-1}^{i+1}\left[-\frac{Fo_j^i}{2}\right]+T_j^{i+1}\left[1+Fo_j^i\right]+T_{j+1}^{i+1}\left[-\frac{Fo_j^i}{2}\right]=$$
$$T_j^i+\frac{Fo_j^i}{2}\left(T_{j-1}^i-2T_j^i+T_{j+1}^i\right)+dFo_j^i\left(T_{j+1}^i-T_{j-1}^i\right)^2 \tag{D.21}$$

2nd-last element

$$T_{N-2}^{i+1}\left[-\frac{Fo_{N-1}^i}{2}\right]+T_{N-1}^{i+1}\left[1+Fo_{N-1}^i\right]=$$
$$T_{N-1}^i+\frac{Fo_{N-1}^i}{2}\left(T_{N-2}^i-2T_{N-1}^i+T_N^i+T_N^{i+1}\right) \tag{D.22}$$

End element

$$T_N^i=known(experimental) \tag{D.23}$$

$$\underset{[N\text{-}1\times N\text{-}1]}{\mathbf{A}} \cdot \underset{[N\text{-}1\times 1]}{\mathbf{x}} = \underset{[N\text{-}1\times 1]}{\mathbf{B}}$$

$$\begin{bmatrix} 1+Fo_1^i+\frac{h_{tot}(T_1^i)\Delta t}{\rho(T_1^i)c_p(T_1^i)\Delta x} & -Fo_1^i & & & & & & \\ & \cdot & & & & & & \\ & & \cdot & & & & & \\ & & & \cdot & & & & \\ & & & -\frac{Fo_j^i}{2} & 1+Fo_j^i & -\frac{Fo_j^i}{2} & & \\ & & & & & \cdot & & \\ & & & & & & \cdot & \\ & & & & & & & \cdot \\ & & & & & & -\frac{Fo_{N-1}^i}{2} & 1+Fo_{N-1}^i \end{bmatrix} \cdot \begin{bmatrix} T_1^{i+1} \\ \cdot \\ \cdot \\ \cdot \\ T_j^{i+1} \\ \cdot \\ \cdot \\ \cdot \\ T_{N-1}^{i+1} \end{bmatrix} = \begin{bmatrix} T_1^i + Fo_1^i(T_2^i - T_1^i) + \frac{\alpha\Delta t}{\rho(T_1^i)c_p(T_1^i)\Delta x}(\dot{q}_{inc}^{''i} + \dot{q}_{inc}^{''i+1}) \\ +\frac{h_{tot}(T_1^i)\Delta t}{\rho(T_1^i)c_p(T_1^i)\Delta x}(2T_\infty - T_1^i) \\ \cdot \\ \cdot \\ \cdot \\ T_j^i + \frac{Fo_j^i}{2}(T_{j-1}^i - 2T_j^i + T_{j+1}^i) + dFo_j^i(T_{j+1}^i - T_{j-1}^i)^2 \\ \cdot \\ \cdot \\ \cdot \\ T_{N-1}^i + \frac{Fo_{N-1}^i}{2}(T_{N-2}^i - 2T_{N-1}^i + T_N^i + T_N^{i+1}) \end{bmatrix} \tag{D.24}$$

4. Single-layer material with known temperature at the surface and known temperature at the back face

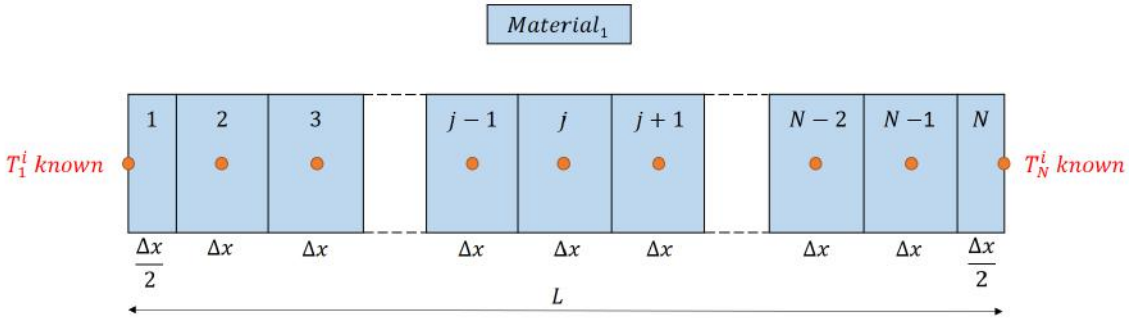

Surface element

$$T_1^i = known(experimental) \tag{D.25}$$

2nd element

$$T_2^{i+1}\left[1+Fo_2^i\right]+T_3^{i+1}\left[-\frac{Fo_2^i}{2}\right]= T_2^i+\frac{Fo_2^i}{2}\left(T_1^i-2T_2^i+T_3^i+T_1^{i+1}\right) \tag{D.26}$$

Middle element

$$T_{j-1}^{i+1}\left[-\frac{Fo_j^i}{2}\right]+T_j^{i+1}\left[1+Fo_j^i\right]+T_{j+1}^{i+1}\left[-\frac{Fo_j^i}{2}\right]= T_j^i+\frac{Fo_j^i}{2}\left(T_{j-1}^i-2T_j^i+T_{j+1}^i\right)+dFo_j^i\left(T_{j+1}^i-T_{j-1}^i\right)^2 \tag{D.27}$$

2nd-last element

$$T_{N-2}^{i+1}\left[-\frac{Fo_{N-1}^i}{2}\right]+T_{N-1}^{i+1}\left[1+Fo_{N-1}^i\right]= T_{N-1}^i+\frac{Fo_{N-1}^i}{2}\left(T_{N-2}^i-2T_{N-1}^i+T_N^i+T_N^{i+1}\right) \tag{D.28}$$

End element

$$T_N^i = known(experimental) \tag{D.29}$$

$$\underset{[\text{N-2}\times\text{N-2}]}{\mathbf{A}} \cdot \underset{[\text{N-2}\times 1]}{\mathbf{x}} = \underset{[\text{N-2}\times 1]}{\mathbf{B}}$$

$$\begin{bmatrix} 1+Fo_2^i & -\frac{Fo_2^i}{2} & & & & & & \\ -\frac{Fo_2^i}{2} & \ddots & \ddots & & & & & \\ & \ddots & \ddots & \ddots & & & & \\ & & -\frac{Fo_j^i}{2} & 1+Fo_j^i & -\frac{Fo_j^i}{2} & & & \\ & & & \ddots & \ddots & \ddots & & \\ & & & & \ddots & \ddots & \ddots & \\ & & & & & \ddots & \ddots & -\frac{Fo_{N-1}^i}{2} \\ & & & & & & -\frac{Fo_{N-1}^i}{2} & 1+Fo_{N-1}^i \end{bmatrix} \cdot \begin{bmatrix} T_2^{i+1} \\ \vdots \\ \vdots \\ \vdots \\ T_j^{i+1} \\ \vdots \\ \vdots \\ \vdots \\ T_{N-1}^{i+1} \end{bmatrix} = \begin{bmatrix} T_2^i + \frac{Fo_2^i}{2}(T_1^i - 2T_2^i + T_3^i + T_1^{i+1}) \\ \vdots \\ \vdots \\ \vdots \\ T_j^i + \frac{Fo_j^i}{2}(T_{j-1}^i - 2T_j^i + T_{j+1}^i) + dFo_j^i(T_{j+1}^i - T_{j-1}^i)^2 \\ \vdots \\ \vdots \\ \vdots \\ \vdots \\ T_{N-1}^i + \frac{Fo_{N-1}^i}{2}(T_{N-2}^i - 2T_{N-1}^i + T_N^i + T_N^{i+1}) \end{bmatrix} \quad \text{(D.30)}$$

Bibliography

[1] Crank J. and Nicolson P. "A practical method for numerical evaluation of solutions of partial differential equations of the heat-conduction type". Advances in Computational Mathematics, vol. 6, pp. 207-226, 1996.

[2] Hidalgo J.P. "Performance-based methodology for the fire safe design of insulation materials in energy efficient buildings". PhD thesis, School of Engineering, The University of Edinburgh, 2015.